Minimized combinatorial CRISPR screens identify genetic interactions in autophagy

Dissertation

zur Erlangung des Doktorgrades

der Naturwissenschaften

vorgelegt beim Fachbereich 14

Biochemie, Chemie und Pharmazie

der Johann Wolfang Goethe-Universität

in Frankfurt am Main

von

Valentina Diehl

geboren am 05.12.1990 in Wachsch

Frankfurt am Main

2021

D30

vom Fachbereich 14 (Biochemie, Chemie und Pharmazie) der

Johann Wolfgang Goethe-Universität als Diessertation angenommen.

Dekan:	Prof. Dr. Clemens Glaubitz
Gutachter:	Prof. Dr. Volker Dötsch
	Prof. Dr. Ivan Dikic

Datum der Disputation:

Decleration of Authorship

Except where stated otherwise by reference or acknowledgment, the work presented in this PhD thesis was generated by myself, Valentina Diehl, between September 2016 and March 2021 under the supervision of Dr. Manuel Kaulich at the Goethe-University Frankfurt, Faculty of Medicine, Institute of Biochemistry II. The data presented in this thesis was published in the following publications:

V. Diehl, M. Wegner, P. Grumati, K. Husnjak, S. Schaubeck, A.Gubas, V. Shah, I. H. Polat, F. Langschied, C. Prieto-Ggarcia, K. Müller, A. Kalousi, I. Ebersberger, C. H. Brandts, I. Dikic and M. Kaulich, **"Minimized combinatorial CRISPR screens identify genetic interactions in autophagy."**, Nucleic Acids Research (2021).
https://doi.org/10.1093/nar/gkab309

M. Wegner, **V. Diehl**, V. Bittl, R. de Bruyn, S. Wiechmann, Y. Matthess, M. Hebel, M.G. Hayes, S. Schaubeck, C. Benner, S. Heinz, A. Bremm, I. Dikic, A. Ernst and M. Kaulich, **"Circular synthesized CRISPR/Cas gRNAs for functional interrogations in the coding and noncoding genome."**, eLife (2019).
https://pubmed.ncbi.nlm.nih.gov/30838976

The work includes the following contributions from colleagues in context of of collaborative reserach:
Martin Wegner (Institute of Biochemistry II, Goethe University Frankfurt) performed sequencing data quality control, read count table generation, enrichment analyses and computation of genetic interaction models.
Konstantin Müller (Institute of Biochemistry II, Goethe University Frankfurt) performed RNA-seq analysis of the monoclonal Cas9-expressing hTERT-RPE1 cell line that was used for CRISPR screening.
This project was carried out in close collaboration with the group of Prof. Dr. Ivan Dikic (Institute of Biochemistry II, Goethe University Frankfurt): Target gene selection and generation of the autophagy multiplex CRISPR library, and the generation of the stable autophagic flux reporter cell line were performed by Dr. Paolo Grumati (Telethon Institute of Genetics and Medicine, Pozzuoli, Italy). Arrayed validation of single essential autophagy genes was performed by Dr. Varun Jayeshkumar Shah (Institute of Biochemistry II, Goethe University Frankfurt) and Dr. Cristian Prieto-Garcia (Institute of Biochemistry II, Goethe University Frankfurt) performed lung squamous cell carcinoma patient survival analysis.
High-throughput sequencing was performed by the groups of Dr. Andrea Ballabio and Dr. Davide Cacchiarelli (Telethon Institute of Genetics and Medicine, Pozzuoli, Italy), and Dr. Sebastian Wagner and Dr. Khalil Abou Elardat (Cancer Genomics Core Facility Frankfurt, Germany).

Contents

List of Figures

List of Tables

Summary

Complex biological phenotypes are orchestrated by the synergistic function of multiple genes. The dissection of the human gene interaction network is a critical step towards understanding how disease arise from gene dysfunction. Accordingly, the systematic identification of context-dependent genetic interactions in various human cell lines, tissues, and under distinct conditions could provide substantial insights into the genotype-to-phenotype relationship, and elucidate how synergistic gene function affects the emergence of complex diseases.

Pooled combinatorial CRISPR (clustered regularly interspaced short palindromic repeats) screens have emerged as a powerful tool to simultaneously study genetic interactions of large numbers of genes. Here, multiplex CRISPR guide RNA (gRNA) libraries are applied to generate pairwise gene knockouts at large scale in mammalian cells. Multiplex CRISPR gRNA libraries can consist of thousands to hundred thousands of plasmids, each encoding a distinct gRNA combination for targeting a specific gene pair. However, large scale genetic interaction screening with multiplex CRISPR gRNA libraries faces additional challenges compared to single gene-targeting CRISPR screens:

First, the construction of highly diverse multiplex CRISPR gRNA libraries becomes more laborious with increasing numbers of target genes because the library diversity, which the total number of different gRNAs or gRNA combinations, is determined by the number of desired target genes. An ideal library would show a uniform library distribution, with the same abundance of all gRNAs or gRNA combinations. However, due to practical constraints, pooled libraries typically exhibit under- and over-represented gRNA sequences. Conventional methods for multiplex gRNA library generation, for instance, rely on iterative, pooled cloning steps and PCR-amplification of oligonucleotides that can result in unevenly distributed or missing gRNA sequences in the final library. This offers potential for optimization.

Second, an increased library diversity of multiplex gRNA libraries, in turn, requires an increased experimental scale with extensive cell culture work, because ensuring reproducible screening results is achieved by applying sufficient screening coverage. The screening coverage describes the average abundance of each gRNA or gRNA combination present in the cell population during the screen. Current guidelines for performing pooled CRISPR screens suggest screening coverages between 200- and 1,000-fold of the library diversity, but lack precise indications which coverage should be used with a given library. Therefore, the required screening coverage constitutes a major challenge that limits the number of targetable gene combinations.

In this study, we present a novel method, called covalently-closed circular-synthesized (3Cs) multiplexing, to rapidly generate highly diverse pooled multiplex gRNA libraries. 3Cs multiplexing circumvents iterative pooled restriction endonuclease-based cloning and PCR-amplification of gRNA-encoding oligonucleotides. We demonstrate that 3Cs multiplexing robustly results in uniformly distributed multiplex gRNA libraries. The library distribution skew, elsewhere termed skew ratio or distribution width, was introduced to measure the library uniformity and is defined as the ratio of the highest and lowest abundant gRNAs of the library. We show that 3Cs multiplex libraries typically show distribution skews below 2.5, values most often unmatched even for single-gRNA libraries.
We hypothesized that the library distribution might affect the robustness of pooled CRISPR screens and that it must be considered before choosing a screening coverage. We aimed at investigating the impact of the library distribution on the screening performance under different coverages. To this end, we generated three artificially skewed multiplex libraries and applied them in proliferation screens with a 20- and 200-fold coverage. Thereby we identified the library distribution skew to be the major determinant for the required screening coverage. Moreover, we demonstrate that, due to their uniform distribution, 3Cs libraries can be applied with minimal screening conditions, resulting in a 10-fold reduction of associated efforts and costs. While previous CRISPR screening guidelines did not account for the initial plasmid library distribution, we recommend choosing a screening coverage based on the library distribution. This will enable to reduce the experimental scale for future screens without compromising the screening performance.

Bulk and selective autophagy are tightly regulated processes that target cellular material for lysosomal degradation. Deregulation of autophagy is implicated in numerous human diseases and can lead to abnormal cell growth or cell death. Since autophagy is integrated into a number of key signaling pathways, it provides therapeutic potential in a variety of human diseases. Identifying and understanding synergistic functions of autophagy genes can lead to new insights on the molecular mechanisms that regulate autophagy, and to novel approaches for the treatment of neurodegenerative diseases and cancer. To investigate autophagy gene interactions, we generated a 3Cs multiplex library targeting human autophagy gene combinations. The 3Cs autophagy multiplex library was composed of 247,032 gRNA combinations targeting known autophagy key players, such as upstream regulators, components of the Unc-51 like autophagy activating kinase 1 (ULK1) and the class III phosphatidylinositol 3-kinase (PIK3C3) complexes, the conjugation machinery, ATG8 homologs, phosphatidylinositol 3-phosphate (PI3P) effectors and components of the autophagosome-lysosome fusion machinery.
To demonstrate the functionality of 3Cs multiplex libraries in coverage-minimized CRISPR screens, we applied the 3Cs autophagy multiplex library in two different pooled screening set ups. In a proliferation screen, we investigated genetic interactions between autophagy genes that affect cell proliferation and identified *WDR45B-PIK3R4* and *ATG7-KEAP1* to result in reduced and enhanced cell proliferation, respectively. In a reporter-based autophagy flux screen,

we identified genetic interactions that are required for autophagic flux, including the paralog pair *ATG2A-ATG2B*, and the genetic interactions *GABARAPL2-WIPI2* and *ULK4-SQSTM1*.

We envision that 3Cs multiplexing will be applicable to a broad range of biological settings and will accelerate the systematic identification of genetic interactions in various contexts and organisms. This will advance the translation into novel drug combinations and lead to new insights into complex human disease phenotypes.

Zusammenfassung

Komplexe biologische Phänotypen resultieren aus einem koordinierten Zusammenspiel von einer Vielzahl von synergistischen Genen. Um zu verstehen, wie Krankheiten durch genetische Dysfunktionen entstehen können, ist es unabdingbar die genetischen Interaktionsnetzwerke in menschlichen Zellen zu entschlüsseln. Eine Identifizierung von Kontext-abhängigen genetischen Interaktionen in verschiedenen Zelllinien, Geweben und unter unterschiedlichen Konditionen kann folglich bedeutende Erkenntnisse über die Beziehung von Phänotyp und Genotyp liefern und erklären, wie synergistische Gen-Funktionen die Entstehung von komplexen Krankheiten bedingen.

Gepoolte, kombinatorische CRISPR (kurz für: clustered regularly interspaced short palindromic repeats) Screens stellen eine wirkungsvolle Methode dar, um potentielle Interaktionen von einer großen Anzahl verschiedener Gene simultan zu untersuchen. Dafür werden sogenannte gepoolte multiplex CRISPR Guide RNA (gRNA)-Bibliotheken verwendet, um vielzählige kombinatorische Gen-Knockouts in Säugetier-Zellen in großangelegten Screens zu generieren. Diese multiplex CRISPR gRNA-Bibliotheken können aus bis zu hunderttausenden Plasmiden bestehen, die jeweils für eine andere gRNA-Kombination kodieren und auf ein spezifisches Gen-Paar abzielen. Im Gegensatz zu gepoolten CRISPR Screens für Einzel-Knockouts gehen solche kombinatorischen multiplex CRISPR Screens zur Identifizierung von genetischen Interaktionen mit zusätzlichen Herausforderungen einher.
Zum einen wächst der verbundene Arbeitsaufwand für die Konstruktion der multiplex CRISPR gRNA-Bibliotheken proportional mit der Anzahl der gewünschten Ziel-Gene. Dies ist dadurch bedingt, dass die finale Diversität der Bibliothek der gesamten Anzahl aller enthaltenen gRNAs oder gRNA-Kombinationen entspricht und somit mit steigender Anzahl von gewünschten Ziel-Genen zunimmt. Für multiplex CRISPR gRNA-Bibliotheken ergibt sich auf Grund der Kombinatorik die Diversität aus dem Quadrat der Anzahl der gewünschten Ziel-Gene.
In einer idealen gRNA-Bibliothek wären alle gRNA-Sequenzen gleich häufig vorhanden. Jedoch weisen gRNA-Bibliotheken aufgrund von technischen Beschränkungen bei konventionellen Herstellungsmethoden typischerweise gRNA-Sequenzen mit höherer, beziehungsweise niedriger Abundanz auf. So basieren konventionelle Methoden zur Herstellung von gRNA-Bibliotheken beispielsweise auf iterativen, gepoolten Klonierungsschritten mit PCR-amplifizierten Oligonukleotiden. Mit jedem zusätzlichen gepoolten Klonierungs- und Amplifikationsschritt ergeben sich zusätzliche Fehlerquellen, welche zu einer Ungleichverteilung oder zum Verlust von gRNA-

Sequenzen führen können. Um die Vollständigkeit der gewünschten Bibliothek zu gewährleisten, müssen mit herkömmlichen Methoden typischerweise mehrere Wiederholungen von gepoolten Reaktionen durchgeführt werden und die Repräsentation aller gRNA-Sequenzen muss durch Sequenzierung bestätigt werden. Daher bieten die herkömmlichen Methoden zur gRNA-Bibliotheken-Generierung Optimierungspotenzial.
Zum anderen erfordert die hohe Bibliotheks-Diversität, die sich wegen der Kombinationen der verschiedenen gRNA-Sequenzen ergibt, gleichzeitig auch eine Vergrößerung des Versuchsmaßstabs und ist mit umfangreichem Zellkultur-Arbeitsaufwand verbunden. Das ist dadurch bedingt, dass die Reproduzierbarkeit der Screen-Ergebnisse durch die sogenannte Screening Coverage sichergestellt werden muss. Die Screening Coverage gibt die durchschnittliche Abundanz der einzelnen gRNA-Sequenzen in der Zellpopulation während des Screens an und kompensiert vor allem für stark unterrepräsentierte, beziehungsweise stark überrepräsentierte gRNA-Sequenzen.
Aktuelle Richtlinien empfehlen eine Screening Coverage, die zwischen dem 200- bis 1000-fachen Wert der Bibliotheks-Diversität liegt, allerdings fehlen bisher genaue Angaben, die auf die Verteilung der verwendeten gRNA-Bibliothek abgestimmt sind. Um die Reproduzierbarkeit des Screens sicherzustellen, wird daher eine sehr hohe Screening Coverage gewählt, was wiederum dazu führt, dass die Durchführbarkeit nur für kleine Bibliotheken mit wenigen Ziel-Genen möglich ist. Deshalb stellt die benötigte Screening Coverage bisher einen limitierenden Faktor dar, der die Anzahl der möglichen Ziel-Genkombinationen in einem Screen beschränkt.

In der vorliegenden Arbeit stellen wir zunächst eine neue Methode vor, die der Generierung von multiplex gRNA Bibliotheken mit hohen Diversitäten dient und die derzeitigen Limitierungen adressiert. Die Methode, genannt 3Cs (covalently-closed circular-synthesized) Multiplexing, umgeht iterative, gepoolte Klonierugsschritte mit Restriktionsenzymen und PCR-Amplifikation von gRNA-kodierenden Oligonukleotiden.
Für das 3Cs Multiplexing wurde zunächst ein sogenanntes Multiplexing Plasmid kloniert, das zwei gRNA-Expressionskassetten beinhaltet, welche jeweils durch unterschiedliche, sequenzspezifische Regionen flankiert sind. Beide Expressionskassetten kodieren zunächst für "Platzhalter-Sequenzen", die später beim 3Cs Multiplexing durch gRNA-Sequenzen ersetzt werden. Zusätzlich enthält das Plasmid einen f1 ori (origin of replication), der eine einzelsträngige Replikation und Verpackung der DNA in Phagenpartikel ermöglicht und beim 3Cs Multiplexing der Isolation von einzelsträngiger zirkulärer DNA des Multiplexing Plasmids dient. An die einzelsträngige DNA werden bei der gepoolten 3Cs Multiplexing Synthese Oligonukleotide annealed, die für alle gewünschten gRNAs kodieren und deren Position durch homologe Bindung an die sequenzspezifischen Regionen der Expressionskassetten bestimmt wird. Nach anschließender Extension und Ligation erfolgt durch Elektroporation in Bakterien eine Amplifikation der finalen Bibliothek, die alle möglichen Kombinationen der verwendeten gRNA-Sequenzen enthält.
Wir zeigen, dass 3Cs Multiplexing auf robuste Weise zur Herstellung von gleichmäßig verteilten

multiplex gRNA Bibliotheken mit hohen Diversitäten verwendet werden kann. Der sogenannte Verteilungs-Skew, auch Skew-Ratio oder Bibliotheksbreite genannt, ist ein Maß zur Ermittlung der Gleichverteilung der gRNA-Sequenzen in der Bibliothek. Er wird über den Quotienten der am häufigsten und am niedrigsten abundanten gRNA-Sequenzen berechnet. Wir zeigen, dass 3Cs multiplex Bibliotheken typischerweise einen Verteilungs-Skew von 2.5 aufweisen, was unter den für gewöhnlich beobachteten Werten von Einzel-gRNA Bibliotheken liegt.
Wir nahmen an, dass die gRNA-Bibliotheksverteilung die Robustheit von gepoolten CRISPR Screens beeinflussen könne und deshalb bei der Auswahl einer geeigneten Screening Coverage berücksichtigt werden müsse. Um den Einfluss der gRNA-Bibliotheksverteilung auf die Screen-Qualität in Abhängigkeit von der verwendeten Screening Coverage zu untersuchen, haben wir zwei künstlich fehlverteilte multiplex gRNA-Bibliotheken generiert und diese, zusätzlich zu einer nahezu gleichverteilten multiplex gRNA-Bibliothek, jeweils mit einer 20- und 200-fachen Screening Coverage in einem kombinatorischen Proliferations-Screen angewandt. Dadurch konnten wir die gRNA-Bibliotheksverteilung als den bestimmenden Parameter für die benötigte Screening Coverage identifizieren. Zusätzlich konnten wir zeigen, dass 3Cs multiplex gRNA-Bibliotheken auf Grund ihrer gleichmäßigen Verteilung mit minimierter Screening Coverage eingesetzt werden können, was zu einer 10-fachen Reduktion des assoziierten Arbeitsaufwands führt. Während bisherige Richtlinien für gepoolte CRISPR Screens die initiale gRNA-Bibliotheksverteilung nicht berücksichtigen, empfehlen wir die Screening Coverage an dieser auszurichten.

Autophagie ist ein streng regulierter zellulärer Prozess, der den Lysosomen Abbau von intrazellulärem Material steuert. Dysregulation von Autophagie steht im Zusammenhang mit zahlreichen menschlichen Erkrankungen und kann auf zellulärer Ebene zu unkontrolliertem Wachstum, aber auch zum Zelltod führen. Da Autophagie in eine Vielzahl von Signalwegen integriert ist, bietet es potenziell außerdem therapeutische Ansatzpunkte zur Behandlung von Krankheiten. Die Identifizierung von synergistischen Funktionen zwischen Autophagie-Genen könnte unser Verständnis über die molekularen Mechanismen, die der Regulation der Autophagie zu Grunde liegen, erweitern und dadurch neuartige Behandlungen für beispielsweise Krebs oder Neurodegeneration ermöglichen.
Um genetische Interaktionen von Autophagie-Genen zu untersuchen haben wir eine 3Cs multiplex gRNA Bibliothek generiert, die auf menschliche Autophagie-Genkombinationen abzielt. Die 3Cs Multiplex Autophagie-Bibliothek enthielt insgesamt 247,032 gRNA-Kombinationen und richtete sich gegen Schlüsselproteine des Autophagie-Prozesses, wie unter anderem vorgeschaltete Transkriptionsfaktoren und Regulatoren, Komponenten der ULK1 (Unc-51like autophagy activating kinase 1) und PIK3C3 (Phosphatidylinositol 3-kinase catalytic subunittype 3) Komplexe, der Konjugations-Maschinerie, ATG8–Homologe und relevante Proteine für die Fusion von Autophagosomen und Lysosomen. Um die Funktionalität der 3Cs Multiplex Autophagie-Bibliothek unter Anwendung minimierter Screening Coverage zu demonstrieren, haben wir sie in zwei verschiedenen Screen-Ausführungen angewandt.

Zunächst verwendeten wir die 3Cs Multiplex Autophagie-Bibliothek in einem Proliferations-Screen, um Autophagie-Geninteraktionen zu identifizieren, deren Verlust zu einer gesteigerten oder verringerten Zellproliferation führt.
Eine genetische Interaktion wird per Definition in einem Screen dann identifiziert, wenn der im Screen gemessene Phänotyp des Doppel-Knockouts einer Genkombination von dem Phänotyp abweicht, der basierend auf den Einzel-Knockouts zu erwarten wäre. Zur Identifikation von genetischen Interaktionen im Proliferations-Screen verwendeten wir eine Summen-Definition, bei der sich der zu erwartenden Phänotyp für einen Doppel-Knockout aus der Summe beider Einzel-Knockouts ergibt.
Unter den identifizierten genetischen Interaktionen resultierte der Knockout von *WDR45B-PIK3R4* zur stärksten Suppression der Proliferation, während die Depletion von *ATG7-KEAP1* zu extrem verstärkter Proliferation beitrug.
Außerdem konnten wir, im Kontext der Proliferation, *PIK3R4*, *ATG7*, und *ATG5* als sogenannte Hub-Gene identifizieren, die Kombination mit über 80% aller getesteten Gene einen Einfluss auf das Proliferationsverhalten hatten.

Während in den letzten Jahren gepoolte gRNA-Bibliotheken, sowohl für Einzel-Gene, als auch für Genetische Interaktionen, bereits mehrfach für Proliferations-Screen eingesetzt wurden, gibt es zum heutigen Stand kaum Anwendungen von kombinatorischen gRNA-Bibliotheken für andere phänotypische Readouts als Proliferation. Um die Anwendbarkeit der 3Cs Multiplex Autophagie-Bibliothek und unserer minimierten Screening Coverage in einem Screen mit einem weiteren, biologisch relevanten phänotypischen Readout zu demonstrieren, haben wir einen etablierten Autophagie-Reporter verwendet. Unter Einsatz einer generierten Zell-Linie mit stabiler Expression des Autophagie-Reporters konnten wir in einem FACS (Fluorescence-activated cell sorting)-basierten Autophagie-Screen genetische Interaktionen aufdecken, die essentiell für den Autophagie-Prozess sind.
Unter der Annahme, dass der Verlust eines zweiten Autophagie-Gens den negativen Effekt auf den Autophagieflux durch den Verlust eines ersten Autophagie-Gens nicht abmildern würde, und aufgrund einer vergleichenden Analyse verschiedener Modelle, verwendeten wir für den FACS-basierten Autophagie-Screen ein Maximal Modell. Nach der Maximal Definition wird eine genetischen Interaktion dann identifiziert, wenn der gemessene kombinatorische Knockout-Phänotyp stärker ist, als der des stärksten Einzel-Phänotyps.
Zu den identifizierten Interaktionen zählen unter anderem die Interaktionen zwischen dem Paralog-Paar *ATG2A-ATG2B*, und zwischen *WIPI2-GABARAPL2*, *SCOC-SIRT2*, *AMBRA1-ZKSCAN3*, *PI4K2A-RAB7B*, *PIK3CA-STK3* und *SQSTM1-UKL4*, die wir ebenso in gesonderten Experimenten ("arrayed") mit separat klonierten gRNAs validieren konnten.
Wie auch im Proliferations-Screen konnten wir im FACS-basierten Multiplex Autophagie-Screen Gene identifizieren, die in Kombination mit einer Vielzahl der getesteten Gene zu einem unerwarteten Phänotyp führten. Zu den Hub-Genen im Kontext des Autophagie-Reporter basierten

Readouts gehörten alle einzel-essentiellen Autophagie-Gene, sowie *AMBRA1*, dessen Knockout alleine keinen Einfluss auf den Autophagieflux hatte. Die starke Konnektivität der Hub-Gene lässt eine wichtige Buffering-Funktion im Autophagie-Signalweg vermuten.

Zusammengefasst haben wir im Rahmen dieser Arbeit die 3Cs Multiplexing Technologie entwickelt und demonstriert, dass 3Cs Multiplexing der robusten Herstellung von kombinatorischen gRNA-Bibliotheken mit hohen Diversitäten und gleichmäßiger Verteilung dient. Wir konnten außerdem, mit Hilfe von unterschiedlich verteilten 3Cs multiplex Bibliotheken in Kombination mit Proliferations-Screens, die Bibliotheksverteilung als bestimmenden Faktor der benötigten Screening Coverage ermitteln. Zusätzlich konnten wir die Anwendbarkeit der 3Cs Multiplexing Technologie zur Identifizierung von genetischen Interaktionen zwischen Autophagie-Genen in zwei unterschiedlichen Screen-Ausführungen mit verschiedenen phänotypischen Readouts zeigen.
Wir glauben, dass 3Cs Multiplexing in Zukunft breite Anwendung in verschiedenen biologisch relevanten Feldern finden wird und die Entschlüsselung von kontext-abhängigen genetischen Interaktionen voranbringen kann. Dadurch kann das Verständnis für die Entstehung von komplexen pathologischen Phänotypen erweitert werden.

Introduction

1.1 Genetic interactions and their biological implications

1.1.1 Defining quantitative genetic interactions

The development of high-throughput technologies for functional genomic screening and whole genome sequencing have not only massively advanced our knowledge on the function of single genes but also uncovered the great impact of GIs on homeostasis and robustness of biological systems. Most phenotypes, in the state of health and disease, are not determined by single gene functions. Instead, multigenic phenotypes result from the orchestrated interplay between multiple genes in a specific environmental context [1]. Accordingly, systematic exploration of GIs and their network topology in human cells can provide substantial insights into the causative effects of synergistic gene function on complex phenotypes and disease [2].

The term *genetic interaction (GI)* describes a group of functional relationships between genes, in which two genes interact if the observed phenotype of their combined perturbation significantly deviates from what is expected based on their individual single mutants [3–5]. Therefore, experimental identification of GIs requires two components: First, a measurement to quantify the phenotypic strength of individual and combinatorial gene perturbation, and second, a mathematical model to predict an expected phenotype for two non-interacting genes [6].
Figure 1.1 illustrates an experimental approach for the identification and classification of different GI types for a proliferative phenotypic read-out: In a hypothetical experiment, the individual proliferation of two mutant cell lines, mutant A and B, is measured and normalized to the proliferation of wild type (wt) cells. Based on the phenotypic strength of the single mutants, an expected phenotype for the combinatorial mutant AB is predicted using a pre-selected mathematical model. This predicted value is expected when both genes do not interact with each other. Accordingly, a GI is identified when the actual measured phenotype for the double mutant AB deviates from the predicted phenotype. Based on the strength and directionality of the deviation, GIs can be classified into positive and negative GIs.
Negative GIs (also aggravating) occur when the combined loss of two genes causes a more severe phenotype than expected (e.g. synthetic sick or synthetic lethal). Synthetic lethality represents the most extreme case of a negative GI, in which two single mutants are viable, while the double mutant is lethal [2, 6, 7]. Conversely, positive GIs (also buffering or alleviating)

arise when the combinatorial perturbation has a less severe phenotypic effect than expected. This includes masking interactions, in which the proliferation of the double mutant corresponds to the sickest single mutant, and genetic suppressive interactions, in which the combinatorial mutant is even healthier than the sickest individual mutant. Masking interactions can emerge when for instance a single gene perturbation leads to complete loss of activity of a non-essential protein complex. In this case the loss of a second gene associated with the same complex will show no additional effect, but resemble the phenotype of the first single mutant [8–10].

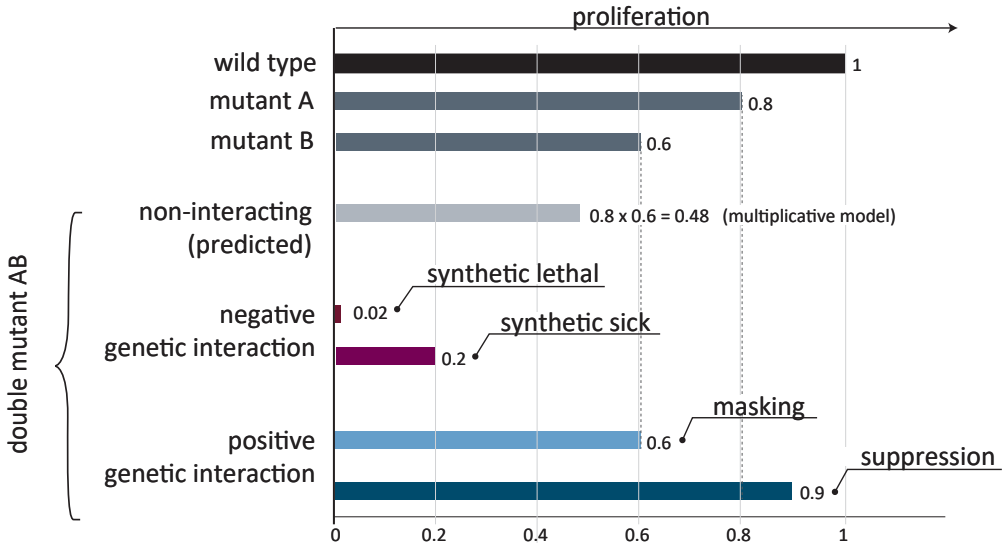

Figure 1.1: Identification and classification of genetic interactions
GIs can be identified by measuring the deviation of a given mutant gene combination (double mutant AB) from a predicted value, which is expected for a non-interacting gene pair. The expected neutral phenotype can be calculated based on the single mutant phenotypes (mutant A and B) by different mathematical models. Here, a multiplicative model is used. A negative GI occurs when the phenotypic quantification of a double mutant AB is more severe than the predicted neutral phenotype. This includes synthetic sick and synthetic lethal interactions. For positive GIs, such as genetic suppression and masking interactions, the measured combinatorial phenotype is less severe than the expected non-interacting prediction. Adapted from [11].

The choice of a suitable model for predicting an expected phenotype for non-interacting genes is a critical parameter for identifying GIs and determines the biological interpretation. Therefore, different models have been tested and used in the past for systematic and large-scale screening for GIs, the most common being the multiplicative, minimum, additive, and logarithmic models [6]. In the minimum model, the expected neutral phenotype for combinatorial mutants corresponds to the single mutant with the most severe phenotype. In case of cell fitness, this corresponds to the least fit single mutant [12–14]. The additive model defines the expected phenotype for non-interacting genes as the sum of the measured phenotypic strength of both individual mutants [15], and in the multiplicative model, the expected phenotype is

predicted as the product of both single mutants. The logarithmic model was developed to determine GIs from measurements on a logarithmic fitness scale. While the multiplicative and logarithmic model have been proven suitable to detect GIs in proliferation and cell viability assays, choosing an adequate model for more complex phenotypes requires further comparative studies [6].
Cell viability, fitness and proliferation are by far the most studied phenotypes in the context of GI mapping. However, any phenotypic read-out that allows quantification can be used as a phenotypic measure. Other phenotypic read-outs include reporter genes for fluorescence-activated cell sorting (FACS) or for high-content screening (HCS), which have been used to assay transcriptional response, protein folding in the endoplasmic reticulum, and other cell biological phenotypes in yeast [16–18]

1.1.2 Genetic interaction properties and network structure

Most of what we know about GIs today was elaborated by systematic profiling of GIs in model organisms, particularly in the budding yeast *Saccharomyces cerevisiae*. The most comprehensive large-scale study on GIs in yeast was conducted by high-throughput *synthetic genetic array (SGA)* analysis and enabled the construction of the first pairwise GI map, which includes almost all essential and non-essential genes of the yeast genome [19]. These studies have fundamentally advanced our understanding of GIs in various aspects, such as the characteristic properties of GI networks and their topology, and how information on gene and protein function can be inferred from GI mapping, as well as the evolution and impact of synergistic gene function on the robustness of biological systems [20–23].

Similar to protein interactions (PIs), GIs are not evenly distributed but show characteristic properties of so-called small-world networks with high local connectivity and small characteristic path lengths [24]. While most genes exhibit few interactions, few genes show multiple interactions and therefore referred to as 'hub-genes'. Hub-genes, such as the chaperone heat shock protein 90 (Hsp90), are associated with pleiotropic function and are highly conserved during evolution [24, 25].
Due to the high diversity of GI networks, interpretation of data, understanding the biological significance and inference of novel information can be challenging. A useful approach to derive information is to organize the nodes of GI networks in modules that share coherent properties [24, 26, 27]. Within GI networks, GIs can occur between and within dense modules of physical interactions (protein-protein interactions (PPIs) and protein-DNA interactions (PDIs)), which are in this context referred to as a 'pathway'. However, depending on the abstraction level these modules can correspond to biological processes, pathways or protein complexes [24, 26–28]. GIs between genes that encode proteins functioning in the same pathway or complex built within-pathway module (WPM) in the global GI network (Figure 1.2 A). For example, if a protein complex consists only of proteins that are essential for its function, disruption of any

gene encoding those proteins will lead to dysfunction of the complex, while a second gene loss will have no further impact. This case constitutes a positive (masking) GI [9, 24, 29]. Negative GIs, on the other hand often bridge two distinct but parallel compensatory or complementary pathways that contribute to the same function and occur in so-called between-pathway modules (BPMs) (Figure 1.2 A). While distinguishing between positive and negative GIs can be an indication of BPM and WPM, a global analysis showed that positive and negative GIs can connect genes between and within complexes or pathways [19]. Interestingly, it was observed that BPMs and WPMs are connected almost exclusively by either positive or negative GIs, a phenomenon referred to as monochromaticity in GI networks [24, 28, 30] (Figure 1.2 A). An example for the monochromatic organization of WPMs and BPMs can be found in GIs associated with the 19S proteasome. The genes that encode the essential 19S proteasome subunits are connected to each other by exclusively negative WPM interactions. In addition, the same genes are linked to anaphase promoting complex (APC)-associated genes by exclusively negative BPM interactions and to the translocon-associated protein complex (TRAP) only by exclusively positive BPM interactions [19].

Moreover, characteristic GI profiles can be used to predict previously unknown gene function [24]. The GI profile of any given gene comprises the complete collection of all its positive and negative GIs. Genes associated with similar biological processes, or genes whose products function in a mutual pathway or complex, share similar GIs (Figure 1.2 B). Thus, various clustering methods that arrange a GI matrix according to the similarity of GI profiles have been used to predict functions for characterized genes [28–32].

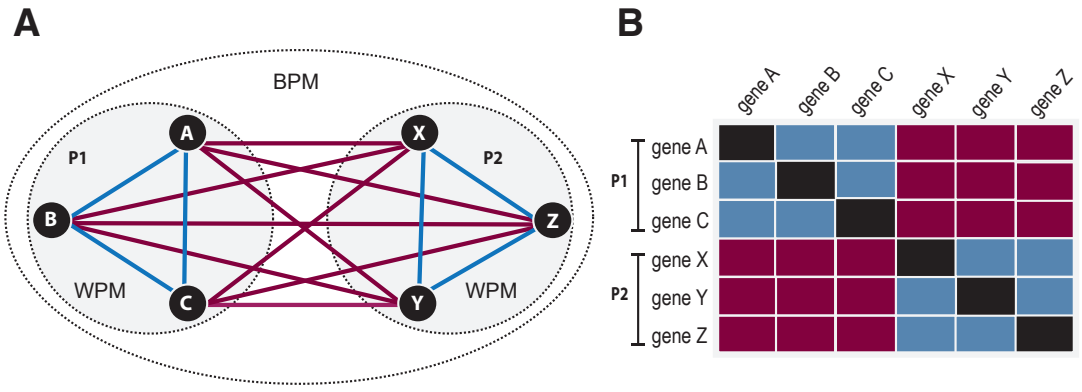

Figure 1.2: Properties of genetic interactions and their networks

Genetic interactions (GIs) are highly organized in networks consisting of interconnected dense modules with coherent characteristic properties that allow predicting gene function. A) By integrating protein interaction data, GIs can be organized in between- and within-pathway modules. Within-pathway modules (WPMs) consist of GIs between genes that correspond to the same pathway or protein complex (A-C and X-Z). In between-pathway modules (BPMs), GIs connect two parallel pathways (P1 and P2). Positive GIs are displayed in red, negative in blue. B) GI profiles can be displayed as a matrix, in which clustering is used to group genes by similarity. Modified from [11].

In summary, GI studies performed in model organisms demonstrate that GI networks are rich in information and are powerful tools to dissect and predict gene function. Although these studies have set the stage for understanding general principles and properties of GI and how information can be derived by large-scale mapping, it remains to be determined to what extent the extracted knowledge can be translated to human cells. The development of efficient GI analysis platforms for human cells will advance our understanding of human GI networks.

1.1.3 Medical implications of genetic interactions

Studying GIs in model organisms, and ultimately humans, can broaden our understanding of synergistic gene function and the robustness of biological systems on a molecular level. Beyond that, GIs are intricately implicated in the human pathology and are therefore critical for clinical research and medicine. More precisely, the investigation of human GI networks can help predicting disease susceptibility to enable prevention, early prognosis and intervention, ultimately leading to advances in drug discovery to improve disease outcomes (Figure 1.3).

The identification of disease-associated genetic biomarkers has improved early detection of predispositions to monogenic disorders, such as Huntington disease [33] and many others [34]. However, complex polygenic diseases are caused by the combined action of more than one gene and lack clear patterns of *Mendelian inheritance*. Therefore, assigning characteristic genetic signatures for diagnosis is more challenging. Disease-causing mutations often show variable *penetrance* and *expressivity* of the disease, which impedes a reliable disease onset prediction [35]. While the underlying molecular mechanisms are often unclear, there is strong evidence that GIs between disease-associated genes and genetic modifier genes within the individuals' genetic background constitute a major cause for variable penetrance and expressivity [36, 37]. For example, one study uncovered the resilience of several individuals showing no pathological symptoms despite having mutations for severe childhood disease. This observed resilience to highly penetrant Mendelian disorders can be explained by additional genetic alterations in the genome leading to genetic suppressive interactions, which abolish the harmful effects caused by the primary disease-associated mutation [38]. An example is the identification of the dominant suppressor locus *deafness recessive, nonsyndromic modifier 1 (DFNM1)*, which rescues *deafness, autosomal recessive 26 (DFNB26)* induced deafness in homozygous individuals [39]. Thus, further identification of genetic susceptibilities and genetic modifier genes to predict risk factors will advance early diagnosis of disease and their therapeutic intervention.

Moreover, GIs play a major role in how patients respond to a given treatment. In most cases, cancer patients carrying the same driver mutations exhibit variable responses to the same drug. GIs between the drug target gene and the specific genetic background of a patient are likely to affect this differential response. As such, the hypersensitivity of *breast cancer susceptibility protein (BRCA)1/2* deficient cells is abolished in patients carrying an additional

tumor protein P53 binding protein 1 (TP53BP1) mutation, resulting in resistance to *poly ADP-ribose polymerase (PARP)1/2* inhibitor treatment [40]. Detection of genetic dependencies between driver mutations and frequent genetic modifiers can help to determine biomarkers for improved drug response prediction.
Furthermore, even a single tumor can be composed of cells that harbor a broad spectrum of different genetic alterations. This cellular heterogeneity of tumors increases the risk for relapse after a first successful treatment. Alterations in genes encoding the target protein of a given drug or mutations in genes that trigger compensatory pathways, thus promoting synthetic viability or genetic suppression, can induce resistance mechanisms. Therefore, precise understanding of how GIs affect a patient's response to a given drug is crucial for effective treatment [37, 41].

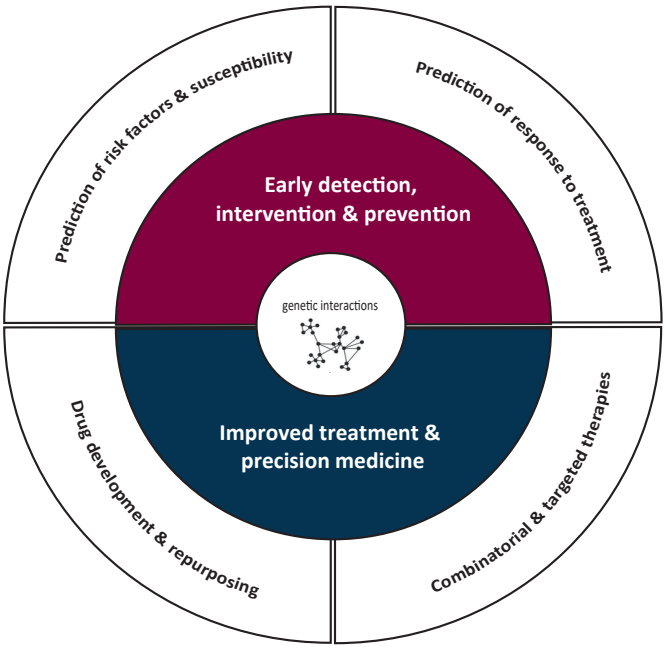

Figure 1.3: Medical implications of genetic interaction studies
Identification of GIs can advance early detection, intervention and prevention of complex diseases and enable their effective and targeted treatment. Modifier genes and genetic susceptibility signatures that are associated with disease onset can serve as biomarkers for early diagnosis and prediction of treatment response. Further, uncovering GIs that cause drug resistance or constitute cancer vulnerabilities will allow drug target discovery and development of targeted and combinatorial therapies for precision medicine.

Apart from diagnosis and prediction of risk factors and treatment response, comprehensive knowledge of underlying GIs that cause resistance to therapeutics can facilitate the rational design for combinatorial therapies and enable targeting of driver gene mutations and their corresponding resistance promoting genes. Early clinical trials showed that combinatorial therapies can help to overcome drug resistance [42–44]. For example, synergistic targeting of the PI3K-AKT and the RAS-MAPK pathway in *epidermal growth factor receptor (EGFR)*-mutated

non-small-cell lung carcinoma (NSLC) showed promise in pre-clinical trials [45, 46]. Additionally, accurate analysis of underlying GIs can reveal cancer vulnerabilities and advance targeted cancer therapy and drug discovery. Cancer is typically driven by gain-of-function mutations in oncogenes and loss-of-function mutations in tumor suppressor genes. Oncogene-driven cancers depend on the acquired activation of the oncogene. This 'oncogene addiction' allows pharmacological targeting of the corresponding oncoprotein [47]. The development of a BCR-ABL (breakpoint cluster region protein-Abelson tyrosine-protein kinase) fusion oncoprotein inhibitor for chronic myelogenous leukemia chronic myelogenous leukemia (CML) and acute lymphocytic leukemia (ALL) treatment provides a successful example for oncogene-targeted therapy [48].

Moreover, synthetic lethal interactions can be translated to novel drug targets. As mentioned before, the interaction between the breast and ovarian cancer genes *BRCA1/2* and the *PARP1* has been exploited by using a small molecule inhibitor of PARP1/2 enzymes to target the hypersensitive BRCA1/2 deficient cells. In 2018, a PARP1 inhibitor was approved by the Food and Drug Administration (FDA) for treatment of germline *BRCA*-mutated, *human epidermal Growth factor receptor 2 (HER2)*-negative metastatic breast cancer, exemplifying the potential of GIs for identification of novel drug targets [49, 50].

Over the past decades, pioneering work in model organisms, especially in yeast, has laid the ground work and provided general principles for GI screening and analysis. It was shown that these findings from model organisms are, at least to some degree regarding the network structure and topology, conserved among higher organisms [51]. It was further demonstrated that hub-genes of GI networks could function as general modifiers of hereditary diseases in humans, highlighting the importance to identify highly connected hub-genes in human genome [52–54]. Nevertheless, the human genome is by far more complex than yeast and the systematic identification and mapping of GIs in human cells is more challenging because it relies on efficient and precise technologies to introduce combinatorial genetic perturbations at a large-scale and in a high-throughput manner. The recent development of advanced gene editing technologies, most notably *RNA interference (RNAi)* [55–58] and clustered regularly interspaced short palindromic repeats and CRISPR-associated protein (CRISPR-Cas) [51], has enabled the first global systematic screening of GIs in human cell lines. This has revealed not only the impact of GIs on the phenotype, but also their strong context-dependent properties [59]. However, further improvement of functional genomic screening technologies constitutes a key challenge for advanced GI mapping in human cells.

1.2 Advances in functional genomic screening by CRISPR-Cas

1.2.1 CRISPR-Cas allows precise genome editing in mammalian cells

Since its discovery, the CRISPR-Cas technology has become the method of choice for editing, cutting and modifying the genome of cells and organisms [60]. Due to their high specificity, great versatility and practicability, CRISPR-Cas tools have advanced the field of genome editing and virtually replaced previous DNA editing technologies, such as transcription activator-like effector nucleases (TALENs), zinc-finger nucleases (ZNFs), and RNAi [61–63]. Most notably, it has revolutionized the field of large-scale functional genomic screening in mammalian cells.

Naturally, CRISPR systems exist in prokaryotes as part of their adaptive immune system, which confers resistance against bacteriophages by destroying foreign genetic material [64]. As of now, various CRISPR systems have been discovered [65]. The type II CRISPR-Cas system with its CRISPR-associated protein 9 (Cas9), derived from *Streptococcus pyogenes* (*S. pyogenes*), was the first to be engineered and adapted for biotechnological purpose [66, 67]. CRISPR-Cas9 systems and alternatives, such as the CRISPR-Cas12 (also known as Cpf1) system, have become invaluable tools in almost every aspect of biological research.
The engineered CRISPR-Cas editing system requires two main components: A Cas protein, which naturally possesses a nuclease activity for DNA cleavage and a guide RNA (gRNA) for target specificity (Figure 1.4 A). The target sequence specificity is mediated by the gRNA via complementary base pairing with the target DNA region, which is also referred to as the protospacer sequence. For CRISPR systems that employ a Cas9 nuclease, the gRNA is composed of a 18-20 nucleotide CRISPR RNA (crRNA), which is specific for the target gene of interest and of a trans-activating CRISPR RNA (tracrRNA), which forms a stem-loop structure and provides a binding scaffold for the Cas9 nuclease to form a ribonucleoprotein (RNP) [68]. In the engineered CRISPR system, the crRNA and tracrRNA are fused together to one single, fully functional, synthetic RNA molecule to improve efficiency and facilitate biotechnological application [68].
Ceavage of the target DNA by the RuvC and HNH nuclease domains of Cas9 requires a particular protospacer adjacent motif (PAM), which is directly following the 3'end of the protospacer sequence to induce a double strand break (DSB) [69, 70]. Different Cas variants require different PAM sequences.For instance, *S. pyogenes* Cas9 requires an 5'-NGG-3' PAM [71], while Cpf1 only exhibits nuclease activity in the presence of a 5'-TTTV-3' [72] or 5'-YTN-3' PAM [73].
In mammalian cells, the cleaved DNA is repaired by two main cellular DNA repair pathways: the non-homologous end joining (NHEJ) or the homology directed repair (HDR) pathway (Figure 1.4 B). Re-ligation of two DNA ends by the NHEJ pathway is fast, efficient and, in contrast to HDR, requires no template DNA strand. However, NHEJ is error-prone and frequently introduces insertion or deletion (Indel) mutations. These can lead to frame shifts, which are likely to disrupt gene expression [66]. Therefore, NHEJ is the preferred repair pathway when

gene knockouts are desired. HDR is the second, naturally occurring DNA repair pathway. It is activated upon DNA damage and promotes error-free DNA repair if a repair template DNA strand is available [74]. HDR can be exploited to generate larger genetic insertions at a defined genomic locus, such as for gene knock-ins or gene tagging. To this end, the sequence that is to be introduced is provided with homology arms corresponding to the cleaved DNA locus and introduced into the cell together with the CRISPR-Cas system. Then, the exogenous DNA is integrated by the cell's HDR machinery at the target site [67, 75].

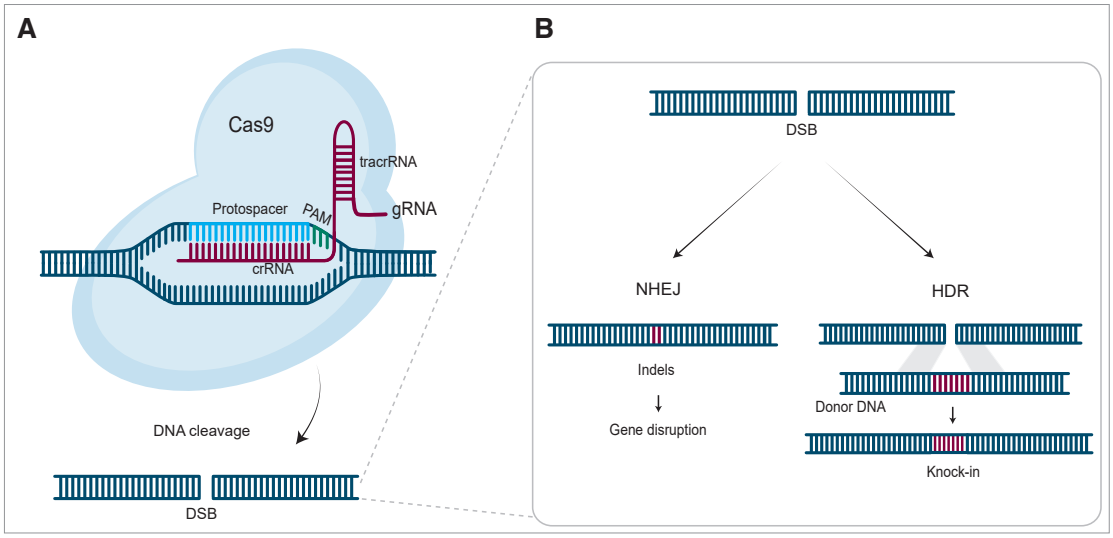

Figure 1.4: Mechanisms of CRIPSR-Cas9 genome editing in mammalian cells
A) CRISPR-Cas genome editing requires two components: A Cas nuclease for DNA cleavage and a guide RNA (gRNA) that mediates target specificity. Most commonly, Cas9 of *S. pyogenes* is used and directed to a specific protospacer sequence of the genomic DNA by the gRNA. In the engineered CRISPR-Cas9 system, CRISPR RNA (crRNA) and trans-activating CRISPR RNA (tracrRNA) are fused to a single synthetic gRNA. In the presence of the protospacer adjacent motif (PAM), sequence specific binding of the crRNA to a complementary protospacer sequence induces DNA cleavage by the Cas9-gRNA ribonucleoprotein. B) The induced double strand break (DSB) can be repaired by two cell endogenous DNA repair pathways. The frequent but error-prone non-homologous end joining (NHEJ) occurs in the absence of a repair template and frequently generates insertion or deletion (Indel) mutations, which can lead to frame shifts and gene disruption. Thus, NHEJ is the desired repair pathway for CRISPR genome editing. The homology directed repair (HDR) pathway is the basis for CRISPR-mediated knock-ins or gene tagging. In the presence of an exogenous donor DNA that is flanked by homology arms, the HDR pathway leads to introduction of the exogenous DNA sequence into the host genome at the DSB site.

For genome editing, the CRISPR-system can be introduced as a dual-component system that includes the gRNA and Cas nuclease, both encoded on a single vector, into the target cell. Alternatively, the gRNA can be introduced separately into cells that already express the Cas nuclease. Transfer methods include transfection, lentiviral or adeno-associated viruses (AAV) mediated transduction and electroporation [76].

DNA cleavage by Cas nucleases is only one way to use the CRISPR technology for genome

editing. There are engineered Cas variants for versatile forms of genetic manipulation, such as the dead CRISPR-associated protein (dCas), in which both catalytic centers are inactivated by mutation [77]. While the DNA cleavage activity of dCas is abolished, the RNA-guided DNA target recognition and binding capability is maintained and can be exploited for transcriptional regulation. For example for *CRISPR inhibition (CRISPRi)* and *CRISPR activation (CRISPRa)* employ effector domains that are fused to the dCas nuclease [78–82]. Similarly, tethering of dCas to fluorescent proteins or specific enzymes enables investigation of chromatin structures [83], base editing [84–87], and epigenetic remodeling [88–90].
The crRNA is variable and, most importantly, programmable to target any desired genetic sequence, solely restricted by the requirement of the PAM. While this constituted a challenge for first CRISPR applications, now more than 20 available Cas variants from different species and their differing PAMs have expanded the range of possible target sites [91]. Additional Cas variants have been engineered with more flexible PAM requirements [92, 93]. These different PAM patterns occur frequently in the genome of all organisms. Thus, practically any site of a host genome can be targeted by selecting a protospacer sequence immediately before a PAM and designing a complementary gRNA [91]. For example, in the human genome, all pathogenic *single-nucleotide polymorphisms (SNPs)* that are documented in the ClinVar database provide an average of almost 30 target sites for CRISPR-based editing by at least one Cas nuclease [91, 94].

The easy delivery, versatility and programmability of the CRISPR-systems have proven to be particularly useful for editing and analyzing not only one specific target gene but for scaling-up experiments to simultaneously test a broad range of target genes in a single batch by functional genomic screens with pooled CRISPR-Cas gRNA libraries.

1.2.2 Functional genomic screening with pooled CRISPR libraries

In the past decades, the development of sequencing technologies has uncovered the extensive volume and diversity of genetic information and fuelled the need for advanced high-throughput technologies and large-scale screening approaches for parallel functional analysis of a myriad of genes. Several pooled genomic screens have applied RNAi to study gene function on a genome-wide scale in mammalian cells [95–98]. While RNAi generates gene knock-downs to reduce gene expression, CRISPR-Cas enables complete depletion of target genes and shows superior target specificity compared to RNAi [62, 99]. The easy programmability and modularity of the CRISPR-Cas system and the pre-existing protocols for RNAi-based screening enabled a rapid adoption and adjustment of the CRISPR-Cas system for pooled functional genomic screening [100].

In contrast to arrayed screening conditions, in which one single genotype is tested per ex-

periment, pooled CRISPR-Cas screening represents an experimental approach for testing the effects of multiple different genetic alterations in parallel, in one single experiment. Pooled screening is based on three components: A genetic perturbation platform, a model system and an assay to screen for phenotypic changes (Figure 1.5A-C).

The genetic perturbation platform allows to simultaneously inducing diverse gene disruptions of a multitude of different target genes. This is provided by so-called pooled CRISPR gRNA libraries, or abbreviated 'CRISPR libraries', which consist of thousands to hundreds of thousands of transfer vectors each encoding one gRNA for a specific target gene. Custom-designed CRISPR libraries are first designed in silico by selecting gRNAs that target the genomic regions of interest. To this end, several computational tools have been developed to score and select gRNA target sites in the genome of most sequenced model organisms. These tools follow previously identified design rules, and employ selection algorithms to identify gRNA sequences with high on-target efficiency and minimized *off-target effects* [101–108]. After gRNA selection, the CRISPR library is constructed by pooled cloning of synthesized oligonucleotides that encode diverse gRNAs into a transfer vector, such as a lentiviral plasmid (Figure 1.5 A). Focused CRISPR libraries can include sub-groups of target genes, for example genes corresponding to a specific pathway, cellular process or protein family, while genome-wide pooled CRISPR libraries are designed to target any possible coding [102, 109–111], or non-coding region of a reference genome [112]. A variety of pre-made CRISPR libraries are available for research purpose, such as the human genome-wide 'Brunello' or 'TKOv3' libraries [102, 113].

The second component of a pooled CRISPR screen is a suitable model system. Theoretically, any cell type or even animal model can be used in a CRISPR screen. However, maintaining sufficient *library coverage*, which is the abundance of any particular gRNA within the complete population, during all steps of the screen is one of the most critical parameters for robust results [91, 114]. This usually requires large amounts of cells or animals, respectively. Thus, animals and cell types that are difficult to expand, such as primary cells, are less suited for large-scale screening. Moreover, generating primary cells that stably express Cas9 is challenging. Therefore, tumor-derived cell lines are often used for mammalian screens because of their easy scalability and cultivation [76]. The CRISPR library is transduced into the selected cell line that stably expresses Cas9 (Figure 1.5 B). Transduction at a low *multiplicity of infection (MOI)* ensures the generation of a heterogeneous mutant cell population, in which the majority of cells carries only one specific genetic alteration in a specific gene. Since lentiviral transduction results in stable integration of the gRNA sequence into the target cell's genome, the gRNA sequence also functions as a unique identifier barcode that directly links each mutant cell phenotype to a specific genetic alteration.

After antibiotic selection of transduced cells follows the third part of the CRISPR screen: a screening assay that allows to measure resulting phenotypic changes, while keeping the linked information to the corresponding genetic cause [114] (Figure 1.5 C). Pooled proliferation screens are the most prominent type of screening assays. In the simplest form of screening, the ability to sustain growth over time constitutes the only selection pressure. Alternatively, a

drug treatment can be applied to screen for resistance or susceptibility. Proliferation screens can be generally divided into positive (enrichment) and negative (depletion) screens, which can be performed with or without applying additional selection pressure.

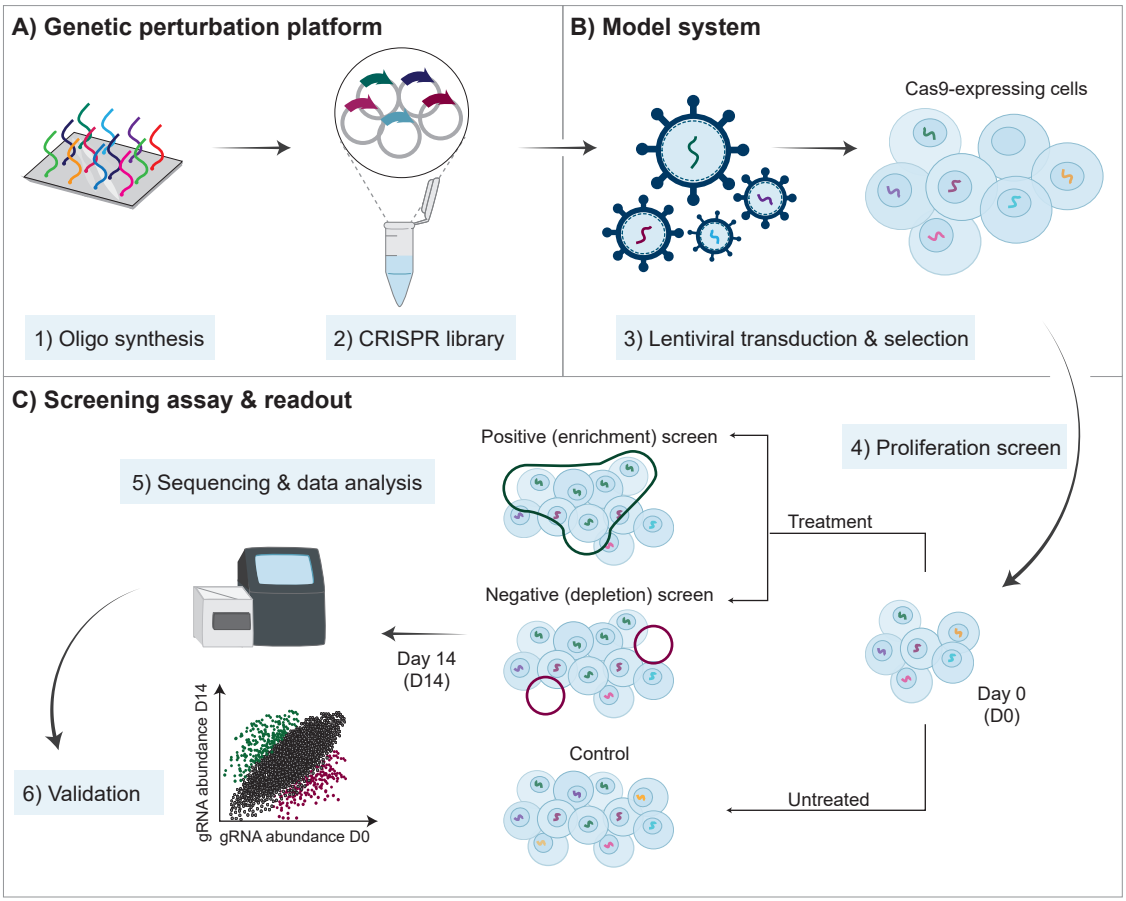

Figure 1.5: Pooled functional genomic screening with CRISPR-Cas
Schematic of a pooled proliferation CRISPR-Cas screening workflow. A pooled CRISPR-Cas screen is based on three components: A) The CRISPR library is generated by cloning of synthesized oligonucleotides (oligos) into lentiviral transfer vectors and provides a genetic perturbation platform for inducing a multitude of different mutations. B) A suitable model cell line is selected and transduced with the lentiviral CRISPR library. Afterwards, transduced cells are selected. C) A screening assay is applied to measure phenotypic changes induced by the gene editing events. Optionally, a drug treatment can be applied. The differential proliferation of heterogeneous mutant cells leads to specific enriched or depleted gRNAs. Since lentiviral transduction results in stable integration of the gRNA sequence within the target cell genome, the gRNA also serves as a unique barcode. At the end of the screen, genomic DNA of the cell population is extracted and the gRNA abundance is determined by sequencing and compared to the initial abundance. Lastly, statistical analysis of the data identifies hits for further validation.

In negative proliferation screens, cells with mutations that decrease cell fitness are depleted or completely lost and therefore identified as drop-outs. This type of screen is powerful for explor-

ing gene essentiality or cancer vulnerabilities to drug treatment [109, 115–117]. Conversely, mutant cells with increased cell proliferation are enriched in positive screens, which typically include drug treatments to identify genes that promote drug resistance [118–120]. In practice, a single proliferation screen can simultaneously identify both, drop-outs and enriched genes. For example, a genome-wide proliferation screen in a cancer cell line can uncover depleted oncogenes and enriched tumor suppressor genes. Flow cytometry-based screening assays provide an alternative to proliferation screens. Here, mutant cells containing reporter constructs can be separated according to their reporter-phenotype, for example by FACS [121–124].
The depletion or enrichment of cells that carry a specific mutation can be determined by measuring the abundance of each gRNA before and after phenotypic selection. This is done by extracting genomic DNA of a representative sample of the cell population and subsequent amplification of the stably integrated lentiviral cassette polymerase chain reaction (PCR). and measuring the gRNA abundance by next-generation sequencing (NGS). Afterwards, gRNA abundances of control and screening samples are compared with each other to identify enriched and depleted genes (Figure 1.5 C).
Several computational tools, statistical packages and pipelines have been developed specifically for pooled screening data analysis [125, 126]. They account for gRNA performance variability, read count normalization, mean-variance modeling, and gRNA and gene ranking, such as MAGeCK [127], CRISPRcloud [128], or PinAPL-Py [129].

Thus far, focused and genome-wide CRISPR libraries have been screened in various mammalian cell lines and have revealed previously unknown gene function of genes involved in cellular fitness and survival [130–134], viral susceptibility [124, 135–137], drug resistance and sensitivity [138–140], cancer vulnerabilities [141–143] and even more [114, 144]. The success of monogenic CRISPR screens, in which every cell receives a single gRNA, has fuelled efforts to adapt pooled CRISPR screening to investigate combinatorial genetic alterations to advance GI studies in mammalian cells. This has led to the development of multiplex CRISPR platforms.

1.3 Multiplex CRISPR libraries for genetic interaction screens

1.3.1 Multiplex CRISPR-Cas systems enable multi-target genome editing

CRISPR-Cas multiplexing describes the simultaneous expression of multiple gRNAs to induce editing of multiple genetic loci in a single cell at the same time [145–147]. Different methods have been established for introducing, expressing, and processing arrays of multiple gRNAs in mammalian cells (Figure 1.6).

The simplest approach for multiplex genome editing is co-transfection of *in vitro* preformed RNPs that consist of purified Cas9 proteins assembled with distinct chemically synthesized gRNAs (Figure 1.6 A). Advantages of using preassembled Cas9-gRNA-RNPs include the fast DNA-free gene editing, the quick degradation in the target cells after the editing event. Moreover, the gRNA molecules do not need to compete for limited Cas9 proteins within the cells [148, 149].
For applications that require stable expression of the CRISPR-Cas system, such as pooled screens, a common method is to express gRNAs from individual promoters (Figure 1.6 B). RNA polymerase III type 3 promoters, such as U6 or 7SK, have been employed for this type of multiplex editing in mammalian cells [116, 150, 151]. While plasmids are available to simultaneously express two gRNAs [116, 150–152], expressing more than two gRNAs can be a concern when using multiple individual promoters due to differential RNA expression levels of the promoters and because of potential size limitations, cloning efficiency and possible recombination during lentiviral packaging [153, 154].
A different approach for multiplex gene editing utilizes Cas12 instead of Cas9 (Figure 1.6 C). In contrast to Cas9, the CRISPR-Cas12 system requires no tracrRNA for nuclease activity and specificity. Moreover, Cas12 can process arrays of up to 25 pre-crRNAs that are transcribed from a single transcript into mature single crRNAs [72, 155]. The smaller size and pre-crRNA processing activity of the CRISPR-Cpf1 system have enabled successful application in human cells [156]. Comparative studies showed that the engineered variants of Cas9 and Cpf1 are highly complementary in terms of off-target effects and specificity. Moreover, Cas9 and Cpf1 can be used in an orthogonal manner for multiplex applications [157]. Thus, Cas9 and Cpf1 enzymes built a versatile toolbox for gene editing [158].
Similar to its natural form in bacteria, several multiplex CRISPR-Cas9 systems have been developed to express multiple gRNAs from a single polycistronic transcript (Figure 1.6 D-F).
One system makes use of the *Pseudomonas aeruginosa* endoribonuclease Csy4, another Cas family endonuclease [159]. Multiple gRNAs are encoded upstream of a single promoter each being flanked by Csy4 recognition sites (Figure 1.6 D). Upon co-expression of Csy4, the arrayed transcript is cleaved and processed into distinct mature gRNAs [160–162]. While Csy4-based gRNA processing is beneficial for expression of numerous gRNAs, the need to co-express Csy4 can be undesirable for some applications [162].
Processing of gRNAs from a single transcript can also be achieved by self-cleaving ribozymes,

which are RNA molecules that exhibit nuclease activity to promote RNA splicing [163–165]. To generate distinct mature gRNAs, an array of gRNAs is encoded upstream of a single promoter and flanked by self-cleaving ribozyme sequences, such as hammerhead or hepatitis delta virus (HDV) ribozyme sequences (Figure 1.6 E).

A third approach with polycistronic gRNA expression exploits the cell endogenous transferRNA (tRNA) processing machinery [166]. Here, multiple gRNAs are separated by pre-tRNA genes that are then recognized and cleaved by the endogenous ribonucleases (RNases) P and Z (Figure 1.6 F). Due to the high evolutionary conservation of the tRNA processing machinery, this approach is functional in a wide range of organisms, including human cells [167–170]. The possibility to express and process multiple gRNAs in an arrayed format can facilitate cloning of the CRISPR expression vector, when the gRNA array can be integrated into the vector as a single insert. However, repetitive sequences that often occur in long gRNA arrays challenge their chemical synthesis [171].

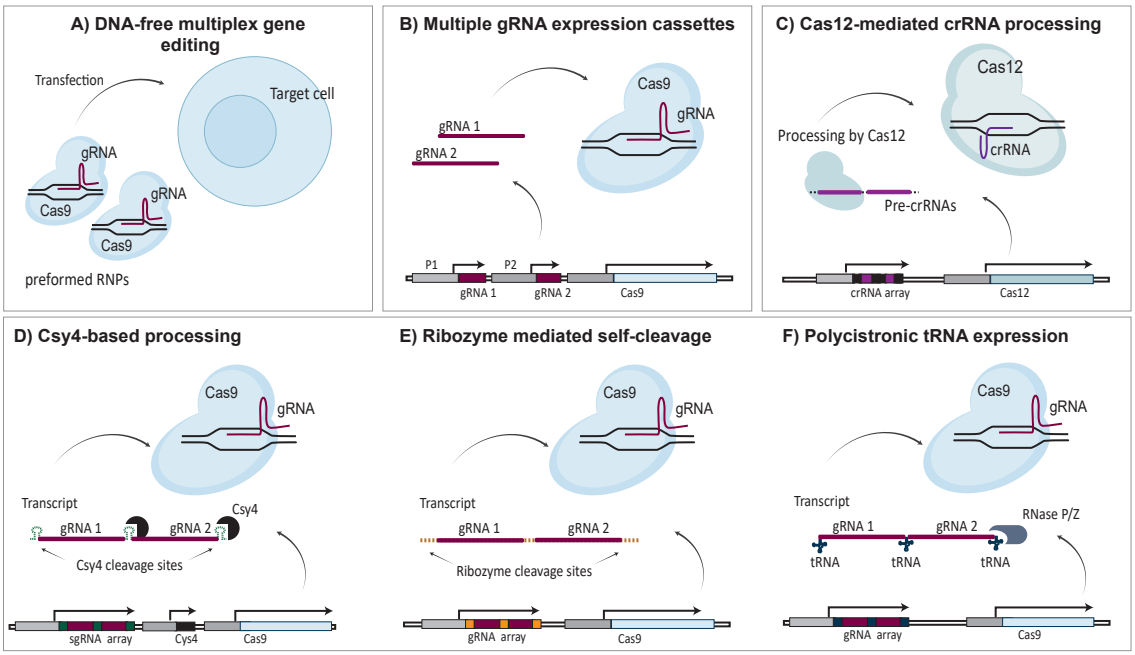

Figure 1.6: Strategies for multiplex gRNA expression in mammalian cells
Different methods have been developed for expressing and processing multiple gRNAs in mammalian cells. A) A DNA-free method is based on transfection of multiple preformed ribonucleoprotein (RNP) that consist of Cas9 proteins loaded with distinct gRNAs. B) Most commonly, two distinct gRNAs are encoded under the control of individual promoters (P1, P2) and separately expressed. C) In contrast to Cas9, Cas12 requires no tracrRNAs and can process an array of multiple short pre-crRNAs into mature crRNAs. D-F) Similar to Cas12-crRNA arrays, there are engineered CRISPR-Cas9 systems that are based on polycistronic expression of multiple gRNAs from a single transcript. D) Co-expression with a Csy4 endonuclease allows processing of gRNAs that are flanked by Csy4 recognition sites from a polycistronic transcript into mature gRNAs. E) Arrayed gRNAs can be flanked by self-cleaving ribozyme sequences to promote processing. F) Endogenous RNases P and Z can be exploited to mediate processing of arrayed pre-gRNAs into mature gRNAs. Adapted from [146].

The development of these CRISPR-Cas multiplex platforms has met the needs of a broad range of different applications in biotechnological research, including genome, strain, and metabolic engineering, multi-input bio-sensing, multi-event recording in living cells and CRISPR-based genetic circuits [147]. Most importantly, just as for monogenic pooled CRISPR screens, the CRISPR-Cas multiplex technology can be scaled-up to enable massive parallel screening for GIs within a myriad of target genes to advance GI mapping in human cells.

1.3.2 Challenges in multiplex CRISPR screening

1.3.2.1 Multiplex CRISPR screening is limited by the required experimental scale

Analogous to monogenic pooled CRISPR-Cas screens, the multiplex CRISPR-Cas system can be applied in mammalian cells in a pooled format to investigate the synergistic effects of pairwise gene depletion at a large scale (Figure 1.7 top panel). To this end, pooled multiplex CRISPR libraries are generated that consist of hundreds of thousands of plasmids each encoding one specific gRNA pair to simultaneously edit two genes in a single cell. The pooled multiplex CRISPR library is then applied to a cell population via retro- or lentiviral transduction. Subsequently, the transduced cells are screened with a desired assay and read-out. After the assay, genomic DNA is extracted and processed for sequencing to identify positive and negative GIs by computational data analysis.
First pooled multiplex CRISPR-Cas screens have been applied in mammalian cells to explore GIs within defined subsets of genes, such as known epigenetic regulators [172], drug targets [151], genes involved in metabolic [173] or cellular signaling pathways [174, 175], and genes implicated in cancer [176, 177]. With at least 20,000 protein-coding genes in the human genome, a genome-wide pairwise screen required testing of at least 400 million dual gene combinations [51, 178, 179]. Thus, a complete genome-wide combinatorial CRISPR screen remains a technically unattainable goal. However, a recent combinatorial screen comprising more than 220,000 gene pairs representing diverse cellular processes and major intracellular compartments [51] demonstrated that, similar to the findings from yeast studies, GIs in the human genome are highly organized into networks with sub-modules of genes belonging to the same processes, pathways and complexes [51]. This study proved the feasibility of large-scale multiplex CRISPR screens on a global level in mammalian cells and highlighted the volume of novel information that can be obtained from combinatorial studies.

Despite this recent progress in multiplex CRISPR screening, for the vast majority of researchers multiplex CRISPR screens in human systems have been hampered by two main technical limitations: First, the sheer diversity and required scale of the screens and the subsequent sample processing and second, the inefficient and time-consuming methods to generate custom-designed multiplex CRISPR libraries.

Figure 1.7 illustrates the practical steps of a pooled CRISPR screen and the experimental scale that is required for each step of a typical monogenic screen that targets one gene per cell (A), and a multiplex CRISPR screen targeting a gene pair (B).

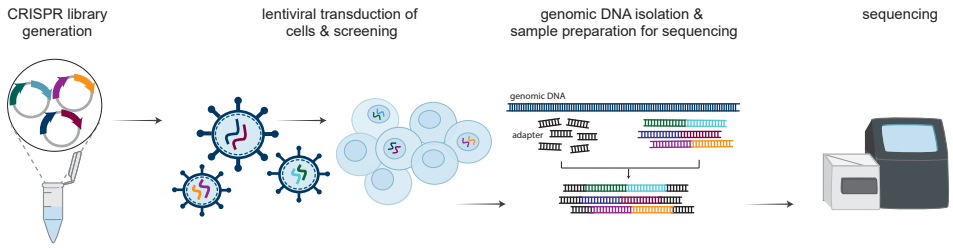

1) library diversity	2) screening coverage	3) sample preparation	4) sequencing
A) monogenic screen			
100 target genes x 4 gRNAs = 400 plasmids	400 plasmids x 500 cov. / 0.5 MOI = 400 x 10^3 cells (T0) 400 plasmids x 500 cov. = 200 x 10^3 cells maintained	200 x 10^3 cells x 6,6 pg DNA = 1.32 µg genomic DNA	400 plasmids x 1,000 (sequencing cov.) = 400 x 10^3 reads
B) multiplex screen			
100 target genes x 4 gRNAs x 100 target genes x 4 gRNAs = 160 x 10^3 plasmids	160 x 10^3 plasmids x 500 cov. / 0.5 MOI = 160 x 10^6 cells (T0) 160 x 10^3 plasmids x 500 cov. = 80 x 10^6 cells maintained	80 x 10^6 cells x 6,6 pg DNA = 528 µg genomic DNA	160 x 10^3 plasmids x 1,000 (sequencing cov.) = 160 x 10^6 reads

Figure 1.7: Experimental scale of monogenic and multiplex pooled CRISPR screens
In order to obtain results from pooled monogenic (A) or multiplex (B) CRISPR screens with statistical confidence, the CRISPR library diversity must be sufficiently covered in all steps of the screen to avoid random loss of any gRNAs due to bottleneck effects. 1) The number of target genes and gRNAs per target gene determine the library diversity. A monogenic CRISPR library with 100 target genes and 4 gRNAs per genes has a library diversity of 400 plasmids. Compared to a monogenic CRISPR screens, the library diversity of a combinatorial library with the same number of target genes is squared. 2) To maintain the library diversity during the screen, a screening coverage between 500- to 1000-fold is recommended. For a monogenic CRISPR library with 100 target genes and 4 gRNAs per genes, a screening coverage of 500-fold corresponds to 400x10^3 cells that need to be transduced at an MOI of 0.5, and 200x10^3 cells that need to be maintained during the screen. For a multiplex library, 160x10^6 cells are required for lentiviral transduction and 80x10^6 cells for maintenance during the screen to provide a 500-fold library coverage. 3) To prepare sequencing samples after the screen, a sufficient amount of genomic DNA must be isolated and processed by PCR to generate a coverage-based sequencing library. The required amount of genomic DNA corresponds to the number of transduced cells with an average DNA content of 6.6 pg per cell. 4) The sequencing depth indicates the library coverage during sequencing. Typically, 1000 reads are obtained for each gRNA or gRNA combination of the library.

Library diversity

Both, monogenic and multiplex CRISPR screens require the generation of pooled CRISPR libraries. The number of desired target genes determines the *library diversity* (also library com-

plexity or size), which is the total number of distinct plasmids that harbor one specific gRNA or one specific gRNA pair for multiplex libraries, respectively (Figure 1.7 (1)). Most commonly, three to ten gRNAs are used to target a given gene, because the number of gRNAs per target gene has a substantial impact on the statistical robustness of results [102, 127, 180, 181]. For a hypothetical single gene-targeting CRISPR library designed to target 100 genes with four gRNAs per target gene, the *library diversity* is 400 (Figure 1.7 A). A multiplex CRISPR library with the same number of target genes, that is designed to target all possible combinations of these genes, has a *library diversity* of $160x10^3$ plasmids (Figure 1.7 B). Since the *library diversity* determines the scale of all subsequent experimental steps, it must be carefully considered before designing a library and planning an experiment.

Library coverage

Hit-calling of pooled CRISPR screens is based on detecting changes in gRNA abundance in the course of the screen that are due to phenotypic changes caused by CRISPR gene editing induced mutations. Therefore, it is crucial that the CRISPR *library diversity* is sufficiently represented during all steps of the screen. In other words, each gRNA, or gRNA combination, of the library must be covered by a sufficient number of cells. The average abundance of each gRNA, or gRNA combination, during the screen, is indicated as the *library coverage*. An insufficient *library coverage* during any practical step of the screen can result in random loss of gRNAs independent of the applied phenotypic selection thereby leading to skewed results. Particularly underrepresented gRNAs with low abundance can lead to false positive hits, due to depletion by a sudden bottleneck effect [76, 114]. While ensuring sufficient coverage is critical for reproducible and data quality, it also significantly affects the required experimental size (Figure 1.7 (2)): For maintaining the *library diversity* during lentiviral transduction of the CRISPR library into target cells and during cell passaging, a *library coverage* of 500 to 1000-fold of the total library diversity is recommended [76, 114]. Consequently, a monogenic CRISPR screen with 100 target genes starts with an initial population of $400x10^3$ cells to provide a 500-fold coverage. The number of required cells drastically increases for multiplex CRISPR screens. Here, for a 500-fold coverage and the same number of target genes in combination, $160x10^6$ cells need to be transduced at an *MOI* of 0.5 and still $80x10^6$ cells must be maintained during the course of the screen (Figure 1.7 (2)). For adherent cell lines, such as hTERT RPE-1 cells, $160x10^6$ cells corresponds to about 650 cell culture flasks with $250x10^3$ cells per flask. Considering this large amount of cell culture work for only one screen, excluding replicates and controls, it becomes evident that library diversity and coverage can set practical limitations in terms of cell culture handling capacity and resources, such as lab equipment, incubator space and growth media. Moreover, some model systems, such as primary cell lines or organoids, cannot be expanded to such high numbers.

Further, the *library diversity* must be maintained during all sample processing steps subsequent to the screen. This includes extraction of genomic DNA of a representative cell population and amplification of the integrated gRNA sequences by PCR to provide the adaptor sequences

that are required for sequencing. This might require to perform hundreds of PCR reactions. For example, processing of 528 µg genomic DNA requires 132 PCR reactions each with 4 µg DNA and subsequent purification of correct PCR products (Figure1.7 (3)).
The so-called sequencing depth indicates the number of average sequencing reads per gRNA, or gRNA combination, respectively. Typically, a 1000-fold sequencing depth is sought, which corresponds to 1000 reads for each gRNA or gRNA combination of the library. Sequencing of multiplex libraries must secure that the information of two combined gRNAs remains linked. Therefore, it requires either one long sequencing read over both gRNAs or a paired-end sequencing strategy. Both approaches are more expensive compared to sequencing single-gRNA libraries. When screening multiplex libraries of high diversity, sequencing of the plasmid library, replicate samples and controls can become expensive [76, 114] (Figure 1.7 (4)).

Conclusively, pooled screens, in particular multiplex CRISPR screens, require balancing a reasonable high *library coverage* in all experimental steps to obtain reproducible results with statistical confidence but also to keep the experimental scale executable and resource efficient.
Published guidelines for planning CRISPR screens provide recommendations for *library coverages* that range from a 200- to 1000-fold. These recommendations are provided based on common practice and lack precise specification based on supporting experimental data [76, 114]. However, the question, whether a screen needs to be performed with a 200- or 1000-fold coverage will decide about the feasibility.

Only recently two studies addressed this problem and provide computational analyses and tools for predicting the minimally required coverage when planning a screen [182, 183]. Most importantly, the work by Imkeller et al., (2020) identifies the *library distribution* as "the limiting parameter that dictates the minimal size of a screening experiment" [182]. However, this has not yet been experimentally tested, and it remains to be analyzed to what degree the library distribution influences the experimental scale and hit-calling confidence.

Library distribution

In an ideal pooled CRISPR library, each plasmid encoding one specific gRNA, or one gRNA combination, is equally abundant. In reality however, CRISPR libraries exhibit a variance of plasmid abundance with low abundant gRNAs that are underrepresented compared to the mean gRNA sequence abundance, and highly abundant gRNAs, compared to the mean gRNA sequence abundance. A measure to specify the uniformity of the *library distribution* is the distribution skew, the ratio between 90th and 10th percentiles of highest and lowest abundant gRNAs [182], which is elsewhere referred to as 'skew ratio' or 'distribution width' [182, 184]. In the above mentioned study, Imkeller et al. simulate the impact of the *library distribution* on the robustness of screen results, such as the reproducibility between replicates (Figure 1.8).

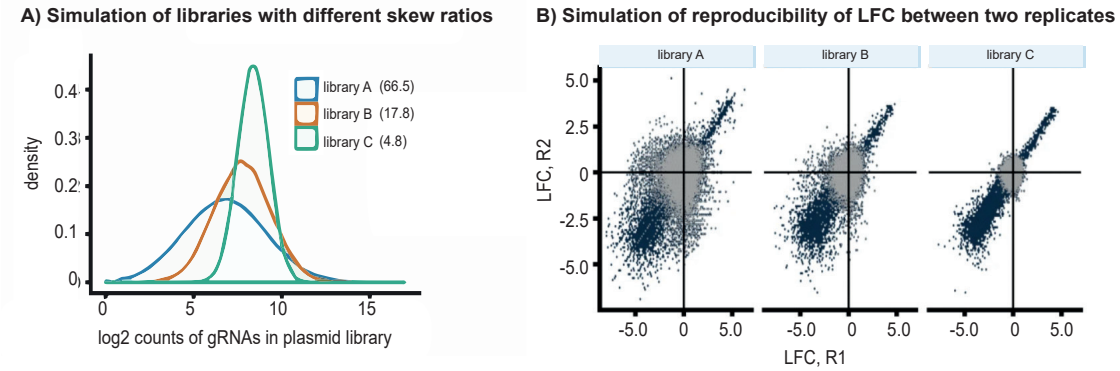

Figure 1.8: Wider library distribution width affects reproducibility.
A) Log2 count distribution of three different simulated gRNA libraries with decreasing distribution width of gRNA abundance distribution (skew ratios: lib.A 66.5; lib.B 17.8; lib.C 4.8). B) Reproducibility of log2-fold change (LFC) between two replicates (R1, R2). Simulations performed with all three libraries showed that higher library width leads to decreased reproducibility between replicates while the frequency of gRNAs with LFC <-1 increased. gRNAs without fitness effects are highlighted in gray, gRNAs with fitness effects in blue. From Imkeller et al., (2020) [182].

Based on their findings they provide indications for choosing an optimal screening coverage according to the *library distribution* width of the CRISPR plasmid library and emphasize that their computational analysis suggests that using CRISPR plasmid libraries with uniform *library distributions* allows to strongly increasing the reproducibility of a screen [182]. Additionally, by analyzing five data sets from published CRISPR libraries, they identify specific sequence properties of highly under- and over-represented gRNAs, such as poly-G-stretches or T-enriched sequences [182]. They hypothesize that the distribution bias they observed for published CRISPR libraries is a result of sequence specific effects during CRISPR library generation [182].

1.3.2.2 Current methods for multiplex CRISPR library generation

These recent findings highlight the strong impact of *library distribution* on the required experimental scale of a CRISPR screen and draw attention to the need for innovative library generation methods that result in uniformly distributed CRISPR libraries. However, current methods for library generation, especially for multiplex CRISPR libraries, are time- and effort-consuming, because they rely on sequential cloning steps that are likely to introduce a distribution bias at several steps of the protocol [147, 185]. There are two main strategies for generating multiplex CRISPR libraries for expression in mammalian (Figure 1.9).
The first approach is based on assembly of single gRNA units to an combined array in a final expression vector (Figure 1.9 A) The distinct single gRNA units can be constructed by annealing of single-stranded DNA (ssDNA) oligonucleotides that encode one specific gRNA and are provided with complementary overhangs to a specific cloning site in the expression vector. The annealed single gRNA units can then be ligated into the predigested vector.

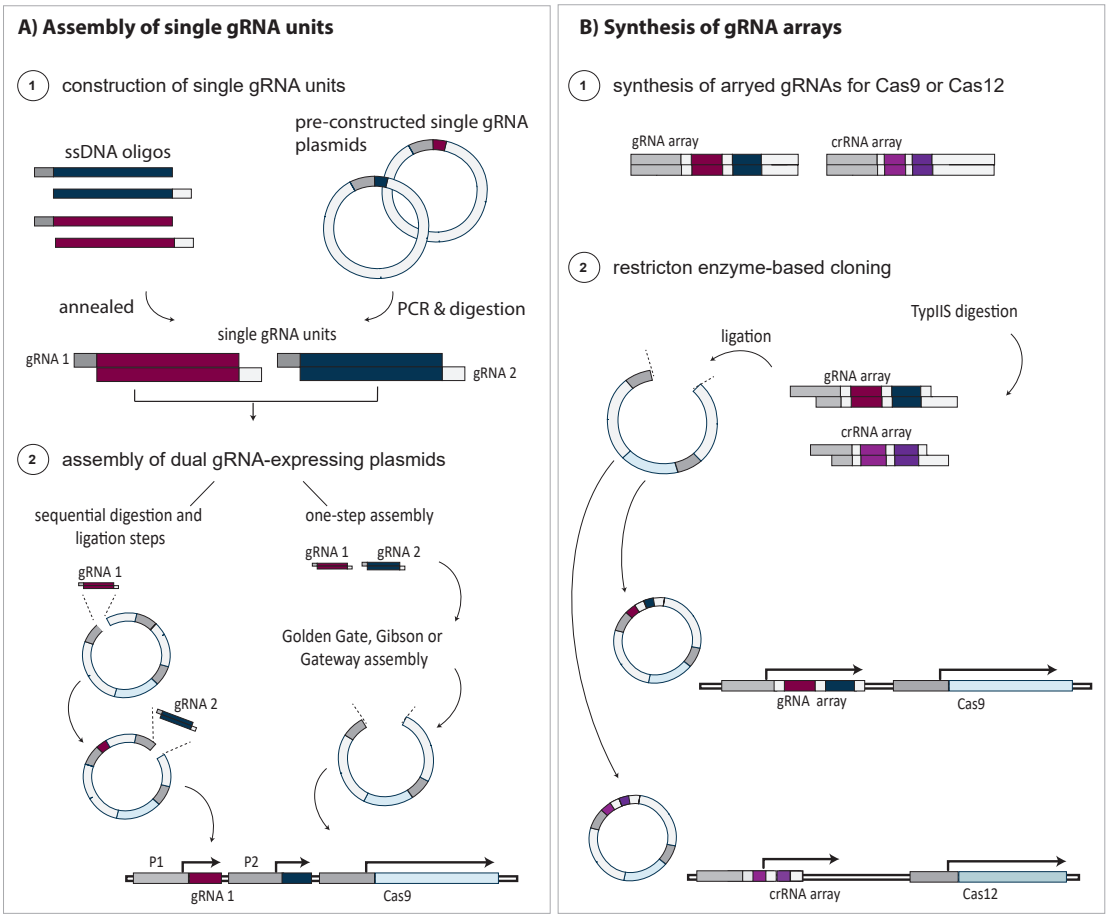

Figure 1.9: Methods for multiplex CRISPR library generation
A) Multiplex CRISPR libraries can be generated by assembly of distinct single gRNA units to a combined array in the final expression vector. Single gRNA units can be generated by annealing complementary ssDNA oligonucleotides that encode gRNAs and are provided with overhangs for restriction enzyme-based cloning into the destination vector. Alternatively, single gRNA units can be PCR-amplified from pre-constructed single gRNA libraries or by extension reactions with additional PCR amplification and subsequent assembly into the target vector by Golden Gate, Gibson or Gateway assembly. B) Alternatively, complete arrays encoding multiple gRNAs can be chemically synthesized and subsequently cloned into an expression vector.

Several plasmid-based multiplex CRISPR tool kits are available that provide expression vectors with multiple gRNA expression cassettes that harbor pre-designed Type IIS restriction enzyme recognition sites to allow cloning and expression of multiple gRNAs from individual promoters [116, 151, 172]. However, these systems require at least two iterative steps of pooled digestions and ligations with each step providing an additional source of error and bottleneck effects that can lead to random loss of gRNAs [151, 172, 186, 187]. Other methods employ Golden Gate assembly [175, 188], Gibson Assembly [176], or Gateway cloning [189] to enable integration of multiple single gRNA units into an expression vector in a single reaction. However, these methods require amplification of single gRNA units from pre-constructed single gRNA libraries by PCR [151, 188], or extension and additional PCR amplification of oligonucleotide pools

to provide them with flanking sequences, specifying the order of each single gRNA unit and allowing their assembly [175, 176]. PCR amplification is another possible source of bias that could explain the observed variance in sequence abundance of published libraries [182].
An alternative approach is based on direct chemical synthesis of a complete array of multiple gRNAs that can then be ligated into a pre-digested expression vector in a single cloning step. This has been used to generate gRNA arrays for Cas9 and Cas12 systems [155, 190] (Figure 1.9 B). While synthesis of long DNA sequences was difficult and expensive in the past, synthesis technologies are rapidly developing. However, these arrays exhibit highly repetitive sequences and, with increasing length, pose an increased source of error that can introduce a sequence distribution bias already in the oligonucleotide pool [191].

We recently published a method for generating highly diverse single gene targeting CRISPR libraries termed covalently-closed-circular-synthesized (3Cs) technology [112]. The 3Cs method is based on *Kunkel mutagenesis* and relies on annealing of ssDNA oligonucleotides, encoding diverse gRNAs, to a ssDNA expression vector. It circumvents PCR amplification of gRNA encoding oligonucleotides and their subsequent ligation. Therefore, we hypothesized that the adaption of our library generation method for multiplex CRISPR libraries will allow increasing quality of multiplex libraries to addressing current limitations in multiplex CRISPR screening.

1.4 Genetic interactions in autophagy

1.4.1 Molecular mechanisms of mammalian autophagy

Autophagy is a catabolic process that is highly conserved among species and plays a key role in intracellular homeostasis. Triggered by stimuli of various stress conditions, such as energy, nutrient or oxygen deprivation and cytotoxic stress, autophagy induction can promote cell survival and protection from cellular damage. This cytoprotective mechanism is tightly regulated to ensure the most beneficial response and adaption of cellular function to unstable external conditions. Deregulation of autophagy is associated with various human disorders, including neurodegeneration, immune disease and cancer [192]. Moreover, modulation of autophagy has recently emerged as potent strategy for therapeutic targeting [193].

The research on autophagy started with the discovery of lysosomes in 1963 by Christian de Duve, who first coined the term 'autophagy'. It derives from the ancient Greek expression for "self-eating" and describes the lysosomal digestion of heterogenic cellular components [194]. In 2016, Yoshinori Ohsumi was awarded the Nobel Prize in Physiology or Medicine for his contribution to elucidating the mechanisms of autophagy and the discovery of autophagy-related genes [195]. Since then, the extensive research on autophagy has uncovered its important role in human physiology and pathology [192, 196].
In mammalian cells, three different types of autophagy are differentiated based on morphological and mechanistic characteristics: macroautophagy, microautophagy, and chaperone-mediated autophagy (CMA) [197]. In microautophagy, intracellular material is directly engulfed and degraded by lysosomes [198]. CMA is based on identification of cargo proteins by chaperones [199]. Macroautophagy is the main and best studied type of autophagy, especially in the context of disease [192, 196, 200].

The hallmark of macroautophagy, hereafter autophagy, is the formation of a double membrane structure called the phagophore, which engulfs intracellular cargo into a vesicle termed an autophagosome and ultimately mediates the degradation of the captured components, thereby enabling their recycling. This process comprises multiple steps [192] (Figure 1.10):
Autophagy initiation (also induction) is triggered by various stress conditions, including invading bacteria, hypoxia, oxidative stress or nutrient deprivation, which lead to the recruitment of autophagy-related (ATG) proteins to specific subdomains on the endoplasmic reticulum (ER) to initiate autophagosome biogenesis. The initiation step includes the activation and recruitment of two major protein complexes, the ULK1 complex and the PIK3C3 complex I. Their recruitment is accompanied by the formation of specific membrane domains called omegasomes, and followed by the nucleation of an isolation membrane named phagophore. The phagophore gradually expands to a cup shape and engulfs cytosolic material (cargo sequestration). Eventually, the phagophore seals and forms the double-membrane autophagosome that contains the cytosolic cargo. The autophagosome is subsequently targeted to the lysosome.

Fusion of the matured autophagosome and the lysosome results in the formation of an autolysosome that is characterized by a hydrolytic milieu that finally promotes cargo degradation [192, 200, 201].
The molecular mechanisms underlying autophagosome biogenesis and its regulation are complex and characterized by a high degree of context-dependency and cross-talk with other cellular pathways. Extensive research over the past decades has led to identification of many autophagic key players and regulatory factors. However, for many of them, the molecular function remains unclear.

1.4.1.1 Initiation of autophagosome biogenesis

In mammalian cells, basal autophagy is constitutively active at low levels, reflecting its important housekeeping role to ensure cellular homeostasis. Moreover, autophagy upregulation is induced upon various stress conditions, such as hypoxia, oxidative stress, invading bacteria and growth factor or nutrient deprivation [202]. Particularly, low levels of amino acids or glucose, are well-studied stimuli of autophagy induction [203, 204].
Amino acid deprivation results in autophagy induction via inactivation of the mechanistic target of rapamycin complex 1 (mTORC1). mTORC1 is a multimeric protein complex and a master regulator of catabolic and anabolic pathways. Its activation promotes synthesis of lipids, proteins and nucleotides, thus enabling cell growth under nutrient-rich conditions. In its active form, mTORC1 also inhibits autophagy by binding and phosphorylating specific sites of ULK1 and ATG13, two components of the ULK1 complex required for the initiation of autophagosome biogenesis [205]. Amino acid starvation results in the inactivation of mTORC1 leading to subsequent dephosphorylation and release of ULK1 from mTORC1. Upon autophosphorylation, ULK1 is able to phosphorylate ATG13 and FIP200 (200-kDa focal adhesion kinase family-interacting protein), enabling the activation of the ULK1 complex and mediating mTORC1-sensed nutrient stress to the autophagic machinery [206, 207].
A decline in cellular energy levels, such as glucose starvation-induced autophagy, is perceived by the kinases 5'AMP-activated protein kinase (AMPK) and serine/threonine kinase 11 (STK11), also known as liver kinase B1 (LKB1). AMPK promotes autophagy upon depletion of ATP by inhibition of mTORC1 through phosphorylation of the regulatory-associated protein of mTOR (RPTOR) and by activation of the tuberous sclerosis 2 (TSC2) complex. The TSC2 complex is further regulated by interaction with WIPI3 (WD repeat domain phosphoinositide interacting 3) and FIP200, two proteins involved in autophagosome formation, thus linking the LKB1-AMPK-TSC2 axis to mTORC1 regulation and autophagosome biogenesis and allowing coordination between autophagy induction and autophagosome formation [202].
The activation of the ULK1 complex marks the initiation of autophagosome biogenesis. The activated ULK1 complex then phosphorylates and activates a second major complex of autophagy initiation, the PIK3C3 complex 1 that consists of vacuolar protein sorting 34, also known as PIK3C3 (VSP34), Beclin 1, ATG14 and the general vesicular transport factor p115 (p115).

Both complexes translocate to specialized subdomains of the ER, the phagophore assembly sites (PASs) where VSP34 mediates the conversion of phosphatidylethanolamine (PE) to PI3P [202, 208] that leads to recruitment of PI3P effector proteins.

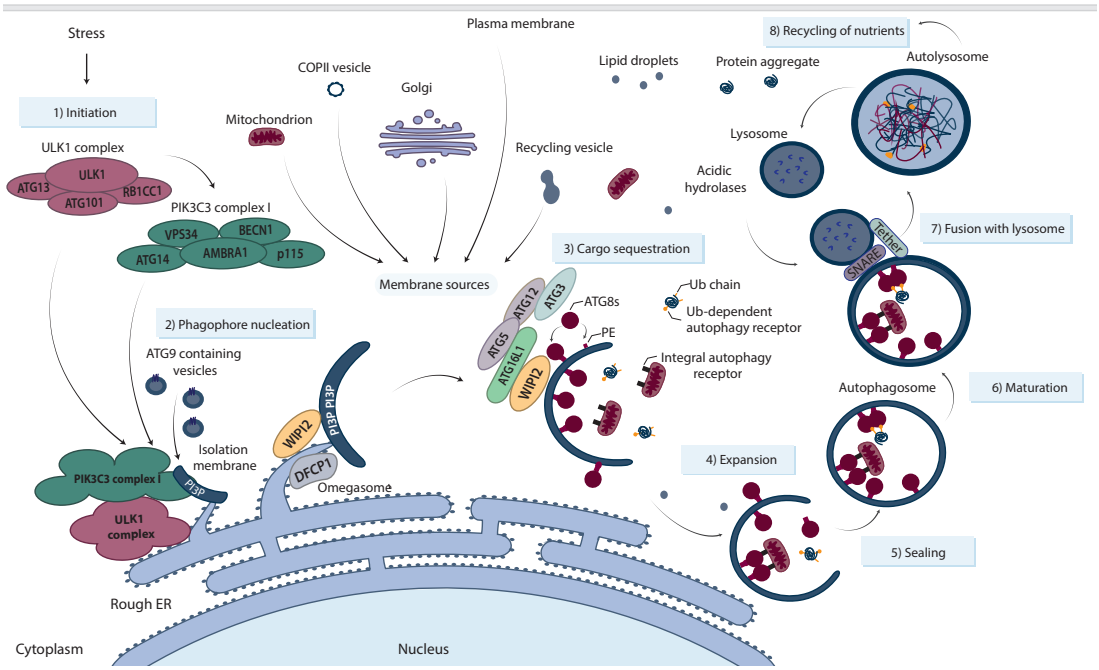

Figure 1.10: Overview of the mammalian autophagy pathway
Cellular stress signals initiate autophagy by activating the ULK1 complex, consisting of ULK1, ATG13, 200-kDa focal adhesion kinase family-interacting protein (FIP200) and ATG101. The ULK1 complex mediates activation of the PIK3C3 complex I, which consists of VSP34, Beclin 1 (BECN1), autophagy and beclin 1 regulator 1 (AMBRA1), p115 and ATG14. VSP34 promotes PI3P production at a specific ER domain termed omegasome, where an isolation membrane is nucleated that expands to a cup-shaped phagophore. PI3P recruits WD repeat domain phosphoinositide interacting (WIPI) proteins. ATG2 possess membrane tethering and lipid transfer activities and binds to WIPI4. WIPI2 directly binds ATG16L1, thus recruiting the ATG12~ATG5 conjugate required for lipidation of ATG8 family proteins, that comprise the light chain 3 (LC3) proteins and gamma-aminobutyric acid receptor-associated proteins (GABARAPs). ATG8 lipidation is ATG3-mediated. LC3s and GABARAPs are conjugated to membrane-bound PE at the inner and outer phagophore membrane. ATG8s are involved in subsequent phagophore expansion, sealing, maturation and in selective sequestration of cargo, such as damaged mitochondria via LC3-interacting region (LIR) containing receptors or protein aggregates with ubiquitin (Ub) dependent receptors. Possible membrane sources for autophagosome biogenesis include mitochondria, coat protein complex II (COPII), Golgi, plasma membrane and recycling endosomes. Maturation of the sealed autophagosome includes clearance of ATG proteins and recruitment of the fusion machinery, including soluble N-ethylmaleimide-sensitive factor attachment protein receptor (SNARE) complexes and several tether proteins. Fusion with the lysosome leads to degradation of the cargo by acidic hydrolases and release of reusable components into the cytoplasm. Modified from [192].

In mammalian cells, autophagosomes can be formed *de novo* upon increased demand at multiple different PASs. The PAS occurrence was reported to coincide with ER–mitochondria

contact sites [209], with autophagy specific *ER exit sites* [210] and closely associated with PI3P-enriched subdomains of the ER, referred to as omegasomes (due to their omega-like shape), which harbor additional pre-autophagic markers, such as the PI3P-binding protein double FYVE-containing protein 1 (DFCP1) [211]. The omegasome serves as a platform for the recruitment of downstream ATG proteins [212]. This includes the only integral transmembrane protein ATG9, which is embedded in 30-60 nm membrane vesicles. A recent study identified the BAR-domain containing protein ADP ribosylation factor interacting protein 2 (ARFIP2) and two phosphatidylinositol 4-Kinases (PI4Ks), also PI4KIIIβ (PI4KB) and also PI4KIIα (PI4K2A), as parts of ATG9 vesicles [213]. Moreover, recent experiments in yeast revealed that the PAS is a liquid-like condensate of Atg proteins and that the Atg1 complex activation induces a liquid droplet formation of the early PAS [214].

1.4.1.2 Phagophore nucleation, expansion and sealing

The coordinated actions of the ULK1 complex, ATG9 vesicles, the PI3P production by the PIK3C3 complex I, and several ER localized proteins (VAPA/B, VMP1, TMEM41B, E-STY and PIS, reviewed in [215]) result in the nucleation of an isolation membrane, referred to as phagophore.

Starvation can induce the formation of a multitude of autophagosomes that require an efficient supply of lipids and membranes. Possible sources have been debated and extensively investigated for over five decades [216, 217]. Although the autophagosomal membrane nucleates from the ER, many additional endomembrane sources, including the ER Golgi intermediate compartment (ERGIC) [218], Golgi [219], mitochondria [220], endosomes [221], the plasma membrane [222] and recently COPII vesicles [223] were suggested as possible membrane donors, but molecular mechanisms remain elusive [201]. Opposed to an early hypothesis, ATG9 vesicles do not appear to be incorporated into autophagosomal membranes in mammalian cells but may supply lipids [201, 224]. Recently, de novo phosphatidylcholine synthesis was shown to be required for autophagosomal membrane formation and maintenance during autophagy [225]. Phagophore nucleation further involves recruitment of four PI3P-binding WIPI proteins.

Phagophore expansion includes the characteristic post-translational modification of Ub-like ATG8 proteins, comprising the LC3 and GABARAP subfamilies [226]. Pro-ATG8s occur in the cytosol in an unlipidated form before they are processed by the protease ATG4 and are lipidated into the membrane-bound, PE-conjugated form at the phagophore outer and inner membranes [226]. Conjugation requires activation of processed ATG8s by the E1-like enzyme ATG7, followed by their conjugation to membrane bound PE mediated by the E2-like ATG3 [209]. ATG3 itself requires activation by the E3-like ATG12~ATG5 conjugate. Ub-like ATG12 is also activated by ATG7 and subsequently conjugated to ATG5 by the E2-like ATG10 [209]. The ATG12~ATG5 conjugate functions in a complex with ATG16L [227, 228], which directly binds the WD repeat domain phosphoinositide interacting protein 2 (WIPI2) at the PAS [229].

The essentiality of ATG8 proteins for autophagosome formation has recently been debated due to evidence that cells can (eventually) form autolysosomes even in the absence of ATG8s [230] or the conjugation systems [231]. However, it has been shown that the loss of the ATG8 conjugation system significantly reduces efficiency of the overall autophagic flux [232].
Besides their role in so-called 'bulk autophagy', which degrades cargo in a non-selective manner, ATG8s are also implicated in selective autophagy [233]. Selective autophagy occurs in cells even during nutrient-rich and contributes to intracellular homeostasis by degrading specific cargo, such as aggregated proteins (aggrephagy), damaged mitochondria (mitophagy), invading pathogens (xenophagy) and many more [234] and relies on mechanisms for recognizing specific cargo while excluding non-cargo material. This selectivity is conferred by cargo receptor proteins [234] that tether a cargo to a nascent autophagosomal membrane by simultaneously binding the cargo and ATG8-family proteins on the membrane. Many receptor proteins recognize poly-Ub chains that are attached to the surface of the cargo and function as degradation labels for selective autophagy, bridging the polyubiquitinated cargo with the autophagy machinery [235–237].
Moreover, in mammalian cells, the ATG8 family proteins might also be involved in phagophore closure, as their depletion leads to accumulation of open autophagosomes [231]. Notably, a conserved ATG2-GABARAP family interaction was recently shown to be critical for phagophore closure [238]. The process of phagophore sealing to form a closed autophagosome appears to be achieved by scission of the inner and outer membrane at the phagophore edges [239], and involves the endosomal sorting complex required for transport (ESCRT) [240–242].

1.4.1.3 Autophagosome maturation and fusion with lysosome

Autophagosome maturation involves gradual clearance of ATG proteins, including conjugated ATG8s from the autophagosome outer membrane [243]. ATG4, a protein involved in ATG8 conjugation, is also required for deconjugation of ATG8s [244]. Formation of the degradative autolysosome requires the recruitment of components mediating the fusion to the lysosome, including RAS-associated binding GTPases (RABs), tethering factors and SNAREs [243]. SNAREs can be divided into autophagosome-localized vesicle SNAREs (v-SNAREs), including syntaxin 17 (STX17) and synaptosome associated protein 29 (SNAP29), and lysosome-localized target membrane SNAREs (t-SNAREs), including the vesicle associated membrane proteins 7 and 8 (VAMP7/8) [245]. Moreover, RAB7 [246], RAB33B [247], and RAB2A [248] have been shown to regulate autophagosome-lysosome fusion, and tethering factors support and stabilize the assembly of the *trans*-SNARE complex that is formed by SNAREs on opposing vesicle membranes. The tethering factors are recruited by binding to RAB proteins, and they include the pleckstrin homology domain-containing family M member 1 (PLEKHM1), the homotypic fusion and protein sorting (HOPS) complex, the ectopic P granules protein 5 homolog (EPG5), ATG14, and the Golgi reassembly-stacking protein of 55 kDa (GRASP55) [243].

Additionally, RAB7 and the ADP ribosylation factor related protein 1 (ARFRP1) mediate binding of cytoskeleton-associated motor protein adaptors, such as FYCO1 (FYVE and coiled-coil domain containing 1), ORP1L (oxysterol-binding protein-related protein 1L), PLEKHM1/2, and the BLOC-1 related (BORC) protein, which are required for the movement of autophagosomes and lysosomes towards each other along the microtubules [243].

Several yeast ATG genes have multiple paralogous genes (or short paralogs) in mammalian cells (Table 1.1) [200]. Paralogs result from gene duplication, which is a major source for the emergence of new genes [249]. Paralogs can share a functional overlap, exhibit unique functions or both, and paralog dependencies are thought to contribute to genetic robustness of human cells [250] as well as to context-dependent differential essentiality of genes [251].
Specific functions and compensatory roles have been reported for several human ATG paralogs. For example, recent evidence indicates differential functions of GABARAPs and LC3s in bulk and selective autophagy, such as different binding specificities to selective substrates [232].

Function	***S. cerevisiae***	**Mammalian paralogs**			
ULK1 complex	Atg1	*ULK1*	*ULK2*	*ULK3*	*ULK4*
PI3P-binding	Atg18	*WIPI1*	*WIPI2*	*WIPI3 (WDR45B)*	*WIPI4 (WDR45)*
ATG9 vesicles	Atg9	*ATG9A*	*ATG9B*		
LC3 conjugation	Atg8	*MAP1LC3A*	*MAP1LC3B*	*MAP1LC3B2*	*MAP1LC3C*
		GABARAP	*GABARAPL1*	*GABARAPL2*	
	Atg4	*ATG4A*	*ATG4B*	*ATG4C*	*ATG4D*
	Atg16	*ATG16L1*	*ATG16L2*		
Others	Atg2	*ATG2A*	*ATG2B*		

Table 1.1 Yeast autophagy-related genes and their homologous mammalian paralogs. Adapted and modified from Kawabata & Yoshimori, (2020) [200].

The yeast Atg18 gene has 4 mammalian paralogs that encode the WIPI family members for which several specific functions have been reported. While the function of WIPI1 is unknown, it is a frequent marker of phagophore formation and recruited before WIPI2 [252]. WIPI2 acts as a scaffold for ATG16L1 at the isolation membrane [229], whereas WIPI3 directly interacts with FIP200 and TSC2 [253], and WIPI4 binds the lipid transfer proteins ATG2A [254] and its paralog ATG2B [255], thus promoting autophagosome elongation [256].
However, many human ATG paralogs lack precise characterization of their specific or compensatory functions in different cellular contexts, and the biological significance of this genetic plurality in higher eukaryotes is largely unknown.
Moreover, it was recently shown that in whole-genome CRISPR screens in human cancer cell lines, paralog genes are less frequently identified as essential genes [251]. A recent study used a multiplex CRISPR approach to identify functional buffering of paralog gene pairs that were undetected in previous monogenic CRISPR knockout screens [257]. Therefore, a multiplex CRISPR screening approach targeting autophagy-associated paralogs might uncover new

specifications, compensatory mechanisms or synergistic essentiality of paralogs involved in autophagy.

1.4.2 Autophagy in human disease

Extensive research over the past decades has led to significant progress in understanding the molecular mechanisms of autophagy and its cytoprotective and homeostatic cellular role. Besides that, dysregulation of autophagy has been linked to various human diseases, including immune and neurodegenerative disease and cancer (Suppl. Table S1) [196].

The role of autophagy in cancer

Autophagy has an ambiguous role in cancer development and progression and is highly context-dependent. It can exhibit opposite functions depending on several factors, such as the tumor progression state, the tumor microenvironment and the genetic context [258–260].

On one hand, the cytoprotective effect of autophagy can promote a tumor-suppression before the onset of malignant transformation and tumorigenesis [261–264]. Conversely, it was also shown that autophagy can promote the survival of cancer cells under stress conditions, including therapy-induced stress, and various cancer types show high autophagic activity [265]. For example, cancers associated with mutant *rat sarcoma (RAS)* genes [266, 267] or pancreatic cancer [265, 268] have been linked to a high autophagy dependency. Additionally, upregulation of autophagy was shown to be a frequent side effect of cancer therapy, and therefore autophagy inhibitors were suggested to increase therapy efficiency by reducing the tumor cells autophagy-dependent adaptive response mechanisms [269–271]. In contrast, autophagy activation has also been shown to increase therapy efficiency [272]. Moreover, there is also evidence of autophagy being involved in shaping tumor environment by *unconventional secretion* of cargo, and in endosomal and exosomal pathways, thereby affecting cancer metastasis and immune responses [273]. Additional cross-talk is observed between autophagy and the *epithelial-mesenchymal transition* (*EMT*) [274]. While autophagy induction was shown to impair EMT [275, 276], which is a critical contributor to metastasis, other studies also show that treatment-induced cyto-protective autophagy could promote melanoma cell EMT [277] and that BECN1 knockdown impairs EMT of colon cancer cells [278]. Notably, autophagy activation was also associated with promoting *anoikis* resistance and metastasis in some tumor models [279, 280].

Taken together, these findings highlight the complex role of autophagy in cancer. While the pharmacological inhibition and activation of autophagy are currently in clinical testing, it still requires more precise knowledge of the molecular mechanisms regulating the outcome of autophagy-dependent therapies and a clear definition of distinction criteria for cancer types that are vulnerable to autophagy inhibition or activation, respectively [259, 265]. It was also shown that the role of autophagy in cancer is highly dependent on the patients' genetic background. For example, the genetic status of *TP53* (tumor protein p53) [281] and *SMAD4*

(*mothers against decapentaplegic homolog 4*) [282] were shown to determine the role of autophagy in pancreatic tumor development, thus highlighting the impact of genetic interactions on cancer therapies.

Autophagy in neurodegenerative disease

Abnormal aggregation and accumulation of misfolded proteins in neuronal cells induces their dysfunction or death and poses a hallmark of several neurodegenerative diseases, including Alzheimer disease, amyotrophic lateral sclerosis (ALS), beta propeller associated neurodegeneration (BPAN), Parkinson's disease, Vici syndrome and many others [196, 283]. As autophagy provides protection against neurodegeneration by removing detrimental or aggregated proteins and damaged mitochondria, numerous neurodegenerative disease are directly linked to mutations of autophagic and lysosomal genes [196, 284] (Suppl. Table S1) [196].

Recessive mutations in *EPG5*, a tethering factor involved in autophagosome and lysosome fusion, cause a multi-system disorder, termed Vici syndrome [285, 286], and mutations in the PI3P effector *WD repeat domain 45 (WDR45)* (WIPI4) were shown to cause BPAN [287, 288]. Furthermore, emerging evidence highlights the role of selective autophagy in neurodegenerative disease. Indeed, mutations in genes encoding autophagy receptors required for selective autophagy, such as *sequestosome-1, also known as p62 (SQSTM1)* and *optineurin (OPTN)*, are linked to familial and early onset of Parkinson's disease, fronto-temporal dementia, and ALS [289, 290]. SQSTM1 binds Ub and is a key player in sequestration and degradation of protein aggregates by autophagosomes [291]. Dysfunctional mitophagy is also suggested as a cause of neurodegenerative disease, because mutations in the *PTEN induced kinase 1 (PINK1)* and the *Parkinson disease protein 2 (PRKN)* gene, two important mitophagy regulators, are associated with recessive and sporadic early-onset Parkinson's disease [292]. Moreover, mutations in the gene encoding TANK binding kinase 1 (TBK1), which is required for phosphorylation of the autophagy receptors OPTN and SQSTM1 to promote sequestration of polyubiquitinated mitochondria in mitophagy [293, 294], were also shown to cause fronto-temporal dementia and ALS [295].

Pharmacological studies in mice indicate that autophagy activation has beneficial therapeutic effects in the context of neurodegenerative disease and holds significant potential for pharmacological intervention [284].

Autophagy in infection, immunity and inflammation

Autophagy can also degrade intracellular pathogens by xenophagy ("foreign-eating"), which is a selective type of autophagy [296]. Invading pathogens are first labelled by various types of Ub chains and galectin. These are recognized by selective autophagy receptors, such as SQSTM1, neighbor of BRCA1 gene 1 protein (NBR1), nuclear domain 10 protein 52, also known as CALCOCO2 (NDP52), OPTN and others, and subsequently sequestered by the phagophore and delivered for autolysosomal degradation. In line with this, xenophagy was shown to be involved in elimination of *Mycobacteria*, *Listeria*, *Salmonella*, *Legionella*, *Shigella* and others

[192, 296, 297].
Other intersections of autophagy with immune functions comprise inflammasome regulation [298], antigen presentation [299, 300], and immune cell development, differentiation and activation [301, 302].
Lastly, genome-wide association studies uncovered mutations in autophagy-associated genes that are linked to chronic inflammatory disease and autoimmune disorders [303, 304]. One example is the increased susceptibility to the inflammatory bowel disease Crohn's disease (CD), which is associated with multiple SNPs in *ATG16L1* and *immunity-related GTPase family M protein (IRGM)* [304, 305]. Moreover, SNPs in *ATG5* and *ATG7* are linked to systemic lupus erythematosus (SLE), an autoimmune disease-causing abnormal inflammation and tissue damage [306].

Taken together, these numerous genetic links connect autophagy to a broad range of different human diseases. Many mammalian ATG genes are functionally diversified and intricately implicated in multiple fundamental cellular processes and signalling pathways. Since therapeutic modulation of autophagy is complex and might indirectly affect intersecting pathways, it requires profound understanding of dependencies between ATG genes and their context specific genetic backgrounds. Improving technologies for GI screening could help to uncover yet unknown genetic dependencies within the autophagy pathway and between autophagy and other cellular processes. This can provide new insights for delineating the role of autophagy in diseases and provide valuable information for the development of therapeutic approaches.

Aim of the work

The systematic mapping of GIs can advance our understanding of higher-level principles of cellular organization and help to reveal how synergistic gene functions result in complex biological phenotypes and disease. However, identification of GIs in higher organisms, especially humans, is difficult because of the high number of genes in the human genome. Moreover, GIs are context-dependent and can differ among cell lines, tissues and conditions. Therefore, establishing a comprehensive functional genetic landscape of a human cell, in the same way as it has been done for yeast, requires efficient and scalable genetic perturbation platforms that will facilitate screening for genetic interactions for large numbers of target genes. In line with this, multiplex CRISPR gRNA libraries have emerged as a powerful tool for combinatorial genetic screening by simultaneously introducing diverse dual-knockouts in a myriad of cells. However, the required experimental scale for GI screens can limit the number of target gene combinations that can be investigated in a single screen. To address this limitation and facilitate GI screening with highly diverse multiplex CRISPR gRNA libraries, in this work, we focused on three main goals:

1. Establish the 3Cs multiplexing technology to enable the generation of combinatorial gRNA libraries with uniform library distributions and demonstrate their functionality for combinatorial gene knockouts in human cells.

2. Investigate the impact of the multiplex gRNA library distribution on the screening performance in relation to distinct screening coverages and determine minimized screening conditions for 3Cs multiplex gRNA libraries based on their library distribution.

3. Demonstrate the applicability of 3Cs multiplex gRNA libraries for two different pooled screening approaches by identifying autophagy gene interactions in cell proliferation and autophagy flux in two coverage-minimized screens.

Material and methods

3.1 Materials

3.1.1 Chemicals, enzymes and consumables

The methods used in this work were performed according to standard protocols or the corresponding manufacturers' specifications. All experiments were performed with deionized water and all standard chemical reagents that are not listed in Table 3.1 were provided by the companies Merck KGaA (Darmstadt) or Carl Roth (Karlsruhe). Mammalian cell culture media and supplements were obtained from Thermo Fischer Scientific/Life Technologies (Darmstadt). All consumables were obtained from Greiner (Solingen), BD Biosciences (Heidelberg) or Corning (Kaiserslautern). Synthesized oligonucleotides were obtained from Integrated DNA Technologies (Interleuvenlaan), or Merck KGaA (Darmstadt). Oligonucleotide sequences used for 3Cs reactions, cloning, and sequencing library preparation are provided in (Supp. Table S2)

Table 3.1 List of chemicals, enzymes, and commercial kits

Chemicals, enzymes, and commercial kits	**Source**
2xYT microbial growth medium (powder)	Carl Roth, Karlsruhe
Adenosine triphosphate (ATP)	New England Biolabs, Frankfurt
Agarose	Carl Roth, Karlsruhe
AleI endonuclease	New England Biolabs, Frankfurt
Ampicillin	Carl Roth, Karlsruhe
BafilomycinA1 (BafA1)	Cayman Chemical, Ann Arbor
BbsI endonuclease	New England Biolabs, Frankfurt
Blasticidin	Carl Roth, Karlsruhe
BsiWI-HF® endonuclease	New England Biolabs, Frankfurt
BsmBI endonuclease	New England Biolabs, Frankfurt
Chloramphenicol	Carl Roth, Karlsruhe
Deoxynucleoside triphosphate (dNTP) mix	Carl Roth, Karlsruhe
Dimethyl sulphoxide (DMSO)	Carl Roth, Karlsruhe
Dithiothreitol (DTT)	Life Technologies, Darmstadt
Dulbecco's Modified Eagle Medium (DMEM)	Life Technologies, Darmstadt
Dulbecco's Modified Eagle Medium (DMEM) F12	Life Technologies, Darmstadt

Table 3.1 List of chemicals, enzymes, and commercial kits

Chemicals, enzymes, and commercial kits	**Source**
E.Z.N.A. M13 DNA extraction kit	Omega Bio-Tek, Norcross
Ethylendiaminetetraacetic acid (EDTA)	Merck KGaA, Darmstadt
Fetal bovine serum (FBS)	Life Technologies, Darmstadt
Gel Loading Dye, Purple (6X)	New England Biolabs, Frankfurt
GeneJET™ Gel extraction kit	Thermo Fisher Scientific, Frankfurt
GeneJET™ Plasmid miniprep kit	Thermo Fisher Scientific, Frankfurt
GeneRuler 1 kb Plus DNA Ladder	Thermo Fisher Scientific, Frankfurt
Geneticin disulphate solution (G418)	Carl Roth, Karlsruhe
Glycerol	Thermo Fisher Scientific, Frankfurt
HEPES (N-2-hydroxyethylpiperazine -N-2-ethane sulfonic acid)	Life Technologies, Darmstadt
Hygromycin	Invivogen, San Diego
I-CeuI endonuclease	New England Biolabs, Frankfurt
I-SceI endonuclease	New England Biolabs, Frankfurt
Isopropanol	Merck KGaA, Darmstadt
Kanamycin	Carl Roth, Karlsruhe
LB broth powder	Carl Roth, Karlsruhe
Lipofectamin 2000	Life Technologies, Darmstadt
M13KO7 helper phage	New England Biolabs, Frankfurt
Methanol	Merck KGaA, Darmstadt
MiSeq 150 cycles sequencing kit	Illumina, San Diego
NEBNext® High-Fidelity 2x PCR master mix	New England Biolabs, Frankfurt
NextSeq 150 cycles sequencing kit	Illumina, San Diego
OneTaq DNA polymerase	New England Biolabs, Frankfurt
Penicillin-streptomycin (Pen/Strep)	Roche, Mannheim
Phosphate buffered saline (PBS)	Life Technologies, Darmstadt
Polybrene	Merck KGaA, Darmstadt
Polyethylene glycol	Carl Roth, Karlsruhe
Proteinase K	Tocris Bioscience, Bristol
PureLink Genomic DNA extraction kit	Life Technologies, Darmstadt
QIAGEN Plasmid Plus Maxi kit	Qiagen, Hilden
QIAGEN RNeasy Mini kit	Qiagen, Hilden
Ribonuclease A	Carl Roth, Karlsruhe
Roti®-Safe Gel Stain	Carl Roth, Karlsruhe
SapI endonuclease	New England Biolabs, Frankfurt
S.O.C. medium	Life Technologies, Darmstadt

Table 3.1 List of chemicals, enzymes, and commercial kits

Chemicals, enzymes, and commercial kits	Source
Sodium chloride	Merck KGaA, Darmstadt
Streptomycin sulfate	Life Technologies, Darmstadt
T4 DNA ligase	New England Biolabs, Frankfurt
T4 polynucleotide kinase	New England Biolabs, Frankfurt
T7 DNA polymerase	New England Biolabs, Frankfurt
Tetracycline Hydrochloride	Carl Roth, Karlsruhe
Torin 1	Selleckchem, Houston
Trypsin-EDTA 0.5%	Life Technologies, Darmstadt
Tween 20	Merck KGaA, Darmstadt
Venor®GeM classic kit	Minerva Biolabs GmbH, Berlin

3.1.2 Mammalian cell lines

Cells that were obtained from other sources than the American Type Culture Collection (ATCC®) were tested for mycoplasma contamination immediately after the arrival of the cells and multiple times during the course of the experiments by using Venor®GeM Classic kit from Minerva Biolabs GmbH, according to the manufacturer's instructions.

Table 3.2 List of mammalian cell lines

Mammalian cell line	Source
Human embryonic kidney (HEK) 293T cells	ATCC®
Human telomerase reverse transcriptase-immortalized retinal pigment epithelial (hTERT-RPE1) cells	ATCC®
Monoclonal Cas9-expressing hTERT-RPE1 cells	generated by lentiviral transduction
Monoclonal GFP-LC3-RFP-expressing hTERT-RPE1 cells	generated by lentiviral transduction
Monoclonal GFP-mCherry-expressing hTERT-RPE1 cells	generated by lentiviral transduction
Puromycin-sensitive hTERT-RPE1 cells	gift from Andrew Holland

The monoclonal human telomerase reverse transcriptase-immortalized retinal pigment epithelia (hTERT-RPE1) cell line with stable expression of *S. pyogenes* Cas9 (SpCas9) was generated by Konstantin Müller by lentiviral transduction of puromycin-resistant hTERT-RPE1 cells with the lentiCRISPRv2-Neo-NHT plasmid (Table 3.3), and subsequent selection with neomycin (geneticin disulphate solution, G418) .
The monoclonal hTERT-RPE1 cell line with stable expression of the GFP-LC3-RFP autophagic flux reporter was generated by Paolo Grumati by lentiviral transduction of monoclonal Cas9-expressing hTERT-RPE1 cells with the pMRX-IP-GFP-LC3-RFP plasmid (Addgene: 84573,

gift from Noboru Mizushima) [307] (Table 3.3).
The monoclonal EGFP-mCherry-expressing hTERT-RPE1 cell line was generated by lentiviral transduction of monoclonal Cas9-expressing hTERT-RPE1 cells with the entiCMV-EGFP-mCherry-Blas plasmid (Vector Builder, (Table 3.3).

3.1.3 Recombinant plasmid DNA

Table 3.3 List of recombinant plasmids

Recombinant plasmids	**Source**
3Cs multiplex vector	cloned
lentiCRISPRv2	Addgene: 52961, gift from Feng Zhang [308]
lentiCRISPRv2-Neo	Addgene: 98292, gift from Brett Stringer [309]
lentiCRISPRv2-Neo-NHT	cloned
lenti-sgRNA blast	Addgene: 104993, gift from Brett Stringer [309]
pKLV2.2-h7SKgRNA5(SapI)- hU6gRNA5(BbsI)-PGKpuroBFP-Wt	Addgene: 72666, gift from Kosuke Yusa [116]
pMRX-IP-GFP-LC3-RFP	Addgene: 84573, gift from Noboru Mizushima [307]
lentiCMV-EGFP-mCherry-Blast	designed and synthesized by VectorBuilder, Frankfurt

The cloning strategy for generating the 3Cs multiplex vector is described in section 3.2.3.2. The lentiCRISPRv2-Neo-NHT plasmid was cloned by BsmBI endonuclease digestion of lenti-CRISPRv2-Neo (Addgene: 98292, gift from Brett Stringer) and subsequent ligation of pre-annealed oligonucleotides encoding a non-human targeting (NHT) gRNA flanked with BsmBI-compatible overhangs (Supp. Table S2). To enable blasticidin selection of dual gRNA constructs, the dual gRNA expressing plasmid pKLV2.2-h7SKgRNA5(SapI)-hU6gRNA5(BbsI)-Blast was cloned by Yves Matthes. To this end, the dual gRNA expression cassette of pKLV2.2-h7SKgRNA5(SapI)-hU6gRNA5(BbsI)-PGKpuroBFP-W (Addgene: 7266, gift Kosuke Yosa) was cloned into the lenti-sgRNA blast plasmid (Addgene: 104993, gift from Brett Stringer) to enable blasticidin selection of dual gRNA constructs. A silent point mutation was introduced to remove the BbsI recognition site within the blasticidin sequence and to allow the subsequent insertion of one gRNA by SapI endonuclease cloning into the human 7SK promoter (h7SK) expression cassette and the second gRNA by BbsI cloning into the human U6 promoter (hU6) expression cassette. Sequences for oligonucleotides used for plasmid cloning are provided in Supp. Table S2.

3.1.4 Bacteria

Table 3.4 List of *Escherichia coli (E. coli)* strains

Strain	Source
XL1-Blue supercompetent cells	Agilent Technologies, Ratingen
10-beta electrocompetent *E. coli*	New England Biolabs, Frankfurt
E. coli K12 CJ236	New England Biolabs, Frankfurt

3.1.5 Hardware

Table 3.5 List of hardware

Hardware	Company
FACSCanto II flow cytometer	BD Bioscience, Heidelberg
ThermoMixer™ F0.5	Eppendorf, Hamburg
Blue light LED illuminator	Analytik Jena, Jena
Light Microscope	Olympus, Hamburg
Thermocycler Mastercycler® Nexus	Eppendorf, Hamburg
Digital block Heater	Thermo Fisher, Frankfurt
Bio-Rad Gene Pulser I System	Bio-Rad, Munich
MiSeq system	Illumina, San Diego
NextSeq 500 System	Illumina, San Diego
Centrifuge 5810 R	Eppendorf, Hamburg
NanoDrop™ One Mikrovolumen-UV/VIS spectral photometer	Thermo Fisher, Frankfurt
Bench-top centrifuge 5424	Eppendorf, Hamburg

3.1.6 Software

Table 3.6 List of software

Software	Source or Reference
Adobe Illustrator 8.0.	Adobe Inc.
Bcl2fastq v2.19.1.403	Illumina, San Diego
Bowtie2 2.3.0	[310]
Cutadapt 2.8	[311]
FACS DIVA Software	BD Bioscience, Heidelberg
FlowJo	BD Bioscience, Heidelberg

Table 3.6 List of software

Software	**Source or Reference**
GraphPad Prism 9	Graphpad Software, Inc.
Python 3	Python Software Foundation
SnapGene	Insightful Science

3.2 Methods

3.2.1 Microbiological methods

3.2.1.1 Cultivation and storage of *E. coli*

Aliquoted *E. coli* were stored at -80°C. For liquid cultivation, bacteria were grown in LB-medium at 37°C by shaking at 225-250 rpm. LB-agar plates (LB medium, 0.5% w/v agar) were incubated at 37°C over night to select single colonies. For the selection of transformed bacteria the appropriate antibiotics were added in the following concentrations:

Table 3.7 Concentrations of antibiotics for bacterial selection

Antibiotic	Concentration
Ampicillin	100 µg/ml
Chloramphenicol	34 µg/ml
Kanamycin	25 µg/ml
Streptomycin	100 µg/ml
Tetracycline	50 µg/ml

3.2.1.2 Transformation of *E. coli* with plasmid DNA

For transformation of plasmid DNA, 10 µl of XL1-Blue supercompetent cells were thawed on ice, then mixed with up to 200 ng plasmid DNA (or 5 µl ligation sample) and incubated on ice for 15 min. Afterwards the cell mixture was placed at 42°C for 45 seconds for heat-pulse and subsequently placed on ice for 2 min. After resuspension in 200 µl S.O.C. medium, cells were placed at 37°C and 300 rpm for 1 h and subsequently plated on a LB-agar plate or resuspended in LB-media with the appropriate antibiotic and incubated overnight at 37°C and 225–250 rpm.

3.2.1.3 Production of KCM competent cells

For generating KCM competent cells, *E. coli* K12 CJ236 were streaked on LB agar plates containing chloramphenicol (34 µg/ml). The next day, 5 ml of LB media supplemented with chloramphenicol (34 µg/ml) and tetracyline (50 µg/ml) was inoculated with one colony and incubated over night at 37°C and 225–250 rpm. The next morning the optical density at a wavelength of 600 nm (OD_{600}) was measured and diluted to 0.05 in 100 mL LB media without antibiotics. After 2 - 4 hrs of further cultivation, at an OD_{600} of 0.3 - 0.6, cells were centrifuged for 5 min at 3000 x g and 4°C. Then each cell pellet was resuspendet in 2.5 ml ice cold TSB (10% PEG, 5% DMSO, 10mM $MgCl_2$, 10mM $MgSO_4$) and incubated on ice for 10 min. After addition of 250 µL cold, sterile Glycerol, aliquots of 55 µl were prepared and flash frozen in liquid nitrogen and stored at -80°C.

3.2.1.4 Transformation of KCM competent cells

To transform KCM competent *E. coli* K12 CJ236 cells, plasmid DNA (100 ng - 1 µg) was mixed with 2 µL of 5x KCM buffer (0.5M KCl, 0.15M $CaCl_2$, 0.25M $MgCl_2$) in a 10 µL reaction volume. Aliquots of 10 µl KCM competent *E. coli* K12 CJ236 cells were thawed on ice. The DNA mixture was added to the cells. After incubation on ice for 10 min, 100 µL S.O.C. medium was added and the cells were placed at 37°C and 225–250 rpm for 1 h. Afterwards, cells were streaked on LB agar plates containing chloramphenicol (34 µg/ml) and ampicillin (100 µg/ml).

3.2.1.5 Production of electrocompetent

To generate electrocompetent cells, *E. coli* C3020K were streaked on LB agar plates supplemented with streptomycin (100 µg/ml). The next day, 200 ml of LB media with 100 µg/ml streptomycin was inoculated with one colony and incubated over night at 37°C and at 225–250 rpm. On the third day, 1.5 L of LB media supplemented with streptomycin (100 µg/ml) was inoculated with 30 ml of the overnight culture and cultivated at 37°C and 225–250 rpm until an OD_{600} of 0.8 was reached. Then, cells were centrifuged for 10 min at 4000 rpm at 4°C. Subsequently, the supernatant was discarded and the pellets were washed three times with 400 ml of 1mM HEPES solution. Each cell pellet was resuspendet in 2.5 ml ice cold TSB (10% PEG, 5% DMSO, 10mM $MgCl_2$, 10mM $MgSO_4$) and incubated on ice for 10 min. After addition of 250 µL ice cold, sterile glycerol, aliquots of 55 µl were prepared, flash frozen in liquid nitrogen and stored at -80°C.

3.2.2 Molecular biological methods

3.2.2.1 Isolation of plasmid DNA of *E. coli*

Plasmid DNA of *E. coli* cells was isolated according to the manufacturer's protocol using the GeneJet Plasmid miniprep kit for up to 25 µg DNA, or the QUIAGEN Plasmid Plus Maxi kit for up to 1 mg DNA. After purification, the DNA concentration was measured using the NanoDrop™ One Mikrovolumen-UV/VIS spectral photometer. Sample purity was ensured by a A260/A280 ratio of 1,7 - 1,9.

3.2.2.2 Polymerase chain reaction (PCR)

DNA amplification by PCR was carried out using NEBNext®High-Fidelity 2X PCR Master Mix in a total reaction volume of 50 µl. Annealing temperature was chosen depending on the melting temperature (Tm) of the used primer pair and the elongation time was adjusted according to the template length with 500 base pairs per minute. The standard reaction mixture was composed of:

Table 3.8 Standard PCR reaction mixture for DNA fragment amplification

Reagent	Volume [µl]
NEBNext® High-Fidelity 2X PCR Master Mix	25.0
Template DNA, 100 ng/µl	1.0
5'-Primer, 10µM	1.5
3'-Primer, 10µM	1.5
H2O	to 50.0

The PCR thermocycler Mastercycler® Nexus was used with the following program:

Table 3.9 Standard PCR programm for DNA fragment amplification

Step	Temperature [°C]	Time [min]	
1. Initial denaturation	98	5	
2. Denaturation	98	0.5	20-40 cycles
3. Annealing	45- 60	0.5	
4. Extension	72	2/kb	
5. Final extension	72	10	

After completion of the program, the reaction was stored at 4°C, visualized by agarose gel electrophoresis using a blue light LED illuminator, extracted using the GeneJET™ Gel extraction kit, and sequenced by Sanger sequencing by Microsynth Seqlab GmbH (Goettingen).

3.2.2.3 Restriction digestion of DNA

DNA digestion was conducted by using restriction endonucleases obtained from New England Biolabs. To digest 1 µg DNA, 10 units (Us) of enzyme and 1 µL of the corresponding 10x buffer were mixed and set up to a 10 µl total reaction volume. The reaction was incubated at the optimum temperature for the respective enzyme for 2 hrs.

3.2.2.4 Ligation

For ligation of PCR-amplified DNA fragments into a vector, the insert and plasmid vector were pre-digested with appropriate restriction endonucleases to create compatible ssDNA overhangs. After purification from an agarose gel using the GeneJET™ Gel extraction kit, the linearized vector and DNA insert were mixed in a 1:7 ratio in a 20 µl reaction with 1x T4 DNA ligation buffer and with 1 µl of T4 DNA ligase. The reaction was incubated for 1 h at room temperatur (RT) or at 16°C over night.

3.2.2.5 Agarose gel electrophoresis

Agarose gel electrophoresis was used to separate DNA depending on the expected DNA fragment size for analytical and preparative analysis. An agarose gel with 0,5-2% (w/v) agarose in 1x TAE buffer (40mM Tris-HCl, 0,1% acetic acid, 1mM EDTA [pH 8.3]) was casted. The agarose was melted in water in a microwave and 1 µg/ml Roti®-Safe Gel Stain was added to the fluid mixture. Afterwards, the melted agarose was poured into a gel tray with a well comb. The comb was removed after solidification of the gel. The samples were mixed with 6x DNA gel loading dye and loaded on the gel together with the GeneRuler 1kb plus DNA marker. To electrophoretically seperate the fragments, the gel was covered with TAE buffer and set to 125 volt for 20 - 30 min. Visualization of DNA was achieved with a blue light LED transilluminator and the size was determined with the loaded DNA ladder.

3.2.2.6 Purification of DNA from agarose gels

For purification of DNA fragments from agarose gels, the DNA was visualized on a blue ight LED transilluminator and the desired bands were cut out. Gel pieces were processed using the GeneJET™ Gel extraction kit according to the manufacturer's protocol. The final elution was done with 30 µl deionized water.

3.2.3 3Cs methods for CRISPR gRNA library generation

3.2.3.1 Cloning of the 3Cs multiplex vector

To clone the 3Cs multiplex vector, pLentiCRISPRv2 was digested with the restriction endonucleases AleI and BsiWI-HF® and gel purified to remove the hU6 gRNA and the Cas9 expression cassettes. The combinatorial gRNA expression cassette of pKLV2.2-h7SKgRNA5(SapI)-hU6gRNA5(BbsI)-PGKpuroBFP-W was digested with AleI and BsiWI-HF® as well. Subsequently, the 2,030 base pair (bp) fragment that encoded the combinatorial gRNA expression cassettes and a PGK promoter was gel purified and cloned into the Cas9-excised, purified backbone of pLentiCRISPRv2. In order to generate unique annealing homology sites for annealing of 3Cs oligonucleotides during 3Cs synthesis and enable template plasmid removal from the final library, the h7SK-associated tracrRNA was replaced by an optimized engineered tracrRNA sequence (tracrRNAv2) [312]. The cloning sites for gRNA integration after the h7SK and hU6 promoters were changed to placeholder sequences encoding I-CeuI and I-SceI homing endonuclease restriction sites, respectively [313].

3.2.3.2 3Cs oligonucleotide design

To discriminate between h7SK and hU6 and enable exclusive annealing to only one gRNA expression cassette, the 3Cs oligonucleotides were designed with two distinct homology sites for either the h7SK or hU6 expression cassette. The homology sites flanked the desired 20 nucleotide gRNA sequence. The 3Cs h7SK oligonucleotides were 57 nucleotides in length (Tm

above 50°C) and matched the 3' end of the h7SK promoter region and the 5' start of the tracrRNAv2. The 3Cs hU6 oligonucleotides were 59 nucleotides in length (Tm above 50°C) and matched the 3' end of the hU6 promoter region and the 5' start of the wildtype SpCas9-tracrRNA in the 3Cs multiplex vector. The oligonucleotide sequences that were used for 3Cs reactions are listed in Supp. Table S2.

3.2.3.3 Purification of single-stranded template DNA

For deoxyuridine single-stranded DNA (dU-ssDNA) template amplification, KCM competent *E. coli* K12 CJ236 cells were transformed by KCM transformation with 100 ng of the 3Cs multiplex vector and streaked out on agar plates containing ampicillin and chloramphenicol and incubated overnight at 37°C. The next morning, a single colony of transformed CJ236 cells was picked into 1 ml of 2xYT media supplemented with M13KO7 helper phage to a final concentration of $1x10^8$ pfu/ml and ampicillin to maintain the host F' episome. After 2 hrs of shaking at 200 rpm and 37°C, kanamycin was added to a final concentration of 25 mg/ml to select for the phagemid. Bacteria were kept at 200 rpm and 37 °C for additional 6 hrs before the culture was transferred to 30 ml of 2xYT media supplemented with ampicillin and kanamycin. After 20 hrs of shaking at 200 rpm and 37°C, the bacterial culture was centrifuged for 10 min at 10,000 rpm and 4°C. To precipitate phage particles, the supernatant was transferred to 6 ml (1/5 of culture volume) PEG/NaCl (20% polyethylene glycol, 2.5 M NaCl), incubated for 1 hr at RT and subsequently centrifuged for 10 min at 10,000 rpm and 4°C. The phage pellet was resuspended in 1 ml phosphate-buffered saline (PBS) and centrifuged at 13,000 rpm for 10 min, before the phage-containing supernatant was stored at 4°C. Circular dU-ssDNA was purified from the resuspended phages with the E.Z.N.A. M13 DNA Mini kit according to the manufacturer's protocol and the purified dU-ssDNA was stored at 4°C.

3.2.3.4 3Cs DNA synthesis

For synthesis of heteroduplex deoxyuridine double-stranded DNA (dU-dsDNA), 600 ng of pooled oligonucleotides were phosphorylated in a 20 µl reaction with 2 µl 10x TM buffer (0.1 M MgCl2, 0.5 M Tris-HCl, pH 7.5), 2 µl 10 mM ATP, 1 µl 100 mM DTT, and 20 units of T4 polynucleotide kinase. The mixture was incubated for 1 h at 37°C. For generation of 3Cs multiplex libraries, 600 ng of each, h7SK and hU6 oligonucleotide pools, were phosphorylated separately. Phosphorylated oligonucleotides were annealed to the circular dU-ssDNA 3Cs multiplex vector by mixing 20 µl of phosphorylation product with 25 µl 10x TM buffer, 20 µg of dU-ssDNA, and water to a total volume of 250 µl. The mixture was denatured for 3 min at 90°C, annealed for 5 min at 50°C and cooled down for 10 min at RT. Afterwards 10 µl of 10 mM ATP, 10 µl of 100 mM dNTP mix, 15 µl of 100 mM DTT, 5 µl of T4 DNA ligase (400,000 units/ml), and 3 µl of T7 DNA polymerase (10,000 units/ml) were added to the annealed oligonucleotide–ssDNA mixture. The 3Cs synthesis mix was incubated for 12 hrs (over night) at RT. The 3Cs synthesis product was then affinity purified and desalted using a the

GeneJET™ Gel extraction kit by adding 500 µl of binding buffer directly to the 3Cs synthesis reaction, before proceeding according to the manufacturer's protocol. For each 3Cs synthesis reaction two columns were used and the DNA was eluted in 50 µl pre-warmed water. The 3Cs reaction product was analyzed by gel electrophoresis along with the dU-ssDNA template on a 0.8% TAE/agarose gel (100 V, 30 min).

3.2.3.5 Electroporation of 3Cs libraries

To amplify 3Cs multiplex and single-gRNA libraries, up to 8 µg of purified 3Cs dsDNA synthesis product was electroporated into 400 µl electrocompetent 10-beta *E. coli* by using a Bio-Rad Gene Pulser (resistance 200 Ω, capacity 25 F, voltage 2.5 kV). After electroporation, cells were rescued in 25 ml of pre-warmed S.O.C. media and incubated for 30 min at 37°C and 200 rpm. After 30 min, the culture was transferred into 400 ml of LB media supplemented with 100 µg/ml ampicillin and shaken overnight at 37°C. To ensure library representation of at least 1,000-fold during and after amplification, the number of transformants was determined by preparing serial dilutions of electroporated bacteria in sterile PBS. The serial dilutions were plated in triplicates on LB agar plates containing 100 µg/ml ampicillin and incubated overnight at 37°C. The next morning, the colonies on the plates were counted and the number of transformed cells in the culture at 30 min after electroporation was calculated. The number of transformants had to be at least 100-fold higher than the library diversity to maintain the representation.

3.2.3.6 Quality control and clean-up of 3Cs libraries

the day after electroporation of 3Cs synthesis product, the plasmid DNA of overnight liquid cultures was purified using a Qiagen Plasmid Plus Maxi DNA kit according to the manufacturer's protocol to obtain the pre-library. To remove residual wild type 3Cs multiplex vector from the pre-library, 2 µg of purified pre-library DNA were digested with 4 µl of I-SceI and I-CeuI (for multiplex libraries), or either I-SceI or I-CeuI (for single-gRNA libraries) with 5 µl of 10X CutSmart® buffer in a 50 µl reaction for a total of 2 hrs at 37°C. To ensure complete removal of wild type sequences, additional 4 µl of I-SceI and I-CeuI, and 5 µl of 10X CutSmart® Buffer were added and the reaction was filled up with water to 100 µl and incubated over night at 37°C. The next day, the digestion reaction was subjected to gel electrophoresis on a 0.8% TAE/agarose gel (125 V, 40 min) to separate undigested 3Cs synthesis product from linearized template plasmid. The band corresponding to the undigested 3Cs synthesis product was purified using a GeneJET™ Gel extraction kit, according to the manufacturer's protocol. Then, 2 µg of purified 3Cs synthesis product was electroporated according to the electroporation protocol described above. The next day, the resulting final 3Cs multiplex library preparation was purified from liquid culture using a Qiagen Plasmid Plus Maxi DNA kit, according to the manufacturer's protocol and the quality was controlled by analytical restriction enzyme digests and sequencing.

3.2.3.7 Generation of artificially skewed 3Cs libraries

For the generating artificially skewed 3Cs multiplex gRNA libraries, two 3Cs oligonucleotide pools, one for each expression cassette of the 3Cs multiplex vector, were designed following the 3Cs oligonucleotide design. The first pool was composed of tumor suppressor and essential gene-targeting gRNAs, whereas the second pool only consisted of non-human targeting (NHT) gRNAs (Supp. Table S2). To generate different libraries with varying sequence distributions, the two oligonucleotide pools were mixed in different ratios with increasing NHT pool ratios (1:1, 1:10, 1:100). The mixed oligonucleotide pools were phosphorylated, annealed to purified dU-ssDNA of the 3Cs multiplex vector. Then the 3Cs synthesis reactions were performed.

3.2.4 Cell biological methods

3.2.4.1 Cultivation of mammalian cell lines

Human embryonic kidney (HEK) 293T cells were maintained in Dulbecco's modified Eagle's medium (DMEM), and hTERT-RPE1 and puromycin-sensitive hTERT-RPE1 cells were maintained in DMEM Nutrient Mixture F-12 (DMEM F12), each supplemented with 10% fetal bovine serum (FBS) and 1% penicillin-streptomycin at 37°C with 5% CO_2. In addition, hTERT-RPE1 cells were supplemented with 0.01 mg/ml hygromycin B. No method to ensure the state of authentication has been applied. Mycoplasma contamination testing was performed immediately after the arrival of the cells and multiple times during the course of the experiments. Cells were passaged every three days and maintained at 20-60% confluency. For passaging, the medium was aspirated, cells were washed twice with sterile phosphate-buffered saline (PBS) and Trypsin-EDTA 0.5% was added to detach cells from the plate. The detached cells were resuspended in fresh medium, counted, diluted as required and seeded into a fresh dish. Cell counting was done using a TC20™ Automated Cell Counter.
For long-term storage, cells were diluted in their appropriate medium without antibiotics containing 10% dimethyl sulfoxide (DMSO) and 20% FBS and transferred into cryogenic tubes. The tubes were frozen at -150°C. To thaw cells, they were put 37°C in a water bath, then resuspended in medium and centrifuged at 1000 rpm for 2 min at RT to remove the DMSO. Lastly, cells were resuspended in their respective medium and cultured as described above.

3.2.4.2 Transfection of mammalian cells

For transfection, for example HEK 293T cells were seeded to 5×10^5 cells/ml. The next day, a transfection mixture was prepared, consisting of DNA and Lipofectamin 2000 transfection reagent at a ratio of 1:3, and 200 µl Opti-MEM. The transfection mixture was incubated for 30 min and then added in a dropwise manner onto the cells. After 24 hrs the medium was changed to regular growth medium.

3.2.4.3 Production of lentiviral supernatant

Lentiviral supernatant was produced by transfecting HEK 293T cells plated in 6, 10 or 15 cm dishes, depending on the required scale, with the following transfection mixtures:

Table 3.10 Transfection mixture for lentiviral supernatant production

cell culture volume	2 ml	10 ml	20 ml
plasmid DNA	3.3 µg	16.5 µg	33.0 µg
pMD2.G	1.0 µg	5.0 µg	10.0 µg
psPAX2	2.7 µg	13.5 µg	27.0 µg
Lipofectamine 2000	21.0 µl	105.0 µl	210.0 µl
Opti-MEM	0.2 ml	1.0 ml	2.0 ml

After 30 min of incubation at RT, the mixture was added onto the cells. The next morning, the transfection medium was replaced with fresh DMEM (10% FBS, 1% PS) medium to remove the transfection reagent. Lentiviral supernatant was harvested 48 hrs after transfection, pooled, aliquoted and stored at -80°C.

3.2.4.4 Determination of lentiviral titer

To determine the lentiviral titer, hTERT-RPE1 cells were plated in a 6-well plate with 50,000 cells per well. The following day, cells were transduced with 8 µg/ml polybrene and a series of 0.5, 1, 5, and 10 µl of viral supernatant. After 2 days of incubation at 37°C, cells were subjected to 2.5 µg/ml puromycin selection for 2 weeks. After 2 weeks, established colonies were counted for each viral dilution. The number of colonies in the highest dilution was then normalized to the volume for obtaining the final lentiviral titer.

3.2.4.5 Lentiviral transduction

To transduce hTERT-RPE1 cells, they were seeded at an appropriate density for each experiment with a maximal confluency of 60 - 70%. On the day of transduction, polybrene was added to the media to a final concentration of 8 µg/ml. The volume of lentiviral supernatant was calculated on the basis of pre-determined lentiviral titer and the number of plated cells to achieve MOI of 0.5. The next morning, the medium was replaced with fresh media and the cells were subjected to antibiotic selection or experimental analysis.

3.2.4.6 Generation of monoclonal cell lines

To generate monoclonal cell lines, transduced cells were selected with the appropriate antibiotic. After selection, cells were plated in 96-well plates with 0.5 cells per well. Single clones were expanded and positive clones were confirmed by FACS.

3.2.4.7 Arrayed validation of autophagy flux blockage

The validation of single and combinatorial autophagy hits was performed in arrayed conditions (one hit gene or hit gene combination per well). To this end, single and dual gene-targeting CRISPR constructs were designed and generated. For each gene, the top scoring guide sequence was selected with Azimuth 2.0 of the GPP sgRNA Designer [102] and purchased as forward and reverse oligonucleotides with compatible overhangs for restriction endonuclease cloning (Supp. Table S2). The two oligonucleotides encoding the gRNAs were annealed and cloned into the restriction enzyme-digested and gel purified vector lenti-sgRNA blast or pKLV2.2-h7SKgRNA5(SapI)-hU6gRNA5(BbsI)-Blast by BbsI and SapI cloning (Table 3.3). After cloning, correct gRNA integration was verified by SANGER sequencing with Microsynth Seqlab GmbH (Goettingen). Next, lentiviral supernatant was generated for each construct as described before. Monoclonal hTERT-RPE1 cells with stable SpCas9 and GFP-LC3-RFP autophagy flux reporter expressions were plated in 6-well plates with 50,000 cells per well. The following day, cells were transduced with lentiviral supernatant with 8 µg/ml polybrene. After 48 hours, the cells were selected with 10 µg/ml blasticidin for 7 days, passaged and cultivated at 40-60% confluency under constant blasticidin selection for additional 7 days. At day 13, cells were treated with Torin1 to induce autophagy for 24 hours. At day 14 they were collected and subjected to FACS to measure single or dual gene knockout-induced autophagy blockage.

3.2.4.8 Tide assay

Guide RNA performance was evaluated by tracking of Indels by decomposition (TIDE) assay, as described previously [314]. For each gRNA sequence, PCR primers flanking the gRNA annealing site around 400 bp upstream and downstream were designed, resulting in a PCR product of 800 to 1,000 bp in length. The area around the gRNA locus was PCR amplified with OneTaq DNA polymerase, using 1 µg of genomic DNA, 40 µM dNTPs (final concentration), 0.2 µM of each forward and reverse primer, 1x OneTaq standard buffer, and 2.5 units of OneTaq DNA polymerase. PCR conditions were used as described above. The PCR products were analyzed on a 0.8% TAE/agarose gel (100 V, 30 min) and purified using a GeneJET™ Gel extraction kit according to the manufacturer's protocol. The purified PCR product was pre-mixed with forward amplification primer and processed by Sanger sequencing by Microsynth Seqlab GmbH (Goettingen). Afterwards, wild type and gRNA-treated Sanger chromatograms were analyzed by TIDE and the percentage of unedited DNA was extracted (https://tide.nki.nl/) [314].

3.2.4.9 RNA-seq

Monoclonal RPE1(Cas9) cells were harvested at 90% confluency and total RNA was purified using the QIAGEN RNeasy Plus Mini Kit, according to the manufacturer's protocol. RNA was stored at -80°C and analyzed by RNA-Seq in quadruplicates. For library preparation, total RNA was quantified using the Qubit 2.0 fluorometric assay (Thermo Fisher Scientific). Sequencing libraries were prepared from 125 ng of total RNA using a 3'DGE mRNA-seq research grade

sequencing service (Next Generation Diagnostics srl) which included library preparation, quality assessment and sequencing on a NovaSeq 6000 sequencing system using a single-end, 100 cycle strategy (Illumina Inc.) [315]. he bioinformatics workflow included analysis of raw data by Next Generation Diagnostics srl proprietary 3'DGE mRNA-seq pipeline (v2.0) which involves a cleaning step by quality filtering and trimming, alignment to the reference genome and counting by gene [316–318]. We filtered out all genes having < 1 cpm in less than n-min samples and Perc MM reads $> 20\%$ simultaneously. Differential expression analysis was performed using edgeR (Supp. Table S8) [319].

3.2.5 Pooled CRISPR screening

3.2.5.1 Calculating the cell number for pooled screening

To determine the required number of cells for pooled CRISPR screening the diversity of the respective library was multiplied by the desired coverage and divided by 0.5 for an MOI of 0.5.

3.2.5.2 Proliferation screens with artificially skewed libraries

To explore the interdependence of the multiplex CRISPR library distribution and the screening coverage in pooled screens, three artificially skewed 3Cs multiplex libraries were generated that represented libraries of different gRNA distributions (described in section 3.2.3.7). All three libraries were screened with a 20-fold and 200-fold coverage, each in triplicates. For the 20-fold screening, for each replicate, 1.1 million SpCas9-expressing hTERT-RPE1 cells were plated (0.37 million cells per flask) and transduced with the respective library with an MOI of 0.5. After 48 hours, cells were selected with 2.5 µg/ml puromycin and kept in growing conditions for 14 days. At day 14, cells were harvested, pooled and stored at -20°C until their genomic DNA was extracted and processed for sequencing. For the 200-fold screening, a total of 11 million (0.5 million cells per flask) SpCas9-expressing hTERT-RPE1 cells were plated and transduced with the respective library with an MOI of 0.5. Further screening was performed identically to the 20-fold screen.

3.2.5.3 Autophagy proliferation screen

Pooled single-gRNA and combinatorial autophagy proliferation screens were performed in biological duplicates in the monoclonal RPE1 cell line stably expressing SpCas9 and the autophagic flux probe [307]. For each replicate, 20 million cells (10 million for each, end time point and day 2 control) were transduced with lentiviral supernatant of the autophagy multiplex library with an MOI of 0.5 and a 1,000- or 20-fold library coverage for single or combinatorial autophagy library screening, respectively. The control time points were harvested 2 days after transduction. The remaining cells were kept in growing conditions until day 7, when the cells were passaged, pooled and reseeded at maintaining the initial library coverage. On day 14 all

cells were harvested, pooled, aliquoted and stored at -80°C until genomic DNA was extracted for sequencing sample preparation.

3.2.5.4 Autophagy flux screen

Pooled single-gRNA and combinatorial autophagy flux screens were performed in biological triplicates in the monoclonal RPE1 cell line stably expressing SpCas9 and the autophagic flux probe [307]. Transduction and passaging of cells until day 13 was performed identical to the autophagy proliferation screen. On day 13, 14 and 15, the cells were treated with Torin 1 for 24 hrs to induce autophagy. After 24 hrs of treatment, cells were collected in three separate batches per day, and FACS-sorted on a FACSCanto II flow cytometer to enrich cells with blocked autophagy. Gating was carried out on the basis of viable and single cells that were identified on the basis of their scatter morphology. In total, for the single-gRNA screen 150,000 - 300,000 cells with blocked autophagy were collected across all replicates. For the combinatorial screening 4.5 - 6.75 million cells with blocked autophagy were collected across all replicates. After sorting, cells were reseeded and expanded for seven days before harvesting, pooled and stored at -20°C until their genomic DNA was extracted and processed for sequencing.

3.2.6 Sequencing sample preparation and sequencing

3.2.6.1 Sequencing sample preparation of 3Cs plasmid libraries

Sample preparation for sequencing of plasmid libraries 3Cs multiplex plasmid libraries were prepared for sequencing as follows: 250 ng of plasmid DNA were used per PCR reaction in a final volume of 50 µl, containing 25 µl Next High-Fidelity 2x PCR Master Mix (New England Biolabs) and 2.5 µl of each 10 µM primer. Depending on the library complexity, up to four 50 µl reactions were performed. Primer sequences are listed separately (Supp. Table S2). Thermal cycler parameters were set as follows: initial denaturation at 98°C for 5 min, 15 cycles of denaturation at 98°C for 30 s, annealing at 65°C for 30 s, extension at 72°C for 40 s, and final extension at 72°C for 5 min. PCR products were purified from a 1.5% TAE/agarose gel using a GeneJET™ Gel extraction kit, according to the manufacturer's protocol.

3.2.6.2 Sequencing sample preparation of of screen samples

Sample preparation for sequencing of screen samples To prepare samples derived from screens for subsequent sequencing, the required amount of genomic DNA for sufficient coverage was calculated first. For the autophagy single and multiplex FACS samples, the amount of required genomic DNA was calculated as the number of FACS sorted cells x screening coverage x 6.6 pg. For the autophagy multiplex proliferation control samples, the amount of required genomic DNA was determined by calculating the library complexity x screening coverage x 6.6 pg. For samples derived from screening with the biased libraries, the amount of required genomic DNA

was calculated as the library complexity x 200 (maximum screening coverage) x 6.6 pg DNA. The calculated amount of genomic DNA was used in the first PCR reaction (PCR1) with 2 - 4 µg of genomic DNA per 50 µl final reaction, using the Next High-Fidelity 2x PCR Master Mix (New England Biolabs) and 2.5 µl of each 10 µM PCR1 primer. Thermal cycler parameters were set as follows: initial denaturation at 98°C for 5 min, 15 cycles of denaturation at 98°C for 55 s, annealing at 65°C for 55 s, extension at 72°C for 110 s, and final extension at 72°C for 7 min. After PCR1, 25 µl of PCR1 product was transferred to a second PCR reaction (PCR2) in a 100 µl reaction with 50 µl High-Fidelity 2x PCR Master Mix and 5 µl of 10 µM PCR2 primers containing Illumina adaptors and barcodes. Primer sequences for PCR1 and PCR2 are listed in Supp. Table S2. Thermal cycler parameters were set as follows: initial denaturation at 98°C for 5 min, 10 cycles of denaturation at 98°C for 30 s, annealing at 65°C for 30 s, extension at 72°C for 40 s, and final extension at 72°C for 5 min. PCR products were purified from a 1.5% TAE/agarose gel and processed for sequencing as described for plasmid libraries.

3.2.6.3 Sequencing

Unless otherwise specified, all DNA sequencing experiments were performed with Illumina technology. Gel-purified PCR products of plasmid libraries or screening samples were denatured and diluted according to Illumina guidelines and set to a final concentration of 2.6 pM in a total volume of 2.2 ml and 15% PhiX control and loaded onto a MiSeq, NextSeq500 or NovaSeq sequencer (Illumina) depending on required read counts (500- to 1,000-fold sequencing depth), according to the manufacturer's protocol. Sequencing was performed with single- or paired-end reads, 75 or 150 cycles, respectively, plus 8 cycles of index reading.

3.2.7 Bioinformatical methods

3.2.7.1 Read count table generation

Raw sequencing data were processed and demultiplexed with bcl2fastq v2.19.1.403 (Illumina). Read counts of individual gRNAs and gRNA combinations were determined using cutadapt 2.8, Bowtie2 2.3.0, and custom Python 3 scripts [310, 311]. Reads were trimmed with cutadapt using 5' adapter sequences, truncated to 20 nucleotides, and aligned to the respective gRNA library using Bowtie2 with no mismatches allowed.

3.2.7.2 Assessment of uniformity of library distributions

The uniformity of each library distribution was assessed by plotting the cumulative distribution of all sequencing reads as a Lorenz curve and determining the area under the curve (AUC). The library distribution skew of each library was determined by plotting the density of read counts and dividing the 90th percentile by the 10th percentile.

3.2.7.3 Cohen's D statistics quality score (QS)

We applied Cohen's d statistics to assess the quality score (QS) of biased library screening performance by measuring the separation of mean LFC values of non-targeting sequences and sequences targeting core essential genes: QS = ((mean LFC of NHT combinations) - (mean LFC of essential combinations)) / (standard deviation (LFC of essential combinations)) [320].

3.2.7.4 Pairwise sample correlations

Pairwise sample correlations were determined with Pearson's correlation of the normalized read counts and visualized with hierarchically clustered heat maps using the Seaborn library 0.10.1 [321].

3.2.7.5 Enrichment analyses

Enrichment analyses using MAGeCK were performed with median or total normalization of read counts with gRNAs having zero counts in the control samples being removed [127]. Down-sampling of the 1:1 dataset was performed by randomly choosing 1–16 gRNA combinations per gene combination without replacement followed by individual MAGeCK analyses to obtain false discovery rate (FDR) and delta log2-fold change (dLFC). gRNA combinations with an FDR $\leq$ 10% and LFC $\leq$ -0.5 were counted as statistically significant hits.

3.2.7.6 Genetic interaction models

GIs were computed according to five established models: SUM, MIN, LOG, MULT [6], and additionally the MAX model was included. Each model assigned a GI to a gene pair xy, if the double mutant phenotype W(xy), deviated from a predicted double mutant phenotype that is expected for no interaction between x and y, E(xy). The phenotype was measured as the LFC of gRNA abundance between respective samples. The expected double mutant phenotype for joint mutations of the genes x and y was defined by the neutrality function of each definition with MIN = min(W(x), W(y)), MULT = (W(x) $\times$ W(y)), LOG = $\log_2[(2^{W(x)} + 1) \times (2^{W(y)} - 1) + 1]$, SUM = (W(x) + W(y)), and MAX = max(W(x), W(y)). The single mutant phenotype for a gene x was defined as the median LFC of all gRNA combinations of NHTs and gRNAs targeting x. For each model, the deviation of observed double mutant phenotypes from their expectation was calculated as their difference and termed dLFC: dLFC = observed – expected. To select the best model for our data, we assumed that GIs were rare for randomly selected gene pairs. Density plots of the dLFC for each model were used to identify the model with the highest number of neutral interactions, indicated by a single large peak around 0 on the x-axis. We kept only combinations with P $\leq$ 0.05 and a dLFC larger than the standard deviation (SD) of all dLFCs. To generate the GI heatmap of core autophagy paralogs, we used MAX model-derived GIs with dLFC $>$ 0 and LFC $>$ 0. Since possible combinations of two genes x

and y are x–y or y–x and both were assumed to show the same phenotype, we averaged xy, yx pairs.

3.2.7.7 Genetic interaction network

To generate a network visualization based on the MAX model-derived autophagy gene interactions, we exported dLFC for all gene interactions and imported them into the open source software platform Cytoscape (3.8.0) [322]. The style of the derived network was manually arranged.

3.2.7.8 Lung squamous cell carcinoma patient survival analysis

Kaplan–Meier curves for lung squamous cell carcinoma (LUSC) patient five-year overall survival rates were estimated with the online tool KM plotter (https://kmplot.com) based on GEO, EGA and TCGA datasets [323–326]. KEAP1 and ATG7 gene expression data were obtained from GEO, caBIG and TCGA databases. Using the KM plotter online tool, patients were split using the option 'Auto select best cutoff' in high or low KEAP1, ATG7 or KEAP1 and ATG7 gene expression groups. The following cutoff values were used: ATG7: 401, KEAP1: 846, KEAP1 and ATG7: 562. P values for log rank tests of the Kaplan–Meier curves were calculated with the KM plotter.
Survival of LUSC patients was analyzed by obtaining ATG7-KEAP1 gene expression data from TCGA in the UCSC Xena online tool [327, 328]. LUSC patients were classified into four categories depending on ATG7 and KEAP1 gene expression in tumors: (i) high expression of ATG7 and KEAP1; (ii) high expression of ATG7 and low expression of KEAP1; (iii) high expression of KEAP1 and low expression of ATG7; 4) low expression of ATG7 and KEAP1. Expression of ATG7 or KEAP1 was defined as high (low) when the respective expression levels were higher (lower) than the median expression levels in all LUSC tumors. Overall survival of a single patient was normalized to the median overall survival of all patients and the median survival were calculated for the previously described 4 groups. R^2 linear regression was calculated using Microsoft Excel.

Results

4.1 Generating combinatorial gRNA libraries by 3Cs multiplexing

4.1.1 Vector design and principles of 3Cs multiplexing

To facilitate GI screening, we expanded our previously reported 3Cs technology for generation of single-gRNA libraries to generating combinatorial gRNA libraries [112]. In contrast to single gRNA-expressing 3Cs libraries, for which commercially available CRISPR vectors can be used, combinatorial pooled gRNA libraries generated by 3Cs multiplexing required cloning of a 3Cs-compatible multiplex CRISPR vector that provided two gRNA expression cassettes with unique homology sites.

The lentiviral 3Cs multiplex vector was cloned by introducing two gRNA expression cassettes into the Cas9-excised lenti-CRISPRv2 vector [308] (Figure 4.1 A). The first expression cassette employed an h7SK and an engineered Cas9-tracrRNA variant (tracrV2) [312]. The second gRNA expression cassette used an hU6 promoter followed by the wild type Cas9-tracrRNA sequence (tracrWT) [329] (Figure 4.1 A). Additionally, we introduced gRNA placeholder sequences, which encoded I-CeuI and I-SceI restriction enzyme sites, respectively, into both gRNA expression cassettes (Figure 4.1 A). Furthermore, the 3Cs multiplex vector encoded a puromycin resistance gene that enabled selection of transduced mammalian cells during the screen (Figure 4.1 A).

3Cs multiplex gRNA library generation was based on *Kunkel mutagenesis* and comprised three essential protocol steps (Figure 4.1 B): first, the generation of dU-ssDNA of the 3Cs multiplex vector; second, the synthesis of heteroduplex 3Cs dU-dsDNA; and third, the amplification of the heteroduplex 3Cs dU-dsDNA and a clean-up step that ensured minimal wild type vector contamination in the final gRNA library (Figure 4.1 B).

For dU-ssDNA generation, the 3Cs multiplex vector was transformed into CJ236 electrocompetent bacteria harboring mutations in the genes encoding uracil-DNA glycosylase (dut^-) and uracil-DNA glycosylase (ung^-), thus leading to increased deoxyuridine triphosphate (dUTP) incorporation into the plasmid DNA [330]. Importantly, the vector encoded an f1 origin of replication (f-ori) for dU-ssDNA replication and packaging into phage particles. Super-infection of a single-colony CJ236 culture with M13KO7 bacteriophage allowed purification of dU-ssDNA of the wild type 3Cs multiplex vector (Figure 4.1 B).

In an *in vitro* 3Cs dU-dsDNA synthesis, two distinct oligonucleotide pool were annealed to the wild type dU-ssDNA. The oligonucleotide pools encoded up to hundreds of thousands of distinct gRNAs depending on the desired *library diversity*. Each gRNA was flanked with 5- and 3-prime homology arms complementary to either the h7SK promoter and tracrV2, or to the hU6 promoter and the tracrWT, respectively, and thereby specified their integration site into the 3Cs multiplex vector. Since the design of the dual gRNA expression cassettes provided unique homology sites, the two oligonucleotide pools selectively annealed to one expression cassette to ensure high 3Cs reaction efficiencies at both sites. The annealed oligonucleotides were subsequently extended with T7 DNA polymerase and ligated with T4 DNA ligase. The resulting heteroduplex dU-dsDNA contained one wild type DNA strand with deoxyuridine (dU) and the complementary dU-free DNA strand harboring the newly integrated gRNA combinations (Figure 4.1 B).
To obtain the final combinatorial CRISPR library, the 3Cs dU-dsDNA synthesis product was electroporated into dut/ung-positive bacteria. Lastly, remnants of the 3Cs multiplex wild type vector were removed in a clean-up step by digestion with I-CeuI and I-SceI restiction enzymes. Thereby, wild type plasmids were linearized while plasmids in which the enzyme restriction site was replaced by gRNA sequences remained undigested. Upon subsequent electroporation, linearized wild type plasmids were removed and gRNA containing plasmids were amplified by bacteria. The resulting multiplex gRNA library contained all possible gRNA combinations encoded in the two oligonucleotide pools (Figure 4.1 B).

3Cs multiplexing circumvented conventional gRNA library generation steps, namely sequential cloning steps of PCR-amplified single gRNAs that pose possible sources for introducing a distribution bias. Therefore, we hypothesized that 3Cs multiplexing would enable generating highly diverse and uniformly distributed combinatorial gRNA libraries.

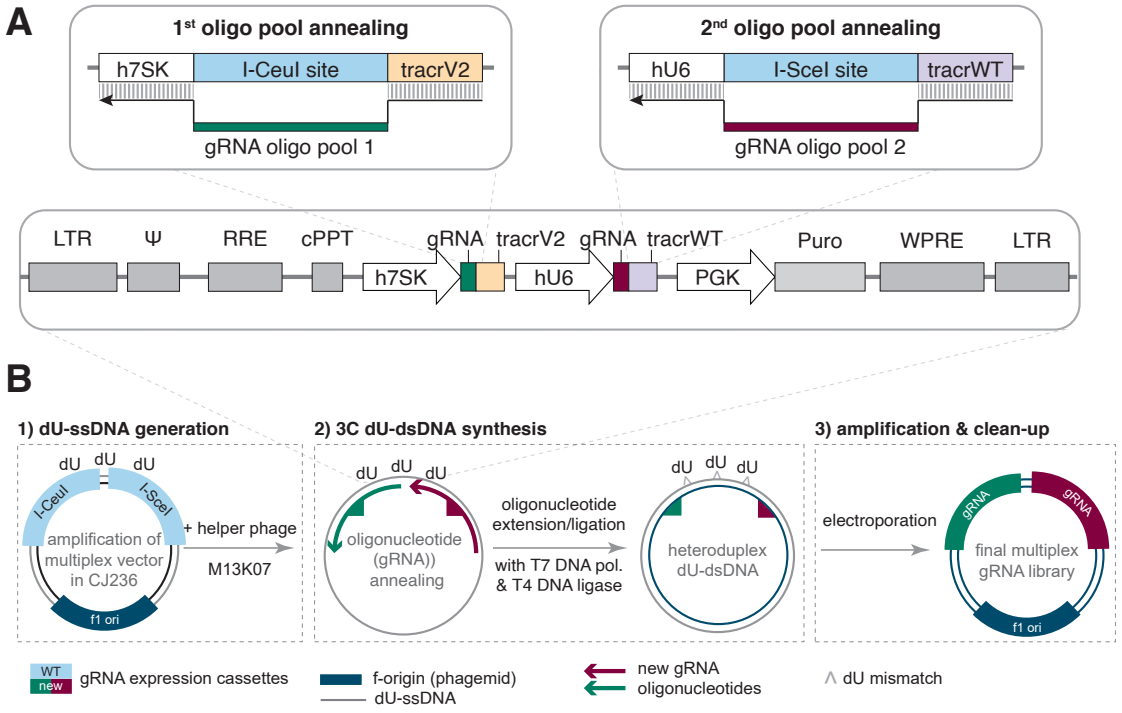

Figure 4.1: Vector design and workflow of 3Cs multiplexing

A) 3Cs multiplex vector design. The lentiviral 3Cs multiplex vector contains two expression cassettes. The first cassette consists of a human 7SK (h7SK) promoter and an engineered Cas9-tracrRNA variant (tracrV2). The second cassette employs a human U6 (hU6) promoter and the wild type Cas9-tracrRNA (tracrWT). Both cassettes provide unique homology sites for selective annealing of two distinct gRNA-encoding oligonucleotide (oligo) pools and contain gRNA placeholder sequences encoding an I-CeuI or I-SceI restriction site, respectively. Additionally, a puromycin (Puro) gene is expressed by a PGK promoter. B) 3Cs multiplexing workflow. First, the wild type (WT) 3Cs multiplex vector is amplified in CJ236 bacteria that incorporate deoxyuridine (dU) into their plasmid DNA. The vector-encoded f1 origin of replication (f-ori) allows deoxyuridine single-stranded DNA (dU-ssDNA) replication and packaging into phage particles by super-infection of a single colony of transformed CJ236 cells with helper phage M13K07. Subsequently, phages and their dU-ssDNA are purified. Next, in the 3Cs reaction, the purified dU-ssDNA is annealed to two oligonucleotides pools encoding all library gRNAs. The pools are designed with unique homology arms to selectively anneal to either the h7SK or the hU6 cassette (green/red triangles). The annealed oligonucleotides are extended with T7 DNA polymerase (pol.) and ligated with T4 DNA ligase. The resulting heteroduplex deoxyuridine double-stranded DNA (dU-dsDNA) consists of a dU-containing WT strand (grey) and a mutated strand encoding all possible combinations of the gRNAs (blue). Lastly, the purified 3Cs dU-dsDNA synthesis product is electroporated into bacteria for amplification and remnants of the WT vector are destroyed by digestion with I-CeuI and I-SceI restriction enzymes.

4.1.2 3Cs multiplexing enables combinatorial gene knockouts in human cells

To investigate the functionality of the 3Cs multiplex vector and to ensure efficient gRNA expression from both cassettes, we designed two gRNA-encoding oligonucleotide pools each containing 50 gRNA sequences targeting a green fluorescent protein (GFP) or mCherry, respectively (Supp. Table S2). While the GFP pool was designed for annealing to the h7sk promoter and tracrV2 scaffold, the mCherry pool annealed to the hU6 promoter and tracrWT. We used both pools in combination to generate a multiplex gRNA library comprising 2,601 gRNA combinations (50 GFP/mCherry gRNAs + wild type I-CeuI/I-SceI sequences: 51x51) that simultaneously target GFP and mCherry genes. Additionally, we generated the respective single-gRNA CRISPR libraries.

Gel electrophoresis of the 3Cs synthesis products of multiplex and single-gRNA libraries showed the typical three-banded pattern of the heteroduplex 3Cs dU-dsDNA (Figure 4.2 A). The upper band of the 3Cs products indicated strand-displaced DNA, the middle band corresponded to nicked DNA resulting from incomplete ligation, and the lower band showed the extended and ligated dU-dsDNA [330]. Due to its higher mobility, the single-stranded 3Cs multiplex vector runs faster than the double-stranded form [331](Figure 4.2 A).

After amplification of final 3Cs synthesis products by bacteria, remnants of non-mutated wild type 3Cs multiplex plasmids were digested with I-SceI and I-CeuI restriction enzymes and removed upon subsequent second electroporation. An analytical digestion of the final libraries with I-CeuI and I-SceI restriction enzymes confirmed minimal remnants of wild type 3Cs - multiplex plasmids (Figure 4.2 B).

Sequencing confirmed the presence of all gRNAs or gRNA combinations for all three libraries (100% completeness), and uniform library distributions indicated by low distribution skews of 1.56 (GFP single), 1.17 (mCherry single), and 1.53 (GFP+mCherry multiplex) (Figure 4.2 C), Supp. Table S3). The area under the curve (AUC) value is a second measure for library uniformity [102, 175]. In line with this, the AUC values of the GFP and mCherry single-gRNA and the multiplex libraries ranged from 0.62 to 0.75 based on the obtained sequencing depths (Supp. Figure S1 A-B).

To test if the 3Cs libraries efficiently induced knockouts in human cells, they were packaged into lentiviral particles and transduced into hTERT-RPE1 cells expressing Cas9, GFP and mCherry. The combinatorial GFP+mCherry gRNA library induced the simultaneous reduction of GFP and mCherry fluorescence while both single libraries selectively reduced either GFP or mCherry fluorescence (Figure 4.2 D).

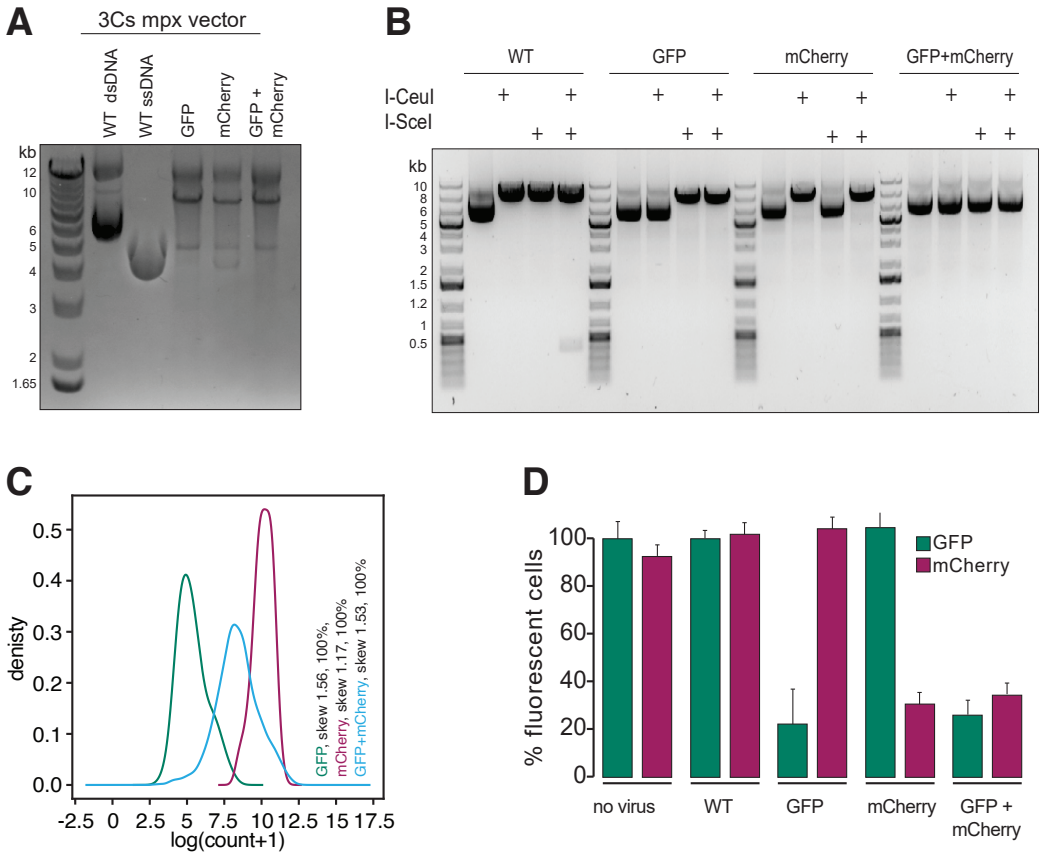

Figure 4.2: Combinatorial GFP-mCherry knockout by 3Cs multiplexing in human cells
A) Gel electrophoresis of wild type (WT) double-stranded DNA (dsDNA) and single-stranded DNA (ssDNA) of the 3Cs multiplex (mpx) vector, and the heteroduplex 3Cs deoxyuridine double-stranded DNA (dU-dsDNA) of the single-gRNA GFP and mCherry, and the multiplex GFP+mCherry libraries. Kb: Kilobase. B) Analytical restriction digestion ensured the 3Cs gRNA library quality. Digested bands indicate WT plasmid sequences. The single-gRNA GFP- and mCherry libraries contain the WT placeholder sequences encoding I-CeuI or I-SceI restriction sites in the hU6 or h7SK cassette, respectively and are therefore linearized with one enzyme. C) Sequencing of all three 3Cs CRISPR libraries confirmed complete library diversity (100%) and distribution skews of 1.56 (GFP), 1.17 (mCherry) and 1.53 (GFP-mCherry). D) Transduction of hTERT-RPE1 cells that express Cas9, GFP and mCherry with lentiviral packed 3Cs CRISPR libraries results in the reduction of only GFP or mCherry fluorescence for both single-gRNA libraries, and in simultaneous reduction of GFP and mCherry signal for the 3Cs multiplex gRNA library.

4.1.3 3Cs multiplexing generates diverse libraries with uniform distributions

To determine how the *library diversity* affects the *library distribution* of 3Cs multiplex libraries, we generated four randomized libraries with increasing diversity by using degenerated oligonucleotide pools in 3Cs reactions. The degenerated oligonucleotide pools encode a NHT-gRNA sequence with either one, two, three or four randomized bases (pool 1N, 2N, 3N and 4N) that can contain any of the four bases and were designed for annealing to both expression cassettes of the 3Cs multiplex vector (Supp. Table S2). Their application in separate 3Cs reactions generated four libraries with increasing diversities with 4x4=16 (1N), 4^2x4^2=256 (2N), 4^3x4^3=4,096 (3N) and 4^2x4^2=65,536 (4N) combinations. Additionally, we generated two non-randomized multiplex libraries, which contained approximately 247,000 and 913,000 different gRNA combinations (Supp. Table S2). We compared the distributions of all libraries by sequencing and confirmed their uniform distributions indicated by AUC values between 0.59 and 0.7 (Figure 4.3), values most often unmatched even for single-gRNA libraries. Sequencing of the libraries confirmed sufficient sequencing depth (Supp. Figure S1 C), and library distribution skews ranging from 1.1 to 1.49 for the randomized gRNA libraries, and 6.02 for the multiplex gRNA library with 913,000 gRNA combinations (Supp. Figure S1 D, Supp. Table S4).

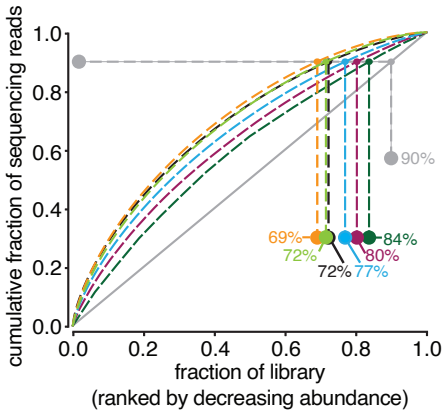

	AUC	combin.
ideal	0.5	
1N	0.59	16
2N	0.63	256
3N	0.66	4,096
4N	0.69	65,536
mpx A	0.7	247,032
mpx B	0.68	913,000

Figure 4.3: Distribution analysis of multiplex libraries with increasing library diversity
The library distribution of six multiplex libraries with increasing library diversity was analyzed by sequencing and is indicated as area under the curve (AUC) values. Four libraries were generated with degenerated oligonucleotide pools with one (1N), two (2N), three (3N) or four (4N) randomized bases, thus generating increasing library diversity ranging from 16 to 65,536 gRNA combinations. Two non-randomized multiplex libraries (mpx A, B) contained approximately 247,000 and 913,000 gRNA combinations. As a reference, a perfectly distributed library (ideal) is shown in grey. Percentages indicate library representations at 90% of cumulative reads. AUC values are indicated next to each library identifier. All libraries showed AUC values $\geq$ 0.7.

4.2 Minimizing the screening conditions for 3Cs multiplex screens

4.2.1 The gRNA library distribution determines the required coverage

Pooled CRISPR screens have been performed at screening coverages of 500- to 1000-fold [76, 114]. However, published guidelines provided no precise indications for selecting an appropriate coverage and do not account for the *library distribution* of the initial plasmid library. We aimed at experimentally investigating to what extent the *library distribution* contributes to hit detection accuracy in CRISPR proliferation screens at different coverages. Therefore, we generated three different libraries with intentionally increasing distribution skews and compared their performance at screening coverages of 20-fold and 200-fold.

To generate libraries with artificially skewed distributions, we designed two oligonucleotide pools (Figure 4.4 A). For the first pool (target pool) we selected a panel of 20 genes comprising 10 core essential and 10 tumor-suppressor genes [113], each targeted by 4 gRNAs, resulting in 80 distinct gRNA sequences (Supp. Table S2). The second pool (NHT pool) consisted of 80 pre-validated NHT gRNA sequences that served as internal negative controls in the proliferation screen [102, 109] (Supp. Table S2). The gRNA sequences in both pools were provided with homology arms for annealing to the h7SK and hU6 expression cassette of the 3Cs multiplex vector, therefore, each pool contained a total of 160 oligonucleotides (Figure 4.4 A). Both oligonucleotide pools were combined in equimolar ratios to generate a gRNA library with a uniform *library distribution* and low distribution skew (library 1:1), and in ratios of increasing NHT sequence molarity for the libraries 1:10 and 1:100 with less uniform *library distributions* and underrepresented target pool sequences compared to NHT sequences (Figure 4.4 B).

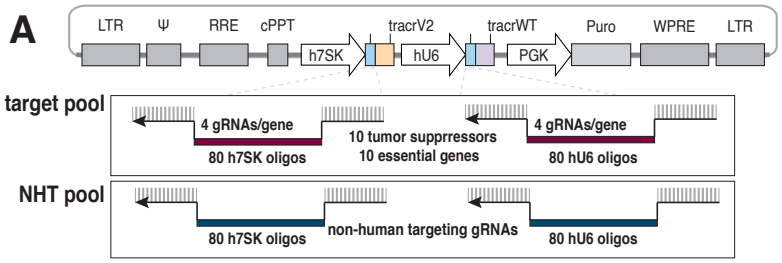

B

	oligo pool ratios	
library	target pool	NHT pool
1:1	1 :	1
1:10	1 :	10
1:100	1 :	100

Figure 4.4: Generation of multiplex 3Cs libraries with artificially skewed distributions
A) Design of two oligonucleotide (oligo) pools. The target pool encodes gRNAs targeting 10 human essential genes and 10 tumor suppressor genes with 4 gRNAs per gene (80 gRNAs). Each gRNA sequence was extended by homology arms to the h7SK and hU6 expression cassette resulting in 160 oligo sequences in the target pool. The non-human targeting (NHT) pool encodes 80 pre-validated control gRNA sequences for annealing to both expression cassettes (160 oligos in total). B) Oligonucleotide pool ratios for 3Cs synthesis. For three separate 3Cs reactions, the target and NHT oligonucleotide pools were mixed at different ratios (1:1, 1:10, and 1:100) of increasing NHT sequence molarity resulting in 3Cs multiplex libraries with variable representations of target gRNA sequences.

Sequencing analysis of the three libraries with artificially skewed distributions revealed an AUC value of 0.65 for library 1:1 , while the 1:10 and 1:100 libraries showed increased AUC values of 0.85 and 0.9, respectively (Figure 4.5 A, Supp. Table S5). Moreover, sequencing confirmed that the distribution skews increased from 1.2 (library 1:1) to 2.4 (library 1:10) and 13.46 (library 1:100) (Figure 4.5 B). For library 1:100, with the highest distribution skew, sequencing analysis could not confirm the presence of all supposed 25,600 gRNA combinations of the library, although the same sequencing depth was used as for the other two libraries. This confirmed the under-representation of target gRNA sequences in the 1:100 library.
Sequencing analysis further confirmed an increased fraction of NHT reads in the 1:10 and 1:100 libraries based on obtained sequencing depths (Supp. Figure S2 A-B, Supp. Table S5). Since the *library distribution* of all three libraries resembled the oligonucleotide pool ratios used for 3Cs reactions, sequencing results of the three libraries demonstrated that the *library distribution* of 3Cs reactions is primarily determined by the sequence distribution of the oligonucleotide pools.

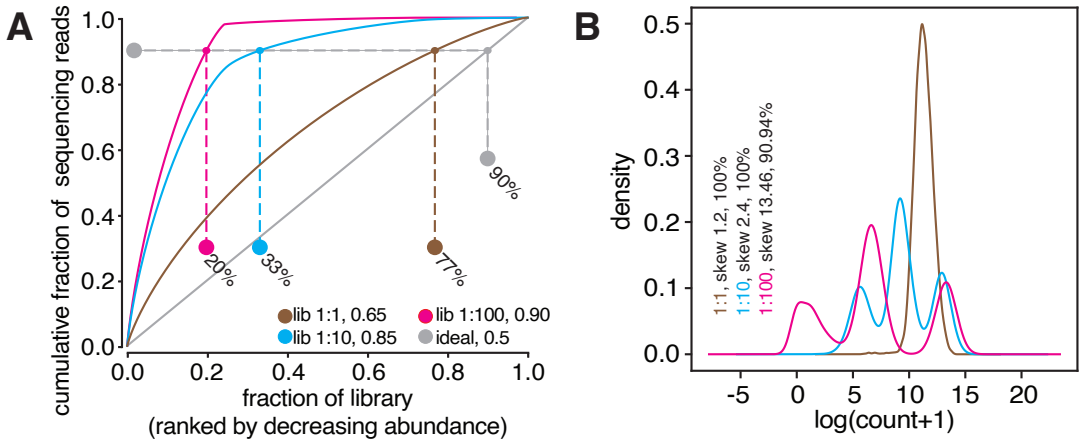

Figure 4.5: Sequencing of 3Cs multiplex libraries with increasing distribution skews
A) The area under the curve (AUC) determination of three libraries generated with different oligonucleotide pool ratios. AUC values are indicated next to each library identifier. As a reference, a perfectly distributed library (ideal) is shown in grey. Percentages indicate the library representations at 90% of cumulative sequencing reads. As expected, library 1:1 showed the lowest AUC value (0.65). B) Analysis of library distribution skew (skew) and completeness (%) per library based on read counts derived from sequencing. In accordance to A), increased skew ratios were observed for lib. 1:10 and 1:100. Lib. 1:100 showed only 90.94% of the complete library diversity.

To determine the influence of different library distributions on the screening robustness, we applied each library in two separate screens with screening coverages of 20- and 200-fold, and evaluated their performance regarding the knockout efficiency of essential genes in a proliferation screen in human Cas9-expressing hTERT-RPE1 cells in biological replicates.
First, we analyzed pairwise guide and gene-level count correlations for all replicate screens (Supp. Figure S3 A-B). The gene level correlations at a 20-fold coverage showed Pearson coefficients of $r = 0.96$ for library 1:1, $r = 1$ for library 1:10, and $r = 0.79$ for library 1:100. At 200-fold coverage, we observed Pearson coefficients of $r = 0.91$-0.98 for library 1:1, $r = 0.96$-

0.97 for library 1:10, and r = 0.98-0.99 for library 1:100 (Supp. Figure S3 A-B).
Next, we analyzed the performance of each library at the 20- and 200-fold coverages by applying a Cohen's d-based quality score (QS). This QS was recently introduced to compare screen performance by measuring the separation of mean LFC values of gRNAs targeting essential genes from the mean LFC values of gRNAs targeting non-essential genes [320]. Since QSs above 2 indicate a good screen quality [332], the QSs for the 1:1 library in both tested coverages were high, with 2.95 and 3.25 for 20x and 200x, respectively, which indicated a clear separation of LFCs of depleted essential genes from NHT controls (Figure 4.6). A decline in screen quality appeared when library distribution skews increased above 2 (library 1:10 and 1:100). At a 20-fold coverage, the QS for library 1:10 was 1.5. Increasing the screening coverage to 200 raised the QS of library 1:10 to 2.68. Thus, screening a less uniformly distributed library with a higher coverage (library 1:10, 200x, QS = 2.68) leads to a similar separation of hit genes from NHT controls as screening a uniformly distributed library at a lower coverage (library 1:1, 20x, QS = 2.95). However, screening a library with a distribution skew >13 resulted in very low QSs (library 1:100, 200x, QS = -1.17, 20x, QS = -0.44). Since Cohen's d QSs below 0.5 are considered as small, even a 200-fold coverage was not sufficient to obtain a robust seperation of essential genes from NHT controls.

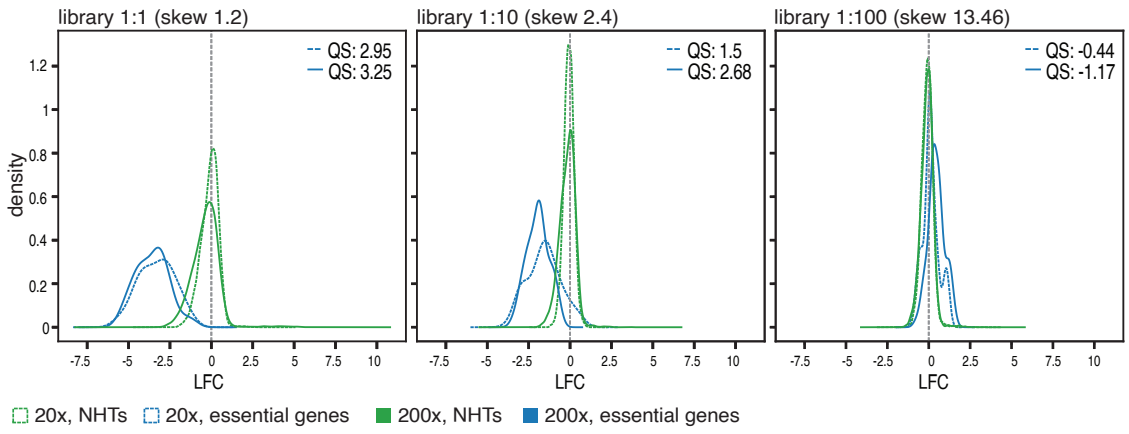

Figure 4.6: Screening performance of artificially skewed gRNA libraries
Density plots showing the log2-fold change (LFC) separation of combinatorial gRNAs targeting essential genes (blue) and non-human targeting (NHT) controls (green) for three libraries with different distribution skews and for screening coverages of 20-fold (20x, dotted) and 200-fold (200x, straight). The highest quality scores (QSs) were observed for library (lib.) 1:1 at a 200-fold coverage with 2.95 and at a 20-fold coverage with 3.25. Decreased QSs were observed for both libraries with distribution skews >2 for both screened coverages.

To confirm the results observed for Cohen's d QSs we applied MAGeCK analyses [127]. We assessed if a higher screening coverage was able to compensate for screening quality loss when screening with an unevenly distributed library and identified essential gene pairs by MAGeCK analyses and cut-off filters set to FDR $<$ 10% and LFC $<$ -0.5. Strikingly, the number of gene pairs detected for library 1:1 and library 1:10 was very similar between 20- and 200-fold coverages (Figure 4.7). For library 1:1, more depleted gene pairs were detected at a 20-fold coverage than at a 200-fold coverage. The number of depleted gene pairs detected for library 1:100 that showed the highest distribution skew, was higher at a 200-fold coverage compared to 20-fold. Thus, increasing the experimental coverage only improved hit detection of depleted essential genes for library 1:100 (distribution skew $<$ 13) to some extent, while it did not improve hit detection for libraries with distribution skews $<$ 2.5.

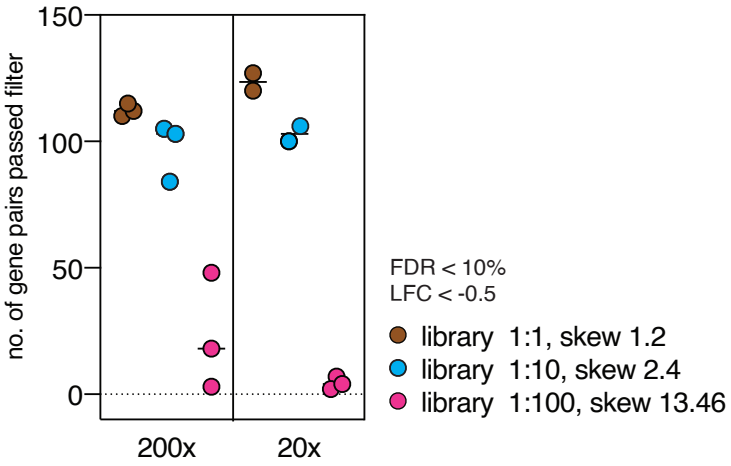

Figure 4.7: Hit detection rates at two different coverages
Analysis of the number (no.) of depleted essential gene pairs detected with MAGeCK analyses at an false discovery rate (FDR) $<$ 10% and log2-fold change (LFC) $<$ -0.5 of screens performed with libraries with increasing distribution skews at 20-fold (20x) and 200-fold (200x) coverages. Increasing the screening coverage from 20 to 200-fold only increased the number of gene pairs passing filters for library 1:100.

4.2.2 The minimal number of gRNAs for robust detection of hit gene pairs

The number of gRNAs per gene has a profound impact on robust identification of hit genes from CRISPR knockout screens [127], but it also determines the *library diversity* and consequently the experimental scale [76]. Choosing the minimal number of gRNAs per target gene that is required for robust hit detection offers potential to reducing the *library diversity* and the required experimental scale. Therefore, we sought to investigate how the number of gRNAs per gene combination affects hit detection in a multiplex CRISPR screens.
To this end, we focused on the data sets of our multiplex proliferation screen performed with the 1:1 library at a 20- and 200-fold coverage. With 10 essential genes on both expression cassettes and four gRNAs per gene, the 1:1 library contained total of 100 essential gene combinations,

each gene combination being covered by 16 different gRNA combinations. Analogous to an analysis that has been done for determining the optimal gRNA number for monogenic screens [181], we down-sampled the data sets that we obtained from screening with library 1:1 with both coverages to distinct read count sub-tables that contained 1 to 16 different gRNA combinations with randomly chosen gRNAs. We analyzed how many of the 100 possible essential gene combinations passed the cut-off filters for a FDR $\leq$ 10% and LFC $\leq$ -0.5 with MAGeCK analyses for each down-sampled read count subset across the two screening coverages (Figure 4.8).
For all 16 read count subsets, the percentages of identified gene pairs were very similar for the 20- and 200-fold coverage, with slightly higher results for the 20-fold coverage (Figure 4.8). As expected, for both coverages, 1 to 4 gRNAs per gene combination yielded less than 20% of all possible essential gene combinations (Figure 4.8). A strong increase, from 20% to 60% was observed for gene combinations covered by 5 to 12 different gRNA combinations. For more than 13 different gRNAs per gene combination, the percentage of identified gene pairs plateaued, and for 16 different gRNA combinations per gene pair, we retrieved the largest number of statistically significant essential gene interactions for the 20- and 200-fold coverages (Figure 4.8). To cover each gene with an equal number of gRNAs on both expression cassettes, we defined (4x4) 16 gRNA combinations per gene pair as the optimal number for our following 3Cs multiplex screens. These results are consistent with previous observations for monogenic CRISPR-Cas9 screens, in which 4 to 6 gRNAs per gene have been identified to be required for robust hit gene detection [181].

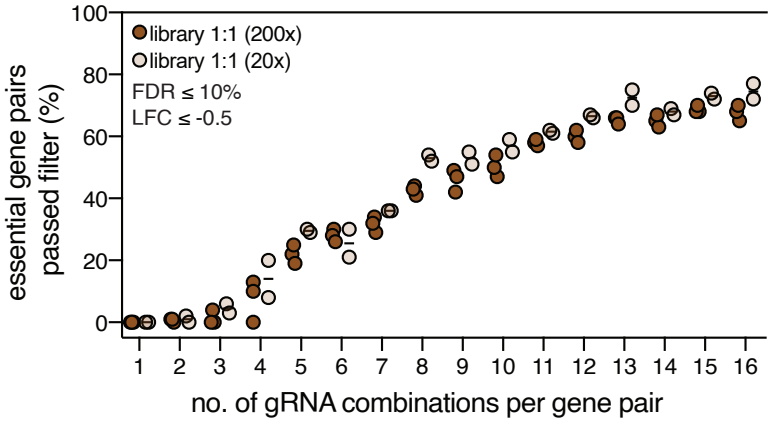

Figure 4.8: The required number of gRNA combinations for detecting hit gene pairs
Determination of the percentage of depleted essential gene pairs that passed the filters for a false discovery rate (FDR) $\leq$ 10% and log2-fold change (LFC) $\leq$ -0.5 from sub-sampled read count tables containing 1 to 16 randomly selected gRNA combinations. The analysis was performed on the data sets resulting from proliferation screens with library 1:1 with 20-fold (20x) and 200-fold (200x) coverages.

4.3 Exploring genetic interactions in autophagy

4.3.1 Generation of a 3Cs autophagy multiplex library

We aimed at applying 3Cs multiplexing and the pre-evaluated minimized screening conditions to investigate GIs between autophagy genes. Therefore, we generated a 3Cs autophagy multiplex library to screen for autophagy GIs in two different screening assays.

To design the autophagy multiplex library, we assembled a literature-curated list of 64 core autophagy genes comprising known autophagy key players, such as upstream regulators, components of the ULK1 and PIK3C3 complexes, the conjugation machinery, ATG8 homologs, PI3P effectors and components of the autophagosome-lysosome fusion machinery. We selected four gRNAs per gene and designed oligonucleotides with homology arms for annealing to the hU6 promoter cassette of our 3Cs multiplex vector (Supp. Table S2). This core autophagy oligonucleotide pool contained additional 26 NHT controls (10% of the complete *library diversity* [102]), resulting in a total of 282 oligonucleotide sequences (Figure 4.9 A). The second oligonucleotide pool, termed extended autophagy pool, was designed for annealing to the h7SK cassette and included all core autophagy genes plus additional gRNAs targeting autophagy related transcription factors, autophagy receptors and ubiquitin-specific proteasess (USPs), among others (Supp. Table S2). With four gRNAs per gene, 80 NHT and 28 essential gene targeting controls, the extended autophagy pool contains 876 gRNAs in total (Figure 4.9 A). By applying the extended autophagy pool in combination with the core autophagy pool in a 3Cs reaction, we created an asymmetric autophagy multiplex library, meaning that the two expression cassettes expressed unequal amounts of gRNAs. The resulting 3Cs multiplex library yielded 247,032 gRNA combinations in total (Figure 4.9 B). Moreover, both oligonucleotide pools were applied alone in separate 3Cs reactions for generating the core and extended single-gRNA libraries (Figure 4.9 B).
For removing remaining wild type 3Cs multiplex plasmids from the final libraries, the electroporated 3Cs reaction products were digested with I-CeuI, I-SceI, or both, respectively. A final analytical restriction enzyme digestion with either I-CeuI or I-SceI, or both confirmed minimal ratios of wild type vector in the final single-gRNA and multiplex libraries (Figure 4.9 C). The extended and core single-gRNA libraries showed no linearized bands with either I-CeuI or I-SceI, respectively and complete linearization with the second enzyme. Gel electrophoresis of the digested autophagy multiplex library showed no linearized bands. This confirmed selective and efficient 3Cs reactions on both cassettes for all libraries.
Sequencing of the extended single-gRNA and autophagy multiplex libraries revealed uniform library distributions with distribution skews of 1.22 and 1.69, respectively (Figure 4.9 D-E), Supp. Table S6). It further confirmed 100% completeness of the extended library, as well as the presence of 99.28% of all 247,032 gRNA combinations for the autophagy multiplex library (Figure 4.9 D-E). The determination of AUC values for both libraries resulted in 0.65 and 0.68, respectively (Figure 4.9 F), supporting our previous observation that 3Cs multiplexing was a

highly robust method for the generating uniformly distributed single-gRNA and combinatorial CRISPR libraries.

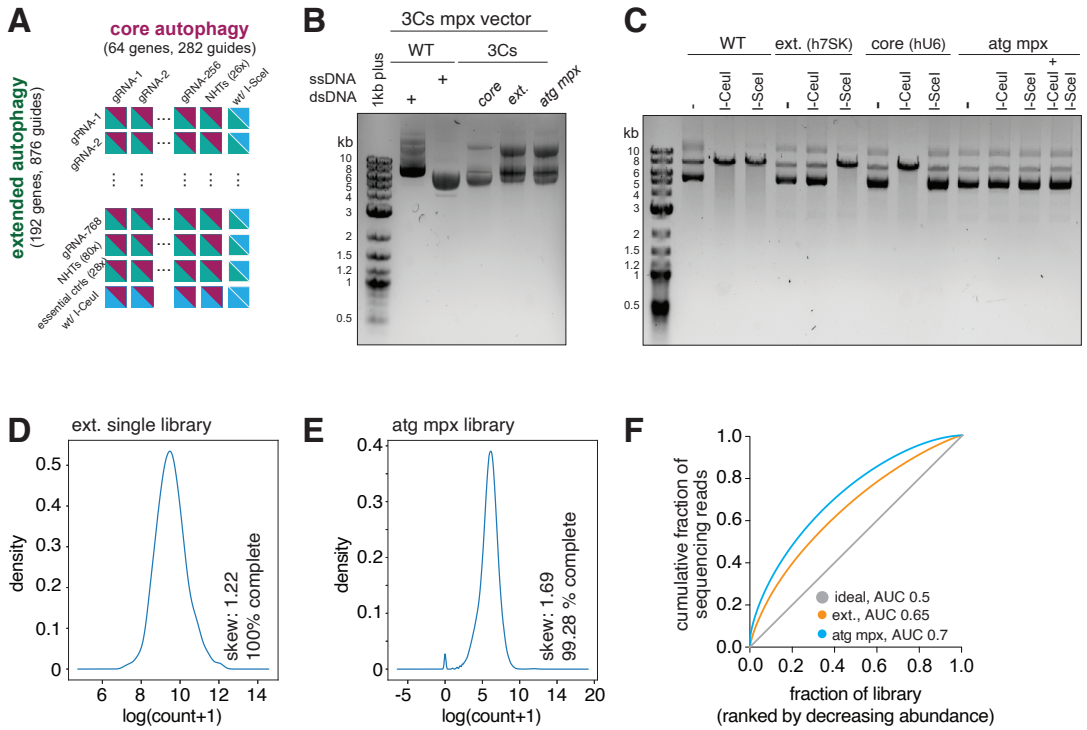

Figure 4.9: Generation of 3Cs single-gRNA and multiplex autophagy libraries
A) Design of two oligonucleotide pools for generating single-gRNA and multiplex autophagy libraries. The core autophagy pool (red) contains 64 autophagy genes with 4 gRNAs per gene and 26 non-human targeting (NHT) gRNAs. The extended autophagy pool (green) includes all core autophagy genes plus additional autophagy-linked target genes, 80 NHT gRNAs, as well as 28 essential gene targeting controls (ctrls). B) Gel electrophoresis of the wild type (WT) 3Cs multiplex (mpx) vector in its double-stranded DNA (dsDNA) and single-stranded DNA (ssDNA) form, and the three 3Cs synthesis products for the extended (ext.) and core single-gRNA libraries, and the autophagy multiplex (atg mpx) library. All 3Cs synthesis products show the characteristic 3-banded pattern. C) Gel electrophoresis of an analytical restriction digestion of each library with only I-CeuI or I-SceI, or both confirms minimal WT vector contamination of final libraries. Linearized bands indicate WT vector remnants in the corresponding expression cassette. D-E) Sequencing analysis of the extended (ext.) and autophagy multiplex (atg mpx) library. The library distribution is indicated by distribution skews and completeness (%) per library based on the obtained sequencing read counts. F) AUC determination of the extended (ext.) and autophagy multiplex (atg mpx) libraries. A perfectly distributed library (ideal) is shown in grey as a reference. AUC values are indicated next to each library identifier.

4.3.2 Establishing screening assays for investigating autophagy gene interactions in cell proliferation and autophagy flux

Using the extended single-gRNA and the autophagy multiplex libraries, we sought to investigate GIs between autophagy genes in two different phenotypic aspects. We aimed at detecting autophagy gene pairs that are essential for autophagic activity by a reporter-based autophagy flux screen, and additionally, we aimed at identifying dual autophagy gene combinations that lead to synergistic proliferative effects by a proliferation screen. While viability and proliferation are common phenotypic read outs used for monogenic and multiplex CRISPR screens, other specific cellular phenotypic read outs, such es autophagy flux, depend on reporter constructs that are introduced into a model cell line. However, reporter-based screens are less common for pooled CRISPR screens, especially for combinatorial screens, experimental protocols, and therefore, guidelines are sparse [76, 114]. To screen for autophagy gene interactions in with GIs that result in both phenotypic readouts, proliferation and autophagic flux, we generated a monoclonal model cell line expressing an established autophagy activity reporter [307] and established two different screening assays (Figure 4.10.

For generating the reporter cell line we employed an established fluorescent autophagic flux reporter that consists of GFP-LC3, which is fused to the N-terminus of RFP [307] (Figure 4.10 A. Its expression in cells leads to seperation of GFP-LC3 and RFP in equimolar amounts due to cleavage of the peptide bond after the C-terminal glycine of LC3 by endogenous ATG4 family proteases. While GFP-LC3 is degraded by autophagy, RFP remains in the cytosol and serves as an internal control. Hence, the autophagic flux can be determined by measuring the GFP/RFP signal ratio [307].
The monoclonal reporter cell line was generated by lentiviral transduction of hTERT-RPE1 cell to stably express Cas9 and the autophagic flux reporter. We confirmed its functionality by FACS analysis. The reporter cell line showed low levels of basal autophagy (6.83%) (Figure 4.10 B). Torin 1 induced mTOR inhibition increased autophagic flux (99.6%) indicated by decreased GFP signal due to GFP-LC3 degradation (Figure 4.10 B). Bafilomycin A1 treatment blocked autophagic flux (Figure 4.10 B).
To facilitate the quantification of proliferative and autophagy flux phenotypes in the same genetic background the reporter cell line was used for the autophagy flux and the proliferation screen (Figure 4.10 C). The screens start with transduction of the monoclonal reporter cells with the extended single-gRNA or autophagy multiplex library. For the autophagy multiplex library, we chose our pre-evaluated minimized conditions (20-fold library coverage) for uniformly distributed CRISPR libraries since we confirmed a low distribution skew. Separate screens were preformed with the extended single-gRNA library in replicates with a 1000-fold library coverage because of the small library diversity. After one week of selection and expansion, cells were passaged while maintaining the initial coverage. In the autophagy flux screen, cells were treated with Torin 1 on day 13 to induce autophagy by mTOR inhibition and subjected to

FACS analysis

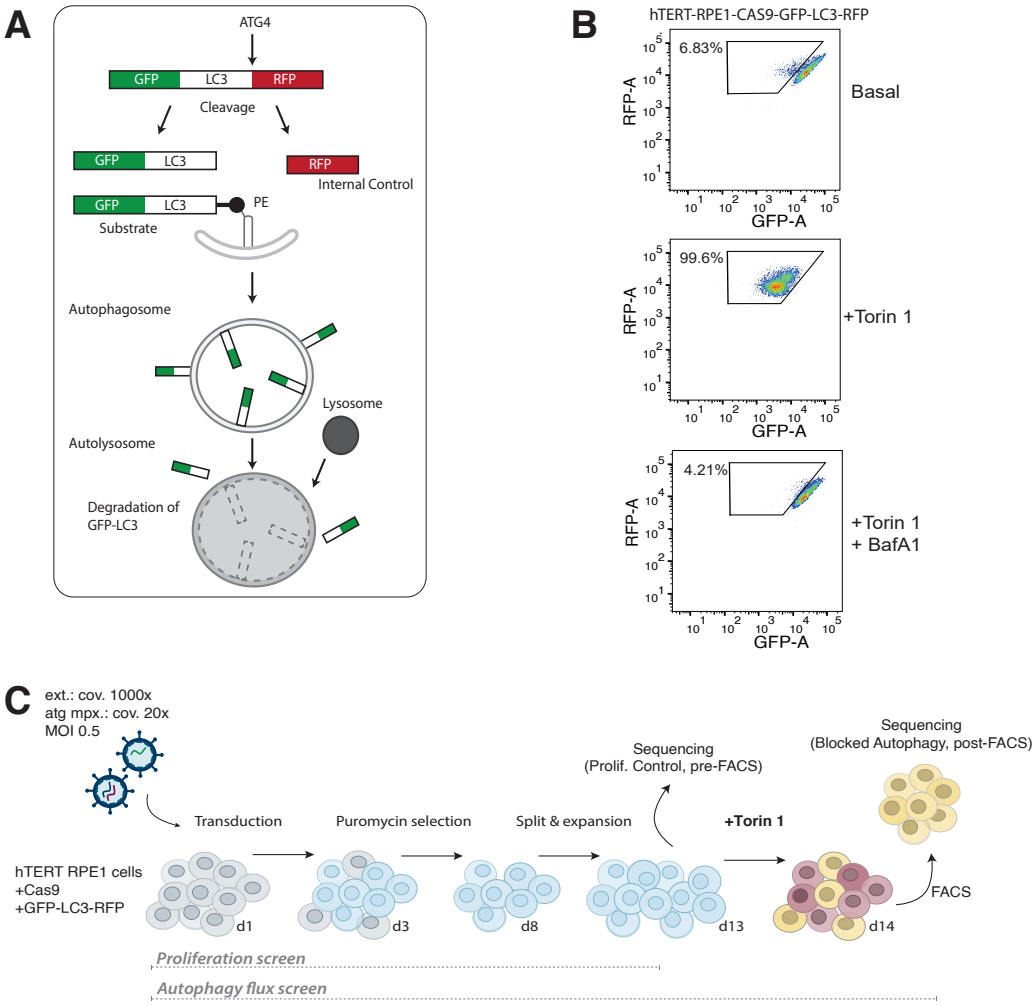

Figure 4.10: Proliferation and autophagy flux screening assay
A)The GFP-LC3-RFP autophagic flux reporter is cleaved by endogenous ATG4 proteases into equimolar amounts of GFP-LC3 and RFP. GFP-LC3 is degraded by autophagy, while RFP remains in the cytosol and serves as an internal control. Adapted from [307]. B) Functionality of the monoconal hTERT-RPE1 cell line expressing Cas9 and the autophagic flux reporter cell line was ensured by FACS. Torin 1 treatment for 24h leads to a shift of the whole cell population, thus indicating high autophagic activity (99.6%). Torin 1 induced autophagy was inhibited by Bafilomycin A1 treatment. C) Screening workflows for identifying single autophagy genes and gene combinations that are essential for autophagy (Autophagy flux screen) and for identifying synergistic proliferative effects (Proliferation screen). hTERT-RPE1 cells expressing Cas9 and an autophagic flux reporter (GFP-LC3-RFP) [307] were transduced with either the extended (ext.) or autophagy multiplex (atg mpx) library at an MOI of 0.5 and a 20-fold or 1000-fold coverage, respectively. In the proliferation screen cells were harvested on day (d) 13. Genomic DNA of a representative cell population was extracted for obtaining proliferation phenotypes by sequencing (pre-FACS). In the autophagy flux screen, cells were treated with Torin 1 on day 13, subjected to FACS and sorted according to their GFP/RFP ratios. Cells with blocked autophagy were collected and expanded before they were processed for sequencing (post-FACS).

on day 14 to sort cells with blocked autophagy (Figure 4.10 C, post-FACS). In the separate identical proliferation screen, cells were harvested on day 13 and a coverage-based cell sample was processed for sequencing analysis (Figure 4.10 C, pre-FACS). Even when screening for other phenotypes than proliferation, proliferative effects are a consequence of gene knockouts, especially in TP53-positive RPE1 cells, and can impair hit detection by confounding gRNA abundance in the final reporter-based sorted cell population. To control for proliferative effects we analyzed the gRNA abundance of the pre-FACS proliferation sample by sequencing, and computed proliferative phenotypes of single and combinatorial gene knockouts (Figure 4.10 C, pre-FACS). This proliferation control screen was used to normalize post-FACS gRNA abundance in the FACS-enriched cell populations.

4.3.3 Identification of autophagy gene interactions in cell proliferation

4.3.3.1 Proliferative effects induced by single autophagy gene depletion

We initially focused on identifying proliferative effects induced by depletion of single autophagy genes. Therefore, we first performed the proliferation screen in duplicates with the extended single-RNA library as described above. Apart from the separate screen with the extended single-gRNA library, single gene proliferation phenotypes were additionally obtained from the autophagy multiplex screen that contained all extended autophagy gRNA sequences paired with NHT control gRNAs (multiplex-inherent single screen).

We applied MAGeCK analyses to the sequenced pre-FACS samples of the separate extended single and multiplex-inherent single screen data sets and excluded already known core essential genes [113] (Figure 4.11). In both screens, we identified the WASH complex subunit 1; also known as FAM39E or WASH1 (WASHC1) to be essential for hTERT-RPE1 cell proliferation (Figure 4.11 A-B). Notably, among the identified depleted genes with LFC$<$-1 were no genes that are considered to be part of the core autophagy machinery. We further found the tumor suppressor TP53 as the single enriched hit gene with a LFC$>$1 (Figure 4.11 A-B).
To assessed the concordance between the separate extended and multiplex-inherent single screens we computed gRNA and gene level correlations (Figure 4.11 C-D). We observed a high overall correlation of $r = 0.97$ on gRNA and gene levels. As expected, essential proliferation genes that belonged to the core-essential gene set published in 2017 by Hart et al. were depleted in both screens [113], while non-targeting controls were slightly enriched (Figure 4.11 C-D).
Although the multiplex-inherent screen was performed with only a 20-fold coverage, the concordance of retrieved hit genes and the high correlation to the separate single screen, which was performed at a 1,000-fold coverage, further support our conclusion that CRISPR libraries with distribution skews of less than 2 could be screened with reduced coverage.

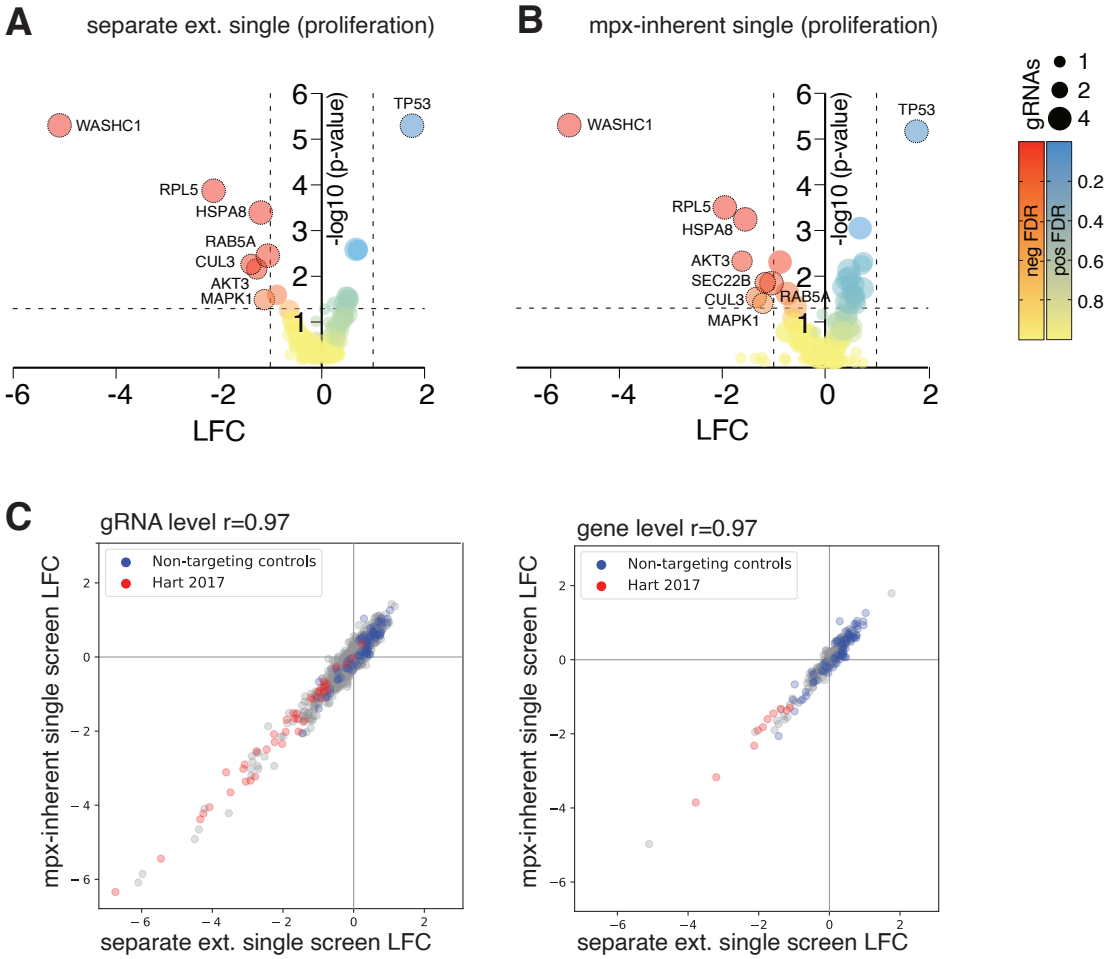

Figure 4.11: Proliferative effects of single autophagy genes
MAGeCK analysis of (A) the separate extended (ext.) single proliferation screen performed with the extended autophagy single-gRNA library and (B) the autophagy multiplex-inherent single proliferation screens. Depleted genes with log2-fold change (LFC) $<$ -1 and enriched genes with LFC $>$ 1 are indicated. Positive and negative false discovery rates (FDRs) are shown by red and blue gradients, respectively. The dot size indicates the number of identified gRNAs. C) Correlation of pre-FACS samples of the autophagy multiplex-inherent and separate extended single screening data on gRNA and gene level. Core essential genes, according to Hart et al., 2017, are highlighted in red [113], non-human targeting (NHT) controls are highlighted in blue.

4.3.3.2 Proliferation-enhancing and suppressive autophagy gene interactions

After having determined the proliferative effects induced by single autophagy gene depletion, we focused on identifying autophagy gene combinations whose loss affected cell proliferation. Therefore, we analyzed the sequenced pre-FACS samples from the autophagy multiplex proliferation screen.

The sequencing analysis and subsequent pairwise correlation between screen duplicates showed a high Pearson correlation coefficient of r=0.99 on gRNA and gene levels, but low correla-

tion to the initial plasmid library (r = 0.4-0.45), indicating selective phenotypic enrichment of knockout cells by proliferation in the course of the screen (Supp. Figure S4, Supp. Table S6).
A MAGeCK analysis resulted in a total of 446 significantly depleted and 732 significantly enriched gene pairs (Figure 4.12 A). The loss of the gene combinations *WDR45B-PIK3R4* and *ATG7-KEAP1* showed the strongest effects on proliferation with LFCs of -2.94 and 2.92, respectively (Figure 4.12 A).
We analyzed the number of interaction partners for each gene within the depleted and enriched gene pairs and identified *PIK3R4*, *ATG7*, and *ATG5* to have 172, 174 and 157 interaction partners, respectively. These three genes had the highest number of interaction partners within the enriched and depleted gene pairs compared to all other genes, and therefore constitute hub genes for proliferation within our tested autophagy gene set (Figure 4.12 B).
Next, we asked if this observed effect on proliferation induced by combinatorial gene depletion could be explained by adding up the individual single gene depletion phenotypes. Therefore, we compared the observed LFCs of combinatorial gene depletion of *WDR45B-PIK3R4* and *ATG7-KEAP1* to the observed LFCs of single gene knockouts that we obtained from the multiplex-inherent single screen (Figure 4.12 C). The observed LFCs of combinatorial gene depletion of *WDR45B-PIK3R4* and *ATG7-KEAP1* were higher than the sum of LFCs of their individual single gene depletion. Notably, the proliferative phenotype for *ATG7-KEAP1* loss was even stronger than that of the tumor suppressor TP53, while the decreased proliferation of *WDR45B-PIK3R4* knockout was milder compared to the depletion of the essential gene WASHC1 (Figure 4.12 B). Since *GIs*, per definition, occur when the observed combinatorial knockout phenotype can not be explained by merely summing up the effects of their individual gene knockout phenotypes [5, 6], our screen identified *WDR45B-PIK3R4* and *ATG7-KEAP1* as GIs.
We aimed to determine how many of all identified enriched and depleted gene pairs in the proliferation screen constituted GIs with combinatorial knockout phenotypes that could not be explained by the combined effects of their single gene depletions. To this end, we applied an additive model (SUM model) to compute expected combinatorial knockout phenotypes for all gene pairs as the sum of their observed LFCs in the multiplex-inherent single screen. This computed combinatorial knockout phenotype was expected when both genes would not interact (Figure 4.12 D). If the observed combinatorial phenotype, namely the LFCs in the multiplex proliferation screen, for a gene pair deviated from the expected combinatorial knockout phenotype, a GI was identified between both genes. In total, we identified 35.4% of the depleted and 52.3% of the enriched gene pairs to constitute GIs according to the SUM model and with a SD of the dLFC above 2 (Figure 4.12 D).

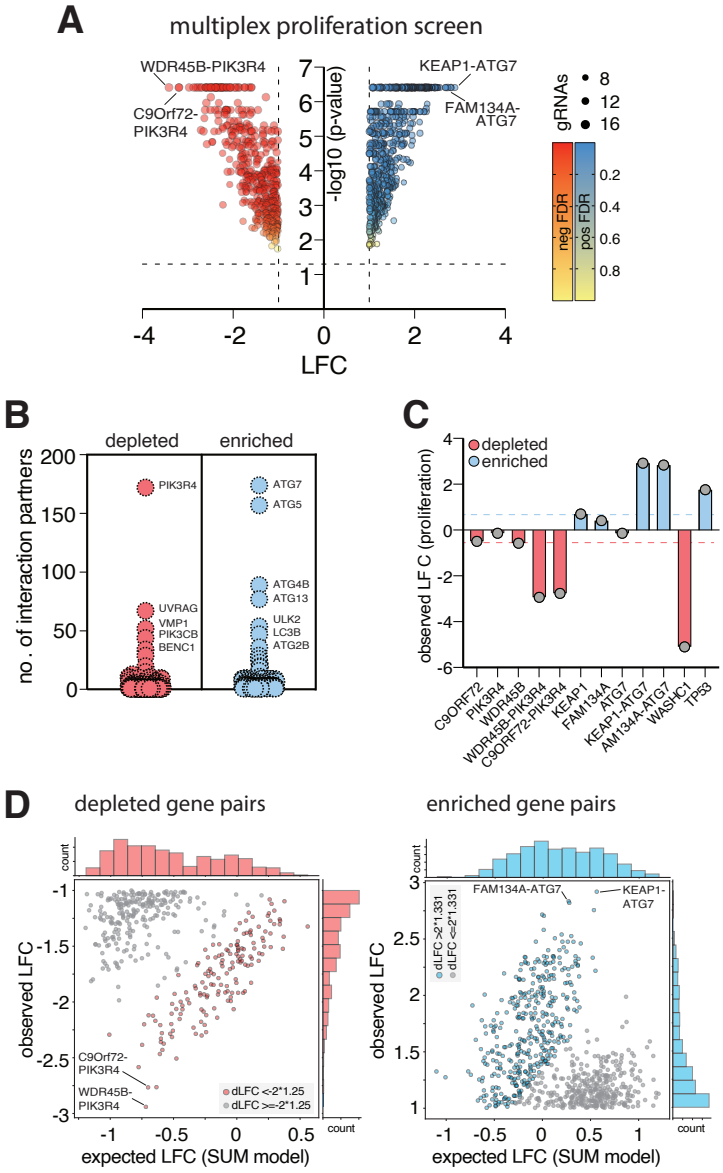

Figure 4.12: Proliferative effects induced by combinatorial autophagy gene depletion
A) Volcano plots of MAGeCK-derived log2-fold change (LFC) values and p-values for the autophagy multiplex proliferation screen. False discovery rates (FDRs) for positive and negative selections are color-coded yellow-red and yellow-blue, respectively. Significant ($p<0.05$) data points with a $LFC > 1$ or $LFC < -1$ have dashed strokes. Dot sizes indicate the number of gRNAs used for MAGeCK hit calling. B) Number of different interaction partners for genes of depleted (red) and enriched (blue) gene pairs in the autophagy multiplex proliferation screen. *PIK3R4* and *ATG7* interact with more than 174 of possible 192 genes. C) Bar graph of observed LFCs of the two most negative (red, depleted) and most positive (blue, enriched) autophagy gene pairs from (A), compared to their single gene LFCs derived from the multiplex-inherent single screen. Dashed lines indicate the strongest positive (blue) and negative (red) single gene deletion phenotypes. WASHC1 and TP53 serve as references for essential gene and tumor suppressor gene depletion, respectively. D) Scatter plots of SUM-model derived expected LFC and observed LFC from the multiplex autophagy proliferation screen. All data points with a $LFC < -1$ (depleted) or a $LFC < 1$ (enriched) are shown. Highlighted are data points with a delta log2 fold-change (dLFC) < -2*1.25 (red) and a $dLFC > 2*1.331$ (blue).

4.3.4 Identification of autophagy gene interactions in autophagy flux

4.3.4.1 Identification of single essential autophagy genes

To identify essential GIs for autophagy flux, we first had to determine to what extent all single genes were essential for autophagy on their own. Therefore, same as for proliferation, we first determined single autophagy gene phenotypes by a separate and a multiplex-inherent single autophagy flux screen.

In the separate single autophagy flux screen, cells with blocked autophagy were sorted by FACS due to their unchanged GFP signal upon Torin 1 treatment. We applied stringent gating to reduce false-positives (Figure 4.13 A).
We sequenced sorted cells and confirmed sufficient sequencing depth for sorted post-FACS samples (Supp. Figure S5 A). Next, we computed pairwise Pearson correlations between biological replicates, which showed high correlation on gRNA ($r = 0.87$) and gene levels ($r = 0.97$) (Supp. Figure S5 B, Supp. Table S6). As expected, due to the phenotypic enrichment by FACS, the correlations between post-FACS samples and the initial plasmid library were very low (gRNA and gene level, $r = 0.05$-0.06) (Supp. Figure S5 B).
We applied MAGeCK analysis to the post-FACS samples of separate single screen and retrieved 12 significantly enriched genes with LFC between 3.76 and 9.12 with an FDR $\leq$ 10% (Figure 4.13 B).
Additionally, we obtained single gene phenotypes from the multiplex-inherent single autophagy flux screen. A MAGeCK analysis identified 10 significantly enriched genes with LFCs between 1.53 and 2.75 (FDR $\leq$ 10%) (Figure 4.13 C). The hit concordance of the separate and multiplex-inherent single autophagy flux data was high and showed an overlap of 7 jointly identified genes that are well known essential genes for bulk autophagy [200, 201, 333] (Figure 4.13 B-C). However, both screens also identified unique hits. In total, five and three hits were identified in only the separate or the multiplex-inherent single screen, respectively. Upon FDR-relaxation (FDR $>$10 %) the concordance of both screens increased to 11 shared hits identified by both screens (Supp. Figure S5 C-D).
We aimed to validate if knockouts of the identified single hit genes were able to block autophagy flux in a FACS analysis when the genes were separately targeted by newly designed single gRNAs. We tested 13 identified single hit genes of both single screens and confirmed blocked autophagy flux for 12 tested single hit genes by arrayed FACS measurement (Figure 4.13 D). However, *RAB1A* showed no autophagy block by arrayed validation (Figure 4.13 D). To confirm the gRNA performance for the validation we quantified the gRNA-induced editing on the genomic level by TIDE analysis (Figure 4.13 D).
We defined the hit genes identified at an FDR $\leq$ 10% from both, the separate and multiplex-inherent single screens, as single essential autophagy genes for our subsequent analysis of combinatorial phenotypes.

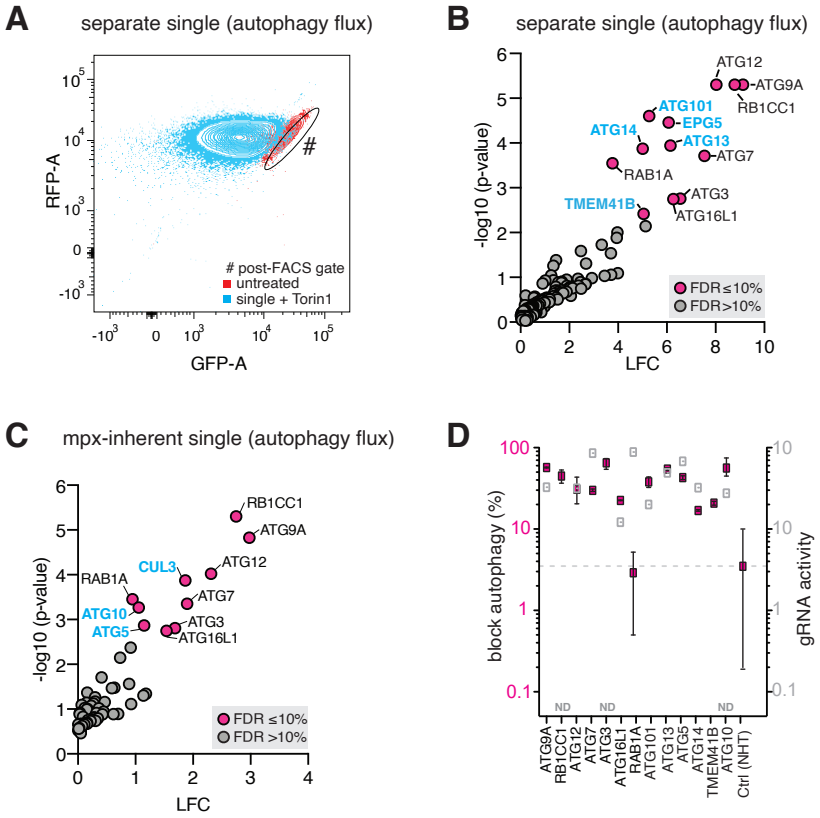

Figure 4.13: Single autophagy flux screens identify essential autophagy genes.
A) Example for gating during FACS analysis of the separate single autophagy flux screen. Untreated cells are highlighted in red, and Torin 1-treated cells in blue. The sorting gate (#, post-FACS) is shown as a black ellipse at the very boundary of the untreated cell population. B-C) To identify enriched genes, MAGeCK analyses were applied to compare the sequencing results of sorted samples with blocked autophagy (post-FACS) to pre-FACS samples of B) the separate single autophagy flux screen and C) the multiplex (mpx)-inherent single autophagy flux screen. Hit genes with a false-discovery rate (FDR) below 10% and p-values ≤ 0.05 are labelled and highlighted in pink. Unique hits that were identified in only one screen are labelled in blue. D) Arrayed validation of autophagy block by FACS analysis for single hit genes derived from B) and C). Evaluation of gRNA activity by TIDE analysis is shown in grey. Error bars represent the standard error of mean (SEM) over three biological replicates per autophagy flux measurement (n=3). ND: not determined.

4.3.4.2 Identification of essential autophagy gene interactions for autophagy flux

In multiplex autophagy flux screen, we applied the same stringent FACS gating as for the single screen to sort cells with blocked autophagy. In contrast to the single screen, in the multiplex screen, we observed a large fraction of cells that showed constant GFP signal after Torin 1 treatment, indicating more cells with blocked autophagy for combinatorial autophagy gene depletions (Figure 4.14 A). Surprisingly, cells transduced with the autophagy multiplex library showed a third cell population in FACS analysis with higher RFP signal compared to untreated wild type cells (Figure 4.14 A). We named this population "high gate" population

and collected the cells for sequencing as well.
Sequencing analysis of the "high gate" cell population confirmed sufficient sequencing depth (Supp. Figure S6 A), and Pearson correlation coefficients between the post-FACS samples of screen replicates ranged from 0.83 and 0.89 on gene levels (Supp. Figure S6 B).
We analyzed the abundance of gRNA sequences in high-gate cell population and found that the majority of reads corresponded to *ATG4B*-targeting gRNA pairs (post-FACS 1, 86.94%; post-FACS 2, 78.03%; post-FACS 3, 75.53%) (Figure 4.14 B). Since the autophagic flux reporter was based on cleavage of GFP-LC3-RFP by endogenous ATG4 [307], we hypothesized that ATG4B loss led to impaired reporter functionality resulting in decreased RFP degradation and therefore, we excluded *ATG4B* from our subsequent analysis.

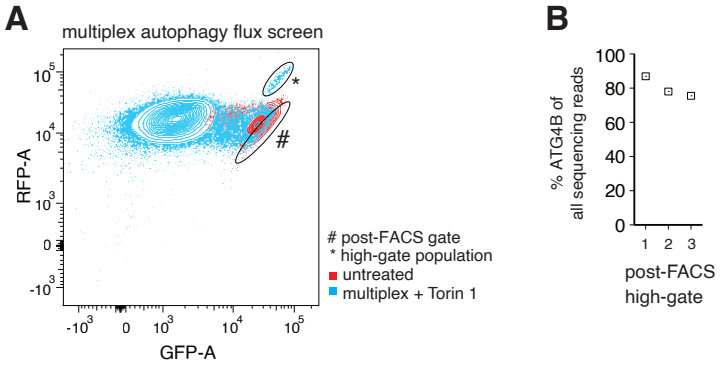

Figure 4.14: FACS analysis of the multiplex autophagy flux screen
A) FACS analysis of the multiplex autophagy flux screen, highlighting untreated (red) and Torin 1-treated (blue) hTERT-RPE1 autophagy reporter cells. Sorting gates (#, post-FACS; *, high-gate) are shown as black ellipses. B) Relative abundance of reads that contain an *ATG4B*-targeting gRNA of post-FACS high-gate replicates.

Next, we sequenced and analyzed the abundance of gRNA-combinations in the post-FACS cell populations with blocked autophagy flux. Pairwise gRNA and gene level correlations of biological replicates of the post-FACS samples resulted in Pearson correlation coefficients of $r = 0.58$, 0.62 and 0.69 on gRNA level and $r = 0.77$, 0.84 and 0.87 on gene level (Figure S4A). As expected, correlations between pre and post-FACS samples were low (gRNA level, $r = 0.15$-0.21; gene level, $r = 0.18$-0.27), confirming selective reporter-based enrichment of cells after FACS (Figure S4A).
While the additive (SUM), multiplicative (MULT), minimum (MIN), and logarithmic (LOG) models have been applied to identify GIs in CRISPR proliferation screens [6], combinatorial screens with reporter-based read outs and suitable analysis strategies have not yet been reported. To choose a suitable model for our multiplex autophagy flux screen, we added the maximum (MAX) model because the knockout of a second autophagy gene was unlikely to ameliorate the knockout of the first autophagy gene. We applied all five models to compute expected phenotypes for non-interacting gene pairs based on the single gene effects that we obtained from the single screens. Then, we computed the dLFC, the deviation of observed

from expected phenotypes (Figure 4.15 A, Supp. Table S7). Previous screens in *Saccharomyces cerevisiae* and human cells revealed GIs to be rare [19, 51]. In line with this, the MAX model detected the fewest deviations of observed combinatorial phenotypes from the predicted value for non-interacting genes (Figure 4.15 A).

We identified a total of 1,570 MAX model-derived GIs (LFC $>$ 0.5, dLFC $>$ 0.05), including GIs containing single essential autophagy genes. To investigate the connectivity of autophagy genes, we determined how many interaction partners each core autophagy gene showed according to the MAX model and found 11 core essential autophagy genes that were highly connected with an average of 241 interactions (of possible 255) (Figure 4.15 B). The phenotypic strength of autophagy genes correlated well with the number of interactions (Figure 4.15 B). In addition, we identified AMBRA1 and ULK1, which were not considered as single essential genes for autophagy flux based on our single autophagy flux screens, as hub genes that interacted with 84 to 25 other core and extended autophagy genes (Figure 4.15 B).

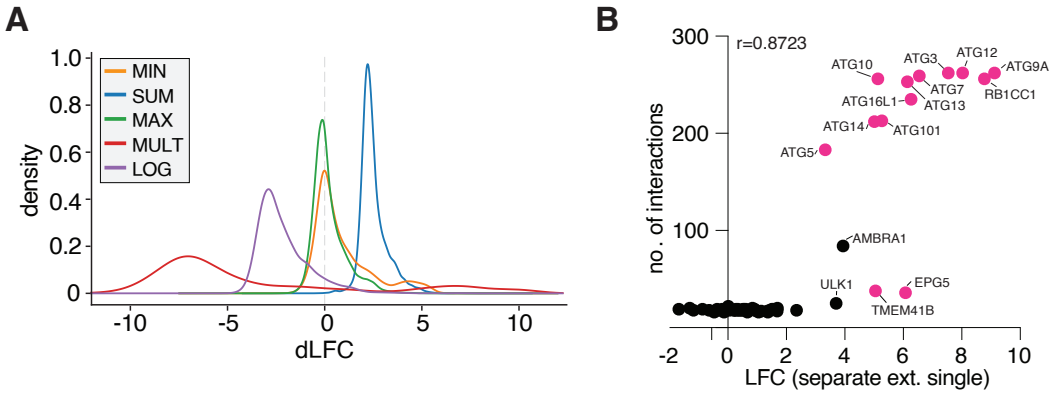

Figure 4.15: Max model-derived autophagy gene interactions required for autophagic flux

A) Density plot of delta log2 fold change (dLFC) distributions of all gRNA combinations in the multiplex autophagy flux screen according to the MIN, MAX, MULT, SUM, LOG genetic interaction models. B) Correlation of the number of interactions for each core autophagy gene and the LFC of core autophagy gene obtained from the separate single screen (r=0.87). Highlighted in red are genes that were identified as single essential autophagy genes in the separate single screen.

Most identified GIs corresponded to gene pairs that consisted of at least one or two single essential autophagy genes. To confirm that the FACS-enrichment of gene-pairs was not driven by the strong phenotype of a single essential autophagy gene, we performed arrayed validations to asses the block of autophagy for of selected combinations that consisted of two single essential genes, one single essential gene, or exclusively non-single essential genes. Targeting combinations of two single essential genes consistently increased the block of autophagy flux compared to targeting one single essential gene, an effect particularly prominent for *ATG5-ATG14* (Figure 4.16 A). Similarly, validations of significantly enriched gene pairs consisting of essential and non-essential genes also increased the fraction of cells with blocked autophagic

flux (Figure 4.16 B). We further confirmed that the interaction of two non-single essential paralogs, namely *ATG2A-ATG2B*, showed a stronger block of autophagy flux, as compared to what was expected based on their single gene depletion effects (Figure 4.16 C).

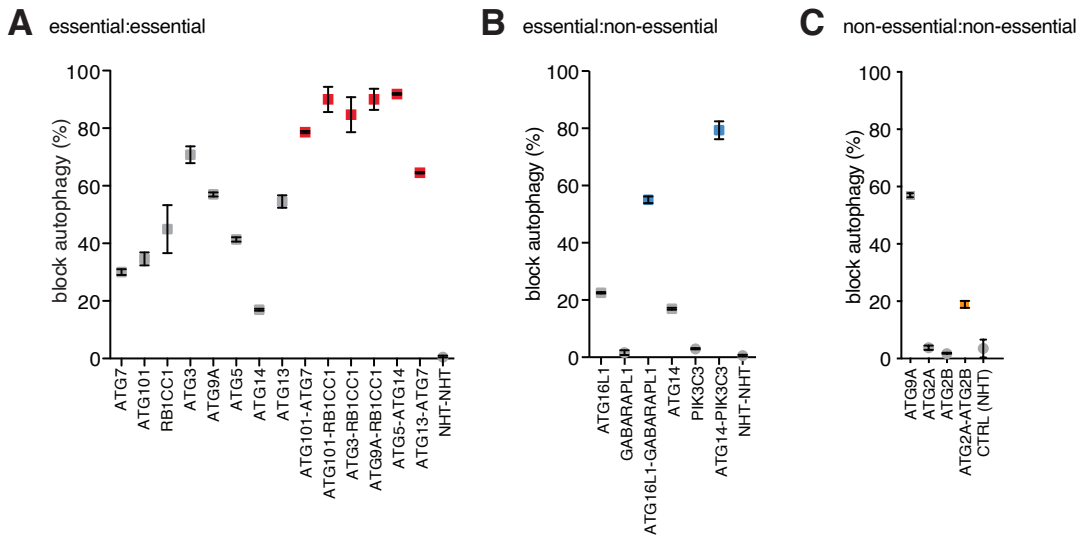

Figure 4.16: Arrayed validation of block in autophagy flux of hit gene pairs
A-C) Arrayed validation of block in autophagy flux of single genes (grey) and hit gene pair depletions derived from Max model analysis. Error bars represent standard error of mean (SEM) over three biological replicates (n=3). Co-depletion of (A) two single essential autophagy genes (red), (B) an essential and a non-essential autophagy gene (blue), and (C) two non-essential autophagy genes (orange) enhances the block in autophagy flux.

Next, we looked in more detail on those GIs that consisted of two non-single essential genes. We excluded all GIs that contained a single essential autophagy gene. In total, 255 GIs remained, which were enriched after FACS (observed LFC >0) and had a positive dLFC according to the MAX model (dLFC >0) (Figure 4.17 A). Of these 255, we selected high-confidence GIs of non-essential autophagy genes with a dLFC >3*SD and LFC >0 (Figure 4.17 A). We integrated these GIs in a network and identified several genes to be connected to selective autophagy (*NBR1*, *PEX13*, *FUNDC1*, *FUNDC2*, *PLEKHM1*, *FAM134B* and *CCPG1*) (Figure 4.17 B). Among these were three GIs linking *ULK4* to the selective autophagy receptors *PEX13*, *FUNDC1* and *SQSTM1*, and two GIs connecting *IRGM* to the ER-phagy pathway genes *CCPG1* and *FAM134B* (Figure 4.17 B). Furthermore, we identified a very strong interaction between the transcription factor *TFEB* and *WAC*.

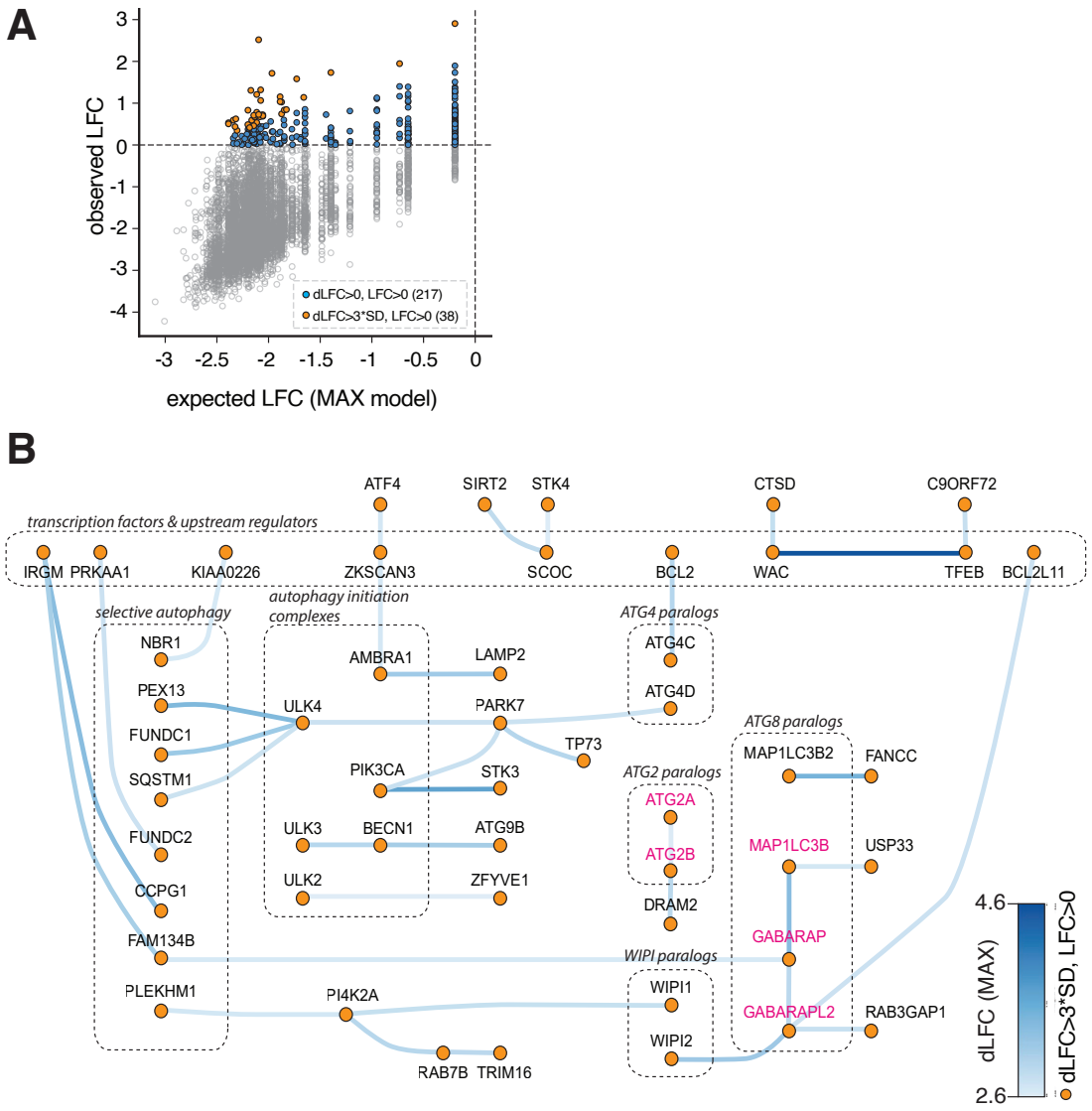

Figure 4.17: Network analysis of non-essential genetic interactions in autophagy
A) MAX model-based comparison of observed and expected combinatorial phenotypes. Highlighted are combinations with a log2-fold change (LFC) > 0, a delta log2-fold change (dLFC) > 0 (blue, 217), and with a delta LFC (dLFC) above 3* standard deviation (SD) (orange, 51). Gene combinations with single essentials genes for autophagy flux and viability (*Hart et al, 2017*), and non-human targeting (NHT) controls are not shown. B) Network analysis of high-confidence GIs with dLFC $>$ 3*SD and LFC > 0 (orange data points from A). Genes and GIs are grouped based on their role in processes, complexes or paralog families. Names of paralog GIs are highlighted in pink. Edge color is set according to GI dLFCs (white to blue).

In addition to *ATG2A-ATG2B*, we validated the *WIPI2-GABARAPL2*, *RAB7B-PI4K2A*, *SCOC-SIRT2*, *SQSTM1-ULK4*, and *PIK3CA-STK3* by arrayed FACS analysis with newly designed gRNAs and confirmed decreased autophagic flux for these hit gene pairs (Figure 4.18).

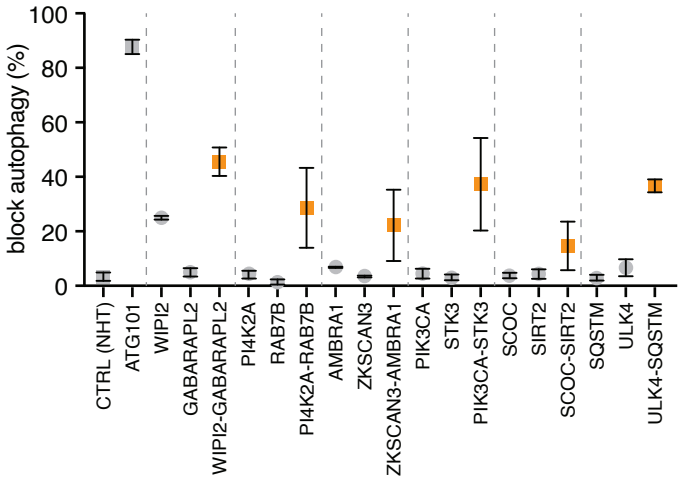

Figure 4.18: Validation of non-essential genetic interactions in autophagy
Arrayed validation of block in autophagy flux of non-single essential autophagy genes (grey) and MAX model-derived hit gene pairs of non-single essential autophagy genes (orange). Error bars represent standard error of mean (SEM) over at least three biological replicates ($n > 3$).

It was shown that paralogs have been less frequently identified as essential genes by monogenic CRISPR screens compared to genes that have no paralogs [251], and it was proposed that their capacity to functionally compensate for each other's loss resulted in the under-representation of paralogs in monogenic CRISPR screens [251, 257]. Therefore, it was hypothesized that combinatorial screens may be able to identify novel gene functions or essentiality for paralog pairs [251, 257]. Since the autophagy pathway includes many paralog genes, we expected to identify genetic interactions between paralogs that are able to compensate for each others loss by our combinatorial autophagy flux screen. However, our network analysis of genetic interactions between non-essential genes showed only three interactions between paralog genes (*ATG2A-ATG2B*, *MAP1LC3B-GABARAP*, *GABARAP-GABARAPL2*) (Figure 4.17 B, highlighted in pink).

4.3.4.3 Genetic interactions of core autophagy paralog genes

To further investigate possible buffering between paralogs, we analyzed all MAX model-derived GIs ($LFC > 0$, $dLFC > 0$) of paralogs of the core autophagy library and compared their genetic interaction profiles, including those GIs that contained single essential autophagy genes Figure 4.19).

As expected from our previous analysis, we identified a GI between the *ATG2A-ATG2B* para-

log pair, indicating that the presence of at least one of the paralogs is required for autophagy flux (Figure 4.19). In addition, within the WIPI gene family, we identified multiple GIs, namely *WIPI1-WIPI2*, *WIPI2-WDR45*, and *WDR45-WDR45B* Figure 4.19). In contrast, we observed no GIs within the *ULK* and *ATG4* paralog families. Additionally, we observed very similar GI profiles for the two essential core autophagy paralogs *ATG9A* and *ATG16L1* and only a few weak interactions for their corresponding paralogs *ATG16L2* and *ATG9B* (Figure 4.19). Moreover, we identified GIs between the members of the ATG8 family (*GABARAP*, *GABARAPL2* and *MAP1LC3B*) (Figure 4.19).

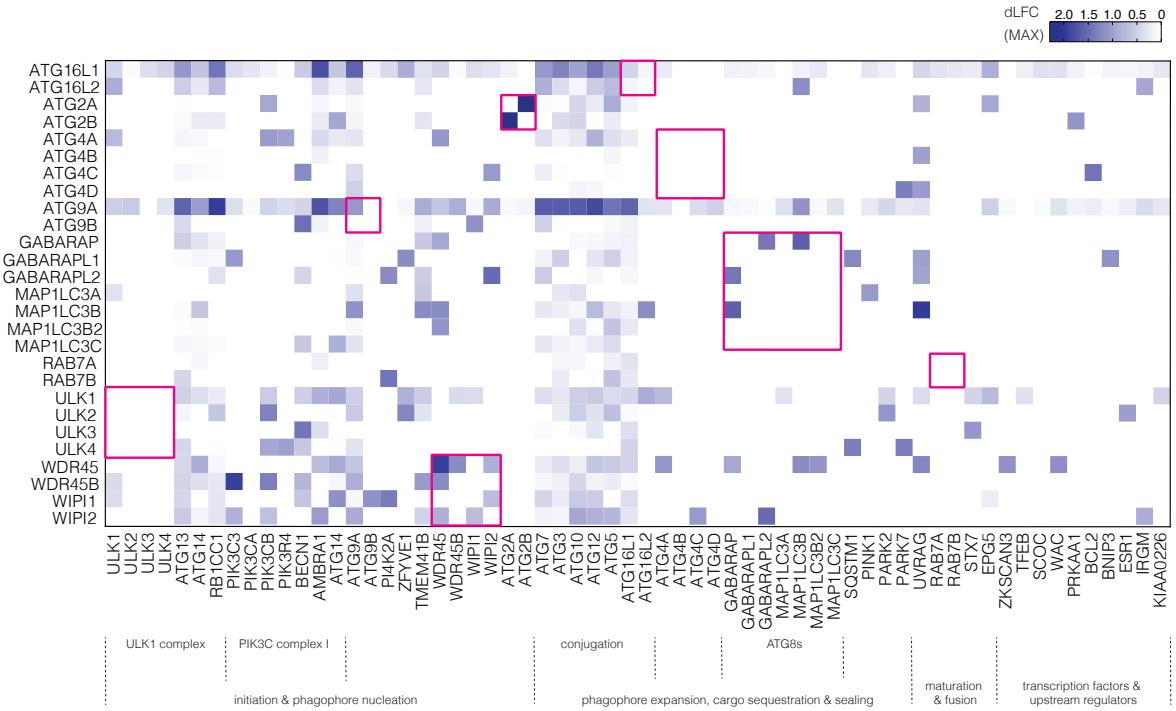

Figure 4.19: Genetic interaction profiles of core autophagy paralogs
Delta log2-fold changes (dLFC) heat map of averaged AB–BA GIs of core autophagy paralog genes across all core autophagy genes. Core autophagy genes are grouped according to their function in autophagy. Red squares highlight GIs of paralog family members. dLFC values are color-coded white to blue.

Discussion

5.1 Advantages and limitations of 3Cs multiplexing

5.1.1 Construction of highly diverse multiplex libraries in a single reaction

In the past years, several technologies have been developed to generate combinatorial CRISPR gRNA plasmids and libraries [51, 130, 151, 173, 175, 176]. All of them are based on cloning techniques that require a restriction endonuclease-based linearization of the library vector for integrating the gRNA-encoding inserts, for instance, by ligation or Gibson assembly [147]. For pooled gRNA libraries, these cloning steps are performed in iterative pooled reactions to integrate first one gRNA, and then the second. Moreover, due to cloning artefacts or low cloning efficiencies, pooled cloning reactions can result in incomplete libraries. Therefore, the intermediate libraries have to be sequenced to determine missing gRNA combinations and to repeat the pooled cloning steps, until the complete desired library diversity is represented in the final library. For example, in the yet biggest genetic interaction screen in human cells a total of 222,784 gene pairs were screened to elucidate the genetic landscape of the human cell [51]. However, of the intended 1,044,844 gRNA combinations, only 964,621 were present in the final library [51]. This highlights the need for robust technologies that allow to generate highly diverse multiplex libraries with complete library diversities.

With our 3Cs multiplexing technology we provide a robust platform for generating highly diverse pooled combinatorial CRISPR gRNA libraries in a single 3Cs synthesis reaction. 3Cs multiplexing requires no linearization of the library vector for integrating pairwise gRNAs but relies on simultaneous annealing of two non-amplified oligonucleotide pools that encode all library gRNAs. We show that 3Cs is capable of generating libraries that contain up to 913,000 gRNA combinations. The complete workflow for generating a 3Cs multiplex gRNA library takes 4 days, but includes several incubation times (Supp. Figure S1 E). The actual time requirements for manual work comprise only 10 hrs and phage particles for dU-ssDNA purification can be prepared in advance for long-term storage. Therefore, the 3Cs multiplexing technology is particularly advantageous for generating multiple different libraries at once or for construction of multiplex libraries on a routine basis.

5.1.2 3Cs multiplex libraries show uniform library distributions

The main advantage of 3Cs multiplexing is the uniformity of library distributions. The 3Cs libraries generated in this work, namely the GFP, mCherry, and autophagy single-gRNA and multiplex libraries, the 1N-4N multiplex libraries and the 1:1 multiplex library, showed distribution skews ranging from 1.1 to 1.69. As a reference, the library distribution skews for five published genome-wide single-gRNA libraries ranged from 2.4 to 8.8. [110, 116, 181, 334, 335] (skews were analyzed in [182]). Of note, the library distribution skews for multiplex libraries generated with conventional cloning methods are expected to be even higher, because the additional cloning steps for integrating the second gRNA provide additional error sources, which can potentially introduce a sequence bias. Sequence analyses showed that unevenly distributed CRISPR libraries tend to have poly-G-stretches in low abundant gRNAs and poly-T-stretches high abundant gRNAs, which is probably due to sequence-specific biases during during synthesis or PCR amplification of gRNAs for library generation [182]. We reasoned that the superior library distribution of 3Cs libraries could be explained by circumventing both, linearization of the library vector and PCR amplification of gRNA sequences. Moreover, the sequencing of artificially skewed libraries (1:1, 1:10 and 1:100) revealed that the ratio of target- to NHT-sequences of the oligonucleotide pool is reflected by the fraction of the respective sequencing reads of the final libraries (Supp. Figure S2 A-B). Therefore, we concluded that the distribution of 3Cs multiplex libraries is primarily determined by the sequence distribution of the initial oligonucleotide pool, and only marginally influenced by technical bias during 3Cs synthesis.

5.1.3 Limitations of 3Cs multiplex library generation

In theory, there is no limitation on the number of gRNA-encoding oligonucleotides, and conclusively on the desired number of target genes that could be multiplexed in a 3Cs synthesis reaction, as long as the amount of dU-ssDNA is proportionally increased and adjusted to the amount of oligonucleotides. Nevertheless, there are technical restrictions that determine the maximum number of possible gRNA combinations for a multiplex library.

First, the 3Cs synthesis reaction is followed by a coverage-based electroporation of purified 3Cs synthesis product. For example, when generating the 3Cs multiplex library with 900,000 gRNA combinations, we have observed that low electroporation efficiencies can lead to bottleneck effects and result in random loss of gRNA sequences, which will be reflected by an increased distribution skew. However, for all subsequent 3Cs multiplex libraries we were able to improve the electroporation efficiencies by scaling up the numbers of bacteria, dU-dsDNA and the electroporation cuvette sizes. A single electroporation results in average in 1×10^{11} transformed cells, which enables electroporation of libraries of up to 1×10^{8} gRNA combinations, while still providing a 1,000-fold coverage. Multiple iterative electroporations are possible as well but each additional reaction provides additional sources for sequence bias, just as with conventional cloning methods.

Further limitations of 3Cs multiplexing relate to the 3Cs multiplex vector design. The two different gRNA expression cassettes employ two distinct RNA pol III promoters and two types of tracrRNAs (tracrWT [329], and tracrV2 [312]), which on one hand are necessary to provide unique homology sites for 3Cs synthesis and prevent recombination during lentiviral packaging, but on the other hand raise concern regarding the expression and activity of the gRNAs from both promoters. On a small scale, knockout of GFP and mCherry in hTERT-RPE1 cells confirmed the functionality of both gRNA expression cassettes in a proof of concept experiment. In addition, on a larger scale, we observed stronger LFCs for gene targeting by dual-gRNAs compared to single-gRNAs (Supp. Figures S2 C-D, S7 A-C), which confirms the activity of gRNAs irrespective of their expression cassette.
Lastly, since the 3Cs multiplex vector does not encode a Cas9, 3Cs multiplex libraries are only applicable for cell lines that have been engineered for stable Cas9-expression, which constitutes a limitation for cell lines with limited expansion capacity, such as primary cell lines. Since 3Cs multiplexing is not limited to knockouts by Cas9, it is possible to expand the 3Cs multiplex tool box in the future by integrating the dual-gRNA expression cassette of the 3Cs multiplex vector into distinct library backbones that contain Cas9 or engineered Cas variants to enable other gene modifications, such as for example gene activation by CRISPRa [79].

5.2 3Cs multiplexing allows coverage-minimized screening for genetic interactions

Computational simulations have recently shown that the screening coverage and library distribution skew are critical factors for screen quality and reproducibility [182]. Indeed, our experimental approach, in which we screened combinatorial libraries with artificially skewed distributions with two different screening coverages (20- and 200-fold), supports this notion. The Cohen's d-based QSs showed increased performance quality for screens with the higher coverage of 200-fold for all three libraries. However, a 200-fold coverage could not improve the QSs for the library with a distribution skew > 13 to an extent that allowed a seperation of LFCs of NHT controls from LFCs of essential genes. Importantly, similar QSs were obtained when screening either a uniform library (distribution skew $= 1.2$) with lower coverage, or a less uniform library (distribution skew $= 2.4$) with higher coverage. In line with the QSs, MAGeCK analyses retrieved similar numbers of gene pairs passing set filters for 20- and 200-fold coverages for both libraries with distribution skew < 2.5. Compared to the 20-fold coverage, the 200-fold coverage only improved MAGeCK hit detection for the library with the highest distribution skew, but still fewer gene pairs passed the set filters compared to both libraries with distribution skews < 2.5. Surprisingly, for the uniformly distributed library, MAGeCK analyses retrieved marginally more hit gene pairs with a 20-fold coverage compared to the 200-fold. This can be explained by technical parameters, which, apart from the screening coverage, can affect the screen quality, namely the coverages during sequencing sample preparation and the sequencing depth. Since we aimed to investigate solely the effect of the screening coverage, the same amount of genomic DNA (200-fold) and the same sequencing depth (1000-fold) were applied to all samples, for both 20- and 200-fold screening coverages. In concordance with our data, computational work suggests that the coverage of genomic DNA for sequencing sample preparation can marginally affect the screen quality [182]. Taken together, our QSs and MAGeCK analyses show (1) that the distribution skew is a critical parameter that should be considered when designing combinatorial CRISPR screens, (2) that increasing the screening coverage even by 10 times is not sufficient to compensate for screening quality loss caused by high a library distribution skew above 13, and (3) that libraries with distribution skews below 2.5 can be screened with minimized screening coverages, without compromising on the data quality.

The correlations of QSs obtained from screens with artificially skewed 3Cs multiplex libraries and their distribution skews serve as an indication for choosing a screening coverage according to the library distribution and provides potential for downsizing current screen sizes, and associated efforts and costs by a factor of at least 10-fold (Figure 5.1). Good screen quality is indicated by QSs above 2, and marginal screen quality by QSs below 1 [332]. However, providing precise screening coverages for libraries with distribution skews > 8 requires further testing of screen performances at coverages above 200-fold. Importantly, the determining impact of the library distribution on the required screening coverage highlights the importance

for robust methods for generating evenly distributed gRNA libraries, such as provided by 3Cs multiplexing.

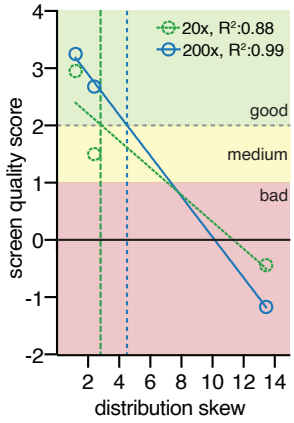

Figure 5.1: The library distribution skew determines the required screening coverage. Correlation of Cohen's d-based screen quality score and library distribution skew. Three artificially skewed 3Cs multiplex libraries were screened at 20-fold (20x, green) and 200-fold (200x, blue) coverages. Indications for high screen performance (green area) is achieved when the screen quality score is above 2 (horizontal grey dashed line).

While our experiments with artificially skewed libraries allowed us to determine minimized screening coverages for reducing the screen sizes for our subsequent screens, the analysis of the optimal number of gRNAs for multiplex screens showed that a reduction of the library diversity by reducing the number of gRNAs per gene combination is not possible. For monogenic screens it was shown that statistically robust hit detection requires at least 4 gRNAs per genes [181]. In a recent approach, it was achieved to reduce the scale of monogenic genome-wide knockout CRISPR screens without sacrificing performance by delivering two randomly paired gRNAs into each cell [336]. In line with this, we hypothesized that the knockout efficiency of target gene combinations would be increased by dual-gRNA targeting, and would therefore enable a reduction of the number of gRNAs per gene for multiplex screens. Indeed, we observed constantly increased knockout efficiencies for dual-gRNA targeting compared to single-gRNA targeting in all screens and in arrayed targeting of single genes by two-gRNAs (Supp. Figures S2 C-D, S7 A-C). However, we identified 16 gRNA combinations, corresponding to 4 gRNAs per gene, to be at least required for pairwise hit detection by MAGeCK analysis. The high number of gRNAs likely compensates for the possibility that selected gRNAs might be inactive, and in the future, improvements for selecting highly active gRNAs will likely enable a reduction of the number of gRNAs for monogenic and multiplex screens.

In summary, our results for determining minimized screening conditions for 3Cs multiplex libraries show (1) that uniformly distributed 3Cs multiplex libraries with distribution skews below 2.5 can be screened with a low coverage without compromising on quality and reproducibility and (2) that 16 gRNA combinations per gene pair are minimally required for reliable detection of hit gene pairs by MAGeCK analysis.

5.3 3Cs multiplex screens identify autophagy gene interactions in cell proliferation and autophagy flux

5.3.1 Single and combinatorial autophagy gene knockouts enhancing and suppressing proliferation

Sustained proliferation of cells, which escaped from regulation by growth signals and cell cycle control, constitutes a hallmark of cancer [337]. Autophagy maintains the genome stability of cells and its disruption has been linked to an increased risk of tumorigenesis [264, 338–340]. At the same time, in established tumors, the role of autophagy in regulating cell proliferation is more complex and highly context-dependent. Cancers with *KRAS* and *BRAF* driver mutations have been associated with high autophagy levels. For instance, pancreatic ductal adenocarcinomas (PDAC) show a high level of basal autophagy that is required for PDAC tumor growth [341, 342]. Likewise, autophagy inhibition by *ATG7* depletion led to tumor regression in a BRAF-driven lung tumors [343]. However, other studies contradict the proliferation promoting effect of high autophagy levels in tumor cells. For example, in breast cancer cells, the autophagy inducer rapamycin has been shown to repress cell proliferation by inducing cell cycle arrest [344]. Therefore, the evidence indicate that autophagy regulates proliferation in a context-dependent manner and autophagy gene interactions might be involved in the coordination of proliferation.

In our single autophagy proliferation screens, we investigated the effects of autophagy gene delpletions and identified WASHC1 to be essential for cell proliferation in hTERT-RPE1 cells. WASHC1 is part of the WASH core complex that functions as a nucleation-promoting factor at the surface of endosomes, and is also involved in endosomal sorting through facilitating tubule fission by activation of the Arp2/3 complex [345]. It was further shown that WASHC1 negatively regulates autophagy by inhibiting BECN1 ubiquitination to inactivate PIK3C3/VPS34 activity [346]. WASHC1 was likely not identified as an essential gene by previous genome-wide screens because the applied genome-wide CRISPR libraries did not include gRNAs targeting WASHC1. We observed no negative or positive proliferative effects when core essential autophagy genes were depleted, suggesting that in hTERT-RPE1 cells, proliferation does not dependent on single autophagy genes.

Our multiplex autophagy proliferation screen identified a total of 446 gene pairs that suppressed cell proliferation, and 732 gene pairs that enhanced cell proliferation upon depletion. The strongest decrease of cell proliferation was observed for knockout of the combination *WDR45B-PIK3R4*. The phospho-inositide-3-kinase regulatory subunit 4, also VPS15 (PIK3R4), constitutes a regulatory subunit of the PI3K complex that mediates the formation of PI3P [347]. A study with high-content microscopy-based assays combined with siRNA-mediated subunit depletions showed that a specific sub-complex, which contained VPS15, VPS34, Beclin 1, UVRAG and BIF-1, regulates receptor degradation and cytokinesis [348]. This opened the possibility that it may also be involved in tumor suppression by downregulation of mitogenic

signalling [348]. The WD repeat-containing protein 45B (WDR45B, also WIPI3) contains seven WD40 repeats that can fold into a beta-propeller structure and are thought to mediate protein-protein interactions. Additionally, it contains a conserved motif that enables interaction with phospholipids and mediates a scaffold function for recruiting other proteins or protein complexes [253]. Based on these observations it might be possible that WDR45B exhibits a specific role as a downstream PI3P effector that could be involved in PI3K-III sub-complex signalling pathways.

Loss of the GI between *KEAP1* and *ATG7* enhanced proliferation to a stronger degree than depletion of the tumor suppressor *TP53*. Due to this strong impact on cell proliferation, and since previous meta-analysis demonstrated that lung tumors with increased proliferative rates were associated with worse prognosis and reduced survival [349], we wondered, if this GI has clinical relevance and could serve as a survival biomarker. We explored the publicly accessible databases Gene Expression Omnibus (GEO) [323], European Genome-phenome Archive of human data (EGA) [324], and cancer Biomedical Informatics Grid (caBIG) [350], and generated Kaplan-Meier curves to analyze the five-year survival rates of lung squamous cell carcinoma (LUSC) patients based on *ATG7*, *KEAP1*, and *ATG7* and *KEAP1* gene expression data (Figure 5.2 A).

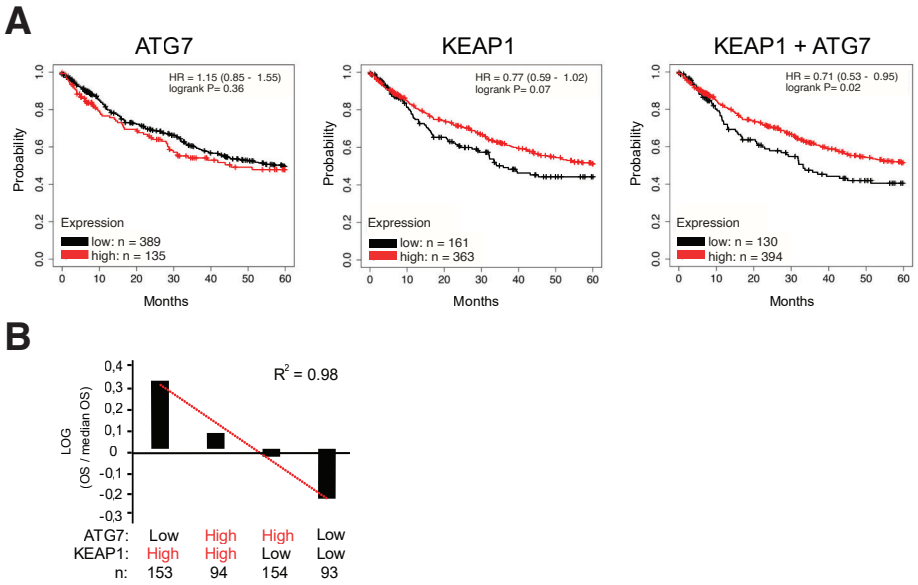

Figure 5.2: Overall survival of lung squamous cell carcinoma patients depending on *ATG7* and *KEAP1* expression

A) Kaplan-Meier curves of five-year overall survival (OS) rates of lung squamous cell carcinoma patients based on ATG7, KEAP1, and KEAP1 and ATG7 gene expression levels. Hazard ratios (HR). B) TCGA analysis of lung squamous cell carcinoma patient survival dependent on ATG7-KEAP1 gene expression profile using the UCSC Xena online tool. Regression line in red color.

The simultaneous downregulation of both genes correlated with reduced five-year survival (Figure 5.2 A). To corroborate our finding, we correlated the *ATG7* and *KEAP1* gene expression

and LUSC patient overall survival obtained from the Pan-Cancer Atlas from The Cancer Genome Atlas (TCGA) [326]. LUSC patients were classified into four categories depending on *ATG7* and *KEAP1* gene expression levels. Interestingly, patients with low expression of *ATG7* and *KEAP1* had the lowest overall survival (Figure 5.2 B).
Moreover, the presence of few highly connected hub genes, also referred to as capacitors that function as buffers for genotypic variation under normal conditions have been previously reported and predicted [351, 352]. Loss of these hub genes can modify the phenotypic consequences of mutations of many different genes [351, 352]. Indeed, we observed that the loss of *PIK3R3*, *ATG5*, or *ATG7* affects cell proliferation in combination with more than 80% of all tested genes. Particularly in cancer, mutations in single genes can exhibit no impact, but promote tumorigenesis in combination with additional mutations, thus leading to poor survival in patients. While our analyses for *KEAP1-ATG7* suggest a potential clinical relevance of *ATG7* and *KEAP1* as a novel LUSC biomarker that, however, requires further investigation, we were not not able to find clinical links for the GIs *KEAP1-ATG5* or *PIK3R4-WDR45B* by similar analyses. The complex and context-dependent nature of GIs complicates their translation to possible novel biomarkers. While these analyses are purely based on correlations and can at most serve as hints for further investigations, they highlight the potential of GIs as biomarkers and the need for an advanced understanding of the phenotypic consequences of synergistic gene functions.

5.3.2 Single genes and gene combinations essential for autophagy flux

The two different types of single autophagy flux screens identified essential autophagy genes with an overlap of 11 genes upon FDR-relaxation (Supp. Figures S5 C-D). Still, the separate single screen identified more single essential genes, for which we were able to confirm a block of autophagy by arrayed FACS validation, such as *TEMEM41B* and *WIPI2*, compared to the multiplex-inherent single screen. We can not exclude that this increased resolution observed for the separate single screen possibly resulted from the higher experimental coverage (1,000-fold) compared to the multiplex-inherent single screen (20-fold). However, the autophagy multiplex screen was intended to identify GIs in autophagy that exhibit strong depletion phenotypes to provide a proof-of-principle for minimized combinatorial CRISPR screens with reporter-based read outs. Increasing the coverage of the multiplex screen for the sake of a higher resolution, would have drastically increased cell culture efforts and FACS-time. The solution we provide for combinatorial FACS-based screens, is to perform a separate single screen with a higher coverage compared to the multiplex screen. This enables extracting more stringent single gene phenotypes that are required to compute expected phenotypes for non-interacting genes, and ultimately to identify high confidence GIs.
Similarly as to in proliferation, we identified hub genes that regulate overall autophagy flux. These include all known single essential core autophagy genes, which blocked autophagy in combination with more than 90% of all other genes of the library to a higher degree as would be

expected. Interestingly, apart from single essential core autophagy genes, we found *AMBRA1* to be highly connected, as the only gene that our and previous screens did not identify as a single essential autophagy gene, nor did the arrayed validation detect a significant block of autophagy for *AMBRA1* depletion alone. The GIs between *AMBRA1* and more than 80 other autophagy genes required for autophagy flux suggest an important buffering role of *AMBRA1* as a hub gene in the context of Torin 1 induced autophagy. AMBRA1 was shown to be a critical regulator of autophagy and to mediate the cross-talk to other cellular pathways, such as apoptosis [353, 354]. Additionally, AMBRA1 itself was shown to link autophagy to cell proliferation by promoting c-Myc dephosphorylation and degradation [264]. The 1,300-amino acid protein, which interacts with numerous proteins and mediates post-translational modifications, is characterized by WD40-domains in the N-terminal region that can serve as platform for the assembly of protein complexes and participate in diverse cellular functions [355]. Apart from the WD40-domains, the AMBRA1 protein sequence is intrinsically disordered, meaning that the rest of the protein sequence lacks recognizable domains [356]. Such intrinsically disordered regions are rich in protein–protein interaction sequences and provide flexibility for conformation changes upon binding to different interacting proteins [357]. This characteristic structure of AMBRA1 accounts for the large number of protein–protein interactions and is supposed to be crucial for the complex interactions within autophagy itself and between autophagy and other pathways [264, 358].

Lastly, our multiplex autophagy screen identified high-confidence GIs that are required for autophagic flux. We were able to validate randomly selected GIs of the network, namely *ATG2A-ATGB*, *WIPI2-GABARAPL2*, *SCOC-SIRT2*, *AMBRA1-ZKSCAN3*, *PI4K2A-RAB7B*, *PIK3CA-STK3*, and *SQSTM1-UKL4* by single and combinatorial gene depletions and quantification of autophagy block by FACS. This confirms our minimized coverage approach and MAX model based GI analysis. Interestingly, in the arrayed validation, we observed that knockout of *WIPI2* alone blocked autophagy to 25.03%. We previously identified *WIPI2* as a unique hit in the separate single screen only under conditions of FDR-relaxation. This result identifies *WIPI2* as a single essential gene for autophagy in hTERT-RPE1 cells. Underlying molecular mechanisms that result in the synergistic gene function of the identified GIs require further investigation in the future.

5.3.3 Genetic interactions between paralogous autophagy genes

Pooled CRISPR-Cas9 screens across distinct human cell lines have identified a set of core essential genes that result in decreased cell viability when they are knocked out [113]. Compared to the high number of constitutively expressed genes in a cell, only few genes constitute essential genes [113]. However, there is emerging evidence that gene essentiality can only be considered in a context-dependent manner and that, at least on an organism level, effectively every gene can be essential under certain conditions [359]. A recent study found that genes that were never identified to be essential across multiple cell lines by different screens include

a high number of paralogs [251]. These observations suggested that functionally redundant paralogs were underrepresented among essential hit genes in monogenic CRISPR-Cas9 screens because their corresponding paralogs would buffer the effects induced by their loss [251, 257]. The autophagy pathway is characterized by a high degree of paralogs, for which unique or compensatory functions are largely unknown. However, among the high-confidence GIs (dLFC $>$ 3*SD, excluding single essentials) that we identified to be essential for autophagy flux in hTERT-RPE1 cells were only three paralog gene pairs, namely *ATG2A-ATGB*, *GABARAP-GABARAPL2*, and *GABARAP-MAP1LC3B*. Among all MAX model-derived GIs (dLFC $>$ 0, LFC $>$ 0, including single essentials) we observed additional GIs among paralogs, such as GIs between members of the WIPI family.

Paralogs result from gene duplication during evolution and four different models have been proposed that describe the fate of paralogous genes after the duplication event, and explain their divergence and development of different functions [360–362]. While the model of neo-functionalization postulates that one gene copy retains the ancestral function and the second gene copy adapts to new function, the model of subfunctionalization proposes that the original gene function is subdivided between both paralogs [363, 364]. Alternatively, one paralog can retain the ancestral function while the gene copy devolves into a pseudogene [365]. Lastly, both gene copies can promote the same function, if increased protein levels provide an advantage [365]. Interpreting whether the identified GIs between paralogs suggest redundant or specific gene functions requires to differentiate between gene families that consist of only two paralog genes, such as ATG2A/B, ATG9A/B and ATG16L1/2, and paralog families that include more than two members, such as *ATG8s*, *ULKs*, *ATG4s*, and *WIPIs*.

The identified GI between *ATG2A* and *ATG2B* suggests compensatory functions of both genes, because the presence of at least one of the paralogs is required for autophagy flux. We observed very similar GI profiles for the two essential core autophagy paralogs *ATG9A* and *ATG16L1* across all core autophagy genes, and only weak interactions with their corresponding paralogs *ATG16L2* and *ATG9B*. Different spatio-temporal or tissue-specific expression profiles have been reported for paralogous genes [366, 367]. To account for context-dependent functions of *ATG9B* and *ATG16L2*, we quantified their transcript levels in RPE1 cells by RNA-seq. As expected, *ATG9A* transcripts were highly abundant, while *ATG9B* transcripts were undetectable (Figure 5.3, Supp. Table S8). In accordance to the distinct tissue-specific roles that have been reported for ATG16L2 and ATG16L1 [366], transcripts levels of *ATG16L2* were much reduced compared to *ATG16L1* (Figure 5.3).

In contrast to GIs between paralog families with two members that suggest redundant functions, the GIs we identified between *WIPI* and *ATG8* paralogs, which contain multiple paralog genes, rather suggest specific functions. For example, the GIs *WIPI1-WIPI2*, *WIPI2-WDR45*, and *WDR45-WDR45B* suggests specific roles of the WIPI members that cannot be compensated for by other members of that family, as was also previously reported [229, 253, 256, 368]. Moreover, the GIs between *GABARAP*, *MAP1LC3B*, and *GABARAPL2* and their observed higher transcript levels suggested specific roles of these three *ATG8s* in hTERT-RPE1 cells

compared to the *ATG8s* paralogs that showed no GIs. Although it has recently been shown that autophagosomes can form eventually even in the absence of all ATG8s [230], we identified GIs between *ATG8s* that might be explained by the pooled, coverage based read-out that allows to detect even subtle reduction of autophagy flux in a fraction of knockout cells. The absence of GI between *ULK* paralogs, suggests potential buffering functions that may only be uncovered by higher-order GI screens.

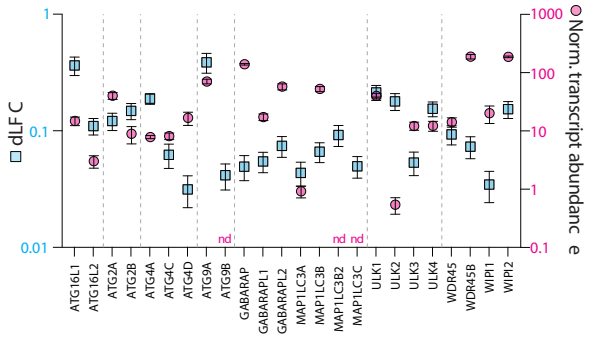

Figure 5.3: Expression levels of autophagy paralogs
Mean of delta log2-fold changes (dLFCs) of genetic interactions (GIs) of core autophagy paralogs across all core autophagy genes (blue squares, left Y-axis) compared to their normalized transcript abundance in hTERT-RPE1 cells (red dots, right Y-axis). Error bars of mean dLFCs represent standard error of mean (SEM) over all GIs. Error bars of normalized transcript abundance represent SEM over three biological replicates (n=3). Not determined (nd).

5.4 Limitations and opportunities of 3Cs multiplex screens

Although the 3Cs multiplexing technology provides a robust platform for generating uniform libraries and thus offers the potential to minimize screening conditions, there are still technical challenges that have yet to be resolved.

For instance, the sample preparation of sequencing libraries from genomic DNA of screen samples requires coverage-based PCR reactions. While computational analysis showed that transduction and PCR only marginally influenced the results in simulated screens [182], the impact of these parameters on the screening performance needs to be investigated by experimental approaches. Moreover, results from pooled monogenic or multiplex screens can be biased by non-cell autonomous effects because in a single dish cross-talk between neighboring cells can mask the true phenotype of other gene functions, for example for knockouts of growth factors. While we show that reporter-based screens can be enabled by reduced coverages and allow investigation of other phenotypes than viability and proliferation, reporter-based screens are limited to genes that are not essential for cell survival and growth because such genes are excluded during the 14 to 21 days of screening.

We hope that, in the future, generating uniform libraries by 3Cs multiplexing will advance combinatorial CRISPR screening at scale and enable investigating more complex phenotypes that

have been difficult to measure due to extensive cell culture efforts. In addition, 3Cs multiplexing might enable screens across numerous cell lines to map core essential and tissue-dependent GIs on a genome-wide scale, in the same way as it has been done for single genes. In the future it might be possible to extend the 3Cs technology to generating higher-order gRNA CRISPR libraries that express more than two gRNA in a single cell. Several different RNA polymerase III promoters from multiple species are available and, together with the new engineered gRNA scaffolds, provide sufficient design space to potentially accommodate up to 5 non-recombining gRNA-expression cassettes with unique 3Cs homology on a single lentiviral plasmid. However, coverage-based amplification and high-throughput sequencing impose practical constraints that need to be considered. And still, their experimental application and analysis is limited by cell culture demands and high-throughput sequencing strategies.

Advances in combinatorial screening will help to reveal synergistic gene functions that underlie complex phenotypes, and benefit the design of therapeutics by identifying buffering or suppressive interactions, which for example can provide molecular targets for inhibitors.

Supplements

6.1 Supplementary Tables

Table S1: Genetic mutations in autophagy related genes associated with human disease

Gene	Disease	Reference
ALFY	Primary microcephaly	[369]
APP	Alzheimer's disease	[370]
AT-1	Spastic paraplegia;	[371]
(SLC33A1)	Developmental delay;	
	Autism spectrum disorders	
ATG16L1	Crohn's disease	[372, 373]
ATG16L2	Systemic lupus erythematosus	[374]
ATG4A/B/C/D	Kashin-Beck disease;	[375, 376]
	Crohn's disease	
ATG5	Autosomal recessive spinocerebral ataxia	[377]
ATP6AP2	X-linked Parkinsonism with spasticity;	[378]
	Multisystem disorder	
BECN1	Brest and ovarian cancer	[379, 380]
C9orf72	Amyotrophic lateral sclerosis;	[381, 382]
	Frontotemporal dementia	
CALCOCO2	Crohn's disease	[383]
(NDP52)		
CLEC16A	Diabetes;	[384, 385]
	Multiple sclerosis	
CTNS	Cystinosis	[386]
EPG5	Vici syndrome	[286]
ERBB2	Breast cancer	[387]
FAM134B	Hereditary sensory and autonomic neuropathy type II	[388]
FANC genes	Fanconi anemia congenital syndrome;	[389]
	Hereditary breast and ovarian cancer;	

Table S1: Genetic mutations in autophagy related genes associated with human disease

Gene	Disease	Reference
	Sporadic cancers	
GPR65	Inflammatory bowel disease	[390]
HTT	Huntington's disease	[391]
(Huntingtin)		
IRGM	Non-alcoholic fatty liver disease;	[392, 393]
	Crohn's disease;	
	Tuberculosis	
LAMP2	Danon's cardiomyopathy	[394]
LRRK2	Crohn's disease;	[395]
	Parkinson's disease	
MTMR3	Inflammatory bowel disease	[396]
OPTN1	Amyotrophic lateral sclerosis;	[397–399]
	Primary open-angle glaucoma;	
	Paget's disease of the bone	
PARK2	Autosomal recessive and	[400, 401]
(Parkin)	sporadic early-onset Parkinson's disease	
	Colon, lung, and brain cancer	
PARK6	Autosomal recessive and	[402]
(PINK1)	sporadic early-onset Parkinson's disease	
PEX13	Zellweger syndrome spectrum disorders	[403]
PIK3R4	Cortical atrophy and epilepsy	[404]
(VPS15)		
PLEKHM1	Osteopetrosis	[405]
PS1	Alzheimer's disease	[406]
PTPN2	Inflammatory bowel disease;	[407]
	Type 1 diabetes;	
	Juvenile arthritis	
RAB7A	Charcot-Marie-Tooth type 2B disease	[408]
SMURF1	Ulcerative colitis	[409]
SNX14	Autosomal recessive spinocerebellar ataxia	[410]
SPG11	Autosomal recessive spastic paraplegia	[411]
SPG15	Autosomal recessive spastic paraplegia	[411]
(ZFYVE26)		
SPG49	Hereditary spastic paraplegia	[411]

Table S1: Genetic mutations in autophagy related genes associated with human disease

Gene	Disease	Reference
(TECPR2)		
SQSTM1	Frontotemporal dementia;	[412, 413]
(p62)	Myotrophic lateral sclerosis	
TBCK	Infantile hypotonia with psychomotor retardation	[414]
	and characterstic facies 3	
TBK1	Amyotrophic lateral sclerosis;	[289, 415]
	Frontotemporal dementia;	
	Other neurodegenerative phenotypes	
TMEM230	Parkinson's disease	[416]
TRIM20	Familial Mediterranean fever	[417]
v-ATPase	Autosomal recessive osteoporosis	[418]
VPS11	Hypomyelinating leukodystrophy	[419, 420]
VPS13D	Ataxia with spasticity	[421]
WASP	Wiskott-Aldrich syndrome	[422]
WDFY3	Autosomal dominant primary microcephaly	[423]
WDR45	Beta-propeller protein-associated neurodegeneration;	[288, 424]
(WIPI4)	Neurodegeneration with brain iron accumulation	
WDR45B	Neurodevelopmental disorder with spastic quadriplegia	[425, 426]
(WIPI3)	and brain abnormalties	
WIPI2	Cerebral palsy;	[368, 427]
	Global developmental disorder	
Adapted from		[192, 196, 420]

Supplementary Tables S2-S8 are provided as excel files on a DVD attached at the last page.

Table S2: DNA oligonucleotide sequences used for 3Cs reactions, cloning, and sequencing library preparation

Table S3: Read counts of GFP-mChery libraries

Table S4: Read counts of randomized libraries (1-4N) and multiplex library B

Table S5: Read counts of artificially skewed libraries and screens

Table S6: Read counts of autophagy single and multiplex libraries and screens

Table S7: GI model summary

Table S8: RNA-seq data of hTERT-RPE1-Cas9 cells

6.2 Supplementary Figures

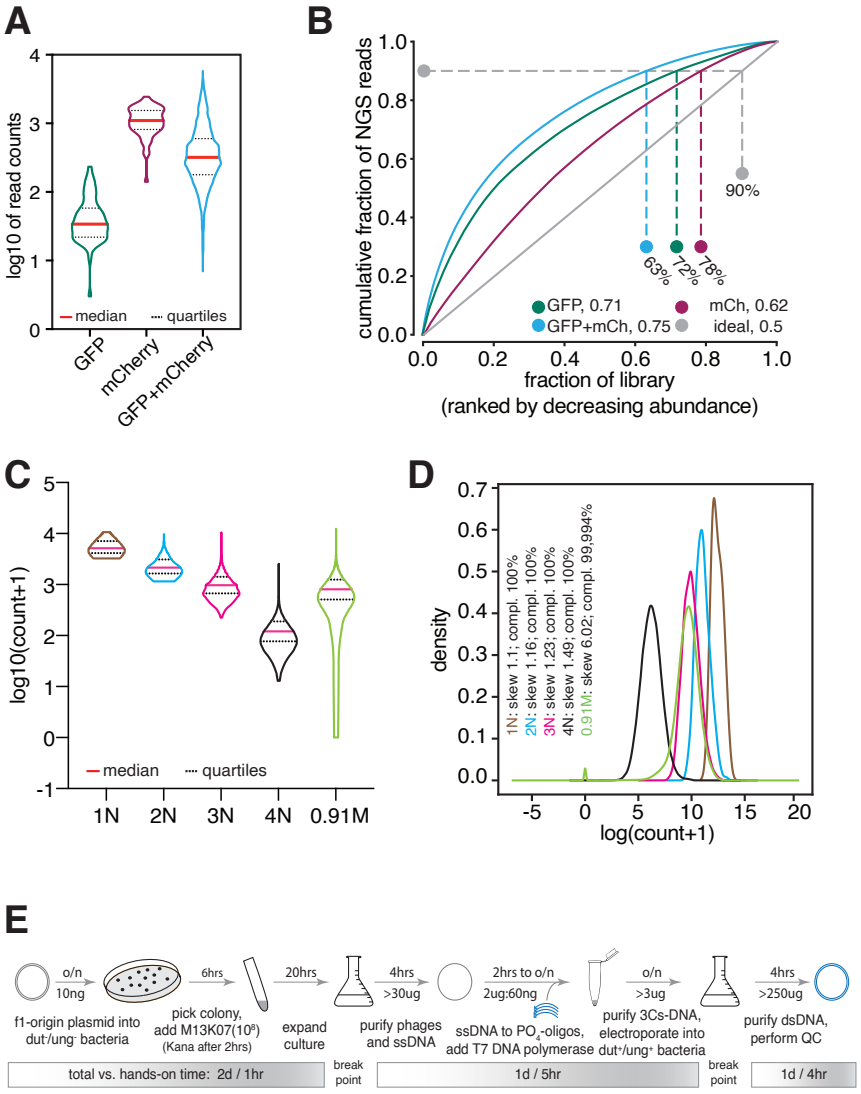

Figure S1: 3Cs multiplexing technology development
A) Sequencing depth of single-gRNA and combinatorial GFP, mCherry, and GFP+mCherry 3Cs libraries. Sample median and quartiles are shown as red straight and black dotted line, respectively. B) Area-under-the-curve (AUC) determination of single and combinatorial GFP, mCherry (mCh), and GFP+mCherry 3Cs library representations. Percentages indicate the library representation at 90% of cumulative reads. AUC values are indicated next to each library identifier. C) Sequencing depth of nucleotide-randomized multiplex 3Cs libraries (1N-4N), and the non-randomized multiplex library with 910,000 gRNA combinations (0.9M). Library median and quartiles are shown as red straight and black dotted line, respectively. D) Analysis of library distribution skews and completeness of the library complexity (%) per library, based on read counts derived from (C). E) Overview of individual steps of the 3Cs and 3Cs multiplexing protocol, and time requirements (on top of grey arrows) and required or expected DNA yields (below arrows) are highlighted. Time requirements are separated by total versus hands-on time (grey scaled bars). Adapted from [112].

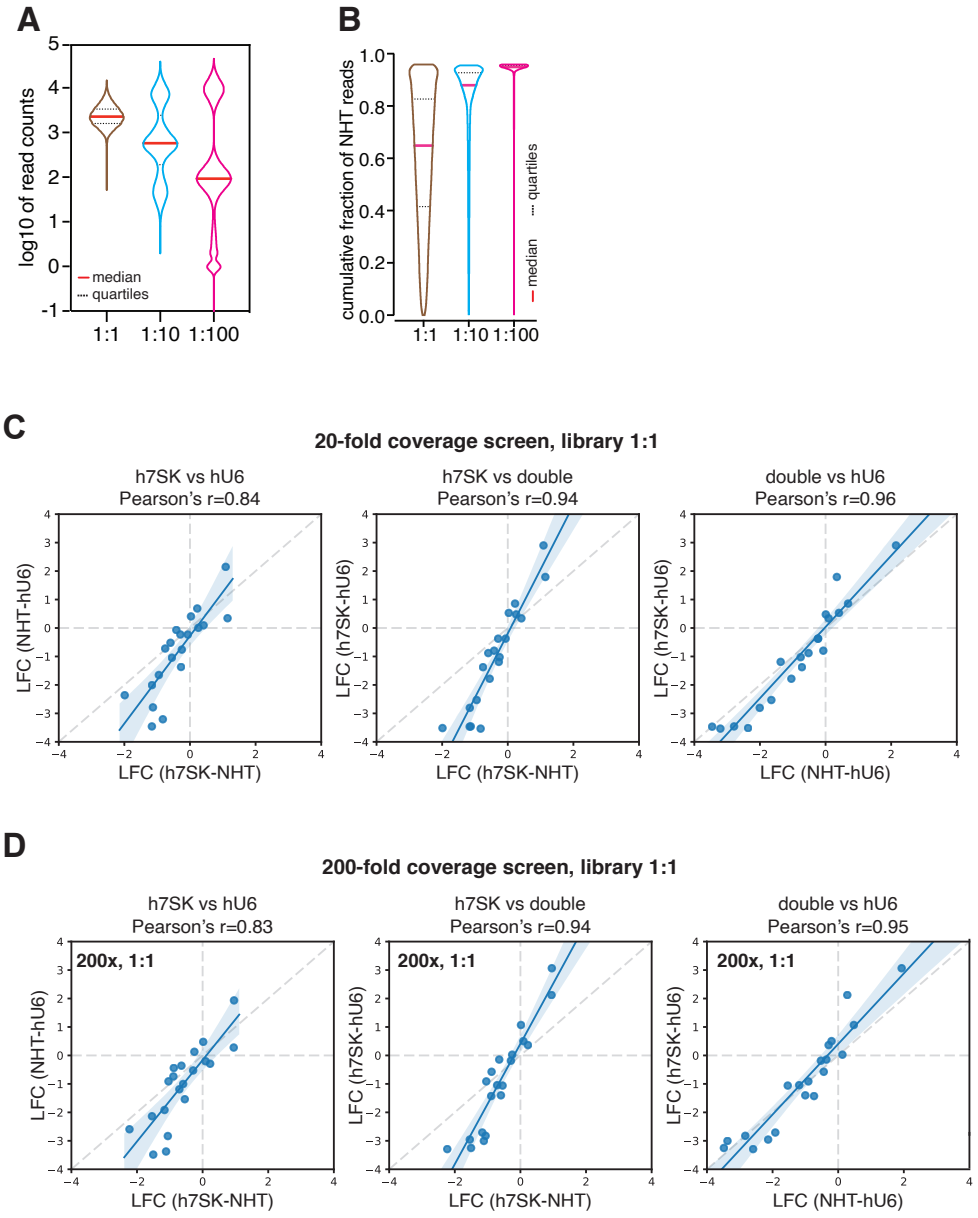

Figure S2: Evaluation of minimized screening conditions for 3Cs multiplex libraries
A) NGS sequencing depth of three multiplexed libraries (1:1, 1:10, 1:100) with biased skew ratios. The median and quartile of each sample is shown as red straight and black dotted line, respectively. B) Analysis of NHT-fraction in three libraries with artificially skewed library distributions. Median and quartiles of the distributions are shown as red straight and black dotted line, respectively. C-D) Concordance of single versus dual-gRNA gene targeting by means of gene-level log 2-fold changes (LFCs) showed stronger LFCs with two gRNAs. This effect was observed in screens performed with the 1:1 library with a 20-fold (C) and 200-fold (D) experimental coverage.

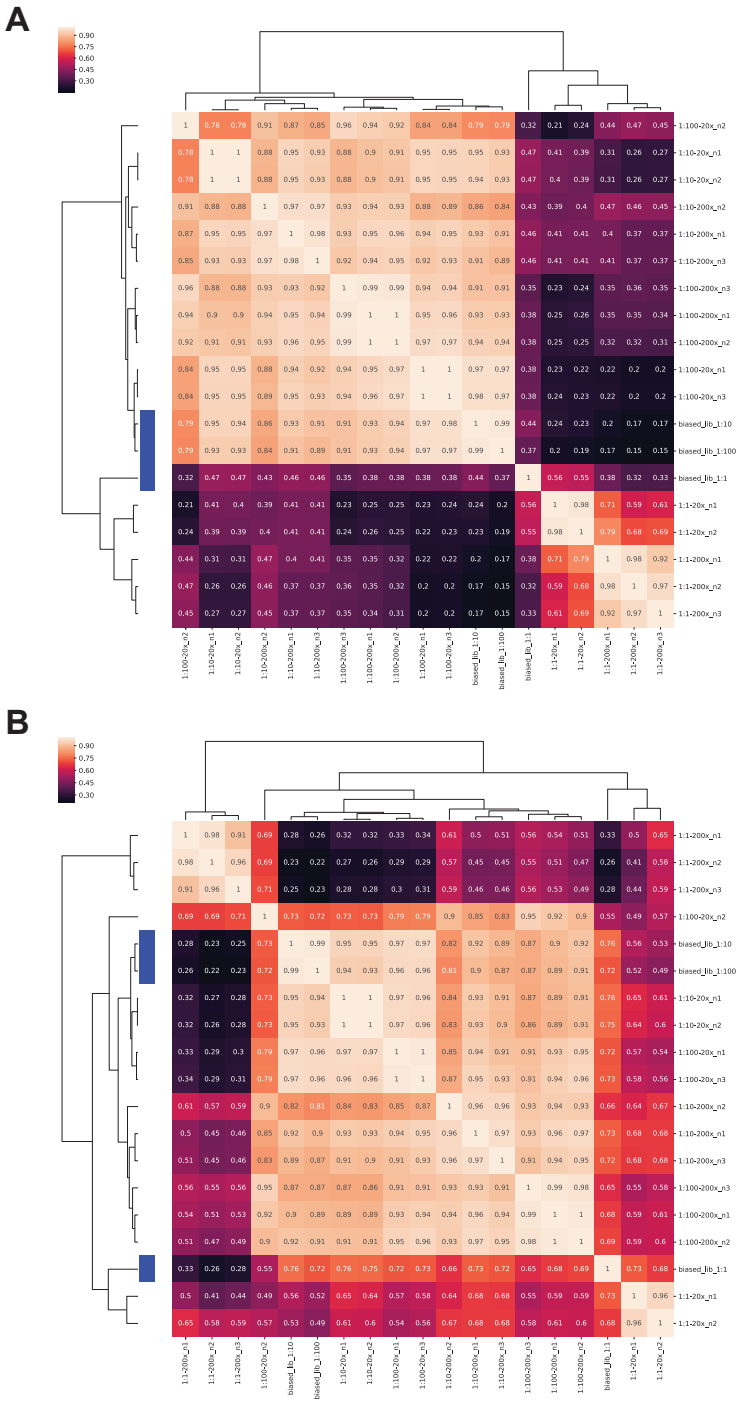

Figure S3: Correlation of libraries with biased skew ratios and corresponding 20-fold and 200-fold coverage screens

A-B) Hierarchically clustered pairwise sample correlation (Pearson's correlation coefficient, r) for all replicates (n1-n3) of the artificially skewed libraries (1:1, 1:10, 1:100) and coverages (20x, 200x). The values in individual cells indicate r of the normalized read counts. The color code visualizes no correlation (black) to high correlation (white), at gRNA (A) and gene (B) level.

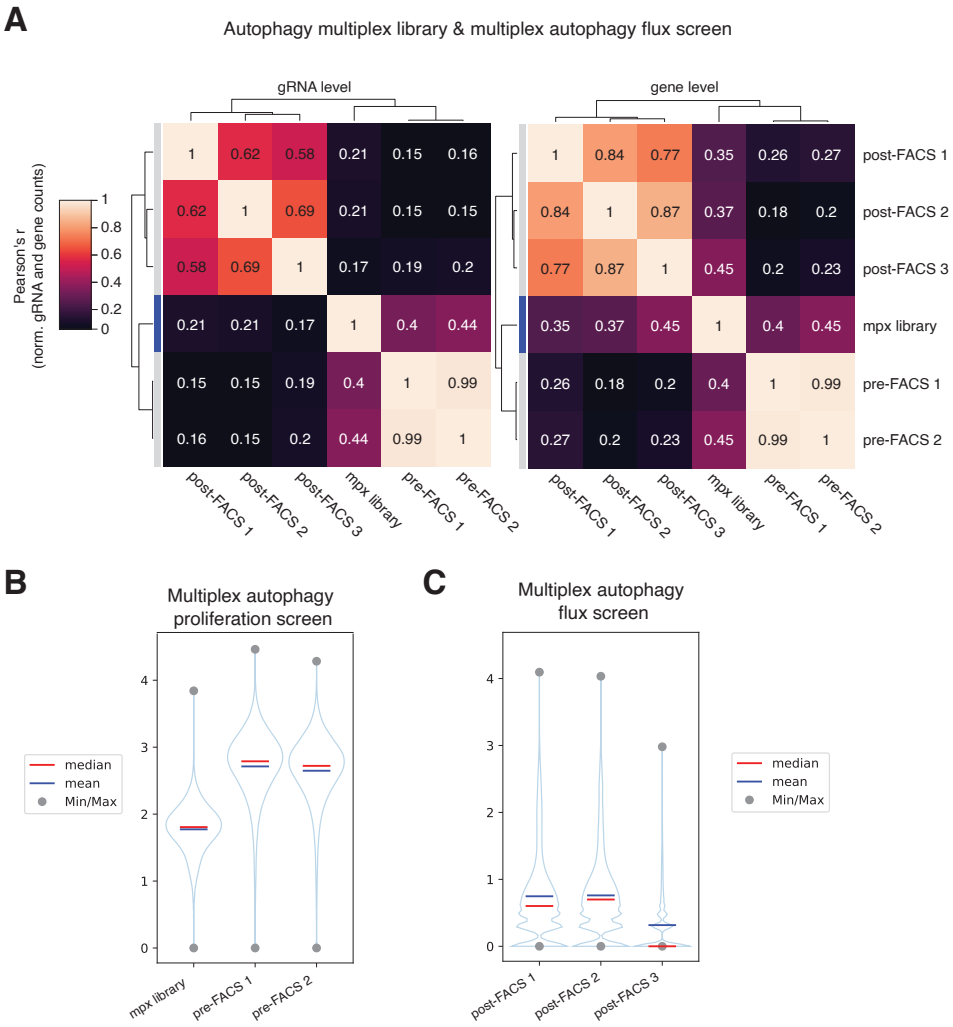

Figure S4: Sequencing analysis of the multiplex proliferation and autophagy flux screen A) Hierarchically clustered pairwise sample correlation (Pearson's correlation coefficient, r) on gRNA and gene levels of the autophagy multiplex (mpx) library and pre- and post-FACS replicates. The values in individual cells indicate r of normalized read counts. Libraries are indicated with a blue bar on the left side of each heatmap. The color code visualizes no correlation (black) to high correlation (white). B-C) Distributions of sequencing depths of replicate samples of the multiplex proliferation screen replicates (pre-FACS 1-2) and the autophagy multiplex (mpx) library (B), and the multiplex autophagy flux screen replicates (post-FACS 1-3) (C).

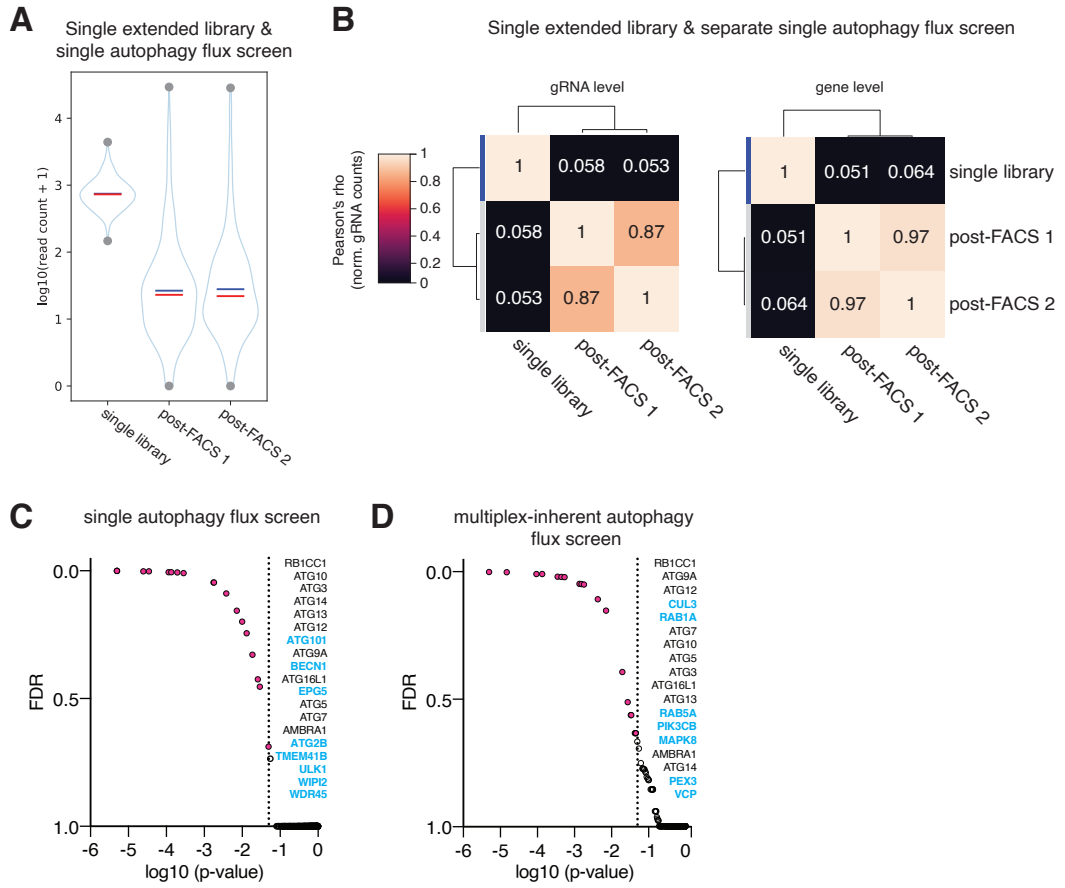

Figure S5: Sequencing analysis of the single autophagy flux screens

A) Distributions of sequencing depths of the extended single autophagy library and separate single autophagy flux screen replicates. B) Hierarchically clustered pairwise sample correlation (Pearson's correlation coefficient, r) on gRNA and gene levels of the autophagy single extended library and post-FACS samples of the separate single autophagy flux screen replicates. The values in individual cells indicate r of normalized read counts. Libraries are indicated with a blue bar on the left side of each heatmap. The color code visualizes no correlation (black) to high correlation (white). C-D) MAGeCK derived significance of enriched genes post-FACS in the separate single (C) and multiplex (mpx)-inherent single (D) screens. Genes with a p-value$<$0.05 are highlighted in red. Significant hit genes unique to the respective analysis are highlighted in blue. False-discovery-rate (FDR).

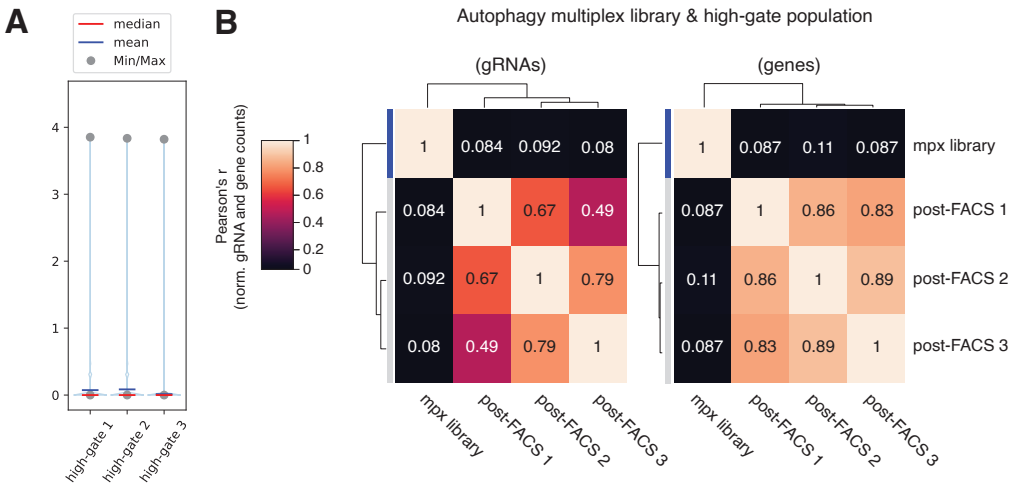

Figure S6: Sequencing analysis of the "high-gate" cell population
A) Distributions of sequencing depths of the "high-gate" cell populations from the autophagy multiplex flux screen replicates. B) Hierarchically clustered pairwise sample correlation (Pearson's correlation coefficient, r) on gRNA and gene levels of the autophagy multiplex (mpx) library and post-FACS "high-gate" cell populations from the autophagy multiplex flux screen replicates (n1-3). The values in individual cells indicate r of normalized read counts. Libraries are indicated with a blue bar on the left side of each heatmap. The color code visualizes no correlation (black) to high correlation (white).

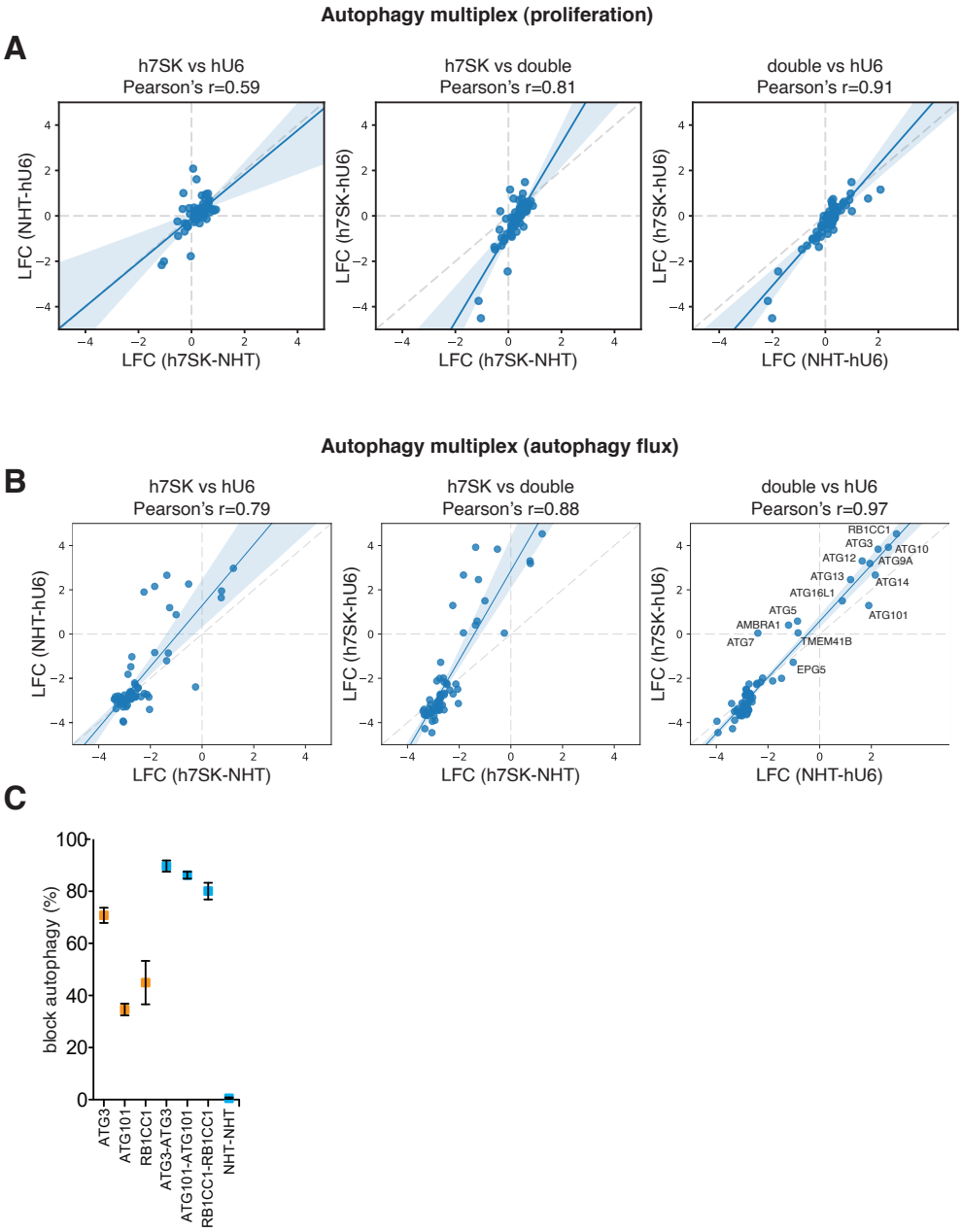

Figure S7: Comparison of dual and single gRNA targeting

A) Comparison of single and double gene log2 fold changes for core essential genes (according to Hart et al., 2017) in the autophagy proliferation screen. Left panel: single phenotypes per cassette (h7SK vs hU6, r=0.59). Middle panel: single h7SK phenotype vs the double phenotype (h7SK vs double, r=0.81). Right panel: single U6 phenotype vs the double phenotypes (double vs hU6, r=0.91). Regression line in blue. B) Comparison of single and double gene log2 fold changes for core essential autophagy genes in the autophagy flux screen. Left panel: single phenotypes per cassette (h7SK vs U6, r=0.79). Middle panel: single h7SK phenotype vs the double phenotype (h7SK vs double, r=0.88). Right panel: double phenotypes versus single U6 phenotype (double vs U6, r=0.97). Regression line in blue. C) Autophagy flux validation of single essential autophagy genes when targeted with one (yellow) or two (blue) gRNAs. Error bars represent standard error of mean (SEM) over three biological replicates (n=3).

Abbraviations

E. coli	*Escherichia coli*
S. pyogenes	*Streptococcus pyogenes*
3Cs	covalently-closed-circular-synthesized
AAV	adeno-associated viruses
ABL	Abelson tyrosine-protein kinase
ALL	acute lymphocytic leukemia
ALS	amyotrophic lateral sclerosis
AMBRA1	autophagy and beclin 1 regulator 1
AMP	ampicillin
AMPK	5'AMP-activated protein kinase
APC	anaphase promoting complex
ARFIP2	ADP ribosylation factor interacting protein 2
ARFRP1	ADP ribosylation factor related protein 1
ATCC®	American Type Culture Collection
ATG	autophagy-related
Atg	autophagy-related, in yeast
AUC	area under the curve
BCL2	B-cell lymphoma 2
BCR	breakpoint cluster region protein
BECN1	Beclin 1
BORC	BLOC-1 related
bp	base pair
BPAN	beta propeller associated neurodegeneration
BPM	between-pathway module
BRCA	breast cancer susceptibility protein
caBIG	cancer Biomedical Informatics Grid
CAR	carbenicillin
Cas12	CRISPR associated protein 12
Cas9	CRISPR-associated protein 9

CD	Crohn's disease
cDNA	complementary DNA
CHL	chloramphenicol
CMA	chaperone-mediated autophagy
CML	chronic myelogenous leukemia
COPII	coat protein complex II
CRISPR-Cas	clustered regularly interspaced short palindromic repeats and CRISPR-associated protein
CRISPRa	CRISPR activation
CRISPRi	CRISPR inhibition
cRNA	complementary RNA
crRNA	CRISPR RNA
dCas	dead CRISPR-associated protein
DFCP1	double FYVE-containing protein 1
DFNB26	deafness, autosomal recessive 26
DFNM1	deafness recessive, nonsyndromic modifier 1
dLFC	delta log2-fold change
DMEM	Dulbecco's modified Eagle's medium
DMSO	dimethyl sulfoxide
DNase	deoxyribonuclease
DRAM1	DNA damage-regulated autophagy modulator protein 1
DSB	double strand break
dsDNA	double-stranded DNA
dU	deoxyuridine
dU-dsDNA	deoxyuridine double-stranded DNA
dU-ssDNA	deoxyuridine single-stranded DNA
DUB	deubiquitinating enzyme
dut	dUTPase
dUTP	deoxyuridine triphosphate
dUTPase	dUTP diphosphatase
EGA	European Genome-phenome Archive of human data
EGFR	epidermal growth factor receptor
EMT	epithelial-mesenchymal transition
EPG5	ectopic P granules protein 5 homolog

ER	endoplasmic reticulum
ERES	ER exit sites
ERGIC	ER Golgi intermediate compartment
ESCRT	endosomal sorting complex required for transport
ext	extended
f-ori	f1 origin of replication
FACS	fluorescence-activated cell sorting
FBS	fetal bovine serum
FDA	Food and Drug Administration
FDR	false discovery rate
FIP200	200-kDa focal adhesion kinase family-interacting protein
FOXO	forkhead-box transcription factor class O
FYCO1	FYVE and coiled-coil domain containing 1
FYVE	Fab1, YOTB, VAC1, EEA1
GABARAP	gamma-aminobutyric acid receptor-associated protein
GAP	GTPase activating protein
GEO	Gene Expression Omnibus
GFP	green fluorescent protein
GI	genetic interaction
GRASP55	Golgi reassembly-stacking protein of 55 kDa
gRNA	guide RNA
h7SK	human 7SK promoter
HCS	high-content screening
HDR	homology directed repair
HDV	hepatitis delta virus
HEK	Human embryonic kidney
HER2	human epidermal Growth factor receptor 2
HMGB1	high mobility group box 1
HOPS	homotypic fusion and protein sorting
Hsp90	heat shock protein 90
hTERT-RPE1	human telomerase reverse transcriptase-immortalized retinal pigment epithelia
hU6	human U6 promoter

Indel	insertion or deletion
IRGM	immunity-related GTPase family M protein
KAN	kanamycin
LC3	light chain 3
LFC	log2-fold change
LIR	LC3-interacting region
LKB1	serine/threonine kinase 11 (STK11), also known as liver kinase B1
LUSC	lung squamous cell carcinoma
MAP1LC3A	microtubule associated protein 1 light chain 3 alpha
MAP1LC3B	microtubule associated protein 1 light chain 3 beta
MAP1LC3C	microtubule associated protein 1 light chain 3 gamma
MAPK	mitogen-activated protein kinase
MOI	multiplicity of infection
mpx	multiplex
mpx atg	multiplex autophagy
mTOR	mechanistic target of rapamycin kinase
mTORC1	mechanistic target of rapamycin complex 1
NBR1	neighbor of BRCA1 gene 1 protein
NDP52	nuclear domain 10 protein 52, also known as CALCOCO2
NGS	next-generation sequencing
NHEJ	non-homologous end joining
NHT	non-human targeting
NK	natural killer
NSLC	non-small-cell lung carcinoma
OD	optical density
OPTN	optineurin
ORP1L	oxysterol-binding protein-related protein 1L
p115	general vesicular transport factor p115
PAM	protospacer adjacent motif
PARP	poly ADP-ribose polymerase
PAS	phagophore assembly site
PBS	phosphate-buffered saline

PCR	polymerase chain reaction
PDAC	pancreatic ductal adenocarcinomas
PDI	protein-DNA interaction
PE	phosphatidylethanolamine
PI	protein interaction
PI3K	phosphoinositide-3-kinase
PI3P	phosphatidylinositol 3-phosphate
PI4K	phosphatidylinositol 4-Kinase
PI4K2A	also PI4KIIα
PI4KB	also PI4KIIIβ
PIK3C3	the class III phosphatidylinositol 3-kinase
PIK3R4	phospho-inositide-3-kinase regulatory subunit 4, also VPS15
PINK1	PTEN induced kinase 1
PLEKHM	pleckstrin homology domain-containing family M member
PNK	polynucleotide kinase
PPI	protein-protein interaction
PRKN	Parkinson disease protein 2
Puro	puromycin
QS	quality score
RAB	RAS-associated binding GTPase
RAB7	RAS-related protein RAB-7
RagD	RAS-related GTP binding D
RAS	rat sarcoma
RFP	red fluorescent protein
RNAi	RNA interference
RNase	ribonuclease
RNP	ribonucleoprotein
RPTOR	regulatory-associated protein of mTOR
RT	room temperatur
SD	standard deviation
SGA	synthetic genetic array
SLE	systemic lupus erythematosus
SMAD4	mothers against decapentaplegic homolog 4
SNAP29	synaptosome associated protein 29

SNARE	soluble N-ethylmaleimide-sensitive factor attachment protein receptor
SNP	single-nucleotide polymorphism
SpCas9	*S. pyogenes* Cas9
SQSTM1	sequestosome-1, also known as p62
ssDNA	single-stranded DNA
STK	
STR	streptomycin
STX17	syntaxin 17
T	thymine
t-SNARE	target membrane SNARE
TALENs	transcription activator-like effector nucleases
TBK1	TANK binding kinase 1
TCGA	The Cancer Genome Atlas
TET	tetracycline
TFEB	transcription factor EB
TIDE	tracking of Indels by decomposition
Tm	melting temperature
TP53	tumor protein p53
TP53BP1	tumor protein P53 binding protein 1
tracrRNA	trans-activating CRISPR RNA
TRAP	translocon-associated protein complex
TRAPPIII	transport protein particle complex 3
tRNA	transferRNA
TSC2	tuberous sclerosis 2
Ub	ubiquitin
ULK1	Unc-51 like autophagy activating kinase 1
ung	uracil-DNA glycosylase
USP	ubiquitin-specific proteases
v-SNARE	vesicle SNARE
VAMP	vesicle associated membrane protein
VAMP8	vesicle associated membrane protein 8
VSP34	vacuolar protein sorting 34, also known as PIK3C3
WASHC1	WASH complex subunit 1; also known as FAM39E or WASH1

WDR45	WD repeat domain 45
WIPI	WD repeat domain phosphoinositide interacting
WPM	within-pathway module
WT	wild type
wt	wild type
ZNFs	zinc-finger nucleases

Glossary

anoikis	Anoikis describes a type of programmed cell death, that occurs in anchorage-dependent cells upon their detachment from the surrounding extracellular matrix (ECM).
contact site	Membrane contact sites are regions of close apposition between organelles and highly conserved in evolution. They are thought to facilitate signalling and promote passaging of small molecules, such as ions, lipids or reactive oxygen species. Important membrane contact sites occur at the endoplasmic reticulum (ER), which is interacting with several organelles, including mitochondria, Golgi, endosomes, lysosomes, peroxisomes, chloroplasts and the plasma membrane. Contact sites can form between most of these organelles [428].
epithelial-mesenchymal transition	Epithelial-mesenchymal transition (ETM) allows polarized epithelial cells, which normally interact with basement membranes, to undergo multiple biochemical changes leading to a mesenchymal cell phenotype with enhanced migratory capacity, invasiveness, and elevated resistance to apoptosis. It occurs during regular embryonic development, tissue regeneration, organ fibrosis, and wound healing. However, it is also involved metastatic expansion during tumor progression and development of tumor cells with stem cell properties, which are major factors mediating resistance to cancer treatment [429].

ER exit site	The ER exit sites (ERES) are specialized zones for cargo transport from the ER to the Golgi. The ER-to-Golgi transport of cargo involves coat protein complex II (COPII) vesicles, which concentrate at the ERES[430].
expressivity	Expressivity describes the degree, to which the symptoms of a given trait can differ among individuals with the same genotype. [36].
hub-gene	Hub genes are defined as genes the highest degree of connectivity in a tested module, meaning that the connectivity ranked at top 10%. For example, for a module size of 1000, the top 100 genes were defined as the hub genes [351, 431].
Kunkel mutagenesis	Kunkel mutagenesis, also (dUTP system mutagenesis or site-directed mutagenesis) is a method for constructing a site-specific mutated gene and selecting it from the wild type (wt). To this end an *E. coli* strain with weak dUTP diphosphatase (dUTPase) activity is used, leading to increased dUTP incorporation into a plasmid DNA. This plasmid is used as a template for DNA synthesis with primers encoding the desired mutation. The resulting duplex DNA contains the wt sequence with dU replacing thymine (T) and a complementary strand, harbouring the usual DNA bases and the mutation. Upon introduction into wt bacteria, inappropriate bases are removed, thus inactivating the dU-DNA strand and leave the mutated strand to be replicated [330, 432].

library complexity	The library complexity, or diversity, is the total number of different plasmids encoding gRNAs or gRNA pairs of a CRISPR library. It is determined by the number of desired target genes and the number of gRNAs per genes.
library coverage	When planing and performing pooled CRISPR screens, the complete library complexity must be maintained at all experimental steps to avoid skewed results. The library coverage, or representation, is a measure of the mean abundance of all gRNAs (or gRNA-pairs in combinatorial libraries) that are present at a given experimental step. For example, for a library of 100,000 gRNAs, 50 million transduced cells correspond to a 500-fold library coverage, meaning that each gRNA is represented by approximately 500 cells.
library distribution	The library distribution measures of the abundance of each gRNA of a CRISPR library. While in an ideal pooled library, each plasmid encoding one specific gRNA is equally distributed real libraries exhibit a variance of plasmid abundance with underrepresented gRNAs compared to highly abundant gRNA. The ratio between 90% and 10% percentiles can be used to specify the library distribution width, also referred to as 'skew ratio' [182, 184].

library diversity	The library diversity is the total number of different plasmids encoding gRNAs or gRNA pairs of a CRISPR library. It is determined by the number of desired target genes and the number of gRNAs per genes. For example, a combinatorial CRISPR library with 10 target genes and 4 gRNAs per gene has a library diversity of (10 genes x 4 gRNAs) x (10 genes x 4 gRNAs)= 1,600 gRNA combinations.
Mendelian inheritance	Mendelian inheritance refers to an biological inheritance pattern originally proposed by Gregor Mendel in 1865 and 1866. Mendelian inheritance comprises the law of uniformity and dominance, the law of segregation, and the law of independent assortment, stating that a gene inherited from either parent segregates at equal frequency. Mendelian disease traits are inherited following three major patterns: autosomal dominant, autosomal recessive, and X-linked [433].
off-target effect	Off-target effects describe an unintended cleavage at sites other than the intended on-target site with mismatches between the sequences of the genomic site and the guide RNA. Cleavage at off-target sites can result in chromosomal rearrangements, mutations or translocations leading to disruption of normal gene expression and possibly activation of oncogenes. Therefore, reducing off-target effects constitutes major challenge in CRISPR genome editing technology [102, 434, 435].

penetrance	Penetrance refers to the proportion of individuals with a specific genotype, who manifest this genotype in their observable phenotype. In other words, how many individuals, that carry the same mutation, actually show the associated disease [436].
unconventional secretion	Unconventional protein secretion pathways mediate delivery of proteins to the plasma membrane and the extracellular space without entering the ER–Golgi conventional pathway of secretion. Unconventional secretion is mainly triggered by stress [437].

References

[1] J. Domingo, P. Baeza-Centurion and B. Lehner, 'The causes and consequences of genetic interactions (epistasis)', *Annual Review of Genomics and Human Genetics*, vol. 20, pp. 433–460, 2019.

[2] P. C. Phillips, S. P. Otto and M. C. Whitlock, 'Beyond the average', *Epistasis and the Evolutionary Process*, pp. 20–38, 2000.

[3] W. Bateson, E. Saunders, R. Punnett and C. Hurst, 'Reports to the Evolution Committee of the Royal Society, Report II. London', *UK: Harrison and Sons*, 1905.

[4] R. A. Fisher, 'The correlation between relatives on the supposition of mendelian inheritance.', *Earth and Environmental Science Transactions of the Royal Society of Edinburgh*, vol. 52, no. 2, pp. 399–433, 1919.

[5] P. C. Phillips, 'The language of gene interaction', *Genetics*, vol. 149, no. 3, pp. 1167–1171, 1998.

[6] R. Mani, R. P. S. Onge, J. L. Hartman, G. Giaever and F. P. Roth, 'Defining genetic interaction', *Proceedings of the National Academy of Sciences*, vol. 105, no. 9, pp. 3461–3466, 2008.

[7] T. Dobzhansky, 'Genetics of natural populations. XIII. Recombination and variability in populations of Drosophila pseudoobscura', *Genetics*, vol. 31, no. 3, p. 269, 1946.

[8] J. Van Leeuwen, C. Pons, J. C. Mellor, T. N. Yamaguchi, H. Friesen, J. Koschwanez, M. M. Ušaj, M. Pechlaner, M. Takar, M. Ušaj *et al.*, 'Exploring genetic suppression interactions on a global scale', *Science*, vol. 354, no. 6312, 2016.

[9] R. P. St Onge, R. Mani, J. Oh, M. Proctor, E. Fung, R. W. Davis, C. Nislow, F. P. Roth and G. Giaever, 'Systematic pathway analysis using high-resolution fitness profiling of combinatorial gene deletions', *Nature Genetics*, vol. 39, no. 2, pp. 199–206, 2007.

[10] B. L. Drees, V. Thorsson, G. W. Carter, A. W. Rives, M. Z. Raymond, I. Avila-Campillo, P. Shannon and T. Galitski, 'Derivation of genetic interaction networks from quantitative phenotype data', *Genome Biology*, vol. 6, no. 4, R38, 2005.

[11] S. J. Dixon, M. Costanzo, A. Baryshnikova, B. Andrews and C. Boone, 'Systematic mapping of genetic interaction networks', *Annual Review of Genetics*, vol. 43, pp. 601–625, 2009.

[12] X. Pan, P. Ye, D. S. Yuan, X. Wang, J. S. Bader and J. D. Boeke, 'A DNA integrity network in the yeast Saccharomyces cerevisiae', *Cell*, vol. 124, no. 5, pp. 1069–1081, 2006.

[13] A. P. Davierwala, J. Haynes, Z. Li, R. L. Brost, M. D. Robinson, L. Yu, S. Mnaimneh, H. Ding, H. Zhu, Y. Chen *et al.*, 'The synthetic genetic interaction spectrum of essential genes', *Nature Genetics*, vol. 37, no. 10, pp. 1147–1152, 2005.

[14] A. H. Y. Tong, M. Evangelista, A. B. Parsons, H. Xu, G. D. Bader, N. Pagé, M. Robinson, S. Raghibizadeh, C. W. Hogue, H. Bussey *et al.*, 'Systematic genetic analysis with ordered arrays of yeast deletion mutants', *Science*, vol. 294, no. 5550, pp. 2364–2368, 2001.

[15] K. Szafraniec, D. M. Wloch, P. Sliwa, R. H. Borts and R. Korona, 'Small fitness effects and weak genetic interactions between deleterious mutations in heterozygous loci of the yeast Saccharomyces cerevisiae', *Genetics Research*, vol. 82, no. 1, pp. 19–31, 2003.

[16] M. C. Jonikas, S. R. Collins, V. Denic, E. Oh, E. M. Quan, V. Schmid, J. Weibezahn, B. Schwappach, P. Walter, J. S. Weissman *et al.*, 'Comprehensive characterization of genes required for protein folding in the endoplasmic reticulum', *Science*, vol. 323, no. 5922, pp. 1693–1697, 2009.

[17] F. J. Vizeacoumar, Y. Chong, C. Boone and B. J. Andrews, 'A picture is worth a thousand words: genomics to phenomics in the yeast Saccharomyces cerevisiae', *FEBS letters*, vol. 583, no. 11, pp. 1656–1661, 2009.

[18] F. J. Vizeacoumar, N. van Dyk, F. S. Vizeacoumar, V. Cheung, J. Li, Y. Sydorskyy, N. Case, Z. Li, A. Datti, C. Nislow *et al.*, 'Integrating high-throughput genetic interaction mapping and high-content screening to explore yeast spindle morphogenesis', *Journal of Cell Biology*, vol. 188, no. 1, pp. 69–81, 2010.

[19] M. Costanzo, B. VanderSluis, E. N. Koch, A. Baryshnikova, C. Pons, G. Tan, W. Wang, M. Usaj, J. Hanchard, S. D. Lee *et al.*, 'A global genetic interaction network maps a wiring diagram of cellular function', *Science*, vol. 353, no. 6306, 2016.

[20] B. Boucher and S. Jenna, 'Genetic interaction networks: better understand to better predict', *Frontiers in Genetics*, vol. 4, p. 290, 2013.

[21] C. Boone, H. Bussey and B. J. Andrews, 'Exploring genetic interactions and networks with yeast', *Nature Reviews Genetics*, vol. 8, no. 6, pp. 437–449, 2007.

[22] M. Costanzo, A. Baryshnikova, C. L. Myers, B. Andrews and C. Boone, 'Charting the genetic interaction map of a cell', *Current Opinion in Biotechnology*, vol. 22, no. 1, pp. 66–74, 2011.

[23] C. Jacobs and D. Segre, 'Organization principles in genetic interaction networks', *Evolutionary Systems Biology*, pp. 53–78, 2012.

[24] A. H. Y. Tong, G. Lesage, G. D. Bader, H. Ding, H. Xu, X. Xin, J. Young, G. F. Berriz, R. L. Brost, M. Chang *et al.*, 'Global mapping of the yeast genetic interaction network', *Science*, vol. 303, no. 5659, pp. 808–813, 2004.

[25] R. Zhao, M. Davey, Y.-C. Hsu, P. Kaplanek, A. Tong, A. B. Parsons, N. Krogan, G. Cagney, D. Mai, J. Greenblatt *et al.*, 'Navigating the chaperone network: an integrative map of physical and genetic interactions mediated by the hsp90 chaperone', *Cell*, vol. 120, no. 5, pp. 715–727, 2005.

[26] I. Ulitsky and R. Shamir, 'Pathway redundancy and protein essentiality revealed in the Saccharomyces cerevisiae interaction networks', *Molecular Systems Biology*, vol. 3, no. 1, p. 104, 2007.

[27] R. Kelley and T. Ideker, 'Systematic interpretation of genetic interactions using protein networks', *Nature Biotechnology*, vol. 23, no. 5, pp. 561–566, 2005.

[28] M. Costanzo, A. Baryshnikova, J. Bellay, Y. Kim, E. D. Spear, C. S. Sevier, H. Ding, J. L. Koh, K. Toufighi, S. Mostafavi *et al.*, 'The genetic landscape of a cell', *Science*, vol. 327, no. 5964, pp. 425–431, 2010.

[29] M. Schuldiner, S. R. Collins, N. J. Thompson, V. Denic, A. Bhamidipati, T. Punna, J. Ihmels, B. Andrews, C. Boone, J. F. Greenblatt *et al.*, 'Exploration of the function and organization of the yeast early secretory pathway through an epistatic miniarray profile', *Cell*, vol. 123, no. 3, pp. 507–519, 2005.

[30] D. Segre, A. DeLuna, G. M. Church and R. Kishony, 'Modular epistasis in yeast metabolism', *Nature Genetics*, vol. 37, no. 1, pp. 77–83, 2005.

[31] R. Deshpande, B. VanderSluis and C. L. Myers, 'Comparison of profile similarity measures for genetic interaction networks', *PloS One*, vol. 8, no. 7, e68664, 2013.

[32] P. Ye, B. D. Peyser, F. A. Spencer and J. S. Bader, 'Commensurate distances and similar motifs in genetic congruence and protein interaction networks in yeast', *BMC Bioinformatics*, vol. 6, no. 1, pp. 1–13, 2005.

[33] R. Ghosh and S. J. Tabrizi, 'Huntington disease', *Handbook of clinical neurology*, vol. 147, pp. 255–278, 2018.

[34] C. R. Haldeman-Englert, T. Jewett, C. B. Mervis, C. A. Morris, B. P. Klein-Tasman, S. L. Velleman, L. R. Osborne, B. M. Finucane, L. L. LGC, D. Arkilo *et al.*, 'GeneReviews®', 2021.

[35] D. N. Cooper, M. Krawczak, C. Polychronakos, C. Tyler-Smith and H. Kehrer-Sawatzki, 'Where genotype is not predictive of phenotype: towards an understanding of the molecular basis of reduced penetrance in human inherited disease', *Human Genetics*, vol. 132, no. 10, pp. 1077–1130, 2013.

[36] J. D. Riordan and J. H. Nadeau, 'From peas to disease: modifier genes, network resilience, and the genetics of health', *The American Journal of Human Genetics*, vol. 101, no. 2, pp. 177–191, 2017.

[37] M. Costanzo, E. Kuzmin, J. van Leeuwen, B. Mair, J. Moffat, C. Boone and B. Andrews, 'Global genetic networks and the genotype-to-phenotype relationship', *Cell*, vol. 177, no. 1, pp. 85–100, 2019.

[38] R. Chen, L. Shi, J. Hakenberg, B. Naughton, P. Sklar, J. Zhang, H. Zhou, L. Tian, O. Prakash, M. Lemire *et al.*, 'Analysis of 589,306 genomes identifies individuals resilient to severe Mendelian childhood diseases', *Nature Biotechnology*, vol. 34, no. 5, pp. 531–538, 2016.

[39] S. Riazuddin, C. M. Castelein, Z. M. Ahmed, A. K. Lalwani, M. A. Mastroianni, S. Naz, T. N. Smith, N. A. Liburd, T. B. Friedman, A. J. Griffith *et al.*, 'Dominant modifier DFNM1 suppresses recessive deafness DFNB26', *Nature Genetics*, vol. 26, no. 4, pp. 431–434, 2000.

[40] A. Aly and S. Ganesan, 'BRCA1, PARP, and 53BP1: conditional synthetic lethality and synthetic viability', *Journal of Molecular Cell Biology*, vol. 3, no. 1, pp. 66–74, 2011.

[41] B. Weigelt and J. S. Reis-Filho, 'Epistatic interactions and drug response', *The Journal of Pathology*, vol. 232, no. 2, pp. 255–263, 2014.

[42] G. Laetitia, S. Sven and J. Fabrice, 'Combinatorial therapies in thyroid cancer: an overview of preclinical and clinical progresses', *Cells*, vol. 9, no. 4, p. 830, 2020.

[43] A. F. Farago, B. Y. Yeap, M. Stanzione, Y. P. Hung, R. S. Heist, J. P. Marcoux, J. Zhong, D. Rangachari, D. A. Barbie, S. Phat *et al.*, 'Combination olaparib and temozolomide in relapsed small-cell lung cancer', *Cancer Discovery*, vol. 9, no. 10, pp. 1372–1387, 2019.

[44] C. B. Johnson and S. Y. Win, 'Combination therapy with PD-1/PD-L1 blockade: an overview of ongoing clinical trials', *Oncoimmunology*, vol. 7, no. 4, e1408744, 2018.

[45] S.-h. Chen and G. Lahav, 'Two is better than one; toward a rational design of combinatorial therapy', *Current Opinion in Structural Biology*, vol. 41, pp. 145–150, 2016.

[46] W.-j. Liu, Y. Du, R. Wen, M. Yang and J. Xu, 'Drug resistance to targeted therapeutic strategies in non-small cell lung cancer', *Pharmacology & Therapeutics*, vol. 206, p. 107 438, 2020.

[47] I. B. Weinstein and A. K. Joe, 'Mechanisms of disease: oncogene addiction—a rationale for molecular targeting in cancer therapy', *Nature Clinical Practice Oncology*, vol. 3, no. 8, pp. 448–457, 2006.

[48] C. S. Huettner, P. Zhang, R. A. Van Etten and D. G. Tenen, 'Reversibility of acute B-cell leukaemia induced by BCR–ABL1', *Nature Genetics*, vol. 24, no. 1, pp. 57–60, 2000.

[49] A. Ashworth, 'A synthetic lethal therapeutic approach: poly (ADP) ribose polymerase inhibitors for the treatment of cancers deficient in DNA double-strand break repair', *Journal of Clinical Oncology*, vol. 26, no. 22, pp. 3785–3790, 2008.

[50] M. Robson, S.-A. Im, E. Senkus, B. Xu, S. M. Domchek, N. Masuda, S. Delaloge, W. Li, N. Tung, A. Armstrong *et al.*, 'Olaparib for metastatic breast cancer in patients with a germline BRCA mutation', *New England Journal of Medicine*, vol. 377, no. 6, pp. 523–533, 2017.

[51] M. A. Horlbeck, A. Xu, M. Wang, N. K. Bennett, C. Y. Park, D. Bogdanoff, B. Adamson, E. D. Chow, M. Kampmann, T. R. Peterson *et al.*, 'Mapping the genetic landscape of human cells', *Cell*, vol. 174, no. 4, pp. 953–967, 2018.

[52] Y. Xiao and Y. Liu, 'Recent advances in the discovery of novel HSP90 inhibitors: an update from 2014', *Current Drug Targets*, vol. 21, no. 3, pp. 302–317, 2020.

[53] J. L. Badano and N. Katsanis, 'Beyond Mendel: an evolving view of human genetic disease transmission', *Nature Reviews Genetics*, vol. 3, no. 10, pp. 779–789, 2002.

[54] J. Tischler, B. Lehner and A. G. Fraser, 'Evolutionary plasticity of genetic interaction networks', *Nature Genetics*, vol. 40, no. 4, pp. 390–391, 2008.

[55] M. Kampmann, M. C. Bassik and J. S. Weissman, 'Functional genomics platform for pooled screening and generation of mammalian genetic interaction maps', *Nature Protocols*, vol. 9, no. 8, p. 1825, 2014.

[56] M. C. Bassik, M. Kampmann, R. J. Lebbink, S. Wang, M. Y. Hein, I. Poser, J. Weibezahn, M. A. Horlbeck, S. Chen, M. Mann *et al.*, 'A systematic mammalian genetic interaction map reveals pathways underlying ricin susceptibility', *Cell*, vol. 152, no. 4, pp. 909–922, 2013.

[57] C. Laufer, B. Fischer, M. Billmann, W. Huber and M. Boutros, 'Mapping genetic interactions in human cancer cells with RNAi and multiparametric phenotyping', *Nature Methods*, vol. 10, no. 5, pp. 427–431, 2013.

[58] A. Roguev, D. Talbot, G. L. Negri, M. Shales, G. Cagney, S. Bandyopadhyay, B. Panning and N. J. Krogan, 'Quantitative genetic-interaction mapping in mammalian cells', *Nature Methods*, vol. 10, no. 5, pp. 432–437, 2013.

[59] L. Henkel, B. Rauscher and M. Boutros, 'Context-dependent genetic interactions in cancer', *Current Opinion in Genetics & Development*, vol. 54, pp. 73–82, 2019.

[60] A. Doudna Jennifer and E. Charpentier, 'The new frontier of genome engineering with CRISPR-Cas9', *Science*, vol. 346, no. 6213, pp. 125–8096, 2014.

[61] B. Evers, K. Jastrzebski, J. P. Heijmans, W. Grernrum, R. L. Beijersbergen and R. Bernards, 'CRISPR knockout screening outperforms shRNA and CRISPRi in identifying essential genes', *Nature Biotechnology*, vol. 34, no. 6, pp. 631–633, 2016.

[62] B. E. Housden and N. Perrimon, 'Comparing CRISPR and RNAi-based screening technologies', *Nature Biotechnology*, vol. 34, no. 6, pp. 621–623, 2016.

[63] M. Boettcher and M. T. McManus, 'Choosing the right tool for the job: RNAi, TALEN, or CRISPR', *Molecular Cell*, vol. 58, no. 4, pp. 575–585, 2015.

[64] R. Barrangou, C. Fremaux, H. Deveau, M. Richards, P. Boyaval, S. Moineau, D. A. Romero and P. Horvath, 'CRISPR provides acquired resistance against viruses in prokaryotes', *Science*, vol. 315, no. 5819, pp. 1709–1712, 2007.

[65] E. V. Koonin, K. S. Makarova and F. Zhang, 'Diversity, classification and evolution of CRISPR-Cas systems', *Current Opinion in Microbiology*, vol. 37, pp. 67–78, 2017.

[66] M. Jinek, A. East, A. Cheng, S. Lin, E. Ma and J. Doudna, 'RNA-programmed genome editing in human cells', *Elife*, vol. 2, e00471, 2013.

[67] P. Mali, L. Yang, K. M. Esvelt, J. Aach, M. Guell, J. E. DiCarlo, J. E. Norville and G. M. Church, 'RNA-guided human genome engineering via Cas9', *Science*, vol. 339, no. 6121, pp. 823–826, 2013.

[68] M. Jinek, K. Chylinski, I. Fonfara, M. Hauer, J. A. Doudna and E. Charpentier, 'A programmable dual-RNA–guided DNA endonuclease in adaptive bacterial immunity', *Science*, vol. 337, no. 6096, pp. 816–821, 2012.

[69] F. J. Mojica, C. Diez-Villaseñor, J. Garcia-Martinez and C. Almendros, 'Short motif sequences determine the targets of the prokaryotic CRISPR defence system', *Microbiology*, vol. 155, no. 3, pp. 733–740, 2009.

[70] S. H. Sternberg, S. Redding, M. Jinek, E. C. Greene and J. A. Doudna, 'DNA interrogation by the CRISPR RNA-guided endonuclease Cas9', *Nature*, vol. 507, no. 7490, pp. 62–67, 2014.

[71] C. Anders, O. Niewoehner, A. Duerst and M. Jinek, 'Structural basis of PAM-dependent target DNA recognition by the Cas9 endonuclease', *Nature*, vol. 513, no. 7519, pp. 569–573, 2014.

[72] B. Zetsche, J. S. Gootenberg, O. O. Abudayyeh, I. M. Slaymaker, K. S. Makarova, P. Essletzbichler, S. E. Volz, J. Joung, J. Van Der Oost, A. Regev *et al.*, 'Cpf1 is a single RNA-guided endonuclease of a class 2 CRISPR-Cas system', *Cell*, vol. 163, no. 3, pp. 759–771, 2015.

[73] I. Fonfara, H. Richter, M. Bratovič, A. Le Rhun and E. Charpentier, 'The CRISPR-associated DNA-cleaving enzyme Cpf1 also processes precursor CRISPR RNA', *Nature*, vol. 532, no. 7600, pp. 517–521, 2016.

[74] F. Liang, M. Han, P. J. Romanienko and M. Jasin, 'Homology-directed repair is a major double-strand break repair pathway in mammalian cells', *Proceedings of the National Academy of Sciences*, vol. 95, no. 9, pp. 5172–5177, 1998.

[75] F. A. Ran, P. D. Hsu, C.-Y. Lin, J. S. Gootenberg, S. Konermann, A. E. Trevino, D. A. Scott, A. Inoue, S. Matoba, Y. Zhang *et al.*, 'Double nicking by RNA-guided CRISPR Cas9 for enhanced genome editing specificity', *Cell*, vol. 154, no. 6, pp. 1380–1389, 2013.

[76] J. G. Doench, 'Am I ready for CRISPR? A user's guide to genetic screens', *Nature Reviews Genetics*, vol. 19, no. 2, p. 67, 2018.

[77] L. S. Qi, M. H. Larson, L. A. Gilbert, J. A. Doudna, J. S. Weissman, A. P. Arkin and W. A. Lim, 'Repurposing CRISPR as an RNA-guided platform for sequence-specific control of gene expression', *Cell*, vol. 152, no. 5, pp. 1173–1183, 2013.

[78] M. H. Larson, L. A. Gilbert, X. Wang, W. A. Lim, J. S. Weissman and L. S. Qi, 'CRISPR interference (CRISPRi) for sequence-specific control of gene expression', *Nature Protocols*, vol. 8, no. 11, pp. 2180–2196, 2013.

[79] M. Kampmann, 'CRISPRi and CRISPRa screens in mammalian cells for precision biology and medicine', *ACS Chemical Biology*, vol. 13, no. 2, pp. 406–416, 2018.

[80] A. A. Dominguez, W. A. Lim and L. S. Qi, 'Beyond editing: repurposing CRISPR–Cas9 for precision genome regulation and interrogation', *Nature Reviews Molecular Cell Biology*, vol. 17, no. 1, p. 5, 2016.

[81] L. R. Polstein, P. Perez-Pinera, D. D. Kocak, C. M. Vockley, P. Bledsoe, L. Song, A. Safi, G. E. Crawford, T. E. Reddy and C. A. Gersbach, 'Genome-wide specificity of DNA binding, gene regulation, and chromatin remodeling by TALE-and CRISPR/Cas9-based transcriptional activators', *Genome Research*, vol. 25, no. 8, pp. 1158–1169, 2015.

[82] S. Konermann, M. D. Brigham, A. E. Trevino, J. Joung, O. O. Abudayyeh, C. Barcena, P. D. Hsu, N. Habib, J. S. Gootenberg, H. Nishimasu *et al.*, 'Genome-scale transcriptional activation by an engineered CRISPR-Cas9 complex', *Nature*, vol. 517, no. 7536, pp. 583–588, 2015.

[83] H. Ma, L.-C. Tu, A. Naseri, M. Huisman, S. Zhang, D. Grunwald and T. Pederson, 'Multiplexed labeling of genomic loci with dCas9 and engineered sgRNAs using CRISPRainbow', *Nature Biotechnology*, vol. 34, no. 5, pp. 528–530, 2016.

[84] H. A. Rees and D. R. Liu, 'Base editing: precision chemistry on the genome and transcriptome of living cells', *Nature Reviews Genetics*, vol. 19, no. 12, pp. 770–788, 2018.

[85] N. M. Gaudelli, A. C. Komor, H. A. Rees, M. S. Packer, A. H. Badran, D. I. Bryson and D. R. Liu, 'Programmable base editing of A▪ T to G▪ C in genomic DNA without DNA cleavage', *Nature*, vol. 551, no. 7681, pp. 464–471, 2017.

[86] A. C. Komor, Y. B. Kim, M. S. Packer, J. A. Zuris and D. R. Liu, 'Programmable editing of a target base in genomic DNA without double-stranded DNA cleavage', *Nature*, vol. 533, no. 7603, pp. 420–424, 2016.

[87] J. Grünewald, R. Zhou, C. A. Lareau, S. P. Garcia, S. Iyer, B. R. Miller, L. M. Langner, J. Y. Hsu, M. J. Aryee and J. K. Joung, 'A dual-deaminase CRISPR base editor enables concurrent adenine and cytosine editing', *Nature Biotechnology*, pp. 1–4, 2020.

[88] A. Vojta, P. Dobrinić, V. Tadić, L. Bočkor, P. Korać, B. Julg, M. Klasić and V. Zoldoš, 'Repurposing the CRISPR-Cas9 system for targeted DNA methylation', *Nucleic Acids Research*, vol. 44, no. 12, pp. 5615–5628, 2016.

[89] J. I. McDonald, H. Celik, L. E. Rois, G. Fishberger, T. Fowler, R. Rees, A. Kramer, A. Martens, J. R. Edwards and G. A. Challen, 'Reprogrammable CRISPR/Cas9-based system for inducing site-specific DNA methylation', *Biology Open*, vol. 5, no. 6, pp. 866–874, 2016.

[90] Y.-H. Huang, J. Su, Y. Lei, L. Brunetti, M. C. Gundry, X. Zhang, M. Jeong, W. Li and M. A. Goodell, 'DNA epigenome editing using CRISPR-Cas SunTag-directed DNMT3A', *Genome Biology*, vol. 18, no. 1, pp. 1–11, 2017.

[91] R. E. Hanna and J. G. Doench, 'Design and analysis of CRISPR–Cas experiments', *Nature Biotechnology*, pp. 1–11, 2020.

[92] H. Nishimasu, X. Shi, S. Ishiguro, L. Gao, S. Hirano, S. Okazaki, T. Noda, O. O. Abudayyeh, J. S. Gootenberg, H. Mori *et al.*, 'Engineered crispr-cas9 nuclease with expanded targeting space', *Science*, vol. 361, no. 6408, pp. 1259–1262, 2018.

[93] B. P. Kleinstiver, M. S. Prew, S. Q. Tsai, V. V. Topkar, N. T. Nguyen, Z. Zheng, A. P. Gonzales, Z. Li, R. T. Peterson, J.-R. J. Yeh *et al.*, 'Engineered CRISPR-Cas9 nucleases with altered PAM specificities', *Nature*, vol. 523, no. 7561, pp. 481–485, 2015.

[94] M. J. Landrum, J. M. Lee, G. R. Riley, W. Jang, W. S. Rubinstein, D. M. Church and D. R. Maglott, 'ClinVar: public archive of relationships among sequence variation and human phenotype', *Nucleic Acids Research*, vol. 42, no. D1, pp. D980–D985, 2014.

[95] N.-Y. Chia, Y.-S. Chan, B. Feng, X. Lu, Y. L. Orlov, D. Moreau, P. Kumar, L. Yang, J. Jiang, M.-S. Lau *et al.*, 'A genome-wide RNAi screen reveals determinants of human embryonic stem cell identity', *Nature*, vol. 468, no. 7321, pp. 316–320, 2010.

[96] M. Colombi, K. Molle, D. Benjamin, K. Rattenbacher-Kiser, C. Schaefer, C. Betz, A. Thiemeyer, U. Regenass, M. Hall and C. Moroni, 'Genome-wide shRNA screen reveals increased mitochondrial dependence upon mTORC2 addiction', *Oncogene*, vol. 30, no. 13, pp. 1551–1565, 2011.

[97] A. Karlas, N. Machuy, Y. Shin, K.-P. Pleissner, A. Artarini, D. Heuer, D. Becker, H. Khalil, L. A. Ogilvie, S. Hess *et al.*, 'Genome-wide RNAi screen identifies human host factors crucial for influenza virus replication', *Nature*, vol. 463, no. 7282, pp. 818–822, 2010.

[98] J. Zuber, J. Shi, E. Wang, A. R. Rappaport, H. Herrmann, E. A. Sison, D. Magoon, J. Qi, K. Blatt, M. Wunderlich *et al.*, 'RNAi screen identifies Brd4 as a therapeutic target in acute myeloid leukaemia', *Nature*, vol. 478, no. 7370, pp. 524–528, 2011.

[99] D. W. Morgens, R. M. Deans, A. Li and M. C. Bassik, 'Systematic comparison of CRISPR/Cas9 and RNAi screens for essential genes', *Nature Biotechnology*, vol. 34, no. 6, pp. 634–636, 2016.

[100] R. Barrangou, A. Birmingham, S. Wiemann, R. L. Beijersbergen, V. Hornung and A. v. B. Smith, 'Advances in CRISPR-Cas9 genome engineering: lessons learned from RNA interference', *Nucleic Acids Research*, vol. 43, no. 7, pp. 3407–3419, 2015.

[101] J. G. Doench, E. Hartenian, D. B. Graham, Z. Tothova, M. Hegde, I. Smith, M. Sullender, B. L. Ebert, R. J. Xavier and D. E. Root, 'Rational design of highly active sgRNAs for CRISPR-Cas9–mediated gene inactivation', *Nature Biotechnology*, vol. 32, no. 12, pp. 1262–1267, 2014.

[102] J. G. Doench, N. Fusi, M. Sullender, M. Hegde, E. W. Vaimberg, K. F. Donovan, I. Smith, Z. Tothova, C. Wilen, R. Orchard *et al.*, 'Optimized sgRNA design to maximize activity and minimize off-target effects of CRISPR-Cas9', *Nature Biotechnology*, vol. 34, no. 2, pp. 184–191, 2016.

[103] A. Radzisheuskaya, D. Shlyueva, I. Müller and K. Helin, 'Optimizing sgRNA position markedly improves the efficiency of CRISPR/dCas9-mediated transcriptional repression', *Nucleic Acids Research*, vol. 44, no. 18, e141–e141, 2016.

[104] A. McKenna and J. Shendure, 'FlashFry: a fast and flexible tool for large-scale CRISPR target design', *BMC Biology*, vol. 16, no. 1, p. 74, 2018.

[105] K. Labun, T. G. Montague, M. Krause, Y. N. Torres Cleuren, H. Tjeldnes and E. Valen, 'CHOPCHOP v3: expanding the CRISPR web toolbox beyond genome editing', *Nucleic Acids Research*, vol. 47, no. W1, W171–W174, 2019.

[106] S. Bae, J. Park and J.-S. Kim, 'Cas-OFFinder: a fast and versatile algorithm that searches for potential off-target sites of Cas9 RNA-guided endonucleases', *Bioinformatics*, vol. 30, no. 10, pp. 1473–1475, 2014.

[107] J. A. Meier, F. Zhang and N. E. Sanjana, 'GUIDES: sgRNA design for loss-of-function screens', *Nature Methods*, vol. 14, no. 9, pp. 831–832, 2017.

[108] F. Heigwer, G. Kerr and M. Boutros, 'E-CRISP: fast CRISPR target site identification', *Nature Methods*, vol. 11, no. 2, pp. 122–123, 2014.

[109] T. Hart, M. Chandrashekhar, M. Aregger, Z. Steinhart, K. R. Brown, G. MacLeod, M. Mis, M. Zimmermann, A. Fradet-Turcotte, S. Sun *et al.*, 'High-resolution CRISPR screens reveal fitness genes and genotype-specific cancer liabilities', *Cell*, vol. 163, no. 6, pp. 1515–1526, 2015.

[110] T. Wang, K. Birsoy, N. W. Hughes, K. M. Krupczak, Y. Post, J. J. Wei, E. S. Lander and D. M. Sabatini, 'Identification and characterization of essential genes in the human genome', *Science*, vol. 350, no. 6264, pp. 1096–1101, 2015.

[111] D. W. Morgens, M. Wainberg, E. A. Boyle, O. Ursu, C. L. Araya, C. K. Tsui, M. S. Haney, G. T. Hess, K. Han, E. E. Jeng *et al.*, 'Genome-scale measurement of off-target activity using Cas9 toxicity in high-throughput screens', *Nature Communications*, vol. 8, no. 1, pp. 1–8, 2017.

[112] M. Wegner, V. Diehl, V. Bittl, R. de Bruyn, S. Wiechmann, Y. Matthess, M. Hebel, M. G. Hayes, S. Schaubeck, C. Benner *et al.*, 'Circular synthesized CRISPR/Cas gRNAs for functional interrogations in the coding and noncoding genome', *Elife*, vol. 8, e42549, 2019.

[113] T. Hart, A. H. Y. Tong, K. Chan, J. Van Leeuwen, A. Seetharaman, M. Aregger, M. Chandrashekhar, N. Hustedt, S. Seth, A. Noonan *et al.*, 'Evaluation and design of genome-wide CRISPR/SpCas9 knockout screens', *G3: Genes, Genomes, Genetics*, vol. 7, no. 8, pp. 2719–2727, 2017.

[114] K. Ford, D. McDonald and P. Mali, 'Functional genomics via CRISPR–Cas', *Journal of Molecular Biology*, vol. 431, no. 1, pp. 48–65, 2019.

[115] T. Wang, H. Yu, N. W. Hughes, B. Liu, A. Kendirli, K. Klein, W. W. Chen, E. S. Lander and D. M. Sabatini, 'Gene essentiality profiling reveals gene networks and synthetic lethal interactions with oncogenic Ras', *Cell*, vol. 168, no. 5, pp. 890–903, 2017.

[116] K. Tzelepis, H. Koike-Yusa, E. De Braekeleer, Y. Li, E. Metzakopian, O. M. Dovey, A. Mupo, V. Grinkevich, M. Li, M. Mazan *et al.*, 'A CRISPR dropout screen identifies genetic vulnerabilities and therapeutic targets in acute myeloid leukemia', *Cell Reports*, vol. 17, no. 4, pp. 1193–1205, 2016.

[117] A. Tsherniak, F. Vazquez, P. G. Montgomery, B. A. Weir, G. Kryukov, G. S. Cowley, S. Gill, W. F. Harrington, S. Pantel, J. M. Krill-Burger *et al.*, 'Defining a cancer dependency map', *Cell*, vol. 170, no. 3, pp. 564–576, 2017.

[118] A. Nagler, D. W. Vredevoogd, M. Alon, P. F. Cheng, S. Trabish, S. Kalaora, R. Arafeh, V. Goldin, M. P. Levesque, D. S. Peeper *et al.*, 'A genome-wide CRISPR screen identifies FBXO42 involvement in resistance toward MEK inhibition in NRAS-mutant melanoma', *Pigment Cell & Melanoma Research*, vol. 33, no. 2, pp. 334–344, 2020.

[119] B. Wang, E. B. Krall, A. J. Aguirre, M. Kim, H. R. Widlund, M. B. Doshi, E. Sicinska, R. Sulahian, A. Goodale, G. S. Cowley *et al.*, 'ATXN1L, CIC, and ETS transcription factors modulate sensitivity to MAPK pathway inhibition', *Cell Reports*, vol. 18, no. 6, pp. 1543–1557, 2017.

[120] E. B. Krall, B. Wang, D. M. Munoz, N. Ilic, S. Raghavan, M. J. Niederst, K. Yu, D. A. Ruddy, A. J. Aguirre, J. W. Kim *et al.*, 'KEAP1 loss modulates sensitivity to kinase targeted therapy in lung cancer', *Elife*, vol. 6, e18970, 2017.

[121] Y. Ma, M. J. Walsh, K. Bernhardt, C. W. Ashbaugh, S. J. Trudeau, I. Y. Ashbaugh, S. Jiang, C. Jiang, B. Zhao, D. E. Root *et al.*, 'CRISPR/Cas9 screens reveal Epstein-Barr virus-transformed B cell host dependency factors', *Cell Host & Microbe*, vol. 21, no. 5, pp. 580–591, 2017.

[122] O. Parnas, M. Jovanovic, T. M. Eisenhaure, R. H. Herbst, A. Dixit, C. J. Ye, D. Przybylski, R. J. Platt, I. Tirosh, N. E. Sanjana *et al.*, 'A genome-wide CRISPR screen in primary immune cells to dissect regulatory networks', *Cell*, vol. 162, no. 3, pp. 675–686, 2015.

[123] M. Brockmann, V. A. Blomen, J. Nieuwenhuis, E. Stickel, M. Raaben, O. B. Bleijerveld, A. M. Altelaar, L. T. Jae and T. R. Brummelkamp, 'Genetic wiring maps of single-cell protein states reveal an off-switch for GPCR signalling', *Nature*, vol. 546, no. 7657, pp. 307–311, 2017.

[124] R. J. Park, T. Wang, D. Koundakjian, J. F. Hultquist, P. Lamothe-Molina, B. Monel, K. Schumann, H. Yu, K. M. Krupzcak, W. Garcia-Beltran *et al.*, 'A genome-wide CRISPR screen identifies a restricted set of HIV host dependency factors', *Nature Genetics*, vol. 49, no. 2, pp. 193–203, 2017.

[125] X. Lin, A. Chemparathy, M. La Russa, T. Daley and L. S. Qi, 'Computational Methods for Analysis of Large-Scale CRISPR Screens', *Annual Review of Biomedical Data Science*, vol. 3, pp. 137–162, 2020.

[126] S. Bodapati, T. P. Daley, X. Lin, J. Zou and L. S. Qi, 'A benchmark of algorithms for the analysis of pooled CRISPR screens', *Genome Biology*, vol. 21, no. 1, pp. 1–13, 2020.

[127] W. Li, H. Xu, T. Xiao, L. Cong, M. I. Love, F. Zhang, R. A. Irizarry, J. S. Liu, M. Brown and X. S. Liu, 'MAGeCK enables robust identification of essential genes from genome-scale CRISPR/Cas9 knockout screens', *Genome Biology*, vol. 15, no. 12, p. 554, 2014.

[128] H.-H. Jeong, S. Y. Kim, M. W. Rousseaux, H. Y. Zoghbi and Z. Liu, 'CRISPRcloud: a secure cloud-based pipeline for CRISPR pooled screen deconvolution', *Bioinformatics*, vol. 33, no. 18, pp. 2963–2965, 2017.

[129] P. N. Spahn, T. Bath, R. J. Weiss, J. Kim, J. D. Esko, N. E. Lewis and O. Harismendy, 'PinAPL-Py: a comprehensive web-application for the analysis of CRISPR/Cas9 screens', *Scientific Reports*, vol. 7, no. 1, pp. 1–8, 2017.

[130] T. Wang, J. J. Wei, D. M. Sabatini and E. S. Lander, 'Genetic screens in human cells using the CRISPR-Cas9 system', *Science*, vol. 343, no. 6166, pp. 80–84, 2014.

[131] H. Koike-Yusa, Y. Li, E.-P. Tan, M. D. C. Velasco-Herrera and K. Yusa, 'Genome-wide recessive genetic screening in mammalian cells with a lentiviral CRISPR-guide RNA library', *Nature Biotechnology*, vol. 32, no. 3, pp. 267–273, 2014.

[132] O. Shalem, N. E. Sanjana, E. Hartenian, X. Shi, D. A. Scott, T. S. Mikkelsen, D. Heckl, B. L. Ebert, D. E. Root, J. G. Doench *et al.*, 'Genome-scale CRISPR-Cas9 knockout screening in human cells', *Science*, vol. 343, no. 6166, pp. 84–87, 2014.

[133] M. A. Horlbeck, S. J. Liu, H. Y. Chang, D. A. Lim and J. S. Weissman, 'Fitness effects of CRISPR/Cas9-targeting of long noncoding RNA genes', *Nature Biotechnology*, vol. 38, no. 5, pp. 573–576, 2020.

[134] J. Xu, C. Zhou, K. S. Foo, R. Yang, Y. Xiao, K. Bylund, M. Sahara and K. R. Chien, 'Genome-wide CRISPR screen identifies ZIC2 as an essential gene that controls the cell fate of early mesodermal precursors to human heart progenitors', *Stem Cells*, vol. 38, no. 6, pp. 741–755, 2020.

[135] B. Li, S. M. Clohisey, B. S. Chia, B. Wang, A. Cui, T. Eisenhaure, L. D. Schweitzer, P. Hoover, N. J. Parkinson, A. Nachshon *et al.*, 'Genome-wide CRISPR screen identifies host dependency factors for influenza A virus infection', *Nature Communications*, vol. 11, no. 1, pp. 1–18, 2020.

[136] J. Wei, M. Alfajaro, R. Hanna, P. DeWeirdt, M. Strine, W. Lu-Culligan, S.-M. Zhang, V. Graziano, C. Schmitz, J. Chen *et al.*, 'Genome-wide CRISPR screen reveals host genes that regulate SARS-CoV-2 infection', *BioRxiv*, 2020.

[137] Y. Li, J. Muffat, A. O. Javed, H. R. Keys, T. Lungjangwa, I. Bosch, M. Khan, M. C. Virgilio, L. Gehrke, D. M. Sabatini *et al.*, 'Genome-wide CRISPR screen for Zika virus resistance in human neural cells', *Proceedings of the National Academy of Sciences*, vol. 116, no. 19, pp. 9527–9532, 2019.

[138] M. Kurata, S. K. Rathe, N. J. Bailey, N. K. Aumann, J. M. Jones, G. W. Veldhuijzen, B. S. Moriarity and D. A. Largaespada, 'Using genome-wide CRISPR library screening with library resistant DCK to find new sources of Ara-C drug resistance in AML', *Scientific Reports*, vol. 6, no. 1, pp. 1–10, 2016.

[139] C. le Sage, S. Lawo, P. Panicker, T. M. Scales, S. A. Rahman, A. S. Little, N. J. McCarthy, J. D. Moore and B. C. Cross, 'Dual direction CRISPR transcriptional regulation screening uncovers gene networks driving drug resistance', *Scientific Reports*, vol. 7, no. 1, pp. 1–10, 2017.

[140] P. Hou, C. Wu, Y. Wang, R. Qi, D. Bhavanasi, Z. Zuo, C. Dos Santos, S. Chen, Y. Chen, H. Zheng *et al.*, 'A genome-wide CRISPR screen identifies genes critical for resistance to FLT3 inhibitor AC220', *Cancer Research*, vol. 77, no. 16, pp. 4402–4413, 2017.

[141] E. H. Yau, I. R. Kummetha, G. Lichinchi, R. Tang, Y. Zhang and T. M. Rana, 'Genome-wide CRISPR screen for essential cell growth mediators in mutant KRAS colorectal cancers', *Cancer Research*, vol. 77, no. 22, pp. 6330–6339, 2017.

[142] K. Han, S. E. Pierce, A. Li, K. Spees, G. R. Anderson, J. A. Seoane, Y.-H. Lo, M. Dubreuil, M. Olivas, R. A. Kamber *et al.*, 'CRISPR screens in cancer spheroids identify 3D growth-specific vulnerabilities', *Nature*, vol. 580, no. 7801, pp. 136–141, 2020.

[143] D. M. Munoz, P. J. Cassiani, L. Li, E. Billy, J. M. Korn, M. D. Jones, J. Golji, D. A. Ruddy, K. Yu, G. McAllister *et al.*, 'CRISPR screens provide a comprehensive assessment of cancer vulnerabilities but generate false-positive hits for highly amplified genomic regions', *Cancer Discovery*, vol. 6, no. 8, pp. 900–913, 2016.

[144] S. Jason and K. Yusa, 'Genome-wide CRISPR-Cas9 screening in mammalian cells', *Methods*, vol. 164, pp. 29–35, 2019.

[145] L. Cong, F. A. Ran, D. Cox, S. Lin, R. Barretto, N. Habib, P. D. Hsu, X. Wu, W. Jiang, L. A. Marraffini *et al.*, 'Multiplex genome engineering using CRISPR/Cas systems', *Science*, vol. 339, no. 6121, pp. 819–823, 2013.

[146] B. Minkenberg, M. Wheatley and Y. Yang, 'Crispr/cas9-enabled multiplex genome editing and its application', *Progress in Molecular Biology and Translational Science*, vol. 149, pp. 111–132, 2017.

[147] N. S. McCarty, A. E. Graham, L. Studená and R. Ledesma-Amaro, 'Multiplexed CRISPR technologies for gene editing and transcriptional regulation', *Nature Communications*, vol. 11, no. 1, pp. 1–13, 2020.

[148] K. Baek, D. H. Kim, J. Jeong, S. J. Sim, A. Melis, J.-S. Kim, E. Jin and S. Bae, 'DNA-free two-gene knockout in Chlamydomonas reinhardtii via CRISPR-Cas9 ribonucleoproteins', *Scientific Reports*, vol. 6, p. 30 620, 2016.

[149] S. Kim, D. Kim, S. W. Cho, J. Kim and J.-S. Kim, 'Highly efficient RNA-guided genome editing in human cells via delivery of purified Cas9 ribonucleoproteins', *Genome Research*, vol. 24, no. 6, pp. 1012–1019, 2014.

[150] D. Maddalo, E. Manchado, C. P. Concepcion, C. Bonetti, J. A. Vidigal, Y.-C. Han, P. Ogrodowski, A. Crippa, N. Rekhtman, E. de Stanchina *et al.*, 'In vivo engineering of oncogenic chromosomal rearrangements with the CRISPR/Cas9 system', *Nature*, vol. 516, no. 7531, pp. 423–427, 2014.

[151] K. Han, E. E. Jeng, G. T. Hess, D. W. Morgens, A. Li and M. C. Bassik, 'Synergistic drug combinations for cancer identified in a CRISPR screen for pairwise genetic interactions', *Nature Biotechnology*, vol. 35, no. 5, p. 463, 2017.

[152] J. A. Vidigal and A. Ventura, 'Rapid and efficient one-step generation of paired gRNA CRISPR-Cas9 libraries', *Nature Communications*, vol. 6, no. 1, pp. 1–7, 2015.

[153] J. M. Coffin, 'Structure, replication, and recombination of retrovirus genomes: some unifying hypotheses', *Journal of General Virology*, vol. 42, no. 1, pp. 1–26, 1979.

[154] A. M. Kabadi, D. G. Ousterout, I. B. Hilton and C. A. Gersbach, 'Multiplex CRISPR/Cas9-based genome engineering from a single lentiviral vector', *Nucleic Acids Research*, vol. 42, no. 19, e147–e147, 2014.

[155] C. C. Campa, N. R. Weisbach, A. J. Santinha, D. Incarnato and R. J. Platt, 'Multiplexed genome engineering by Cas12a and CRISPR arrays encoded on single transcripts', *Nature Methods*, vol. 16, no. 9, pp. 887–893, 2019.

[156] Y. E. Tak, B. P. Kleinstiver, J. K. Nuñez, J. Y. Hsu, J. E. Horng, J. Gong, J. S. Weissman and J. K. Joung, 'Inducible and multiplex gene regulation using CRISPR–Cpf1-based transcription factors', *Nature Methods*, vol. 14, no. 12, pp. 1163–1166, 2017.

[157] J. Kweon, A.-H. Jang, D.-e. Kim, J. W. Yang, M. Yoon, H. R. Shin, J.-S. Kim and Y. Kim, 'Fusion guide RNAs for orthogonal gene manipulation with Cas9 and Cpf1', *Nature Communications*, vol. 8, no. 1, pp. 1–6, 2017.

[158] D. C. Swarts and M. Jinek, 'Cas9 versus Cas12a/Cpf1: Structure–function comparisons and implications for genome editing', *Wiley Interdisciplinary Reviews: RNA*, vol. 9, no. 5, e1481, 2018.

[159] R. E. Haurwitz, M. Jinek, B. Wiedenheft, K. Zhou and J. A. Doudna, 'Sequence-and structure-specific RNA processing by a CRISPR endonuclease', *Science*, vol. 329, no. 5997, pp. 1355–1358, 2010.

[160] R. Ferreira, C. Skrekas, J. Nielsen and F. David, 'Multiplexed CRISPR/Cas9 genome editing and gene regulation using Csy4 in Saccharomyces cerevisiae', *ACS Synthetic Biology*, vol. 7, no. 1, pp. 10–15, 2018.

[161] M. Kurata, N. K. Wolf, W. S. Lahr, M. T. Weg, M. G. Kluesner, S. Lee, K. Hui, M. Shiraiwa, B. R. Webber and B. S. Moriarity, 'Highly multiplexed genome engineering using CRISPR/Cas9 gRNA arrays', *PLoS One*, vol. 13, no. 9, e0198714, 2018.

[162] L. Nissim, S. D. Perli, A. Fridkin, P. Perez-Pinera and T. K. Lu, 'Multiplexed and programmable regulation of gene networks with an integrated RNA and CRISPR/Cas toolkit in human cells', *Molecular Cell*, vol. 54, no. 4, pp. 698–710, 2014.

[163] Y. Gao and Y. Zhao, 'Self-processing of ribozyme-flanked RNAs into guide RNAs in vitro and in vivo for CRISPR-mediated genome editing', *Journal of Integrative Plant Biology*, vol. 56, no. 4, pp. 343–349, 2014.

[164] R. T. H. Lee, A. S. M. Ng and P. W. Ingham, 'Ribozyme mediated gRNA generation for in vitro and in vivo CRISPR/Cas9 mutagenesis', *PloS One*, vol. 11, no. 11, e0166020, 2016.

[165] L. Xu, L. Zhao, Y. Gao, J. Xu and R. Han, 'Empower multiplex cell and tissue-specific CRISPR-mediated gene manipulation with self-cleaving ribozymes and tRNA', *Nucleic Acids Research*, vol. 45, no. 5, e28–e28, 2017.

[166] K. Xie, B. Minkenberg and Y. Yang, 'Boosting CRISPR/Cas9 multiplex editing capability with the endogenous tRNA-processing system', *Proceedings of the National Academy of Sciences*, vol. 112, no. 11, pp. 3570–3575, 2015.

[167] Y. Zhang, J. Wang, Z. Wang, Y. Zhang, S. Shi, J. Nielsen and Z. Liu, 'A gRNA-tRNA array for CRISPR-Cas9 based rapid multiplexed genome editing in Saccharomyces cerevisiae', *Nature Communications*, vol. 10, no. 1, pp. 1–10, 2019.

[168] W. Qi, T. Zhu, Z. Tian, C. Li, W. Zhang and R. Song, 'High-efficiency CRISPR/Cas9 multiplex gene editing using the glycine tRNA-processing system-based strategy in maize', *BMC Biotechnology*, vol. 16, no. 1, p. 58, 2016.

[169] F. Port and S. L. Bullock, 'Augmenting CRISPR applications in Drosophila with tRNA-flanked sgRNAs', *Nature Methods*, vol. 13, no. 10, p. 852, 2016.

[170] F. Dong, K. Xie, Y. Chen, Y. Yang and Y. Mao, 'Polycistronic tRNA and CRISPR guide-RNA enables highly efficient multiplexed genome engineering in human cells', *Biochemical and Biophysical Research Communications*, vol. 482, no. 4, pp. 889–895, 2017.

[171] R. A. Hughes and A. D. Ellington, 'Synthetic DNA synthesis and assembly: putting the synthetic in synthetic biology', *Cold Spring Harbor Perspectives in Biology*, vol. 9, no. 1, a023812, 2017.

[172] A. S. Wong, G. C. Choi, C. H. Cui, G. Pregernig, P. Milani, M. Adam, S. D. Perli, S. W. Kazer, A. Gaillard, M. Hermann *et al.*, 'Multiplexed barcoded CRISPR-Cas9 screening enabled by CombiGEM', *Proceedings of the National Academy of Sciences*, vol. 113, no. 9, pp. 2544–2549, 2016.

[173] M. Aregger, K. A. Lawson, M. Billmann, M. Costanzo, A. H. Tong, K. Chan, M. Rahman, K. R. Brown, C. Ross, M. Usaj *et al.*, 'Systematic mapping of genetic interactions for de novo fatty acid synthesis identifies C12orf49 as a regulator of lipid metabolism', *Nature Metabolism*, pp. 1–15, 2020.

[174] B. Adamson, T. M. Norman, M. Jost, M. Y. Cho, J. K. Nuñez, Y. Chen, J. E. Villalta, L. A. Gilbert, M. A. Horlbeck, M. Y. Hein *et al.*, 'A multiplexed single-cell CRISPR screening platform enables systematic dissection of the unfolded protein response', *Cell*, vol. 167, no. 7, pp. 1867–1882, 2016.

[175] F. J. Najm, C. Strand, K. F. Donovan, M. Hegde, K. R. Sanson, E. W. Vaimberg, M. E. Sullender, E. Hartenian, Z. Kalani, N. Fusi *et al.*, 'Orthologous CRISPR–Cas9 enzymes for combinatorial genetic screens', *Nature Biotechnology*, vol. 36, no. 2, p. 179, 2018.

[176] J. P. Shen, D. Zhao, R. Sasik, J. Luebeck, A. Birmingham, A. Bojorquez-Gomez, K. Licon, K. Klepper, D. Pekin, A. N. Beckett *et al.*, 'Combinatorial CRISPR–Cas9 screens for de novo mapping of genetic interactions', *Nature Methods*, vol. 14, no. 6, pp. 573–576, 2017.

[177] M. Boettcher, R. Tian, J. A. Blau, E. Markegard, R. T. Wagner, D. Wu, X. Mo, A. Biton, N. Zaitlen, H. Fu *et al.*, 'Dual gene activation and knockout screen reveals directional dependencies in genetic networks', *Nature Biotechnology*, vol. 36, no. 2, p. 170, 2018.

[178] P. C. DeWeirdt, A. K. Sangree, R. E. Hanna, K. R. Sanson, M. Hegde, C. Strand, N. S. Persky and J. G. Doench, 'Genetic screens in isogenic mammalian cell lines without single cell cloning', *Nature Communications*, vol. 11, no. 1, pp. 1–15, 2020.

[179] S. L. Salzberg, 'Open questions: How many genes do we have?', *BMC Biology*, vol. 16, no. 1, pp. 1–3, 2018.

[180] J. Kweon and Y. Kim, 'High-throughput genetic screens using CRISPR–Cas9 system', *Archives of Pharmacal Research*, vol. 41, no. 9, pp. 875–884, 2018.

[181] S. H. Ong, Y. Li, H. Koike-Yusa and K. Yusa, 'Optimised metrics for CRISPR-KO screens with second-generation gRNA libraries', *Scientific Reports*, vol. 7, no. 1, pp. 1–10, 2017.

[182] K. Imkeller, G. Ambrosi, M. Boutros and W. Huber, 'gscreend: modelling asymmetric count ratios in CRISPR screens to decrease experiment size and improve phenotype detection', *Genome Biology*, vol. 21, no. 1, pp. 1–13, 2020.

[183] T. Nagy and M. Kampmann, 'CRISPulator: a discrete simulation tool for pooled genetic screens', *BMC Bioinformatics*, vol. 18, no. 1, pp. 1–12, 2017.

[184] J. Joung, S. Konermann, J. S. Gootenberg, O. O. Abudayyeh, R. J. Platt, M. D. Brigham, N. E. Sanjana and F. Zhang, 'Genome-scale CRISPR-Cas9 knockout and transcriptional activation screening', *Nature Protocols*, vol. 12, no. 4, pp. 828–863, 2017.

[185] J. Cao, Q. Xiao and Q. Yan, 'The multiplexed CRISPR targeting platforms', *Drug Discovery Today: Technologies*, vol. 28, pp. 53–61, 2018.

[186] T. Sakuma, A. Nishikawa, S. Kume, K. Chayama and T. Yamamoto, 'Multiplex genome engineering in human cells using all-in-one CRISPR/Cas9 vector system', *Scientific Reports*, vol. 4, no. 1, pp. 1–6, 2014.

[187] J. M. Replogle, T. M. Norman, A. Xu, J. A. Hussmann, J. Chen, J. Z. Cogan, E. J. Meer, J. M. Terry, D. P. Riordan, N. Srinivas *et al.*, 'Combinatorial single-cell CRISPR screens by direct guide RNA capture and targeted sequencing', *Nature Biotechnology*, pp. 1–8, 2020.

[188] J. Cao, L. Wu, S.-M. Zhang, M. Lu, W. K. Cheung, W. Cai, M. Gale, Q. Xu and Q. Yan, 'An easy and efficient inducible CRISPR/Cas9 platform with improved specificity for multiple gene targeting', *Nucleic Acids Research*, vol. 44, no. 19, e149–e149, 2016.

[189] J. Albers, C. Danzer, M. Rechsteiner, H. Lehmann, L. P. Brandt, T. Hejhal, A. Catalano, P. Busenhart, A. F. Goncalves, S. Brandt *et al.*, 'A versatile modular vector system for rapid combinatorial mammalian genetics', *The Journal of Clinical Investigation*, vol. 125, no. 4, pp. 1603–1619, 2015.

[190] C. Liao, F. Ttofali, R. A. Slotkowski, S. R. Denny, T. D. Cecil, R. T. Leenay, A. J. Keung and C. L. Beisel, 'Modular one-pot assembly of CRISPR arrays enables library generation and reveals factors influencing crRNA biogenesis', *Nature Communications*, vol. 10, no. 1, pp. 1–14, 2019.

[191] S. Kosuri and G. M. Church, 'Large-scale de novo DNA synthesis: technologies and applications', *Nature Methods*, vol. 11, no. 5, p. 499, 2014.

[192] I. Dikic and Z. Elazar, 'Mechanism and medical implications of mammalian autophagy', *Nature Reviews Molecular Cell Biology*, vol. 19, no. 6, pp. 349–364, 2018.

[193] L. Galluzzi, J. M. Bravo-San Pedro, B. Levine, D. R. Green and G. Kroemer, 'Pharmacological modulation of autophagy: therapeutic potential and persisting obstacles', *Nature Reviews Drug Discovery*, vol. 16, no. 7, p. 487, 2017.

[194] C. De Duve, B. Pressman, R. Gianetto, R. Wattiaux and F. Appelmans, 'Tissue fractionation studies. 6. Intracellular distribution patterns of enzymes in rat-liver tissue', *Biochemical Journal*, vol. 60, no. 4, pp. 604–617, 1955.

[195] Y. Ohsumi, 'The Nobel Prize in Physiology or Medicine 2016', *Stockholm, Sweden: The Nobel Assembly at Karolinska Institute*, 2016.

[196] B. Levine and G. Kroemer, 'Biological functions of autophagy genes: a disease perspective', *Cell*, vol. 176, no. 1-2, pp. 11–42, 2019.

[197] M. Oku and Y. Sakai, 'Three distinct types of microautophagy based on membrane dynamics and molecular machineries', *Bioessays*, vol. 40, no. 6, p. 1 800 008, 2018.

[198] D. Mijaljica, M. Prescott and R. J. Devenish, 'Microautophagy in mammalian cells: revisiting a 40-year-old conundrum', *Autophagy*, vol. 7, no. 7, pp. 673–682, 2011.

[199] A. C. Massey, C. Zhang and A. M. Cuervo, 'Chaperone-mediated autophagy in aging and disease', *Current Topics in Developmental Biology*, vol. 73, pp. 205–235, 2006.

[200] T. Kawabata and T. Yoshimori, 'Autophagosome biogenesis and human health', *Cell Discovery*, vol. 6, no. 1, pp. 1–14, 2020.

[201] S. A. Walker and N. T. Ktistakis, 'Autophagosome biogenesis machinery', *Journal of Molecular Biology*, 2019.

[202] A. Abada and Z. Elazar, 'Getting ready for building: signaling and autophagosome biogenesis', *EMBO Reports*, vol. 15, no. 8, pp. 839–852, 2014.

[203] A. González and M. N. Hall, 'Nutrient sensing and TOR signaling in yeast and mammals', *EMBO Journal*, vol. 36, no. 4, pp. 397–408, 2017.

[204] L. Bar-Peled and D. M. Sabatini, 'Regulation of mTORC1 by amino acids', *Trends in Cell Biology*, vol. 24, no. 7, pp. 400–406, 2014.

[205] T. J. Mercer, A. Gubas and S. A. Tooze, 'A molecular perspective of mammalian autophagosome biogenesis', *Journal of Biological Chemistry*, vol. 293, no. 15, pp. 5386–5395, 2018.

[206] N. Hosokawa, T. Hara, T. Kaizuka, C. Kishi, A. Takamura, Y. Miura, S.-i. Iemura, T. Natsume, K. Takehana, N. Yamada *et al.*, 'Nutrient-dependent mTORC1 association with the ULK1–Atg13–FIP200 complex required for autophagy', *Molecular Biology of the Cell*, vol. 20, no. 7, pp. 1981–1991, 2009.

[207] C. H. Jung, C. B. Jun, S.-H. Ro, Y.-M. Kim, N. M. Otto, J. Cao, M. Kundu and D.-H. Kim, 'ULK-Atg13-FIP200 complexes mediate mTOR signaling to the autophagy machinery', *Molecular Biology of the Cell*, vol. 20, no. 7, pp. 1992–2003, 2009.

[208] E. Itakura and N. Mizushima, 'Characterization of autophagosome formation site by a hierarchical analysis of mammalian Atg proteins', *Autophagy*, vol. 6, no. 6, pp. 764–776, 2010.

[209] M. Hamasaki, N. Furuta, A. Matsuda, A. Nezu, A. Yamamoto, N. Fujita, H. Oomori, T. Noda, T. Haraguchi, Y. Hiraoka *et al.*, 'Autophagosomes form at ER–mitochondria contact sites', *Nature*, vol. 495, no. 7441, pp. 389–393, 2013.

[210] E. Karanasios, S. A. Walker, H. Okkenhaug, M. Manifava, E. Hummel, H. Zimmermann, Q. Ahmed, M.-C. Domart, L. Collinson and N. T. Ktistakis, 'Autophagy initiation by ULK complex assembly on ER tubulovesicular regions marked by ATG9 vesicles', *Nature Communications*, vol. 7, no. 1, pp. 1–17, 2016.

[211] T. Nishimura, N. Tamura, N. Kono, Y. Shimanaka, H. Arai, H. Yamamoto and N. Mizushima, 'Autophagosome formation is initiated at phosphatidylinositol synthase-enriched ER subdomains', *EMBO Journal*, vol. 36, no. 12, pp. 1719–1735, 2017.

[212] E. L. Axe, S. A. Walker, M. Manifava, P. Chandra, H. L. Roderick, A. Habermann, G. Griffiths and N. T. Ktistakis, 'Autophagosome formation from membrane compartments enriched in phosphatidylinositol 3-phosphate and dynamically connected to the endoplasmic reticulum', *The Journal of Cell Biology*, vol. 182, no. 4, pp. 685–701, 2008.

[213] D. Judith, H. B. Jefferies, S. Boeing, D. Frith, A. P. Snijders and S. A. Tooze, 'ATG9A shapes the forming autophagosome through Arfaptin 2 and phosphatidylinositol 4-kinase IIIβ', *Journal of Cell Biology*, vol. 218, no. 5, pp. 1634–1652, 2019.

[214] Y. Fujioka, J. M. Alam, D. Noshiro, K. Mouri, T. Ando, Y. Okada, A. I. May, R. L. Knorr, K. Suzuki, Y. Ohsumi *et al.*, 'Phase separation organizes the site of autophagosome formation', *Nature*, vol. 578, no. 7794, pp. 301–305, 2020.

[215] N. T. Ktistakis, 'ER platforms mediating autophagosome generation', *Biochimica et Biophysica Acta (BBA)-Molecular and Cell Biology of Lipids*, vol. 1865, no. 1, 2020.

[216] S. A. Tooze and T. Yoshimori, 'The origin of the autophagosomal membrane', *Nature Cell Biology*, vol. 12, no. 9, pp. 831–835, 2010.

[217] D. M. Hollenstein and C. Kraft, 'Autophagosomes are formed at a distinct cellular structure', *Current Opinion in Cell Biology*, vol. 65, pp. 50–57, 2020.

[218] L. Ge, D. Melville, M. Zhang and R. Schekman, 'The ER–Golgi intermediate compartment is a key membrane source for the LC3 lipidation step of autophagosome biogenesis', *Elife*, vol. 2, e00947, 2013.

[219] J. Geng and D. J. Klionsky, 'The Golgi as a potential membrane source for autophagy', *Autophagy*, vol. 6, no. 7, pp. 950–951, 2010.

[220] D. W. Hailey, A. S. Rambold, P. Satpute-Krishnan, K. Mitra, R. Sougrat, P. K. Kim and J. Lippincott-Schwartz, 'Mitochondria supply membranes for autophagosome biogenesis during starvation', *Cell*, vol. 141, no. 4, pp. 656–667, 2010.

[221] C. Puri, M. Renna, C. F. Bento, K. Moreau and D. C. Rubinsztein, 'Diverse autophagosome membrane sources coalesce in recycling endosomes', *Cell*, vol. 154, no. 6, pp. 1285–1299, 2013.

[222] B. Ravikumar, K. Moreau, L. Jahreiss, C. Puri and D. C. Rubinsztein, 'Plasma membrane contributes to the formation of pre-autophagosomal structures', *Nature Cell Biology*, vol. 12, no. 8, pp. 747–757, 2010.

[223] T. Shima, H. Kirisako and H. Nakatogawa, 'COPII vesicles contribute to autophagosomal membranes', *Journal of Cell Biology*, vol. 218, no. 5, pp. 1503–1510, 2019.

[224] A. Orsi, M. Razi, H. Dooley, D. Robinson, A. Weston, L. Collinson and S. Tooze, 'Dynamic and transient interactions of Atg9 with autophagosomes, but not membrane integration, are required for autophagy', *Molecular Biology of the Cell*, vol. 23, no. 10, pp. 1860–1873, 2012.

[225] G. Andrejeva, S. Gowan, G. Lin, A.-C. L. Wong Te Fong, E. Shamsaei, H. G. Parkes, J. Mui, F. I. Raynaud, Y. Asad, G. Vizcay-Barrena *et al.*, 'De novo phosphatidylcholine synthesis is required for autophagosome membrane formation and maintenance during autophagy', *Autophagy*, vol. 16, no. 6, pp. 1044–1060, 2020.

[226] J. D. Lane, M. R. Slobodkin and Z. Elazar, 'The Atg8 family: multifunctional ubiquitin-like key regulators of autophagy', *Essays in Biochemistry*, vol. 55, pp. 51–64, 2013.

[227] Kuma, A and Mizushima, N and Ishihara, N and Ohsumi, Y, 'Formation of the approximately 350-kda apg12-apg5.apg16 multimeric complex, mediated by apg16 oligomerization, is essential for autophagy in yeast.', *Journal of Biological Chemistry*, vol. 277, no. 2, pp. 18 619–18 625, 2002.

[228] Y. Fujioka, N. N. Noda, H. Nakatogawa, Y. Ohsumi and F. Inagaki, 'Dimeric coiled-coil structure of Saccharomyces cerevisiae Atg16 and its functional significance in autophagy', *Journal of Biological Chemistry*, vol. 285, no. 2, pp. 1508–1515, 2010.

[229] H. C. Dooley, M. Razi, H. E. Polson, S. E. Girardin, M. I. Wilson and S. A. Tooze, 'WIPI2 links LC3 conjugation with PI3P, autophagosome formation, and pathogen clearance by recruiting Atg12–5-16L1', *Molecular Cell*, vol. 55, no. 2, pp. 238–252, 2014.

[230] T. N. Nguyen, B. S. Padman, J. Usher, V. Oorschot, G. Ramm and M. Lazarou, 'Atg8 family LC3/GABARAP proteins are crucial for autophagosome–lysosome fusion but not autophagosome formation during PINK1/Parkin mitophagy and starvation', *Journal of Cell Biology*, vol. 215, no. 6, pp. 857–874, 2016.

[231] K. Tsuboyama, I. Koyama-Honda, Y. Sakamaki, M. Koike, H. Morishita and N. Mizushima, 'The ATG conjugation systems are important for degradation of the inner autophagosomal membrane', *Science*, vol. 354, no. 6315, pp. 1036–1041, 2016.

[232] N. Mizushima, 'The ATG conjugation systems in autophagy', *Current Opinion in Cell Biology*, vol. 63, pp. 1–10, 2020.

[233] T. Johansen and T. Lamark, 'Selective autophagy: ATG8 family proteins, LIR motifs and cargo receptors', *Journal of Molecular Biology*, vol. 432, no. 1, pp. 80–103, 2020.

[234] V. Kirkin and V. V. Rogov, 'A diversity of selective autophagy receptors determines the specificity of the autophagy pathway', *Molecular Cell*, vol. 76, no. 2, pp. 268–285, 2019.

[235] V. Kirkin, D. G. McEwan, I. Novak and I. Dikic, 'A role for ubiquitin in selective autophagy', *Molecular Cell*, vol. 34, no. 3, pp. 259–269, 2009.

[236] A. Khaminets, C. Behl and I. Dikic, 'Ubiquitin-dependent and independent signals in selective autophagy', *Trends in Cell Biology*, vol. 26, no. 1, pp. 6–16, 2016.

[237] A. Stolz, A. Ernst and I. Dikic, 'Cargo recognition and trafficking in selective autophagy', *Nature Cell Biology*, vol. 16, no. 6, pp. 495–501, 2014.

[238] M. Bozic, L. van den Bekerom, B. A. Milne, N. Goodman, L. Roberston, A. R. Prescott, T. J. Macartney, N. Dawe and D. G. McEwan, 'A conserved ATG2-GABARAP family interaction is critical for phagophore formation', *EMBO Reports*, vol. 21, no. 3, e48412, 2020.

[239] R. L. Knorr, R. Lipowsky and R. Dimova, 'Autophagosome closure requires membrane scission', *Autophagy*, vol. 11, no. 11, pp. 2134–2137, 2015.

[240] Y. Takahashi, X. Liang, T. Hattori, Z. Tang, H. He, H. Chen, X. Liu, T. Abraham, Y. Imamura-Kawasawa, N. J. Buchkovich *et al.*, 'VPS37A directs ESCRT recruitment for phagophore closure', *Journal of Cell Biology*, vol. 218, no. 10, pp. 3336–3354, 2019.

[241] Y. Takahashi, H. He, Z. Tang, T. Hattori, Y. Liu, M. M. Young, J. M. Serfass, L. Chen, M. Gebru, C. Chen *et al.*, 'An autophagy assay reveals the ESCRT-III component CHMP2A as a regulator of phagophore closure', *Nature Communications*, vol. 9, no. 1, pp. 1–13, 2018.

[242] Y. Zhen, H. Spangenberg, M. J. Munson, A. Brech, K. O. Schink, K.-W. Tan, V. Sørensen, E. M. Wenzel, M. Radulovic, N. Engedal *et al.*, 'ESCRT-mediated phagophore sealing during mitophagy', *Autophagy*, vol. 16, no. 5, pp. 826–841, 2020.

[243] Y. G. Zhao and H. Zhang, 'Autophagosome maturation: an epic journey from the ER to lysosomes', *Journal of Cell Biology*, vol. 218, no. 3, pp. 757–770, 2019.

[244] Z.-Q. Yu, T. Ni, B. Hong, H.-Y. Wang, F.-J. Jiang, S. Zou, Y. Chen, X.-L. Zheng, D. J. Klionsky, Y. Liang *et al.*, 'Dual roles of Atg8- PE deconjugation by Atg4 in autophagy', *Autophagy*, vol. 8, no. 6, pp. 883–892, 2012.

[245] E. Itakura, C. Kishi-Itakura and N. Mizushima, 'The hairpin-type tail-anchored SNARE syntaxin 17 targets to autophagosomes for fusion with endosomes/lysosomes', *Cell*, vol. 151, no. 6, pp. 1256–1269, 2012.

[246] M. G. Gutierrez, D. B. Munafó, W. Berón and M. I. Colombo, 'Rab7 is required for the normal progression of the autophagic pathway in mammalian cells', *Journal of Cell Science*, vol. 117, no. 13, pp. 2687–2697, 2004.

[247] T. Itoh, E. Kanno, T. Uemura, S. Waguri and M. Fukuda, 'OATL1, a novel autophagosome-resident Rab33B-GAP, regulates autophagosomal maturation', *Journal of Cell Biology*, vol. 192, no. 5, pp. 839–853, 2011.

[248] X. Ding, X. Jiang, R. Tian, P. Zhao, L. Li, X. Wang, S. Chen, Y. Zhu, M. Mei, S. Bao *et al.*, 'RAB2 regulates the formation of autophagosome and autolysosome in mammalian cells', *Autophagy*, vol. 15, no. 10, pp. 1774–1786, 2019.

[249] J. F. Brookfield, 'Genetic redundancy: screening for selection in yeast', *Current Biology*, vol. 7, no. 6, R366–R368, 1997.

[250] R. Dandage and C. R. Landry, 'Paralog dependency indirectly affects the robustness of human cells', *Molecular Systems Biology*, vol. 15, no. 9, e8871, 2019.

[251] B. De Kegel and C. J. Ryan, 'Paralog buffering contributes to the variable essentiality of genes in cancer cell lines', *PLoS Genetics*, vol. 15, no. 10, e1008466, 2019.

[252] T. Proikas-Cezanne and S. G. Pfisterer, 'Assessing mammalian autophagy by WIPI-1/Atg18 puncta formation', *Methods in Enzymology*, vol. 452, pp. 247–260, 2009.

[253] D. Bakula, A. J. Müller, T. Zuleger, Z. Takacs, M. Franz-Wachtel, A.-K. Thost, D. Brigger, M. P. Tschan, T. Frickey, H. Robenek *et al.*, 'WIPI3 and WIPI4 β-propellers are scaffolds for LKB1-AMPK-TSC signalling circuits in the control of autophagy', *Nature Communications*, vol. 8, no. 1, pp. 1–18, 2017.

[254] D. P. Valverde, S. Yu, V. Boggavarapu, N. Kumar, J. A. Lees, T. Walz, K. M. Reinisch and T. J. Melia, 'ATG2 transports lipids to promote autophagosome biogenesis', *Journal of Cell Biology*, vol. 218, no. 6, pp. 1787–1798, 2019.

[255] T. Osawa, Y. Ishii and N. N. Noda, 'Human ATG2B possesses a lipid transfer activity which is accelerated by negatively charged lipids and WIPI4', *Genes to Cells*, vol. 25, no. 1, pp. 65–70, 2020.

[256] M. Graef, 'Membrane tethering by the autophagy ATG2A-WIPI4 complex', *Proceedings of the National Academy of Sciences*, vol. 115, no. 42, pp. 10 540–10 541, 2018.

[257] M. Dede, M. McLaughlin, E. Kim and T. Hart, 'Multiplex enCas12a screens show functional buffering by paralogs is systematically absent from genome-wide CRISPR/Cas9 knockout screens', *BioRxiv*, 2020.

[258] X. Li, S. He and B. Ma, 'Autophagy and autophagy-related proteins in cancer', *Molecular Cancer*, vol. 19, no. 1, p. 12, 2020.

[259] F. Nazio, M. Bordi, V. Cianfanelli, F. Locatelli and F. Cecconi, 'Autophagy and cancer stem cells: molecular mechanisms and therapeutic applications', *Cell Death & Differentiation*, vol. 26, no. 4, pp. 690–702, 2019.

[260] M. Garg, 'Epithelial plasticity, autophagy and metastasis: potential modifiers of the crosstalk to overcome therapeutic resistance', *Stem Cell Reviews and Reports*, pp. 1–8, 2020.

[261] R. Mathew, C. M. Karp, B. Beaudoin, N. Vuong, G. Chen, H.-Y. Chen, K. Bray, A. Reddy, G. Bhanot, C. Gelinas *et al.*, 'Autophagy suppresses tumorigenesis through elimination of p62', *Cell*, vol. 137, no. 6, pp. 1062–1075, 2009.

[262] W. Liu, Y. Meng, C. Zong, S. Zhang and L. Wei, 'Autophagy and Tumorigenesis', in *Autophagy: Biology and Diseases*, Springer, 2020, pp. 275–299.

[263] L. Mainz and M. T. Rosenfeldt, 'Autophagy and cancer–insights from mouse models', *The FEBS journal*, vol. 285, no. 5, pp. 792–808, 2018.

[264] V. Cianfanelli, C. Fuoco, M. Lorente, M. Salazar, F. Quondamatteo, P. F. Gherardini, D. De Zio, F. Nazio, M. Antonioli, M. D'Orazio *et al.*, 'AMBRA1 links autophagy to cell proliferation and tumorigenesis by promoting c-Myc dephosphorylation and degradation', *Nature Cell Biology*, vol. 17, no. 1, pp. 20–30, 2015.

[265] R. K. Amaravadi, A. C. Kimmelman and J. Debnath, 'Targeting autophagy in cancer: recent advances and future directions', *Cancer Discovery*, vol. 9, no. 9, pp. 1167–1181, 2019.

[266] J. Y. Guo, H.-Y. Chen, R. Mathew, J. Fan, A. M. Strohecker, G. Karsli-Uzunbas, J. J. Kamphorst, G. Chen, J. M. Lemons, V. Karantza *et al.*, 'Activated Ras requires autophagy to maintain oxidative metabolism and tumorigenesis', *Genes & Development*, vol. 25, no. 5, pp. 460–470, 2011.

[267] S. Seton-Rogers, 'Eliminating protective autophagy in KRAS-mutant cancers', *Nature Reviews Cancer*, vol. 19, no. 5, pp. 247–247, 2019.

[268] K. L. Bryant and C. J. Der, 'Blocking autophagy to starve pancreatic cancer', *Nature Reviews Molecular Cell Biology*, vol. 20, no. 5, pp. 265–265, 2019.

[269] A. Apel, I. Herr, H. Schwarz, H. P. Rodemann and A. Mayer, 'Blocked autophagy sensitizes resistant carcinoma cells to radiation therapy', *Cancer Research*, vol. 68, no. 5, pp. 1485–1494, 2008.

[270] D. Liu, Y. Yang, Q. Liu and J. Wang, 'Inhibition of autophagy by 3-MA potentiates cisplatin-induced apoptosis in esophageal squamous cell carcinoma cells', *Medical Oncology*, vol. 28, no. 1, pp. 105–111, 2011.

[271] T. Shingu, K. Fujiwara, O. Bögler, Y. Akiyama, K. Moritake, N. Shinojima, Y. Tamada, T. Yokoyama and S. Kondo, 'Inhibition of autophagy at a late stage enhances imatinib-induced cytotoxicity in human malignant glioma cells', *International Journal of Cancer*, vol. 124, no. 5, pp. 1060–1071, 2009.

[272] L. Galluzzi, J. M. Bravo-San Pedro, S. Demaria, S. C. Formenti and G. Kroemer, 'Activating autophagy to potentiate immunogenic chemotherapy and radiation therapy', *Nature Reviews Clinical Oncology*, vol. 14, no. 4, p. 247, 2017.

[273] M.-E. Papandreou and N. Tavernarakis, 'Crosstalk between Endo/Exocytosis and Autophagy in Health and Disease', *Biotechnology Journal*, p. 1 900 267, 2020.

[274] H.-T. Chen, H. Liu, M.-J. Mao, Y. Tan, X.-Q. Mo, X.-J. Meng, M.-T. Cao, C.-Y. Zhong, Y. Liu, H. Shan *et al.*, 'Crosstalk between autophagy and epithelial-mesenchymal transition and its application in cancer therapy', *Molecular Cancer*, vol. 18, no. 1, pp. 1–19, 2019.

[275] M. Catalano, G. D'Alessandro, F. Lepore, M. Corazzari, S. Caldarola, C. Valacca, F. Faienza, V. Esposito, C. Limatola, F. Cecconi *et al.*, 'Autophagy induction impairs migration and invasion by reversing EMT in glioblastoma cells', *Molecular Oncology*, vol. 9, no. 8, pp. 1612–1625, 2015.

[276] Q. Lv, W. Wang, J. Xue, F. Hua, R. Mu, H. Lin, J. Yan, X. Lv, X. Chen and Z.-W. Hu, 'DEDD interacts with PI3KC3 to activate autophagy and attenuate epithelial–mesenchymal transition in human breast cancer', *Cancer Research*, vol. 72, no. 13, pp. 3238–3250, 2012.

[277] Y. Bao, Z. Ding, P. Zhao, J. Li, P. Chen, J. Zheng and Z. Qian, 'Autophagy inhibition potentiates the anti-EMT effects of alteronol through TGF-β/Smad3 signaling in melanoma cells', *Cell Death & Disease*, vol. 11, no. 4, pp. 1–10, 2020.

[278] H. Shen, L. Yin, G. Deng, C. Guo, Y. Han, Y. Li, C. Cai, Y. Fu, S. Liu and S. Zeng, 'Knockdown of Beclin-1 impairs epithelial-mesenchymal transition of colon cancer cells', *Journal of Cellular Biochemistry*, vol. 119, no. 8, pp. 7022–7031, 2018.

[279] H.-D. Zhu, L. Liu, H. Deng, Z.-B. Li, J.-Q. Sheng, X.-X. He, D.-A. Tian and P.-Y. Li, 'Astrocyte elevated gene 1 (AEG-1) promotes anoikis resistance and metastasis by inducing autophagy in hepatocellular carcinoma', *Journal of Cellular Physiology*, vol. 235, no. 6, pp. 5084–5095, 2020.

[280] Y.-F. Peng, Y.-H. Shi, Z.-B. Ding, A.-W. Ke, C.-Y. Gu, B. Hui, J. Zhou, S.-J. Qiu, Z. Dai and J. Fan, 'Autophagy inhibition suppresses pulmonary metastasis of HCC in mice via impairing anoikis resistance and colonization of HCC cells', *Autophagy*, vol. 9, no. 12, pp. 2056–2068, 2013.

[281] M. T. Rosenfeldt, J. O'Prey, J. P. Morton, C. Nixon, G. MacKay, A. Mrowinska, A. Au, T. S. Rai, L. Zheng, R. Ridgway *et al.*, 'p53 status determines the role of autophagy in pancreatic tumour development', *Nature*, vol. 504, no. 7479, pp. 296–300, 2013.

[282] C. Liang, J. Xu, Q. Meng, B. Zhang, J. Liu, J. Hua, Y. Zhang, S. Shi and X. Yu, 'TGFB1-induced autophagy affects the pattern of pancreatic cancer progression in distinct ways depending on SMAD4 status', *Autophagy*, vol. 16, no. 3, pp. 486–500, 2020.

[283] F. Chiti and C. M. Dobson, 'Protein misfolding, functional amyloid, and human disease', *Annual Reviews in Biochemistry*, vol. 75, pp. 333–366, 2006.

[284] F. M. Menzies, A. Fleming, A. Caricasole, C. F. Bento, S. P. Andrews, A. Ashkenazi, J. Füllgrabe, A. Jackson, M. J. Sanchez, C. Karabiyik *et al.*, 'Autophagy and neurodegeneration: pathogenic mechanisms and therapeutic opportunities', *Neuron*, vol. 93, no. 5, pp. 1015–1034, 2017.

[285] Z. Wang, G. Miao, X. Xue, X. Guo, C. Yuan, Z. Wang, G. Zhang, Y. Chen, D. Feng, J. Hu *et al.*, 'The Vici syndrome protein EPG5 is a Rab7 effector that determines the fusion specificity of autophagosomes with late endosomes/lysosomes', *Molecular Cell*, vol. 63, no. 5, pp. 781–795, 2016.

[286] T. Cullup, A. L. Kho, C. Dionisi-Vici, B. Brandmeier, F. Smith, Z. Urry, M. A. Simpson, S. Yau, E. Bertini, V. McClelland *et al.*, 'Recessive mutations in EPG5 cause Vici syndrome, a multisystem disorder with defective autophagy', *Nature Genetics*, vol. 45, no. 1, pp. 83–87, 2013.

[287] T. Ozawa, R. Koide, Y. Nakata, H. Saitsu, N. Matsumoto, K. Takahashi, I. Nakano and S. Orimo, 'A novel WDR45 mutation in a patient with static encephalopathy of childhood with neurodegeneration in adulthood (SENDA)', *American Journal of Medical Genetics Part A*, vol. 164, no. 9, pp. 2388–2390, 2014.

[288] H. Saitsu, T. Nishimura, K. Muramatsu, H. Kodera, S. Kumada, K. Sugai, E. Kasai-Yoshida, N. Sawaura, H. Nishida, A. Hoshino *et al.*, 'De novo mutations in the autophagy gene WDR45 cause static encephalopathy of childhood with neurodegeneration in adulthood', *Nature Genetics*, vol. 45, no. 4, pp. 445–449, 2013.

[289] E. T. Cirulli, B. N. Lasseigne, S. Petrovski, P. C. Sapp, P. A. Dion, C. S. Leblond, J. Couthouis, Y.-F. Lu, Q. Wang, B. J. Krueger *et al.*, 'Exome sequencing in amyotrophic lateral sclerosis identifies risk genes and pathways', *Science*, vol. 347, no. 6229, pp. 1436–1441, 2015.

[290] Y. A. Abramzon, P. Fratta, B. J. Traynor and R. Chia, 'The overlapping genetics of amyotrophic lateral sclerosis and frontotemporal dementia', *Frontiers in Neuroscience*, vol. 14, p. 42, 2020.

[291] S. Pankiv, T. H. Clausen, T. Lamark, A. Brech, J.-A. Bruun, H. Outzen, A. Øvervatn, G. Bjørkøy and T. Johansen, 'p62/SQSTM1 binds directly to Atg8/LC3 to facilitate degradation of ubiquitinated protein aggregates by autophagy', *Journal of Biological Bhemistry*, vol. 282, no. 33, pp. 24 131–24 145, 2007.

[292] A. M. Pickrell and R. J. Youle, 'The roles of PINK1, parkin, and mitochondrial fidelity in Parkinson's disease', *Neuron*, vol. 85, no. 2, pp. 257–273, 2015.

[293] G. Matsumoto, T. Shimogori, N. Hattori and N. Nukina, 'TBK1 controls autophagosomal engulfment of polyubiquitinated mitochondria through p62/SQSTM1 phosphorylation', *Human Molecular Genetics*, vol. 24, no. 15, pp. 4429–4442, 2015.

[294] B. Richter, D. A. Sliter, L. Herhaus, A. Stolz, C. Wang, P. Beli, G. Zaffagnini, P. Wild, S. Martens, S. A. Wagner *et al.*, 'Phosphorylation of OPTN by TBK1 enhances its binding to Ub chains and promotes selective autophagy of damaged mitochondria', *Proceedings of the National Academy of Sciences*, vol. 113, no. 15, pp. 4039–4044, 2016.

[295] A. Freischmidt, T. Wieland, B. Richter, W. Ruf, V. Schaeffer, K. Müller, N. Marroquin, F. Nordin, A. Hübers, P. Weydt *et al.*, 'Haploinsufficiency of TBK1 causes familial ALS and fronto-temporal dementia', *Nature Neuroscience*, vol. 18, no. 5, pp. 631–636, 2015.

[296] V. Sharma, S. Verma, E. Seranova, S. Sarkar and D. Kumar, 'Selective autophagy and xenophagy in infection and disease', *Frontiers in Cell and Developmental Biology*, vol. 6, p. 147, 2018.

[297] A. Reggio, V. Buonomo and P. Grumati, 'Eating the unknown: Xenophagy and ER-phagy are cytoprotective defenses against pathogens', *Experimental Cell Research*, pp. 112–276, 2020.

[298] T. Liu, 'Regulation of inflammasome by autophagy', in *Autophagy Regulation of Innate Immunity*, Springer, 2019, pp. 109–123.

[299] C. Münz, 'Autophagy proteins in antigen processing for presentation on MHC molecules', *Immunological Reviews*, vol. 272, no. 1, pp. 17–27, 2016.

[300] L. Van Kaer, V. V. Parekh, J. L. Postoak and L. Wu, 'Role of autophagy in MHC class I-restricted antigen presentation', *Molecular Immunology*, vol. 113, pp. 2–5, 2019.

[301] T. Riffelmacher, F. C. Richter and A. K. Simon, 'Autophagy dictates metabolism and differentiation of inflammatory immune cells', *Autophagy*, vol. 14, no. 2, pp. 199–206, 2018.

[302] A. J. Clarke and A. K. Simon, 'Autophagy in the renewal, differentiation and homeostasis of immune cells', *Nature Reviews Immunology*, vol. 19, no. 3, pp. 170–183, 2019.

[303] H. Yin, H. Wu, Y. Chen, J. Zhang, M. Zheng, G. Chen, L. Li and Q. Lu, 'The therapeutic and pathogenic role of autophagy in autoimmune diseases', *Frontiers in Immunology*, vol. 9, p. 1512, 2018.

[304] B. Verstockt, K. G. Smith and J. C. Lee, 'Genome-wide association studies in Crohn's disease: Past, present and future', *Clinical & Translational Immunology*, vol. 7, no. 1, e1001, 2018.

[305] P. Nath, K. K. Jena, S. Mehto, N. R. Chauhan, R. Sahu, K. Dhar, K. Srinivas, S. Chauhan and S. Chauhan, 'IRGM links autoimmunity to autophagy', *Autophagy*, pp. 1–3, 2020.

[306] Y.-y. Qi, X.-j. Zhou and H. Zhang, 'Autophagy and immunological aberrations in systemic lupus erythematosus', *European Journal of Immunology*, vol. 49, no. 4, pp. 523–533, 2019.

[307] T. Kaizuka, H. Morishita, Y. Hama, S. Tsukamoto, T. Matsui, Y. Toyota, A. Kodama, T. Ishihara, T. Mizushima and N. Mizushima, 'An autophagic flux probe that releases an internal control', *Molecular Cell*, vol. 64, no. 4, pp. 835–849, 2016.

[308] N. E. Sanjana, O. Shalem and F. Zhang, 'Improved vectors and genome-wide libraries for CRISPR screening', *Nature Methods*, vol. 11, no. 8, p. 783, 2014.

[309] B. W. Stringer, B. W. Day, R. C. D'Souza, P. R. Jamieson, K. S. Ensbey, Z. C. Bruce, Y. C. Lim, K. Goasdoué, C. Offenhäuser, S. Akgül *et al.*, 'A reference collection of patient-derived cell line and xenograft models of proneural, classical and mesenchymal glioblastoma', *Scientific Reports*, vol. 9, no. 1, pp. 1–14, 2019.

[310] B. Langmead and S. L. Salzberg, 'Fast gapped-read alignment with Bowtie 2', *Nature Methods*, vol. 9, no. 4, p. 357, 2012.

[311] M. Martin, 'Cutadapt removes adapter sequences from high-throughput sequencing reads', *EMBnet. Journal*, vol. 17, no. 1, pp. 10–12, 2011.

[312] Y. Dang, G. Jia, J. Choi, H. Ma, E. Anaya, C. Ye, P. Shankar and H. Wu, 'Optimizing sgRNA structure to improve CRISPR-Cas9 knockout efficiency', *Genome Biology*, vol. 16, no. 1, pp. 1–10, 2015.

[313] B. Chen, L. A. Gilbert, B. A. Cimini, J. Schnitzbauer, W. Zhang, G.-W. Li, J. Park, E. H. Blackburn, J. S. Weissman, L. S. Qi *et al.*, 'Dynamic imaging of genomic loci in living human cells by an optimized CRISPR/Cas system', *Cell*, vol. 155, no. 7, pp. 1479–1491, 2013.

[314] E. K. Brinkman, T. Chen, M. Amendola and B. van Steensel, 'Easy quantitative assessment of genome editing by sequence trace decomposition', *Nucleic Acids Research*, vol. 42, no. 22, e168–e168, 2014.

[315] Y. Xiong, M. Soumillon, J. Wu, J. Hansen, B. Hu, J. G. Van Hasselt, G. Jayaraman, R. Lim, M. Bouhaddou, L. Ornelas *et al.*, 'A comparison of mRNA sequencing with random primed and 3-directed libraries', *Scientific Reports*, vol. 7, no. 1, pp. 1–12, 2017.

[316] A. Dobin, C. A. Davis, F. Schlesinger, J. Drenkow, C. Zaleski, S. Jha, P. Batut, M. Chaisson and T. R. Gingeras, 'STAR: ultrafast universal RNA-seq aligner', *Bioinformatics*, vol. 29, no. 1, pp. 15–21, 2013.

[317] S. Anders, P. T. Pyl and W. Huber, 'HTSeq—a Python framework to work with high-throughput sequencing data', *Bioinformatics*, vol. 31, no. 2, pp. 166–169, 2015.

[318] B. Bushnell, 'BBMap: a fast, accurate, splice-aware aligner', Lawrence Berkeley National Lab., Berkeley, CA (United States), Tech. Rep., 2014.

[319] M. D. Robinson, D. J. McCarthy and G. K. Smyth, 'edgeR: a Bioconductor package for differential expression analysis of digital gene expression data', *Bioinformatics*, vol. 26, no. 1, pp. 139–140, 2010.

[320] E. Kim and T. Hart, 'Improved analysis of CRISPR fitness screens and reduced off-target effects with the BAGEL2 gene essentiality classifier', *BioRxiv*, 2020.

[321] M. Waskom, O. Botvinnik, J. Ostblom, M. Gelbart, S. Lukauskas, P. Hobson, D. C. Gemperline, T. Augspurger, Y. Halchenko, J. B. Cole *et al.*, 'Mwaskom/seaborn: V0. 10.1', *Zenodo*, 2020.

[322] P. Shannon, A. Markiel, O. Ozier, N. S. Baliga, J. T. Wang, D. Ramage, N. Amin, B. Schwikowski and T. Ideker, 'Cytoscape: a software environment for integrated models of biomolecular interaction networks', *Genome Research*, vol. 13, no. 11, pp. 2498–2504, 2003.

[323] R. Edgar, M. Domrachev and A. E. Lash, 'Gene Expression Omnibus: NCBI gene expression and hybridization array data repository', *Nucleic Acids Research*, vol. 30, no. 1, pp. 207–210, 2002.

[324] I. Lappalainen, J. Almeida-King, V. Kumanduri, A. Senf, J. D. Spalding, G. Saunders, J. Kandasamy, M. Caccamo, R. Leinonen, B. Vaughan *et al.*, 'The European Genome-phenome Archive of human data consented for biomedical research', *Nature Genetics*, vol. 47, no. 7, pp. 692–695, 2015.

[325] Á. Nagy, A. Lánczky, O. Menyhárt and B. Győrffy, 'Validation of mirna prognostic power in hepatocellular carcinoma using expression data of independent datasets', *Scientific reports*, vol. 8, no. 1, pp. 1–9, 2018.

[326] J. N. Weinstein, E. A. Collisson, G. B. Mills, K. R. M. Shaw, B. A. Ozenberger, K. Ellrott, I. Shmulevich, C. Sander and J. M. Stuart, 'The cancer genome atlas pan-cancer analysis project', *Nature Genetics*, vol. 45, no. 10, pp. 1113–1120, 2013.

[327] M. Goldman, B. Craft, M. Hastie, K. Repečka, F. McDade, A. Kamath, A. Banerjee, Y. Luo, D. Rogers, A. Brooks *et al.*, *The UCSC Xena platform for public and private cancer genomics data visualization and interpretation. BioRxiv, 326470*, 2019.

[328] M. J. Goldman, B. Craft, M. Hastie, K. Repečka, F. McDade, A. Kamath, A. Banerjee, Y. Luo, D. Rogers, A. N. Brooks *et al.*, 'Visualizing and interpreting cancer genomics data via the Xena platform', *Nature Biotechnology*, vol. 38, no. 6, pp. 675–678, 2020.

[329] B. C. Cross, S. Lawo, C. R. Archer, J. R. Hunt, J. L. Yarker, A. Riccombeni, A. S. Little, N. J. McCarthy and J. D. Moore, 'Increasing the performance of pooled CRISPR–Cas9 drop-out screening', *Scientific Reports*, vol. 6, no. 1, pp. 1–8, 2016.

[330] T. A. Kunkel, 'Rapid and efficient site-specific mutagenesis without phenotypic selection', *Proceedings of the National Academy of Sciences*, vol. 82, no. 2, pp. 488–492, 1985.

[331] R. Huang, P. Fang and B. K. Kay, 'Improvements to the Kunkel mutagenesis protocol for constructing primary and secondary phage-display libraries', *Methods*, vol. 58, no. 1, pp. 10–17, 2012.

[332] E. Kim and T. Hart, 'Improved analysis of CRISPR fitness screens and reduced off-target effects with the BAGEL2 gene essentiality classifier', *Genome Medicine*, vol. 13, no. 1, pp. 1–11, 2021.

[333] K. Morita, Y. Hama, T. Izume, N. Tamura, T. Ueno, Y. Yamashita, Y. Sakamaki, K. Mimura, H. Morishita, W. Shihoya *et al.*, 'Genome-wide CRISPR screen identifies TMEM41B as a gene required for autophagosome formation', *Journal of Cell Biology*, vol. 217, no. 11, pp. 3817–3828, 2018.

[334] R. M. Meyers, J. G. Bryan, J. M. McFarland, B. A. Weir, A. E. Sizemore, H. Xu, N. V. Dharia, P. G. Montgomery, G. S. Cowley, S. Pantel *et al.*, 'Computational correction of copy number effect improves specificity of CRISPR–Cas9 essentiality screens in cancer cells', *Nature Genetics*, vol. 49, no. 12, pp. 1779–1784, 2017.

[335] S. M. Sidik, D. Huet, S. M. Ganesan, M.-H. Huynh, T. Wang, A. S. Nasamu, P. Thiru, J. P. Saeij, V. B. Carruthers, J. C. Niles *et al.*, 'A genome-wide CRISPR screen in Toxoplasma identifies essential apicomplexan genes', *Cell*, vol. 166, no. 6, pp. 1423–1435, 2016.

[336] E. M. Peets, L. Crepaldi, Y. Zhou, F. Allen, R. Elmentaite, G. Noell, G. Turner, V. Iyer and L. Parts, 'Minimized double guide RNA libraries enable scale-limited CRISPR/Cas9 screens', *BioRxiv*, p. 859 652, 2019.

[337] D. Hanahan and R. A. Weinberg, 'Hallmarks of cancer: the next generation', *Cell*, vol. 144, no. 5, pp. 646–674, 2011.

[338] S. Ambrosio and B. Majello, 'Autophagy Roles in Genome Maintenance', *Cancers*, vol. 12, no. 7, p. 1793, 2020.

[339] X. H. Liang, S. Jackson, M. Seaman, K. Brown, B. Kempkes, H. Hibshoosh and B. Levine, 'Induction of autophagy and inhibition of tumorigenesis by beclin 1', *Nature*, vol. 402, no. 6762, pp. 672–676, 1999.

[340] A. Takamura, M. Komatsu, T. Hara, A. Sakamoto, C. Kishi, S. Waguri, Y. Eishi, O. Hino, K. Tanaka and N. Mizushima, 'Autophagy-deficient mice develop multiple liver tumors', *Genes & Development*, vol. 25, no. 8, pp. 795–800, 2011.

[341] S. Yang, X. Wang, G. Contino, M. Liesa, E. Sahin, H. Ying, A. Bause, Y. Li, J. M. Stommel, G. Dell'Antonio *et al.*, 'Pancreatic cancers require autophagy for tumor growth', *Genes & Development*, vol. 25, no. 7, pp. 717–729, 2011.

[342] A. Yang, N. Rajeshkumar, X. Wang, S. Yabuuchi, B. M. Alexander, G. C. Chu, D. D. Von Hoff, A. Maitra and A. C. Kimmelman, 'Autophagy is critical for pancreatic tumor growth and progression in tumors with p53 alterations', *Cancer Discovery*, vol. 4, no. 8, pp. 905–913, 2014.

[343] J. Y. Guo, G. Karsli-Uzunbas, R. Mathew, S. C. Aisner, J. J. Kamphorst, A. M. Strohecker, G. Chen, S. Price, W. Lu, X. Teng *et al.*, 'Autophagy suppresses progression of K-ras-induced lung tumors to oncocytomas and maintains lipid homeostasis', *Genes & Development*, vol. 27, no. 13, pp. 1447–1461, 2013.

[344] A. Chatterjee, S. Mukhopadhyay, K. Tung, D. Patel and D. A. Foster, 'Rapamycin-induced G1 cell cycle arrest employs both TGF-β and Rb pathways', *Cancer Letters*, vol. 360, no. 2, pp. 134–140, 2015.

[345] T. S. Gomez and D. D. Billadeau, 'A FAM21-containing WASH complex regulates retromer-dependent sorting', *Developmental Cell*, vol. 17, no. 5, pp. 699–711, 2009.

[346] P. Xia, S. Wang, Y. Du, Z. Zhao, L. Shi, L. Sun, G. Huang, B. Ye, C. Li, Z. Dai *et al.*, 'WASH inhibits autophagy through suppression of Beclin 1 ubiquitination', *EMBO Journal*, vol. 32, no. 20, pp. 2685–2696, 2013.

[347] X. Yu, Y. C. Long and H.-M. Shen, 'Differential regulatory functions of three classes of phosphatidylinositol and phosphoinositide 3-kinases in autophagy', *Autophagy*, vol. 11, no. 10, pp. 1711–1728, 2015.

[348] S. B. Thoresen, N. M. Pedersen, K. Liestøl and H. Stenmark, 'A phosphatidylinositol 3-kinase class III sub-complex containing VPS15, VPS34, Beclin 1, UVRAG and BIF-1 regulates cytokinesis and degradative endocytic traffic', *Experimental Cell Research*, vol. 316, no. 20, pp. 3368–3378, 2010.

[349] D.-m. Wei, W.-j. Chen, R.-m. Meng, N. Zhao, X.-y. Zhang, D.-y. Liao and G. Chen, 'Augmented expression of Ki-67 is correlated with clinicopathological characteristics and prognosis for lung cancer patients: an up-dated systematic review and meta-analysis with 108 studies and 14,732 patients', *Respiratory Research*, vol. 19, no. 1, pp. 1–19, 2018.

[350] D. Fenstermacher, C. Street, T. McSherry, V. Nayak, C. Overby and M. Feldman, 'The cancer biomedical informatics grid (caBIG TM)', in *2005 IEEE Engineering in Medicine and Biology 27th Annual Conference*, IEEE, 2006, pp. 743–746.

[351] A. Bergman and M. L. Siegal, 'Evolutionary capacitance as a general feature of complex gene networks', *Nature*, vol. 424, no. 6948, pp. 549–552, 2003.

[352] C. Queitsch, T. A. Sangster and S. Lindquist, 'Hsp90 as a capacitor of phenotypic variation', *Nature*, vol. 417, no. 6889, pp. 618–624, 2002.

[353] G. M. Fimia, A. Stoykova, A. Romagnoli, L. Giunta, S. Di Bartolomeo, R. Nardacci, M. Corazzari, C. Fuoco, A. Ucar, P. Schwartz *et al.*, 'Ambra1 regulates autophagy and development of the nervous system', *Nature*, vol. 447, no. 7148, pp. 1121–1125, 2007.

[354] G. M. Fimia, M. Corazzari, M. Antonioli and M. Piacentini, 'Ambra1 at the crossroad between autophagy and cell death', *Oncogene*, vol. 32, no. 28, pp. 3311–3318, 2013.

[355] C. U. Stirnimann, E. Petsalaki, R. B. Russell and C. W. Müller, 'WD40 proteins propel cellular networks', *Trends in Biochemical Sciences*, vol. 35, no. 10, pp. 565–574, 2010.

[356] Y. Mei, M. Su, G. Soni, S. Salem, C. L. Colbert and S. C. Sinha, 'Intrinsically disordered regions in autophagy proteins', *Proteins: Structure, Function, and Bioinformatics*, vol. 82, no. 4, pp. 565–578, 2014.

[357] H. J. Dyson and P. E. Wright, 'Intrinsically unstructured proteins and their functions', *Nature Reviews Molecular Cell Biology*, vol. 6, no. 3, pp. 197–208, 2005.

[358] V. Cianfanelli, F. Nazio and F. Cecconi, 'Connecting autophagy: AMBRA1 and its network of regulation', *Molecular & Cellular Oncology*, vol. 2, no. 1, e970059, 2015.

[359] A. K. Ramani, T. Chuluunbaatar, A. J. Verster, H. Na, V. Vu, N. Pelte, N. Wannissorn, A. Jiao and A. G. Fraser, 'The majority of animal genes are required for wild-type fitness', *Cell*, vol. 148, no. 4, pp. 792–802, 2012.

[360] C. R. Baker, V. Hanson-Smith and A. D. Johnson, 'Following gene duplication, paralog interference constrains transcriptional circuit evolution', *Science*, vol. 342, no. 6154, pp. 104–108, 2013.

[361] C. Roth, S. Rastogi, L. Arvestad, K. Dittmar, S. Light, D. Ekman and D. A. Liberles, 'Evolution after gene duplication: models, mechanisms, sequences, systems, and organisms', *Journal of Experimental Zoology Part B: Molecular and Developmental Evolution*, vol. 308, no. 1, pp. 58–73, 2007.

[362] J. P. Gogarten and L. Olendzenski, 'Orthologs, paralogs and genome comparisons', *Current Opinion in Genetics & Development*, vol. 9, no. 6, pp. 630–636, 1999.

[363] S. Rastogi and D. A. Liberles, 'Subfunctionalization of duplicated genes as a transition state to neofunctionalization', *BMC Evolutionary Biology*, vol. 5, no. 1, pp. 1–7, 2005.

[364] S. R. Sandve, R. V. Rohlfs and T. R. Hvidsten, 'Subfunctionalization versus neofunctionalization after whole-genome duplication', *Nature Genetics*, vol. 50, no. 7, pp. 908–909, 2018.

[365] S. W. Cheetham, G. J. Faulkner and M. E. Dinger, 'Overcoming challenges and dogmas to understand the functions of pseudogenes', *Nature Reviews Genetics*, vol. 21, no. 3, pp. 191–201, 2020.

[366] B. Khor, K. L. Conway, A. S. Omar, M. Biton, A. L. Haber, N. Rogel, L. A. Baxt, J. Begun, P. Kuballa, J. D. Gagnon *et al.*, 'Distinct tissue-specific roles for the disease-associated autophagy genes atg16l2 and atg16l1', *The Journal of Immunology*, vol. 203, no. 7, pp. 1820–1829, 2019.

[367] S. Lian, Y. Zhou, Z. Liu, A. Gong and L. Cheng, 'The differential expression patterns of paralogs in response to stresses indicate expression and sequence divergences', *BMC Plant Biology*, vol. 20, no. 1, pp. 1–16, 2020.

[368] M. Jelani, H. C. Dooley, A. Gubas, H. S. A. Mohamoud, M. T. M. Khan, Z. Ali, C. Kang, F. Rahim, A. Jan, N. Vadgama *et al.*, 'A mutation in the major autophagy gene, WIPI2, associated with global developmental abnormalities', *Brain*, vol. 142, no. 5, pp. 1242–1254, 2019.

[369] R. Kadir, T. Harel, B. Markus, Y. Perez, A. Bakhrat, I. Cohen, M. Volodarsky, M. Feintsein-Linial, E. Chervinski, J. Zlotogora *et al.*, 'ALFY-controlled DVL3 autophagy regulates Wnt signaling, determining human brain size', *PLoS Genetics*, vol. 12, no. 3, e1005919, 2016.

[370] P. H. Reddy, X. Yin, M. Manczak, S. Kumar, J. A. Pradeepkiran, M. Vijayan and A. P. Reddy, 'Mutant APP and amyloid beta-induced defective autophagy, mitophagy, mitochondrial structural and functional changes and synaptic damage in hippocampal neurons from Alzheimer's disease', *Human Molecular Genetics*, vol. 27, no. 14, pp. 2502–2516, 2018.

[371] Y. Peng, S. L. Shapiro, V. C. Banduseela, I. A. Dieterich, K. J. Hewitt, E. H. Bresnick, G. Kong, J. Zhang, K. L. Schueler, M. P. Keller *et al.*, 'Increased transport of acetyl-CoA into the endoplasmic reticulum causes a progeria-like phenotype', *Aging Cell*, vol. 17, no. 5, e12820, 2018.

[372] K. G. Lassen, P. Kuballa, K. L. Conway, K. K. Patel, C. E. Becker, J. M. Peloquin, E. J. Villablanca, J. M. Norman, T.-C. Liu, R. J. Heath *et al.*, 'Atg16L1 T300A variant decreases selective autophagy resulting in altered cytokine signaling and decreased antibacterial defense', *Proceedings of the National Academy of Sciences*, vol. 111, no. 21, pp. 7741–7746, 2014.

[373] A. Murthy, Y. Li, I. Peng, M. Reichelt, A. K. Katakam, R. Noubade, M. Roose-Girma, J. DeVoss, L. Diehl, R. R. Graham *et al.*, 'A Crohn's disease variant in Atg16l1 enhances its degradation by caspase 3', *Nature*, vol. 506, no. 7489, pp. 456–462, 2014.

[374] J. E. Molineros, W. Yang, X.-j. Zhou, C. Sun, Y. Okada, H. Zhang, K. Heng Chua, Y.-L. Lau, Y. Kochi, A. Suzuki *et al.*, 'Confirmation of five novel susceptibility loci for systemic lupus erythematosus (SLE) and integrated network analysis of 82 SLE susceptibility loci', *Human Molecular Genetics*, vol. 26, no. 6, pp. 1205–1216, 2017.

[375] S. Cabrera, A. F. Fernandez, G. Marino, A. Aguirre, M. F. Suarez, Y. Espanol, J. A. Vega, R. Laura, A. Fueyo, M. S. Fernandez-Garcia *et al.*, 'ATG4B/autophagin-1 regulates intestinal homeostasis and protects mice from experimental colitis', *Autophagy*, vol. 9, no. 8, pp. 1188–1200, 2013.

[376] J. Z. Liu, S. Van Sommeren, H. Huang, S. C. Ng, R. Alberts, A. Takahashi, S. Ripke, J. C. Lee, L. Jostins, T. Shah *et al.*, 'Association analyses identify 38 susceptibility loci for inflammatory bowel disease and highlight shared genetic risk across populations', *Nature Genetics*, vol. 47, no. 9, pp. 979–986, 2015.

[377] M. Kim, E. Sandford, D. Gatica, Y. Qiu, X. Liu, Y. Zheng, B. A. Schulman, J. Xu, I. Semple, S.-H. Ro *et al.*, 'Mutation in ATG5 reduces autophagy and leads to ataxia with developmental delay', *Elife*, vol. 5, e12245, 2016.

[378] O. Korvatska, N. S. Strand, J. D. Berndt, T. Strovas, D.-H. Chen, J. B. Leverenz, K. Kiianitsa, I. F. Mata, E. Karakoc, J. L. Greenup *et al.*, 'Altered splicing of ATP6AP2 causes X-linked parkinsonism with spasticity (XPDS)', *Human Molecular Genetics*, vol. 22, no. 16, pp. 3259–3268, 2013.

[379] G. Valente, F. Morani, G. Nicotra, N. Fusco, C. Peracchio, R. Titone, O. Alabiso, R. Arisio, D. Katsaros, C. Benedetto *et al.*, 'Expression and clinical significance of the autophagy proteins BECLIN 1 and LC3 in ovarian cancer', *BioMed Research International*, vol. 2014, 2014.

[380] H. Tang, S. Sebti, R. Titone, Y. Zhou, C. Isidoro, T. S. Ross, H. Hibshoosh, G. Xiao, M. Packer, Y. Xie *et al.*, 'Decreased BECN1 mRNA expression in human breast cancer is associated with estrogen receptor-negative subtypes and poor prognosis', *EBioMedicine*, vol. 2, no. 3, pp. 255–263, 2015.

[381] A. Corrionero and H. R. Horvitz, 'A C9orf72 ALS/FTD ortholog acts in endolysosomal degradation and lysosomal homeostasis', *Current Biology*, vol. 28, no. 10, pp. 1522–1535, 2018.

[382] M. Nassif, U. Woehlbier and P. A. Manque, 'The enigmatic role of C9ORF72 in autophagy', *Frontiers in Neuroscience*, vol. 11, p. 442, 2017.

[383] D. Ellinghaus, H. Zhang, S. Zeissig, S. Lipinski, A. Till, T. Jiang, B. Stade, Y. Bromberg, E. Ellinghaus, A. Keller *et al.*, 'Association between variants of PRDM1 and NDP52 and Crohn's disease, based on exome sequencing and functional studies', *Gastroenterology*, vol. 145, no. 2, pp. 339–347, 2013.

[384] P. G. Bronson, D. Chang, T. Bhangale, M. F. Seldin, W. Ortmann, R. C. Ferreira, E. Urcelay, L. F. Pereira, J. Martin, A. Plebani *et al.*, 'Common variants at PVT1, ATG13–AMBRA1, AHI1 and CLEC16A are associated with selective IgA deficiency', *Nature Genetics*, vol. 48, no. 11, pp. 1425–1429, 2016.

[385] S. A. Soleimanpour, A. Gupta, M. Bakay, A. M. Ferrari, D. N. Groff, J. Fadista, L. A. Spruce, J. A. Kushner, L. Groop, S. H. Seeholzer *et al.*, 'The diabetes susceptibility gene Clec16a regulates mitophagy', *Cell*, vol. 157, no. 7, pp. 1577–1590, 2014.

[386] B. P. Festa, Z. Chen, M. Berquez, H. Debaix, N. Tokonami, J. A. Prange, G. van de Hoek, C. Alessio, A. Raimondi, N. Nevo *et al.*, 'Impaired autophagy bridges lysosomal storage disease and epithelial dysfunction in the kidney', *Nature Communications*, vol. 9, no. 1, pp. 1–17, 2018.

[387] S. Vega-Rubin-de-Celis, Z. Zou, A. F. Fernandez, B. Ci, M. Kim, G. Xiao, Y. Xie and B. Levine, 'Increased autophagy blocks HER2-mediated breast tumorigenesis', *Proceedings of the National Academy of Sciences*, vol. 115, no. 16, pp. 4176–4181, 2018.

[388] A. Khaminets, T. Heinrich, M. Mari, P. Grumati, A. K. Huebner, M. Akutsu, L. Liebmann, A. Stolz, S. Nietzsche, N. Koch *et al.*, 'Regulation of endoplasmic reticulum turnover by selective autophagy', *Nature*, vol. 522, no. 7556, pp. 354–358, 2015.

[389] R. Sumpter Jr, S. Sirasanagandla, Á. F. Fernández, Y. Wei, X. Dong, L. Franco, Z. Zou, C. Marchal, M. Y. Lee, D. W. Clapp *et al.*, 'Fanconi anemia proteins function in mitophagy and immunity', *Cell*, vol. 165, no. 4, pp. 867–881, 2016.

[390] K. G. Lassen, C. I. McKenzie, M. Mari, T. Murano, J. Begun, L. A. Baxt, G. Goel, E. J. Villablanca, S.-Y. Kuo, H. Huang *et al.*, 'Genetic coding variant in GPR65 alters lysosomal pH and links lysosomal dysfunction with colitis risk', *Immunity*, vol. 44, no. 6, pp. 1392–1405, 2016.

[391] A. Ashkenazi, C. F. Bento, T. Ricketts, M. Vicinanza, F. Siddiqi, M. Pavel, F. Squitieri, M. C. Hardenberg, S. Imarisio, F. M. Menzies *et al.*, 'Polyglutamine tracts regulate beclin 1-dependent autophagy', *Nature*, vol. 545, no. 7652, pp. 108–111, 2017.

[392] Y.-C. Lin, P.-F. Chang, H.-F. Lin, K. Liu, M.-H. Chang and Y.-H. Ni, 'Variants in the autophagy-related gene IRGM confer susceptibility to non-alcoholic fatty liver disease by modulating lipophagy', *Journal of Hepatology*, vol. 65, no. 6, pp. 1209–1216, 2016.

[393] S. Chauhan, M. A. Mandell and V. Deretic, 'Mechanism of action of the tuberculosis and Crohn disease risk factor IRGM in autophagy', *Autophagy*, vol. 12, no. 2, pp. 429–431, 2016.

[394] I. Nishino, J. Fu, K. Tanji, T. Yamada, S. Shimojo, T. Koori, M. Mora, J. E. Riggs, S. J. Oh, Y. Koga *et al.*, 'Primary LAMP-2 deficiency causes X-linked vacuolar cardiomyopathy and myopathy (Danon disease)', *Nature*, vol. 406, no. 6798, pp. 906–910, 2000.

[395] K. Y. Hui, H. Fernandez-Hernandez, J. Hu, A. Schaffner, N. Pankratz, N.-Y. Hsu, L.-S. Chuang, S. Carmi, N. Villaverde, X. Li *et al.*, 'Functional variants in the LRRK2 gene confer shared effects on risk for Crohn's disease and Parkinson's disease', *Science Translational Medicine*, vol. 10, no. 423, 2018.

[396] A. Lahiri, M. Hedl and C. Abraham, 'MTMR3 risk allele enhances innate receptor-induced signaling and cytokines by decreasing autophagy and increasing caspase-1 activation', *Proceedings of the National Academy of Sciences*, vol. 112, no. 33, pp. 10 461–10 466, 2015.

[397] I. A. Silva, N. Conceiçao, É. Gagnon, H. Caiado, J. P. Brown, F. Gianfrancesco, L. Michou and M. L. Cancela, 'Effect of genetic variants of OPTN in the pathophysiology of Paget's disease of bone', *Biochimica et Biophysica Acta (BBA)-Molecular Basis of Disease*, vol. 1864, no. 1, pp. 143–151, 2018.

[398] M. S. Shim, Y. Takihara, K.-Y. Kim, T. Iwata, B. Y. Yue, M. Inatani, R. N. Weinreb, G. A. Perkins and W.-K. Ju, 'Mitochondrial pathogenic mechanism and degradation in optineurin E50K mutation-mediated retinal ganglion cell degeneration', *Scientific Reports*, vol. 6, no. 1, pp. 1–17, 2016.

[399] Y. C. Wong and E. L. Holzbaur, 'Optineurin is an autophagy receptor for damaged mitochondria in parkin-mediated mitophagy that is disrupted by an ALS-linked mutation', *Proceedings of the National Academy of Sciences*, vol. 111, no. 42, E4439–E4448, 2014.

[400] T. Kitada, S. Asakawa, N. Hattori, H. Matsumine, Y. Yamamura, S. Minoshima, M. Yokochi, Y. Mizuno and N. Shimizu, 'Mutations in the parkin gene cause autosomal recessive juvenile parkinsonism', *Nature*, vol. 392, no. 6676, pp. 605–608, 1998.

[401] L. Xu, D.-c. Lin, D. Yin and H. P. Koeffler, 'An emerging role of PARK2 in cancer', *Journal of Molecular Medicine*, vol. 92, no. 1, pp. 31–42, 2014.

[402] P. Jiang and N. Mizushima, 'Autophagy and human diseases', *Cell Research*, vol. 24, no. 1, pp. 69–79, 2014.

[403] M. Y. Lee, R. Sumpter Jr, Z. Zou, S. Sirasanagandla, Y. Wei, P. Mishra, H. Rosewich, D. I. Crane and B. Levine, 'Peroxisomal protein PEX 13 functions in selective autophagy', *EMBO Reports*, vol. 18, no. 1, pp. 48–60, 2017.

[404] T. Gstrein, A. Edwards, A. Přistoupilová, I. Leca, M. Breuss, S. Pilat-Carotta, A. H. Hansen, R. Tripathy, A. K. Traunbauer, T. Hochstoeger *et al.*, 'Mutations in Vps15 perturb neuronal migration in mice and are associated with neurodevelopmental disease in humans', *Nature Neuroscience*, vol. 21, no. 2, pp. 207–217, 2018.

[405] G. Stenbeck and F. P. Coxon, 'Role of vesicular trafficking in skeletal dynamics', *Current Opinion in Pharmacology*, vol. 16, pp. 7–14, 2014.

[406] J.-H. Lee, W. H. Yu, A. Kumar, S. Lee, P. S. Mohan, C. M. Peterhoff, D. M. Wolfe, M. Martinez-Vicente, A. C. Massey, G. Sovak *et al.*, 'Lysosomal proteolysis and autophagy require presenilin 1 and are disrupted by Alzheimer-related PS1 mutations', *Cell*, vol. 141, no. 7, pp. 1146–1158, 2010.

[407] M. Scharl, K. A. Wojtal, H. M. Becker, A. Fischbeck, P. Frei, J. Arikkat, T. Pesch, S. Kellermeier, D. L. Boone, A. Weber *et al.*, 'Protein tyrosine phosphatase nonreceptor type 2 regulates autophagosome formation in human intestinal cells', *Inflammatory Bowel Diseases*, vol. 18, no. 7, pp. 1287–1302, 2012.

[408] D. Colecchia, M. Stasi, M. Leonardi, F. Manganelli, M. Nolano, B. M. Veneziani, L. Santoro, E.-L. Eskelinen, M. Chiariello and C. Bucci, 'Alterations of autophagy in the peripheral neuropathy Charcot-Marie-Tooth type 2B', *Autophagy*, vol. 14, no. 6, pp. 930–941, 2018.

[409] L. H. Franco, V. R. Nair, C. R. Scharn, R. J. Xavier, J. R. Torrealba, M. U. Shiloh and B. Levine, 'The ubiquitin ligase Smurf1 functions in selective autophagy of Mycobacterium tuberculosis and anti-tuberculous host defense', *Cell Host & Microbe*, vol. 21, no. 1, pp. 59–72, 2017.

[410] N. Akizu, V. Cantagrel, M. S. Zaki, L. Al-Gazali, X. Wang, R. O. Rosti, E. Dikoglu, A. B. Gelot, B. Rosti, K. K. Vaux *et al.*, 'Biallelic mutations in SNX14 cause a syndromic form of cerebellar atrophy and lysosome-autophagosome dysfunction', *Nature Genetics*, vol. 47, no. 5, pp. 528–534, 2015.

[411] D. Ebrahimi-Fakhari, A. Saffari, L. Wahlster, J. Lu, S. Byrne, G. F. Hoffmann, H. Jungbluth and M. Sahin, 'Congenital disorders of autophagy: an emerging novel class of inborn errors of neuro-metabolism', *Brain*, vol. 139, no. 2, pp. 317–337, 2016.

[412] A. Goode, J. E. Long, B. Shaw, S. H. Ralston, M. R. Visconti, F. Gianfrancesco, T. Esposito, L. Gennari, D. Merlotti, D. Rendina *et al.*, 'Paget disease of bone-associated UBA domain mutations of SQSTM1 exert distinct effects on protein structure and function', *Biochimica et Biophysica Acta (BBA)-Molecular Basis of Disease*, vol. 1842, no. 7, pp. 992–1000, 2014.

[413] Y. Lee, P. H. Jonson, J. Sarparanta, J. Palmio, M. Sarkar, A. Vihola, A. Evilä, T. Suominen, S. Penttilä, M. Savarese *et al.*, 'TIA1 variant drives myodegeneration in multisystem proteinopathy with SQSTM1 mutations', *The Journal of Clinical Investigation*, vol. 128, no. 3, pp. 1164–1177, 2018.

[414] E. Zapata-Aldana, D. D. Kim, S. Remtulla, C. Prasad, C.-T. Nguyen and C. Campbell, 'Further delineation of TBCK-infantile hypotonia with psychomotor retardation and characteristic facies type 3', *European Journal of Medical Genetics*, vol. 62, no. 4, pp. 273–277, 2019.

[415] N. van Beek, D. J. Klionsky and F. Reggiori, 'Genetic aberrations in macroautophagy genes leading to diseases', *Biochimica et Biophysica Acta (BBA)-Molecular Cell Research*, vol. 1865, no. 5, pp. 803–816, 2018.

[416] M. J. Kim, H.-X. Deng, Y. C. Wong, T. Siddique and D. Krainc, 'The Parkinson's disease-linked protein TMEM230 is required for Rab8a-mediated secretory vesicle trafficking and retromer trafficking', *Human Molecular Genetics*, vol. 26, no. 4, pp. 729–741, 2017.

[417] T. Kimura, A. Jain, S. W. Choi, M. A. Mandell, K. Schroder, T. Johansen and V. Deretic, 'TRIM-mediated precision autophagy targets cytoplasmic regulators of innate immunity', *Journal of Cell Biology*, vol. 210, no. 6, pp. 973–989, 2015.

[418] N. Ochotny, I. Voronov, C. Owen, J. E. Aubin and M. F. Manolson, 'The R740 S mutation in the V-ATP ase a3 subunit results in osteoclast apoptosis and defective early-stage autophagy', *Journal of Cellular Biochemistry*, vol. 114, no. 12, pp. 2823–2833, 2013.

[419] K. Hörtnagel, I. Krägeloh-Mann, A. Bornemann, M. Döcker, S. Biskup, H. Mayrhofer, F. Battke, G. Du Bois and K. Harzer, 'The second report of a new hypomyelinating disease due to a defect in the VPS11 gene discloses a massive lysosomal involvement', *Journal of Inherited Metabolic Disease*, vol. 39, no. 6, pp. 849–857, 2016.

[420] J. Zhang, V. Lachance, A. Schaffner, X. Li, A. Fedick, L. E. Kaye, J. Liao, J. Rosenfeld, N. Yachelevich, M.-L. Chu *et al.*, 'A founder mutation in VPS11 causes an autosomal recessive leukoencephalopathy linked to autophagic defects', *PLoS Genetics*, vol. 12, no. 4, e1005848, 2016.

[421] E. Seong, R. Insolera, M. Dulovic, E.-J. Kamsteeg, J. Trinh, N. Brüggemann, E. Sandford, S. Li, A. B. Ozel, J. Z. Li *et al.*, 'Mutations in VPS13D lead to a new recessive ataxia with spasticity and mitochondrial defects', *Annals of neurology*, vol. 83, no. 6, pp. 1075–1088, 2018.

[422] P. P. Lee, D. Lobato-Márquez, N. Pramanik, A. Sirianni, V. Daza-Cajigal, E. Rivers, A. Cavazza, G. Bouma, D. Moulding, K. Hultenby *et al.*, 'Wiskott-Aldrich syndrome protein regulates autophagy and inflammasome activity in innate immune cells', *Nature Communications*, vol. 8, no. 1, pp. 1–13, 2017.

[423] A. Fleming and D. C. Rubinsztein, 'Autophagy in neuronal development and plasticity', *Trends in Neurosciences*, 2020.

[424] T. B. Haack, P. Hogarth, M. C. Kruer, A. Gregory, T. Wieland, T. Schwarzmayr, E. Graf, L. Sanford, E. Meyer, E. Kara *et al.*, 'Exome sequencing reveals de novo WDR45 mutations causing a phenotypically distinct, X-linked dominant form of NBIA', *The American Journal of Human Genetics*, vol. 91, no. 6, pp. 1144–1149, 2012.

[425] J. Suleiman, D. Allingham-Hawkins, M. Hashem, H. Shamseldin, F. Alkuraya and A. El-Hattab, 'WDR45B-related intellectual disability, spastic quadriplegia, epilepsy, and cerebral hypoplasia: A consistent neurodevelopmental syndrome', *Clinical Genetics*, vol. 93, no. 2, pp. 360–364, 2018.

[426] C. Ji, H. Zhao, D. Li, H. Sun, J. Hao, R. Chen, X. Wang, H. Zhang and Y. G. Zhao, 'The role of Wdr45b in maintaining neural autophagy and cognitive function', *Autophagy*, vol. 16, no. 4, pp. 615–625, 2020.

[427] G. McMichael, M. Bainbridge, E. Haan, M. Corbett, A. Gardner, S. Thompson, B. Van Bon, C. Van Eyk, J. Broadbent, C. Reynolds *et al.*, 'Whole-exome sequencing points to considerable genetic heterogeneity of cerebral palsy', *Molecular Psychiatry*, vol. 20, no. 2, pp. 176–182, 2015.

[428] L. Scorrano, M. A. De Matteis, S. Emr, F. Giordano, G. Hajnóczky, B. Kornmann, L. L. Lackner, T. P. Levine, L. Pellegrini, K. Reinisch *et al.*, 'Coming together to define membrane contact sites', *Nature Communications*, vol. 10, no. 1, pp. 1–11, 2019.

[429] T. Brabletz, R. Kalluri, M. A. Nieto and R. A. Weinberg, 'EMT in cancer', *Nature Reviews Cancer*, vol. 18, no. 2, p. 128, 2018.

[430] K. Kurokawa and A. Nakano, 'The ER exit sites are specialized ER zones for the transport of cargo proteins from the ER to the Golgi apparatus', *The Journal of Biochemistry*, vol. 165, no. 2, pp. 109–114, 2019.

[431] B. Lehner, C. Crombie, J. Tischler, A. Fortunato and A. G. Fraser, 'Systematic mapping of genetic interactions in Caenorhabditis elegans identifies common modifiers of diverse signaling pathways', *Nature Genetics*, vol. 38, no. 8, pp. 896–903, 2006.

[432] P. Handa, S. Thanedar and U. Varshney, 'Rapid and reliable site-directed mutagenesis using Kunkel's approach', in *In Vitro Mutagenesis Protocols*, Springer, 2002, pp. 1–6.

[433] T. Harel, D. Pehlivan, C. T. Caskey and J. R. Lupski, 'Mendelian, non-Mendelian, multigenic inheritance, and epigenetics', in *Rosenberg's Molecular and Genetic Basis of Neurological and Psychiatric Disease*, Elsevier, 2015, pp. 3–27.

[434] A. Veres, B. S. Gosis, Q. Ding, R. Collins, A. Ragavendran, H. Brand, S. Erdin, C. A. Cowan, M. E. Talkowski and K. Musunuru, 'Low incidence of off-target mutations in individual CRISPR-Cas9 and TALEN targeted human stem cell clones detected by whole-genome sequencing', *Cell Stem Cell*, vol. 15, no. 1, pp. 27–30, 2014.

[435] H. A. Han, J. K. S. Pang and B.-S. Soh, 'Mitigating off-target effects in CRISPR/Cas9-mediated in vivo gene editing', *Journal of Molecular Medicine*, pp. 1–18, 2020.

[436] Mahdavi, Morteza and Nassiri, Mohammadreza and Kooshyar, Mohammad Mahdi and Vakili-Azghandi, Masoume and Avan, Amir and Sandry, Ryan and Pillai, Suja and Lam, Alfred King-yin and Gopalan, Vinod, 'Hereditary breast cancer; Genetic penetrance and current status with BRCA', *Journal of Cellular Physiology*, vol. 234, no. 5, pp. 5741–5750, 2019.

[437] C. Rabouille, 'Pathways of unconventional protein secretion', *Trends in Cell Biology*, vol. 27, no. 3, pp. 230–240, 2017.

Danksagung

Zu Beginn möchte ich mich bei meinem Betreuer Dr. Manuel Kaulich bedanken, der die Durchführung dieser Arbeit ermöglicht hat und mich bei der Bearbeitung stets durch zielführende Diskussionen und anhaltende Hilfestellung begleitet hat.

Mein Dank gilt auch Prof. Dr. Ivan Dikic für seine zahlreichen konstruktiven Anregungen, seine fachliche Expertise und für die enge und erfolgreiche Kollaboration mit seiner Arbeitsgruppe zur Anwendung der 3Cs Multiplexing Technologie im Kontext von Autophagie.

Ich danke außerdem Prof. Dr. Volker Dötsch für die Erstellung des Erstgutachtens und allen Mitgliedern der Prüfungskommission für Ihre Zeit und Ihr Interesse an dieser Arbeit.

Außerdem gilt mein Dank auch Dr. Paolo Grumati und Dr. Varun Shah für ihre Unterstützung bei der Durchführung und Validierung des Autophagie-Screens.

Ganz besonders möchte ich mich bei Dr. Koraljka Husnjak bedanken, die bei fachlichen Fragen und experimentellen Problemen nicht nur ein offenes Ohr, sondern vor allem auch stets hilfreiche Lösungsansätze hatte.

Ich bedanke mich auch bei allen Mitgliedern des Instituts für Biochemie II für das anregende Arbeitsklima und die Hilfsbereitschaft.

Besonderer Dank gebührt meinen Kollegen aus der Arbeitsgruppe von Dr. Manuel Kaulich. Insbesondere danke ich Konstantin Müller für seine Freundschaft und für alle unsere Diskussionen über forschungsrelevanten und -irrelevante Themen. Ich möchte mich außerdem bei Simone Schaubeck bedanken, die einen entscheidenden Beitrag zum Gelingen dieser Arbeit geleistet hat. Vor allem aber werde ich dank ihrer lustigen und warmherzigen Art meine Promotionszeit immer mit wundervollen Erinnerungen verbinden. Vielen Dank für die Ratschläge, die moralische Unterstützung und deine Freundschaft.

Mein ganz besonderer Dank gilt meiner Familie und meinen Freunden, ohne die diese Arbeit nicht möglich gewesen. Danke, dass Ihr immer an mich geglaubt und mich auch in schwierigen Situationen stets unterstützt und motiviert habt.

Eidesstattliche Erklärung

Hiermit erkläre ich, Valentina Diehl, geboren am 5.Dezember 1990 in Wachsch, dass ich die vorliegende Dissertation mit dem Titel:

„Minimized combinatorial CRISPR screens identify genetic interactions in autophagy“

selbstständig angefertigt und mich anderer Hilfsmittel als der in ihr angegebenen nicht bedient habe, insbesondere, dass alle Entlehnungen aus anderen Schriften mit Angabe der betreffenden Schrift gekennzeichnet sind.

Ich versichere, die Grundsätze der guten wissenschaftlichen Praxis beachtet, und nicht die Hilfe einer kommerziellen Promotionsvermittlung in Anspruch genommen zu haben.

Frankfurt am Main, ... Valentina Diehl . . . . . .

Ich erkläre hiermit, dass ich mich bisher keiner Doktorprüfung im mathematisch/naturwissenschaftlichen Bereich unterzogen habe.

Frankfurt am Main, ... Valentina Diehl . . . . . .

Publications and patent

Publications:

1. **V. Diehl**, M. Wegner, P. Grumati, K. Husnjak, S. Schaubeck, A.Gubas, V. Shah, I. H. Polat, F. Langschied, C. Prieto-Ggarcia, K. Müller, A. Kalousi, I. Ebersberger, C. H. Brandts, I. Dikic and M. Kaulich, **"Minimized combinatorial CRISPR screens identify genetic interactions in autophagy."**, Nucleic Acids Research (2021). https://doi.org/10.1093/nar/gkab309

2. M. Wegner, **V. Diehl**, V. Bittl, R. de Bruyn, S. Wiechmann, Y. Matthess, M. Hebel, M.G. Hayes, S. Schaubeck, C. Benner, S. Heinz, A. Bremm, I. Dikic, A. Ernst and M. Kaulich, **"Circular synthesized CRISPR/Cas gRNAs for functional interrogations in the coding and noncoding genome."**, eLife (2019). https://pubmed.ncbi.nlm.nih.gov/30838976

Patent:
The Goethe University Frankfurt has filed a patent application related to this work, on which Valentina Diehl, Martin Wegner, Ivan Dikic and Manuel Kaulich are inventors (WO2017EP84625).

Curriculum vitae

Valentina Diehl

PERSONAL INFORMATION

Born:	**05.12.1990, in Wachsch, Tadjikistan**
Address:	**Morgensternstraße 37, 60596 Frankfurt am Main**
Phone:	**+49 17655850745**
Email:	**valentinadiehl@web.de**

EDUCATION AND EMPLOYMENT HISTORY

09/2016 - 03/2021 **PhD candidate**
At the Institute of Biochemistry II, University Hospital in Frankfurt am Main in the gene editing group of Dr. Manuel Kaulich.
Topic: Combinatorial CRISPR-Cas9 screening for genetic interactions in the human autophagy pathway.

03 - 09/2016 **Master thesis**
At the Institute of Biochemistry II, University Hospital in Frankfurt am Main in the gene editing group of Dr. Manuel Kaulich.
Topic: Design and validation of a subset-specific CRISPR-Cas9 gRNA library targeting cyclin-dependent kinase 4 (CDK4) substrates.
Grade: 1.1

03/2015 - 09/2015 **Internship**
At Roche Diagnostics GmbH in Penzberg in the group of Dr. Sven Markert.
Topic: Seed train characterization by cell physiological assays.

10/2013 - 09/2016 **Master's study**
At the University of Freiburg.
Major subjects: Applied Bioscience, Plant Biology and Immunology.
Final grade: 1.3

10/2010 - 08/2013	**Bachelor's study**
	At the Karlsruhe Institute of Technology.
	Final grade: 1.9
06/2010	**Abitur**
	At Markgrafengymnasium Karlsruhe.
	Grade: 2.2

Frankfurt am Main, ...

Valentina Diehl . . . . . .